



Hard exclusive processes beyond the leading twist

Adrien Besse

► To cite this version:

Adrien Besse. Hard exclusive processes beyond the leading twist. Other [cond-mat.other]. Université Paris Sud - Paris XI; National centre for nuclear research (Otwock-Świerk), 2013. English. NNT : 2013PA112106 . tel-00855281

HAL Id: tel-00855281

<https://theses.hal.science/tel-00855281>

Submitted on 29 Aug 2013

HAL is a multi-disciplinary open access archive for the deposit and dissemination of scientific research documents, whether they are published or not. The documents may come from teaching and research institutions in France or abroad, or from public or private research centers.

L'archive ouverte pluridisciplinaire **HAL**, est destinée au dépôt et à la diffusion de documents scientifiques de niveau recherche, publiés ou non, émanant des établissements d'enseignement et de recherche français ou étrangers, des laboratoires publics ou privés.



THÈSE

Présentée pour obtenir
LE GRADE DE DOCTEUR EN SCIENCES
DE L'UNIVERSITÉ PARIS-SUD XI
en cotutelle avec le
NATIONAL CENTRE FOR NUCLEAR RESEARCH
Spécialité: Physique théorique

par

Adrien BESSE

soutenue publiquement le Mardi 02 juillet 2013

Réactions dures exclusives au twist sous-dominant

Directeurs de thèse: Lech SZYMANOWSKI
Samuel WALLON

Composition du jury

<i>Président du jury:</i>	Dr. Damir BECIREVIC
<i>Rapporteurs:</i>	Pr. Krzysztof GOLEC-BIERNAT Dr. Stéphane MUNIER
<i>Examineurs:</i>	Pr. Krzysztof KUREK Dr. Laurent SCHOEFFEL



Thèse préparée au
Département de Physique d'Orsay,
Laboratoire de Physique Théorique
(UMR 8627),
Bât. 210, Université Paris-Sud 11,
91405 Orsay Cedex

Résumé

Cette thèse porte sur le calcul des amplitudes d'hélicités de la leptoproduction diffractive exclusive du méson ρ dans la limite de Regge perturbative au-delà du twist dominant. La compréhension de ce processus et autres processus exclusifs en terme d'interactions entre les constituents fondamentaux de la QCD, constitue un enjeu majeur pour comprendre la structure des hadrons. L'approche suivie par le modèle présenté ici est basée d'une part sur la k_T -factorisation à petits x , c'est-à-dire dans la limite des hautes énergies dans le centre de masse $W \sim \sqrt{s}$ et d'autre part sur la factorisation colinéaire du méson ρ dans la limite des hautes virtualités Q du photon virtuel interagissant avec le nucléon.

Dans l'approche de la k_T -factorisation, l'amplitude est scindée en deux pièces principales, le facteur d'impact correspondant à la transition du photon virtuel au méson ρ ($\gamma^*(\lambda_\gamma) \rightarrow \rho(\lambda_\rho)$) et le facteur d'impact du nucleon cible. Ces deux facteurs d'impacts interagissent par l'échange d'un poméron dans la voie t qui contient toute la dépendance en énergie du processus. Le poméron est décrit à l'ordre dominant par l'échange de deux gluons et à l'ordre dominant en $\ln(1/x)$ avec $x \sim Q^2/W^2$ par l'échange d'une échelle de gluons dans la voie t .

La haute virtualité du photon justifie l'application de la QCD perturbative pour calculer le facteur d'impact $\gamma^*(\lambda_\gamma) \rightarrow \rho(\lambda_\rho)$ en utilisant la factorisation colinéaire pour séparer les contributions dominantes au twist 2 et au twist 3. Cette approche a été employée par Ginzburg, Panfil et Serbo en 1985 pour calculer les termes de twist 2 des facteurs d'impacts des transitions où le photon virtuel est polarisé soit longitudinalement soit transversalement et où le méson ρ est polarisé longitudinalement. Ces transitions sont dénotées respectivement " $\gamma_L^* \rightarrow \rho_L$ " et " $\gamma_T^* \rightarrow \rho_L$ ". L'approche a ensuite été poussée au twist 3 en 2010 par Anikin, Ivanov, Pire, Szymanowski et Wallon, pour obtenir le terme de twist 3 du facteur d'impact de la transition " $\gamma_T^* \rightarrow \rho_T$ " où le photon virtuel et le méson ρ sont polarisés transversalement. Ces résultats sont invariants de jauge et font apparaître les distributions d'amplitudes du méson ρ paramétrisant la production du méson à partir des états de Fock intermédiaires quark-antiquark et quark-antiquark-gluon.

Dans cette thèse nous présentons un premier modèle se basant sur ces résultats pour les facteurs d'impacts, pour décrire les rapports d'amplitudes d'hélicités associés à ce processus en utilisant un modèle phénoménologique pour le facteur d'impact du nucléon cible. On utilise aussi un modèle pour les distributions d'amplitudes du méson ρ basé sur le développement conforme de celles-ci. Les résultats de ce modèle sont ensuite comparés aux données de HERA et nous discutons les résultats obtenus.

Une seconde approche est présentée où les facteurs d'impacts aux twist 2 et 3 des transitions $\gamma_L^* \rightarrow \rho_L$ et $\gamma_T^* \rightarrow \rho_T$ sont redérivés dans la représentation des paramètres d'impacts. On montre que ces résultats sont équivalents à ceux obtenus dans l'approche dans l'espace des impulsions et permettent d'avoir une image en terme des configurations de dipôles de couleurs contenues dans l'état partonique intermédiaire de la transition $\gamma^* \rightarrow \rho$. Les amplitudes d'hélicités ainsi obtenues se décomposent en une convolution entre le recouvrement des fonctions d'onde du photon virtuel et du méson ρ calculé dans l'approximation colinéaire,

avec l'amplitude d'interaction d'un dipôle de couleur avec le nucléon cible. Cette dernière amplitude est universelle et déterminée à partir d'autres processus tels que le processus de diffusion profondément inélastique. Nous obtenons ainsi une expression pour les amplitudes d'hélicités où nous pouvons combiner des modèles d'amplitude de diffusion dipôle-nucléon avec le recouvrement des fonctions d'onde issus des calculs de factorisation colinéaire aux twists 2 et 3. Nous présentons les prédictions, comparées aux données de HERA, pour les sections efficaces polarisées de la production diffractive exclusive du méson ρ obtenues à partir des amplitudes d'hélicités. Les prédictions sont en accord avec les données pour des virtualités supérieures à $5\text{-}7\text{ GeV}^2$. Nous présentons une analyse de ces résultats, notamment nous discutons le rôle des corrections de twists supérieurs et nous comparons nos résultats avec des recouvrements de fonctions d'onde obtenus par d'autres modèles existants.

Mots-clefs: Processus exclusifs, Chromodynamique Quantique perturbative, Amplitudes d'hélicités, Factorisation colinéaire, k_T -factorisation, Dipôles de couleurs.

Abstract

This thesis, entitled "Hard exclusive processes beyond the leading twist", deals with the computation of the helicity amplitudes of the exclusive diffractive ρ -meson leptonproduction in the perturbative Regge limit beyond the leading twist. The understanding of such exclusive processes in terms of the elementary constituents of QCD is a serious challenge to understand the hadronic structure. The approach we follow here, first relies on the k_T -factorization in the small- x regime, i.e. when there is a high energy $W \sim \sqrt{s}$ in the center of mass of the photon-proton system. It secondly relies on the collinear factorization scheme for large virtualities Q of the photon, to factorize the ρ -meson soft part of the process.

Within the k_T -factorization approach, the amplitude splits in two main pieces, the $\gamma^*(\lambda_\gamma) \rightarrow \rho(\lambda_\rho)$ impact factor, with λ_γ and λ_ρ the polarizations of the virtual photon and the ρ -meson, and the nucleon impact factor. The impact factors are interacting with the exchange of a pomeron in the t -channel which corresponds to the exchange of two t -channel gluons at leading order and a ladder of gluons at leading $\log(1/x)$ order, with $x \sim Q^2/W^2$.

At high virtualities of the photon, the perturbative QCD techniques are justified to compute the $\gamma^*(\lambda_\gamma) \rightarrow \rho(\lambda_\rho)$ impact factor using the collinear factorization scheme to get the twist 2 and twist 3 terms. This approach was first used in 1985 by Ginzburg, Panfil and Serbo to compute the twist 2 $\gamma_L^* \rightarrow \rho_L$ and $\gamma_T^* \rightarrow \rho_L$ impact factors. In 2010 the twist 3 term of the $\gamma_T^* \rightarrow \rho_T$ impact factor was derived by Anikin, Ivanov, Pire, Szymanowski and Wallon. The results obtained are gauge invariant and they involve the twist 2 and twist 3 distribution amplitudes of the ρ -meson that parameterize the meson production from the quark antiquark and the quark antiquark gluon intermediate Fock states.

In this thesis we present a model based on these impact factor results to get predictions for the ratios of helicity amplitudes associated to the ρ -meson diffractive leptonproduction using a phenomenological model for the proton impact factor. We also use a model for the distribution amplitudes based on the conformal expansion. The predictions are then compared to HERA data and we discuss the results of this approach.

A second approach is presented where the twist 2 and twist 3 impact factors are derived in the impact parameter representation. We show that the results are equivalent to the ones obtained in the momentum space representation. The results in impact parameter representation give information about the dipole configuration content of the intermediate state involved in the $\gamma^* \rightarrow \rho$ impact factors. As a result of this approach, the helicity amplitudes factorize as the convolution of two parts, the first one is the overlap of the virtual photon and the ρ -meson wave functions computed in the collinear approximation and the second one is the dipole-target scattering amplitude. The dipole-target scattering amplitude is well determined on other processes such as deep inelastic scattering processes. Combining a model for the dipole cross-section with the results obtained within the collinear factorization scheme for the overlap of the wave functions, we get a model for helicity amplitudes and the longitudinal and transverse polarized cross-sections. We compare our predictions to HERA data and get a good agreement for virtualities of the photon larger than $Q^2 \sim 5 - 7 \text{ GeV}^2$.

We discuss the results, in particular the role of higher twist corrections and we compare our results with the overlaps of wave functions obtained from other models that exist within the color dipole picture.

Keywords: Exclusive processes, Perturbative quantum chromodynamics, Helicity amplitudes, Collinear factorization, k_T -factorization, Color dipoles.

Remerciements

Je voudrais remercier tout d'abord mes directeurs de thèse Samuel Wallon et Lech Szymanowski ainsi que notre proche collaborateur Bernard Pire pour ces trois années de thèse où ils m'ont fait partager leur enthousiasme pour la recherche. J'ai énormément appris grâce à leurs conseils et à nos discussions et je leur suis profondément reconnaissant autant pour leur investissement dans mon apprentissage que pour tout le savoir qu'ils ont réussi à me communiquer. Je les remercie d'avoir toujours été disponibles et à l'écoute lorsque j'ai eu besoin de leur aide qui s'est toujours révélée très précieuse dans l'avancement de mes travaux de thèse. Cela aura été un vrai plaisir de travailler avec eux ainsi qu'une expérience très enrichissante.

Je remercie le directeur du laboratoire Henk Hilhorst, pour m'avoir accueilli au LPT et m'avoir permis d'aller à un grand nombre de conférences et d'écoles qui m'ont beaucoup apportées. J'aimerais aussi remercier toute l'équipe administrative du LPT, Mireille Calvet, Philippe Molle, Jocelyne Puech et Odile Heckenauer, ainsi que l'équipe "informatique" du laboratoire, Philippe Boucaud et Olivier Brand-Foissac, pour leur disponibilité et l'aide qu'ils m'ont tous apporté durant ces trois années.

Je tiens à remercier nos collaborateurs polonais Krzysztof Golec-Biernat, Leszek Motyka et Mariusz Sadzikowski pour leur accueil et pour nos discussions lors de mes séjours à Cracovie. Je voudrais remercier Stéphane Munier et Cyrille Marquet pour leurs conseils concernant mes travaux de thèse, ainsi que Christophe Royon pour ses nombreuses invitations à des conférences internationales. Un grand merci à Hervé Moutarde et Franck Sabatié pour me donner la chance de continuer à travailler sur d'intéressants problèmes de physique hadronique et pour m'avoir accepté au sein de leur nouveau projet.

Merci à tous les membres de mon jury pour avoir accepté de prendre de leur temps pour examiner ma thèse. Je les remercie pour les remarques très pertinentes qui ont été soulevées durant la soutenance et qui permettent d'envisager de nouvelles perspectives au travail qui a été fait dans cette thèse.

Un grand merci aussi aux doctorants du laboratoire pour les bons moments passés dans la cafétéria du LPT. Je remercie particulièrement Cédric Weiland avec qui j'ai partagé mon bureau durant ces trois années pour son agréable compagnie et pour toutes les discussions intéressantes que nous avons eu ensemble.

Merci à mon ami Axel avec qui nous avons suivi nos études depuis les classes préparatoires jusqu'à la thèse et à qui je dois énormément. Je le remercie pour son soutien tout au long de nos études où nous avons partagé notre passion pour la physique. Je remercie mes parents et mon frère pour leurs incessants encouragements durant toutes mes années d'études. Merci aussi à tous mes amis pour les bons moments passés ensemble durant ces trois années, Antoine, Gabriel, Olga, Roberto, Béa, Charles, ainsi que tous ceux que je ne peux citer ici mais que je n'oublie pas. Enfin je ne peux que remercier ma bien-aimée Katyusha pour son immense soutien durant ces deux dernières années de thèse.

Merci à vous tous!

Acknowledgments

First I would like to thank my supervisors Samuel Wallon and Lech Szymanowski as well as our close collaborator Bernard Pire, for having shared with me their enthusiasm for research during these three years of thesis. I have learned a lot thanks to their advices and our discussions and I am deeply grateful for their investment in my formation as well as for all the knowledge they gave me. I thank them for being always available and attentive when I needed their assistance which has always been very helpful in my work. It was a great pleasure working with them and it was for me a very rewarding experience.

I would like to thank the director of the laboratory, Henk Hilhorst, for welcoming me at the LPT and for all the conferences and the schools that he allowed me to participate and where I have learned a lot. I would like also to thank the administrative team of the LPT, Mireille Calvet, Philippe Molle, Jocelyne Puech and Odile Heckenauer, as well as the "computer" team, Olivier Brand-Foissac and Philippe Boucaud for their availability and for all the assistance they provided me during these three years.

I want to thank our colleagues from Poland, Krzysztof Golec-Biernat, Leszek Motyka and Mariusz Sadzikowski for their hospitality and for our discussions during my visits in Krakow. I would like to thank Stéphane Munier and Cyrille Marquet for their advices on my thesis work and Christophe Royon for his invitations to international conferences. Many thanks to Hervé Moutarde and Franck Sabatié for giving me the opportunity to continue to work on interesting hadronic physics problems and for accepting me in their new project.

Many thanks also to all the members of the jury for taking from their time to examine my thesis. I thank them for all the relevant remarks that have been told during the defense which allow to consider new perspectives to the work of my thesis.

A big thank you to all the PhD students of the LPT for the good time we spent in the caf   of the lab. I am particularly thankful to C  dric Weiland with whom I was sharing my office during these three years for his very pleasant company and the interesting discussions we have had.

Many thanks to my friend Axel with whom we shared our taste for physics since our first years at the university, and to whom I owe a lot. I thank my parents and my brother for their constant support all along my studies. Many thanks to all my friends for the good time we spent together during these three years, Antoine, Gabriel, Olga, Roberto, B  a, Charles, and all others that I don't name here but who are not forgotten. I finally thank my beloved Katyusha for her huge support during these two last years of PhD.

Thank you very much!

Contents

Introduction	1
1 High energy QCD	5
1.1 Introduction	5
1.1.1 Postulates and consequences	5
1.1.2 Regge trajectories and the pomeron intercept	8
1.1.3 Cutkosky rules	10
1.2 Scattering amplitudes in the Regge limit	11
1.2.1 The color octet exchange	11
1.2.2 The singlet color exchange in t -channel	14
1.2.3 Impact factor representation of the quark-quark scattering amplitude	16
1.2.4 The k_T factorization scheme	20
1.3 Deep inelastic scattering amplitude in the perturbative Regge kinematics . .	24
1.3.1 Introduction to DIS observables	24
1.3.2 Impact factors $\gamma_{L,T}^* \rightarrow \gamma_{L,T}^*$	30
1.3.3 Color dipole picture	33
1.3.4 Models for the dipole target interactions	40
2 Light-Cone Collinear Factorization applied to the ρ-meson production	51
2.1 Introduction	51
2.1.1 Diffractive exclusive vector electroproduction	51
2.1.2 The underlying ideas of our approach	55
2.2 Light-cone collinear factorization up to twist 3 accuracy	56
2.2.1 Soft parts and hard parts	56
2.2.2 Factorization of the spinor indices	59
2.2.3 Factorization of the color indices	62
2.2.4 Factorization in the momentum space around the light cone direction p	63
2.3 Parameterizing the vacuum to rho-meson matrix elements	68
2.3.1 Light-cone wave functions and distribution amplitudes	69
2.3.2 Lorentz decomposition and parity analysis	70
2.4 Reduction to a minimal set of DAs	77
2.4.1 DA relations from the equations of motion of QCD	77

2.4.2	Equations from the n -independence condition	79
2.4.3	Wandzura-Wilczek and genuine solutions	82
2.4.4	The dictionary	86
2.5	Conformal expansion and scale dependence of DAs	88
2.5.1	Goal of the conformal expansion	88
2.5.2	Conformal expansion of the DAs	90
2.5.3	Scale dependence of the DAs	91
2.6	QCD sum rules	98
2.7	Impact factors $\gamma^*(\lambda_\gamma) \rightarrow \rho(\lambda_\rho)$	100
2.7.1	Kinematics	101
2.7.2	The $\gamma_L^* \rightarrow \rho_L$ transition	102
2.7.3	The $\gamma_T^* \rightarrow \rho_L$ impact factor	103
2.7.4	The $\gamma_T^* \rightarrow \rho_T$ impact factor	104
2.8	Helicity amplitudes	109
2.8.1	Measurement of helicity amplitudes and spin matrix elements	110
2.8.2	A proton impact factor model	112
2.8.3	Helicity amplitudes T_{11} and T_{00} at $t = t_{min}$ - Comparison of obtained predictions with H1 data	112
2.8.4	Helicity amplitudes T_{00} and T_{01} for $t \neq t_{min}$	117
2.8.5	Discussion of the results	123
3	LCCF in the impact parameter representation	125
3.1	Introduction	125
3.2	The $q\bar{q}$ intermediate state contributions	126
3.2.1	Equivalent LCCF procedure in impact parameter representation	126
3.2.2	Impact factor calculation for the $q\bar{q}$ contribution	128
3.2.3	Interpretation of the result obtained in the WW approximation	133
3.2.4	Equivalence of momentum and impact parameter calculations	135
3.2.5	The impact parameter representation of the $\gamma_L^* \rightarrow \rho_L$ impact factor	135
3.3	The $q\bar{q}g$ intermediate state contribution to the $\gamma_T^* \rightarrow \rho_T$ impact factor	136
3.3.1	LCCF in impact parameter representation for the $q\bar{q}g$ amplitude	137
3.3.2	The color dipole configurations of the hard part	138
3.3.3	Fourier transforms of the 3-parton diagrams in the collinear limit	143
3.3.4	Spin non-flip and spin flip $q\bar{q}g$ impact factor	147
3.4	The twist 3 $\gamma_T^* \rightarrow \rho_T$ impact factor in the dipole picture	151
3.4.1	The dipole picture arising from the equations of motion of QCD	151
3.4.2	Equivalence with the results obtained in momentum space in the light- cone collinear factorization scheme	153
3.4.3	Complete twist 3 result of the $\gamma_T^* \rightarrow \rho_T$ impact factor	155
3.5	Helicity amplitudes and polarized cross-sections	156
3.6	Comparison with the HERA data	159

3.7	Interacting dipole distributions	162
3.7.1	Overlaps and distributions	163
3.7.2	Comparison of overlaps	170
3.8	Discussion	173
Conclusions		175
Appendix		177
REFERENCES		182

Introduction

Inclusive processes, such as the deep inelastic scattering (DIS) processes have provided a lot of information about the nature of strong interactions and the nucleon structure. These processes first described by the naive parton model proposed by Feynman and Bjorken [1, 2] to explain the approximate Bjorken scaling observed at SLAC in late 60's, allowed to disentangle the hadronic structure as made of elementary asymptotically free constituents called "partons". The mysterious facts that in a strongly bound hadronic state the partons are acting like free and the fact that quarks without their color degrees of freedom are violating the Pauli exclusion principle were solved with the apparition of the quantum chromodynamics (QCD) to describe the strong interactions. Indeed, QCD which is a non-abelian gauge quantum field theory based on the $SU(3)$ color group, is an asymptotically free theory given the number of flavors we know, as demonstrated in 1973 by Wilczek, Politzer and Gross [3, 4, 5]. This is due to the non-abelian character of QCD and the running of α_s is very well reproduced by the data.

Another important feature of QCD is the confinement of quarks and gluons into colorless hadronic states which makes the direct observation of partons as external particles impossible. The experimental evidence for gluons at PETRA in 1979 comes from 3-jet events, due to an energetic gluon radiation $q\bar{q} \rightarrow q\bar{q}g$ in the hard sub-process $e^-e^+ \rightarrow q\bar{q}$. The confinement of the emitted quark antiquark and gluon leads to the observation of 3-jet events. These events are also used to determine the coupling constant of the strong interaction α_s .

Many techniques exist to study the QCD properties. The perturbative QCD (pQCD) approach is one of them and it relies on the factorization of a process into a hard part where large energy scales are involved and a soft part involving the long distance dynamics of the partons inside the hadrons. The presence of a hard scale Q in the collision is needed to justify the perturbative expansion in $\alpha_s(Q)$ of the hard part and the factorization into hard and soft pieces. Under kinematic assumptions, one can derive pQCD evolution equations such as the Dokshitzer-Gribov-Lipatov-Altarelli-Parisi (DGLAP), Efremov-Radyushkin-Brodsky-Lepage (ERBL) or Balitsky-Fadin-Kuraev-Lipatov (BFKL) equations, for the soft parts but pQCD cannot provide information on non-perturbative aspects of soft parts. Other techniques can supply information on non-perturbative quantities such as lattice QCD, effective field theories or QCD sum rules techniques.

Inclusive processes have also provided a deep understanding of the structure of the hadrons and the partonic distribution functions (PDFs), which are known on a wide kinematic range. They have been the testing ground of theoretical innovations such as the operator product expansion (OPE) formalism first introduced in particle physics by Wilson in the 70's [6] and then applied to DIS [7, 4]. However inclusive process observables give only information on the forward kinematics where there is no momentum transferred in t -channel. With the increasing improvement of the experiments, the measurements on exclusive processes, where one is interesting to a specific final state, have begun to bring additional information on the hadronic structure. For example, the generalized parton distributions (GPDs) parameterizing

the nucleon in the non-forward limit have to take into account not only the x dependence of the partonic distributions but also the skewness dependence. The exclusive processes such as the diffractive production of vector mesons, or the deep virtual Compton scattering (DVCS) have been studied for more than 25 years and are still the subject of many studies and experiments. For our purpose, we should name more particularly the HERA collider collaborations H1 and ZEUS as they have provided data for very small values of x and moderate Q^2 , which is the kinematic region of interest in this thesis. The low- x physics is an interesting limit of QCD. Alternative approaches from the usual collinear factorization scheme are based on k_T -factorization, such as the dipole models by Nikolaev, Zakharov [8, 9] and Mueller [10, 11] or the CGC formalism [12, 13, 14, 15, 16, 17]. Such approaches are used to understand the transition from a diluted to a dense partonic system due to the emission of gluons by Bremsstrahlung which takes place in the small- x limit. This transition poses the interesting question of saturation effects inside the hadrons.

In this thesis we developed a model for the diffractive ρ -meson production in the perturbative Regge limit, i.e. at small x and at high enough Q^2 to use pQCD techniques. This approach will be presented in chapter 2 and chapter 3, while the first chapter will be devoted to introduce the main tools of this treatment on a DIS process.

In the chapter 1, we will introduce basics of different techniques that are used in this thesis. We will present the k_T -factorization on the simplest examples to explain how the amplitudes can be factorized in the high energy limit, in sub-processes called "impact factors". Next, after a brief general introduction to DIS, we will focus on a DIS process to show how these impact factors can be interpreted in the language of dipole models. This permits us to discuss the importance and different ways of incorporation into the dipole model of saturation effects.

In the chapter 2, we will present the Light-Cone Collinear Factorization (LCCF) scheme beyond the leading twist and its application to the computation of the impact factor $\Phi^{\gamma^*(\lambda_\gamma) \rightarrow \rho(\lambda_\rho)}$ of the transition of the virtual photon of helicity λ_γ into a ρ -meson of helicity λ_ρ . In this approach, the soft part associated to the production of the ρ -meson is parameterized by the distribution amplitudes (DAs) of the ρ -meson. We will discuss the energy scale dependence of the DAs and the QCD sum rule technique to get non-perturbative parameters that enters the DAs. Finally we will present a phenomenological model to get predictions on helicity amplitudes of the diffractive ρ -meson production at HERA. This model will naturally lead us to the next chapter topic.

In the chapter 3, we will connect the impact factor $\Phi^{\gamma^*(\gamma) \rightarrow \rho \lambda_\rho}$ obtained in the previous chapter in the collinear approximation, to the color dipole picture. From this result, one can get phenomenological models by combining our results for the impact factors with dipole models that are already known from DIS analysis and that contains the x -dependence of the helicity amplitudes. These dipole models include the saturation dynamics of the nucleon target. We compare the predictions of the polarized cross-sections of the ρ -meson electroproduction with HERA data and discuss our results.

In the chapters 2 and 3, some parts are based on our own contributions like the phenomenological model [18] at the end of the chapter 2, and the chapter 3 which is based on

the studies [19] and [20].

Chapter 1

High energy QCD

In this chapter we present basics of the concepts and tools necessary to tackle the phenomenology of hadronic reactions in the small- x physics.

After an introduction on the Regge theory and the pomeron trajectory sec. 1.1, we explain on the quark-quark scattering the k_T -factorization procedure, first in the case of one gluon exchanged in t -channel and then in the case of a color singlet exchange (two gluon exchange) in sec. 1.2. We show how the impact factors emerge from this picture and briefly discuss the resummation at leading $\log(1/x)$ of the gluon ladder exchange in the t -channel.

We present some basics of DIS process in sec. 1.3, and show how the amplitude can be factorized in the dipole picture into the photon wave functions and the dipole cross-section. We present finally different models of dipole cross-section that include the saturation effects, as well as the equations that governs the energy dependence of the dipole cross-section in the diluted and dense regimes.

1.1 Introduction

1.1.1 Postulates and consequences

Before QCD was applied to describe the strong interactions, physicists relied on the basic postulates of the Lorentz invariance, the unitarity and the analyticity of the S -matrix in order to get information on the hadronic scattering.

Lorentz invariance of the S -matrix implies that the S -matrix element corresponding to the process

$$a(p_A, \lambda_A) + b(p_B, \lambda_B) \rightarrow c(p_C, \lambda_C) + d(p_D, \lambda_D), \quad (1.1)$$

can be expressed in terms of Lorentz invariant quantities such as the Mandelstam variables and the masses of the particles. For the particular case of the process (1.1) where two particles in the initial state give two particles in the final state, the scattering amplitude can be expressed in terms of the Mandelstam variables $s = (p_A + p_B)^2$, $t = (p_A - p_C)^2$ and $u = (p_A - p_D)^2$ which satisfy

$$s + t + u = \sum_i m_i^2, \quad (1.2)$$

where m_i denotes the mass of the particle i .

The unitarity condition of the S -matrix

$$S^\dagger S = S S^\dagger = 1, \quad (1.3)$$

expresses the fact that the probability for an initial state to give any final state is equal to one. Let us consider an *in*-state $|a\rangle$ and an *out*-state $|b\rangle$ which are respectively states of free particles at the times $t \rightarrow -\infty$ and $t \rightarrow \infty$. The corresponding S -matrix element is

$$S_{ab} = \langle b | a \rangle. \quad (1.4)$$

Let us introduce now the T -matrix element such as $S = 1 + iT$, and the scattering amplitude \mathcal{A}_{ab} and the cross-section σ_{ab} associated to this process,

$$S_{ab} = \delta_{ab} + iT_{ab} = \delta_{ab} + i(2\pi)^4 \delta^4\left(\sum_a p_a - \sum_b p_b\right) \mathcal{A}_{ab}. \quad (1.5)$$

The cross-section σ_{ab} of the event $a \rightarrow b$ is related to the probability of this event to happen, it is then proportional to the square of the scattering amplitude,

$$\sigma_{ab} = \frac{1}{F} \int d\Pi_b |\mathcal{A}_{ab}|^2, \quad (1.6)$$

with F the flux factor and Π_b the phase space of the n -body particles of the b final state. The flux factor in the case of the process (1.1) is given by

$$F = 2\sqrt{\lambda(s, m_A^2, m_B^2)} \quad (1.7)$$

where $\lambda(s, m_A^2, m_B^2)$ is the standard kinematic variable,

$$\lambda(s, m_A^2, m_B^2) = (s - (m_A + m_B)^2) (s - (m_A - m_B)^2). \quad (1.8)$$

The expression (1.7) for the flux factor remains true for the production of n particles in the final state from a two-particle initial state. Note that in the large s limit where the masses can be neglected compared to s , the flux factor is just $F = 2s$.

The unitarity condition of the S -matrix (1.3) implies then the following condition on the T -matrix elements

$$\begin{aligned} \sum_c (\delta_{ac} + iT_{ac}) (\delta_{cb} - iT_{cb}^\dagger) &= \delta_{ab} \\ i(T_{ab}^\dagger - T_{ab}) &= \sum_c T_{ac} T_{cb}^\dagger, \end{aligned} \quad (1.9)$$

where c is any physical state, i.e. the particles of this state are on the mass-shell. In terms of the scattering amplitudes, using the fact that

$$2i\mathcal{I}m \mathcal{A}_{ab} = \mathcal{A}_{ab} - \mathcal{A}_{ab}^\dagger, \quad (1.10)$$

the relation (1.9) reads

$$2\mathcal{I}m \mathcal{A}_{ab} = (2\pi)^4 \delta^4(\sum_a p_a - \sum_b p_b) \sum_c \mathcal{A}_{ac} \mathcal{A}_{cb}^\dagger. \quad (1.11)$$

This relation has very important consequences as it leads to the Cutkosky rules c.f. sec. 1.1.3 and, in the special case where one put identical *in*- and *out*- states, it leads to the optical theorem. The theorem reads

$$2\mathcal{I}m \mathcal{A}_{aa}(s, t=0) = (2\pi)^4 \delta^4(\sum_a p_a - \sum_b p_b) \sum_c |\mathcal{A}_{ac}|^2. \quad (1.12)$$

As a consequence of the optical theorem, the total cross-section σ_{tot} , associated to the process " $a \rightarrow$ any physical state", is given up to a coefficient by the imaginary part of the amplitude $\mathcal{A}_{aa}(s, t=0)$,

$$2\mathcal{I}m \mathcal{A}_{aa}(s, t=0) = F \sigma_{tot}. \quad (1.13)$$

The third postulate is the analyticity of the S -matrix elements, meaning that the S -matrix is an analytical function of the Lorentz invariants seen as complex variables. Analyticity has been shown to be a consequence of the causality, which prevents two regions separated by a space-like distance to influence on each other. Some consequences of the analyticity are:

- the crossing symmetry of the scattering amplitudes,
- the dispersion relations which allows to get the real part of the amplitude from the imaginary part.

The crossing symmetry in the case of the two to two particle process (1.1) reads

$$\mathcal{A}_{a+\bar{c} \rightarrow \bar{b}+d}(s, t) = \mathcal{A}_{a+b \rightarrow c+d}(t, s) \quad (1.14)$$

$$\mathcal{A}_{a+\bar{d} \rightarrow \bar{b}+c}(s, u) = \mathcal{A}_{a+b \rightarrow c+d}(u, s) \quad (1.15)$$

where \bar{b} , \bar{c} and \bar{d} are the antiparticles associated to b , c and d . In the case where $\mathcal{I}m \mathcal{A}(s, t)$ falls to zero when $z \rightarrow \infty$, the dispersion relation which relates the amplitude to its imaginary part is obtained by deforming the integration contour which surround the cuts,

$$\mathcal{A}(s, t) = \frac{1}{\pi} \int_{s_{th}^+}^{\infty} ds' \frac{\mathcal{I}m \mathcal{A}(s', t)}{s' - s} + \frac{1}{\pi} \int_{-\infty}^{s_{th}^-} ds' \frac{\mathcal{I}m \mathcal{A}(s', t)}{s' - s}, \quad (1.16)$$

where s^{th+} and s^{th-} are the thresholds of particle production along the real positive and real negative axis. If the asymptotic behavior of the integrand when $|s| \rightarrow \infty$ is not falling fast enough then the dispersion relation (1.16) is not valid and should be replaced by a subtracted dispersion relation where the integrand is divided by as many factors $(s' - s_0)$ as it is necessary

to ensure the convergence of the integrand with s_0 an arbitrary point. For the addition of one of the factor $s' - s_0$, the subtracted dispersion relation reads

$$\begin{aligned} \mathcal{A}(s, t) = & \mathcal{A}(s_0, t) + \frac{(s - s_0)}{\pi} \int_{s_{th}^+}^{\infty} ds' \frac{\mathcal{I}m \mathcal{A}(s', t)}{(s' - s)(s' - s_0)} \\ & + \frac{s - s_0}{\pi} \int_{-\infty}^{s_{th}^-} ds' \frac{\mathcal{I}m \mathcal{A}(s', t)}{(s' - s)(s' - s_0)}. \end{aligned} \quad (1.17)$$

Note that these relations require the knowledge of the asymptotic behavior of the scattering amplitudes which is the subject of the Regge theory.

These so-called "bootstrap" relations, that relate the imaginary part of the amplitude to the amplitude itself and to the sum of product of other amplitudes due to the analyticity and unitarity postulates, are obtained without for now specifying the underlying quantum field theory and are very general considerations.

1.1.2 Regge trajectories and the pomeron intercept

In the high energy limit $s \rightarrow \infty$ with fixed t , called the Regge limit, the asymptotic behavior of the amplitude of the process

$$a + b \rightarrow c + d, \quad (1.18)$$

is connected to the angular momentum l of the particle exchanged in s -channel of the crossed channel process,

$$a + \bar{c} \rightarrow \bar{b} + d. \quad (1.19)$$

The partial wave expansion of the amplitude of the crossed process (1.19),

$$\mathcal{A}_{a+\bar{c} \rightarrow \bar{b}+d}(s, t) = \sum_{l=0} (2l+1) a_l(s) P_l(1 + 2\frac{t}{s}), \quad (1.20)$$

allows to decouple the contribution given by elementary particle of angular momentum l and mass M exchanged in the s -channel. The crossing symmetry implies that for the process $a+b \rightarrow c+d$ where the role of the Mandelstam variables are exchanged, $s \leftrightarrow t$, the amplitude is essentially given by the resonance and takes the form,

$$\begin{aligned} \mathcal{A}_{ab \rightarrow cd}(s, t = M^2) &= \mathcal{A}_{a\bar{c} \rightarrow \bar{b}d}(t = M^2, s) \\ &= A_l(t) P_l(1 + 2\frac{s}{t}) = \frac{G_{a\bar{c}}(t) G_{\bar{b}d}(t)}{t - M^2} (\sigma_t + (-1)^l) P_l(1 + 2s/t), \end{aligned} \quad (1.21)$$

where σ_t is the signature which is 1 for crossing even amplitudes and -1 for crossing odd amplitudes, $G_{a\bar{c}}(t)$ is the vertex of the particle exchanged in the t -channel with the external particles. The process $t = M^2$ is not in the physical region of the s -channel and in eq. (1.21) an analytical continuation of the Legendre polynomials in the physical region of the process (1.18) allows to derive the asymptotic behavior of the amplitude of the process,

$$\mathcal{A}_{a+b \rightarrow c+d}(s, t) = \frac{g_{ac}(t) g_{bd}(t)}{t - M^2} s^l. \quad (1.22)$$

Note that the fact that the vertices G_{ij} do not depend on s at high energy is an universal feature that we will see also when describing the impact factor approach in k_T -factorization scheme. The amplitude depends on s only through the particles exchanged in t -channel.

This asymptotic behavior violates the unitarity of the theory. Indeed it was proven long ago by Froissart [21] using unitarity and partial wave expansion that hadronic cross-sections has to increase slower than $\ln^2(s)$,

$$\sigma_{tot} < A \ln^2(s),$$

with $A \sim 60$ mb. This is equivalent to bound the asymptotic amplitudes by,

$$A(s, t) < s \ln^2(s),$$

which from (1.22) is clearly violated for $l > 1$.

The way to solve this problem is to use the Sommerfeld-Watson integral transformation to express the partial wave expansion. The pole structure in the complex variable l of the partial wave amplitude $A_l(t) = A(l, t)$ will then fix the complex angular momentum of the resonance. The resonance angular momentum given by the pole $\alpha_R(t)$ of maximal real value will dominate the asymptotic power behavior of the amplitude, this pole is called the Regge pole and the effective "resonance" associated to this pole, of complex angular momentum $l = \alpha_R(t)$ is called reggeon. The underlying assumption is that poles are simple poles, but in practice logarithms appearing in the perturbation theory can gives branch cuts. The pole $\alpha_R(t)$ is a Regge trajectory and $\alpha_R(0)$ the reggeon intercept. The trajectories $l = \alpha_R(t)$ are universal objects that only depends on the quantum numbers of the particle exchanged in t -channel.

For $t < 0$, the t -dependence of the Regge pole can be experimentally obtained by fitting the energy dependence of the s -channel amplitudes. As explained above, the reggeon can be seen as resonances at $t = M^2$ of angular momentum l . The idea of so-called Chew Frautschi plots was then to show the masses of known resonances ρ, ω, \dots , as a function of their angular momentum. It turns out that the data are aligned on straight-lines and by extrapolating to the physical region $t < 0$, the straight-lines give a relatively good descriptions of the data obtained from experiments, leading to linear Regge trajectories

$$\alpha_R(t = M^2) = \alpha_R(0) + \alpha'_R t.$$

The Regge theory allows to complete the bootstrap relation as it allows to obtain the asymptotic behavior of the amplitude.

Using the optical theorem, the s -power like dependence of the total cross-section is

$$\sigma_{tot} \propto \text{Im} \mathcal{A}(s, t = 0) \propto s^{\alpha_R(t=0)-1}. \quad (1.23)$$

It was demonstrated by Pommeranchuk that the cross-section vanishes asymptotically in the case where there is a charge exchange in the t -channel. A Regge trajectory with $\alpha_R(0) > 1$ corresponds then to a reggeon that carries the vacuum quantum numbers and which is called

the "pomeron" (for a pedagogical review on the pomeron in QCD see [22]). The pomeron intercept is denoted $\alpha_P(0)$. Donnachie and Landshoff [23] have proposed a fit of the total cross-sections for pp and $p\bar{p}$ collisions as

$$\sigma_{tot} = X s^\epsilon + Y s^{-\eta},$$

where the first term can be interpreted as the exchange of a pomeron while the second term corresponds to the exchange of a reggeon. The best fits were

$$\begin{aligned}\sigma_{tot}^{pp} &= 21.7 s^{0.08} + 56.1 s^{-0.45}, \\ \sigma_{tot}^{p\bar{p}} &= 21.7 s^{0.08} + 98.4 s^{-0.45}.\end{aligned}$$

These fits highlights the fact that the pomeron couplings to the antiproton and the proton are the same which is due to the fact that the pomeron carries vacuum quantum numbers. The value $\eta = 0.45$, corresponds to the Regge trajectory close to the one given by the linear fits of Chew Frautschi plots based on the spectrum of $\{\rho, \omega \dots\}$ resonances.

The pomeron intercept $\alpha_P(0) = 1.08$ violates the unitarity bound from the Froissart theorem but one can show that with this value of the pomeron intercept, the violation occurs only at the Planck scale.

The quark and gluon content of the pomeron can be studied in diffractive dissociation processes where for example in ep collision, the pomeron is seen like a parton of the proton that interacts with the electron to give any final state X. This reaction is analogous to deep inelastic scattering where the pomeron replaces the proton which allows to study its partonic content.

1.1.3 Cutkosky rules

In the case of QED or QCD one can check that the imaginary part of an amplitude $\mathcal{A}(s, t)$ arises when a virtual particle goes on-shell due to the $i\epsilon$ term in the propagator denominators $p^2 + i\epsilon$. Branch cuts appear for s real such as $s > s_0$ with s_0 the threshold where a physical state can be produced. Due to analyticity we have the relations

$$\text{Re } \mathcal{A}(s + i\epsilon, t) = \text{Re } \mathcal{A}(s - i\epsilon, t), \quad (1.24)$$

$$\text{Im } \mathcal{A}(s + i\epsilon, t) = -\text{Im } \mathcal{A}(s - i\epsilon, t), \quad (1.25)$$

the discontinuity of the amplitude around the branch cut along the real axis reads

$$\text{Disc}_s \mathcal{A}(s, t) = \text{Lim}_{\epsilon \rightarrow 0} (\mathcal{A}(s + i\epsilon, t) - \mathcal{A}(s - i\epsilon, t)) = 2i \text{Im } \mathcal{A}(s + i\epsilon, t). \quad (1.26)$$

It can be shown that the discontinuity of the amplitude can be obtained by replacing in the propagators

$$\frac{1}{p^2 + i\epsilon} \rightarrow -2i\pi \delta(p^2 - m^2) \theta(p^0). \quad (1.27)$$

The $\theta(p^0)$ ensures that the particle has positive energy, i.e. is a physical particle. For any diagram the discontinuity can be directly obtained by following the so-called "Cutkosky rules" [24],

1. the diagrams must be cut in all possible ways such that the cut propagators can be put on shell simultaneously,
2. the cut propagators are replaced following eq. (1.27),
3. the discontinuity is given by the sum of all the cut diagrams.

We will use these rules in the following parts in order to get the imaginary part of the amplitudes by computing their discontinuities with the Cutkosky rules.

1.2 Scattering amplitudes in the Regge limit

In this section, we introduce the approximations to get the dominant contribution of the amplitudes in the perturbative Regge limit, using the fact that in this limit $s/|t|$ is very large. We first consider the quark-quark scattering amplitude with one gluon exchange in the t -channel to show the kinematics of the dominant contribution in powers of $1/s$. Then we compute the quark-quark amplitude of a color singlet exchange in t -channel involving a two gluon exchange in t -channel. This example is particularly relevant for hadronic processes in the perturbative Regge limit, as the color singlet exchange dominates the colorless states scattering. We finally show how the amplitude can be factorized into the so-called "impact factors" and the t -channel gluons Green function. Note that the approach presented in this section, is based on Feynman gauge calculations and the calculations beyond the Born order approximation would be different within another gauge. Of course, the final results for gauge invariant quantities are gauge independent.

1.2.1 The color octet exchange

At leading order the scattering of two quarks in QCD is given by the tree diagram shown in fig. 1.1, where a gluon carrying the color charge a is exchanged between the two quarks. We will assume that a hard scale justifies the use of pQCD for example $|t| \gg \Lambda_{QCD}^2$ and the fact that $s \gg |t|$.

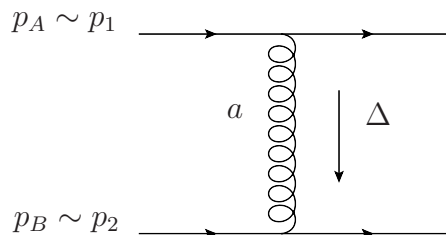


Figure 1.1: Quark-quark scattering amplitude at the tree level with an octet exchange in t -channel.

We denote respectively p_A and p_B the momenta of the upper quark and lower quark and m_A, m_B their masses. The Mandelstam variable $S_{AB} = (p_A + p_B)^2$ is large by assumption and

we can neglect the masses of the quarks and then assume that their momenta p_A and p_B are very close to two light-like vectors p_1 and p_2 of opposite directions such as $S_{AB} \sim s = 2p_1 \cdot p_2$, where s is the large scale. We can expand p_A and p_B on this Sudakov basis as,

$$\begin{aligned} p_A &= p_1 + \frac{m_A^2}{s} p_2, \quad p_B = p_2 + \frac{m_B^2}{s} p_1, \\ S_{AB} &= (p_A + p_B)^2 = m_B^2 + m_A^2 + 2p_A \cdot p_B \sim 2p_1 \cdot p_2 = s. \end{aligned}$$

The momentum of the gluon exchanged in t -channel can also be decomposed on this basis as,

$$\Delta = \alpha p_1 + \beta p_2 + k_\perp. \quad (1.28)$$

It is conventional to use a two-dimensional euclidean vector, that we underline (\underline{x}), to replace the Minkowskian transverse vector x_\perp , such as $x_\perp^2 = -\underline{x}^2$. We will use this convention all along the manuscript.

Assuming that the particles are on the mass-shell (we neglect now the masses of the quarks), one has the two following conditions,

$$(p_A - \Delta)^2 = 0 \quad (1.29)$$

$$(p_B + \Delta)^2 = 0 \quad (1.30)$$

which lead to

$$-(1 - \alpha)\beta + \frac{\Delta_\perp^2}{s} = 0, \quad (1.31)$$

$$(1 + \beta)\alpha + \frac{\Delta_\perp^2}{s} = 0. \quad (1.32)$$

Substituting in eq. (1.32) the expression of β by,

$$\beta = \frac{\Delta_\perp^2}{s(1 - \alpha)}, \quad (1.33)$$

leads to a second order equation in α ,

$$\alpha^2 - \alpha - \frac{\Delta_\perp^2}{s} = 0. \quad (1.34)$$

The two couples of solutions for α and β up to first order in $\frac{\Delta_\perp^2}{s}$ are,

$$\alpha = 1 + \frac{\Delta_\perp^2}{s}, \quad \beta = -1, \quad (1.35)$$

and

$$\alpha = -\frac{\Delta_\perp^2}{s}, \quad \beta = \frac{\Delta_\perp^2}{s}. \quad (1.36)$$

The first couple of solutions is not relevant as it would imply that $t = \Delta^2 \sim -s$, which violates our first assumption $s \gg -t$. The second couple of solution gives,

$$\Delta = -\frac{\Delta_\perp^2}{s} p_1 + \frac{\Delta_\perp^2}{s} p_2 + \Delta_\perp. \quad (1.37)$$

We get then that $t = \Delta^2 \sim \Delta_\perp^2 = -\underline{\Delta}^2$. Note that it justifies a posteriori that $\Delta_\perp^2/s \sim t/s$ can be neglected.

We will now introduce another approximation to simplify the vertex expression, called the eikonal approximation. The upper vertex gives the contribution,

$$ig\bar{u}_r(p_1 - \Delta)\gamma^\mu t_{ij}^a u_s(p_1), \quad (1.38)$$

where we put explicitly the spinor indices r, s , of the Dirac spinors. The spinor $\bar{u}_r(p_1 - \Delta)$ depends on the vector $p_1 - \Delta$ which is approximately equal to p_1 as $|\beta| \sim |\alpha| \sim |\Delta_\perp^2|/s \ll 1$. Thus, the upper vertex simplifies as,

$$ig\bar{u}_r(p_1)\gamma^\mu t_{ij}^a u_s(p_1) = 2igp_1^\mu \delta_{r,s} t_{ij}^a, \quad (1.39)$$

where we have used the Gordon identity,

$$\bar{u}_r(p')\gamma^\mu u_s(p) = \frac{1}{2m}\bar{u}_r(p')((p'^\mu + p^\mu) + i\sigma^{\mu\nu}(p' - p)_\nu)u_s(p), \quad (1.40)$$

with m the mass of the fermion and

$$\sigma^{\mu\nu} = \frac{i}{2}[\gamma^\mu, \gamma^\nu], \quad (1.41)$$

for $p' = p = p_1$, and the normalizations of the spinors $\bar{u}_r(p)u_s(p) = 2m\delta_{r,s}$. This approximation is known as the "eikonal approximation" and can be used as long as a soft gauge particle is exchanged. Finally, using for the lower vertex the same approximation one gets for the scattering amplitude,

$$\begin{aligned} i\mathcal{M} &= ig^2(2p_1^\mu)\frac{g_{\mu\nu}}{\Delta^2}(2p_2^\nu)\delta_{r_1,s_1}\delta_{r_2,s_2}t_{ij}^a t_{kl}^a \\ &= i8\pi\alpha_s \frac{s}{t}\delta_{r_1,s_1}\delta_{r_2,s_2}t_{ij}^a t_{kl}^a. \end{aligned} \quad (1.42)$$

Note that the upper and lower vertices are respectively proportional to p_1^μ and p_2^ν , thus if we decompose the metric tensor into the following tensor components

$$g_{\mu\nu} = \frac{2}{s}p_{2\mu}p_{1\nu} + \frac{2}{s}p_{1\mu}p_{2\nu} + g_{\mu\nu}^\perp, \quad (1.43)$$

only the component $\frac{2}{s}p_{2\mu}p_{1\nu}$ gives a non-vanishing contribution. As the metric tensor is coming from the sum over the polarizations of the propagator of the gluon, this component can be seen as the tensor product of the so-called "non-sense" polarizations,

$$\varepsilon_\mu^{\text{up}} = \sqrt{\frac{2}{s}}p_{2\mu}, \quad \varepsilon_\nu^{\text{down}} = \sqrt{\frac{2}{s}}p_{1\nu}, \quad (1.44)$$

such as $g_{\mu\nu}$ can be replaced due to the eikonal approximation by $\varepsilon_\mu^{\text{up}}\varepsilon_\nu^{\text{down}}$. Now the amplitude \mathcal{M} reads

$$i\mathcal{M} = \frac{-i}{\Delta^2}(ig)^2(\bar{u}_{\lambda'}(p_1)\not{\varepsilon}^{\text{up}}t_{ij}^a u_\lambda(p_1))(\bar{u}_{\lambda'}(p_2)\not{\varepsilon}^{\text{down}}t_{kl}^a u_\lambda(p_2)). \quad (1.45)$$

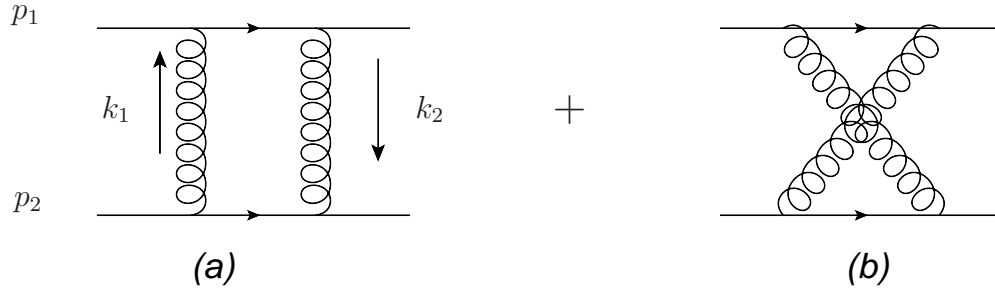


Figure 1.2: Diagrams of the singlet exchange at Born order.

1.2.2 The singlet color exchange in t -channel

In diffractive processes the quantum numbers exchanged in t -channel are those of the vacuum and consequently, we have to consider a singlet color exchange in t -channel. Let us consider the color singlet exchange on the quark-quark scattering amplitude.

A color singlet exchange in t -channel involves at least two gluons. At Born order, the scattering of two quarks is given by the two diagrams shown in fig. 1.2. These two diagrams are related by crossing symmetry. Let us define $\Delta = k_1 - k_2$ the momentum exchanged in t -channel. The diagram (b) can be obtained from diagram (a) results, up to the color factor that are different by

$$\mathcal{A}_{(b)}(s, t, u) = \mathcal{A}_{(a)}(u, t, s) \approx \mathcal{A}_{(a)}(-s, t, s), \quad (1.46)$$

where we use for the last equality, the fact that at large s and fixed t ,

$$s \approx -u.$$

The color factor for a singlet exchange of the diagrams (a) and (b) are equal and given by

$$(t^a t^b)_{ij} \frac{\delta_{ij}}{N} (t^a t^b)_{kl} \frac{\delta_{kl}}{N} = \frac{1}{N^2} \left(\frac{\delta^{ab}}{2} \right) \left(\frac{\delta^{ab}}{2} \right) = \frac{N^2 - 1}{4N^2}. \quad (1.47)$$

Let us compute the imaginary part of the diagram (a) by using the Cutkosky rules,

$$\mathcal{Im} \mathcal{A} = \frac{1}{2} \frac{N^2 - 1}{4N^2} \int d\Pi_2^{\text{Cut.}} \mathcal{A}^{\text{tree}}(k_1) \mathcal{A}^{\text{tree}\dagger}(-k_2 = \Delta - k_1). \quad (1.48)$$

In fig. 1.3 the cut of the fermionic line of diagram (a) is represented by the dashed line.

The color factors are put apart of the amplitude $\mathcal{A}^{\text{tree}}$. The expression of $\mathcal{A}^{\text{tree}}(k)$ is given by (1.42),

$$\mathcal{A}^{\text{tree}}(k) = -8\pi\alpha_s \frac{s}{\underline{k}^2}. \quad (1.49)$$

The integral measure $d\Pi_2^{\text{Cut.}}$ on the phase space is given by,

$$\begin{aligned} \int d\Pi_2^{\text{Cut.}} &= \int \frac{d^4 l_1}{(2\pi)^4} \frac{d^4 l_2}{(2\pi)^4} (2\pi)\delta(l_1^2) (2\pi)\delta(l_2^2) (2\pi)^4 \delta^{(4)}(p_1 + p_2 - l_1 - l_2) \\ &= \int \frac{d^4 k_1}{(2\pi)^4} d^4 l_2 (2\pi)\delta((p_1 + k_1)^2) (2\pi)\delta(l_2^2) \delta^{(4)}(p_2 - l_2 - k_1) \\ &= \int \frac{d^4 k_1}{(2\pi)^2} \delta((p_1 + k_1)^2) \delta((p_2 - k_1)^2), \end{aligned} \quad (1.50)$$

$$(1.51)$$

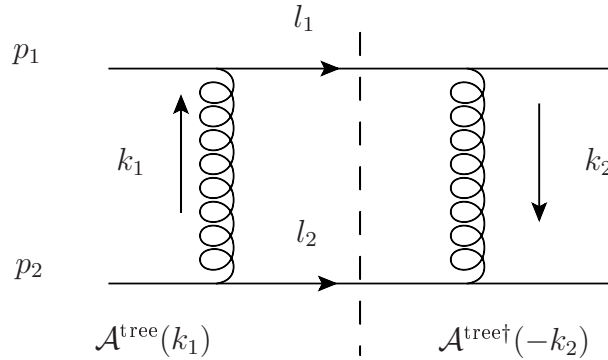


Figure 1.3: Cut of the diagram (a).

where in the second line we have shifted the momentum l_1 by the $k_1 = l_1 - p_1$. The mass shell conditions $l_1^2 = 0$ and $l_2^2 = 0$ being imposed by the Dirac factors. Using the Sudakov decomposition of the momentum k_1 ,

$$k_1 = \alpha_1 p_1 + \beta_1 p_2 + k_{1\perp}, \quad (1.52)$$

$d\Pi_2$ reads,

$$\int d\Pi_2^{\text{Cut.}} = \frac{s}{2} \int \frac{d\alpha_1 d\beta_1 d^2 k_{1\perp}}{(2\pi)^2} \delta(\beta s(1 + \alpha) - \underline{k}_1^2) \delta(-\alpha s(1 - \beta) - \underline{k}_1^2). \quad (1.53)$$

The factor $s/2$ comes from the Jacobian of the coordinate transformation from $k_1 = (k_1^0, \vec{k}_1)$ to $k_1 = (\alpha, \beta, k_{1\perp})$ with $p_1 \cdot p_2 = s/2$.

The imaginary part of the amplitude reads

$$\begin{aligned} \mathcal{Im} \mathcal{A}_{(a)} &= \frac{N^2 - 1}{4N^2} \frac{1}{2} \frac{s}{2} \int \frac{d\alpha_1 d\beta_1 d^2 k_{1\perp}}{(2\pi)^2} \delta(\beta s(1 + \alpha) - \underline{k}_1^2) \delta(-\alpha s(1 - \beta) - \underline{k}_1^2) \\ &\times (-8\pi\alpha_s s)^2 \frac{1}{\underline{k}_1^2 \underline{k}_2^2} \end{aligned} \quad (1.54)$$

$$= \frac{N^2 - 1}{4N^2} 16\pi^2 \alpha_s^2 s \int \frac{d^2 \underline{k}_1}{(2\pi)^2} \frac{1}{\underline{k}_1^2 \underline{k}_2^2}, \quad (1.55)$$

where $\underline{k}_2 = \underline{k}_1 - \underline{\Delta}$.

A full computation of the amplitude at one loop would lead to terms proportional to $\ln(s/t) = \ln(s/|t|) - i\pi$, where the imaginary contribution to the full amplitude arises from the factor $-i\pi$. Keeping this in mind, we see that we can get the real part of the amplitude by replacing $-i\pi \rightarrow \ln(s/|t|)$ in our result,

$$\mathcal{Re} \mathcal{A}_{(a)} = -\frac{N^2 - 1}{4N^2} 16\pi\alpha_s^2 \frac{s}{t} \ln\left(\frac{s}{|t|}\right) \int \frac{d^2 \underline{k}_1}{(2\pi)^2} \frac{-\Delta^2}{\underline{k}_1^2 (\underline{k}_1 - \Delta)^2}. \quad (1.56)$$

Using the crossing symmetry relation (1.46) the full amplitude at one loop of the diagram (b) is

$$\mathcal{A}_{(b)} = -\frac{N^2 - 1}{4N^2} 16\pi\alpha_s^2 \frac{-s}{t} \ln\left(\frac{-s}{t}\right) \int \frac{d^2 \underline{k}_1}{(2\pi)^2} \frac{-\Delta^2}{\underline{k}_1^2 (\underline{k}_1 - \Delta)^2}. \quad (1.57)$$

Note that there is no contribution to the imaginary part as $-s/t > 0$, which is consistent that the diagram b does not contribute to the discontinuity, it is only necessary for convergence in the s complex plane. The expression (1.57) is the opposite of the real part of the contribution of the diagram (a). Consequently the real parts of the two diagrams cancel and only the imaginary part of diagram (a) remains at the end,

$$\mathcal{A}_{(a)+(b)} = \mathcal{I}m \mathcal{A}_{(a)} . \quad (1.58)$$

Note that this cancellation is due to the fact that the color factors are the same for the diagrams (a) and (b), as we are interesting here in a color singlet exchange. It is not the case for a color octet exchange where the real parts are not canceling each other.

1.2.3 Impact factor representation of the quark-quark scattering amplitude

We will introduce here the k_T -factorization scheme [25, 26, 27, 28, 29, 30, 31] which is valid in the perturbative Regge limit where the amplitude is factorized into an upper and a lower so-called impact factors that exchange at Born level two t -channel gluons in a singlet color state.

Let us show on the particular example of the scattering of two quarks in the forward limit $\Delta = 0$, $k_1 = k$ and $k_2 = k$, the procedure of k_T -factorization.

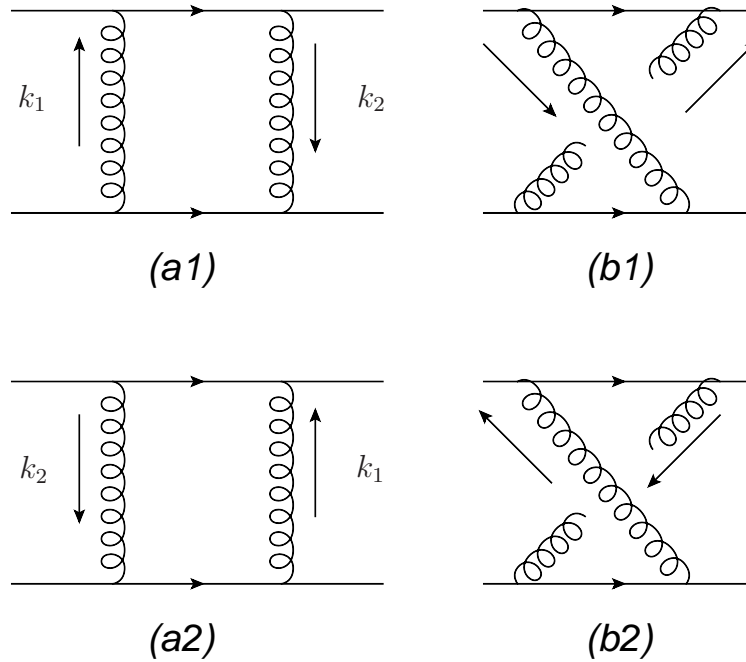


Figure 1.4: Diagrams of the singlet exchange.

In fig. 1.4 are shown four diagrams which when they are summed corresponds to twice the amplitude at the Born level of the singlet exchange, $\mathcal{A} = \frac{1}{2}(\mathcal{A}_{(a1)} + \mathcal{A}_{(b1)} + \mathcal{A}_{(a2)} + \mathcal{A}_{(b2)})$. The factor $1/2$ prevent from overcounting the diagram contributions due to the loop-integration

where we integrate over all configurations of the momenta k_1, k_2 . The amplitude of the diagram (a1), putting apart the color factor $\frac{N^2-1}{4N^2}$ reads

$$\begin{aligned} i\mathcal{A}_{(a1)} &= \frac{s}{2} \int \frac{d\alpha d\beta d^2\mathbf{k}}{(2\pi)^4} \left(\bar{u}(p_1) i g \gamma^\mu \frac{i(\not{p}_1 + \not{k})}{(p_1 + k)^2 + i\epsilon} i g \gamma^\nu u(p_1) \right)_{\text{up}} \\ &\times \left(\bar{u}(p_2) i g \gamma^\alpha \frac{i(\not{p}_2 - \not{k})}{(p_2 - k)^2 + i\epsilon} i g \gamma^\beta u(p_2) \right)_{\text{down}} \frac{-i g_{\mu\alpha}}{k^2 + i\epsilon} \frac{-i g_{\nu\beta}}{k^2 + i\epsilon}, \end{aligned} \quad (1.59)$$

where "up" and "down" subscripts identify the upper and lower parts of the diagram (a1) fig. 1.2. Now using the eikonal approximation, we can replace

$$g_{\mu\nu} \rightarrow \frac{2}{s} p_{2\mu}^{\text{up}} p_{1\nu}^{\text{down}}, \quad (1.60)$$

and we can approximate $k = \alpha p_1 + \beta p_2 + k_\perp$ by

$$k^{\text{up}} = \beta p_2 + k_\perp, \quad k^{\text{down}} = \alpha p_1 + k_\perp, \quad (1.61)$$

as the p_1 (resp. p_2) component is negligible compared to one in the upper (resp. lower) part of the diagram. We also approximate $k^2 = -\underline{k}^2$. After these simplifications we get,

$$\begin{aligned} i\mathcal{A}_{(a1)} &= \frac{s}{2} \int \frac{d\alpha d\beta d^2\mathbf{k}}{(2\pi)^4} \left(\frac{2i(ig)^2}{s} \bar{u}(p_1) \frac{\not{p}_2 \not{p}_1 \not{p}_2}{\beta s - \underline{k}^2 + i\epsilon} u(p_1) \right)_{\text{up}} \\ &\times \left(\frac{2i(ig)^2}{s} \bar{u}(p_2) \frac{\not{p}_1 \not{p}_2 \not{p}_1}{-\alpha s - \underline{k}^2 + i\epsilon} u(p_2) \right)_{\text{down}} \frac{i}{\underline{k}^2} \frac{i}{\underline{k}^2}. \end{aligned} \quad (1.62)$$

Using the Clifford algebra of the Dirac matrix $\{\gamma^\mu, \gamma^\nu\} = 2g^{\mu\nu}$, and the fact that p_1 and p_2 are light-cone vectors we have

$$\bar{u}(p_1) \not{p}_2 \not{p}_1 \not{p}_2 u(p_1) = s \bar{u}(p_1) \not{p}_2 u(p_1) = s^2, \quad (1.63)$$

where we have for the last equality used the Gordon identity and the normalization of the spinors. The amplitude reads now,

$$\begin{aligned} i\mathcal{A}_{(a1)} &= \frac{s}{2} \int \frac{d^2\mathbf{k}}{(2\pi)^2} \frac{-1}{(\underline{k}^2)^2} \\ &\times \left(2i(ig)^2 \int \frac{d\beta}{2\pi} \frac{1}{\beta - \frac{\underline{k}^2}{s} + i\epsilon} \right)_{\text{up}} \\ &\times \left(2i(ig)^2 \int \frac{d\alpha}{2\pi} \frac{1}{-\alpha - \frac{\underline{k}^2}{s} + i\epsilon} \right)_{\text{down}}. \end{aligned} \quad (1.64)$$

Let us rewrite this result as

$$i\mathcal{A}_{(a1)} = \frac{s}{2} \int \frac{d^2\mathbf{k}}{(2\pi)^2} \frac{-1}{(\underline{k}^2)^2} \left(\int \frac{d\beta}{2\pi} \phi(\beta, \underline{k}) \right)_{\text{up}} \left(\int \frac{d\alpha}{2\pi} \phi(-\alpha, -\underline{k}) \right)_{\text{down}}, \quad (1.65)$$

with

$$\phi(x, \underline{\ell}) = \frac{2i(ig)^2}{x - \frac{\underline{\ell}^2}{s} + i\epsilon}. \quad (1.66)$$

The contributions of the diagrams (b1), (a2) and (b2), are obtained by changing the signs of k in the propagators leading to

$$i\mathcal{A}_{(b1)} = \frac{s}{2} \int \frac{d^2 \underline{k}}{(2\pi)^2} \frac{-1}{(\underline{k}^2)^2} \left(\int \frac{d\beta}{2\pi} \phi(-\beta, -\underline{k}) \right)_{\text{up}} \left(\int \frac{d\alpha}{2\pi} \phi(-\alpha, -\underline{k}) \right)_{\text{down}}, \quad (1.67)$$

$$i\mathcal{A}_{(a2)} = \frac{s}{2} \int \frac{d^2 \underline{k}}{(2\pi)^2} \frac{-1}{(\underline{k}^2)^2} \left(\int \frac{d\beta}{2\pi} \phi(-\beta, -\underline{k}) \right)_{\text{up}} \left(\int \frac{d\alpha}{2\pi} \phi(\alpha, \underline{k}) \right)_{\text{down}}, \quad (1.68)$$

$$i\mathcal{A}_{(b2)} = \frac{s}{2} \int \frac{d^2 \underline{k}}{(2\pi)^2} \frac{-1}{(\underline{k}^2)^2} \left(\int \frac{d\beta}{2\pi} \phi(\beta, \underline{k}) \right)_{\text{up}} \left(\int \frac{d\alpha}{2\pi} \phi(\alpha, \underline{k}) \right)_{\text{down}}. \quad (1.69)$$

The total contribution reads

$$\begin{aligned} i\mathcal{A} &= \frac{s}{2} \int \frac{d^2 \underline{k}}{(2\pi)^2} \frac{-1}{(\underline{k}^2)^2} \times 2 \\ &\times \frac{1}{2} \left(\int \frac{d\beta}{2\pi} (\phi(\beta, \underline{k}) + \phi(-\beta, -\underline{k})) \right)_{\text{up}} \\ &\times \frac{1}{2} \left(\int \frac{d\alpha}{2\pi} (\phi(\alpha, \underline{k}) + \phi(-\alpha, -\underline{k})) \right)_{\text{down}}, \end{aligned} \quad (1.70)$$

where the factor $\frac{1}{2}$ are symmetrically inserted in front of the upper and lower parts of the process. As we know that $i\mathcal{A} = \frac{1}{2}(\mathcal{A}_{(a1)} + \mathcal{A}_{(a2)} + \mathcal{A}_{(b1)} + \mathcal{A}_{(b2)})$ because of the fact we have considered twice more diagrams than it was necessary, we have a global factor $(\frac{1}{2})_{\text{up}} \times (\frac{1}{2})_{\text{down}} \times 2 = \frac{1}{2}$ where the extra factor 2 has been put in the t -channel gluon propagator part of the amplitude. This factor 2 is coming from the fact that there are two possibilities to combine the indices of the $g_{\mu\alpha}g_{\nu\beta}$ of the propagator and $g_{\mu\beta}g_{\nu\alpha}$, in other words this factor is absorbed in the 4-point green function of the t -channel gluons. As we took care of keeping the coefficient that belong respectively to the upper and lower part of the process, we see that eq. (1.70) can be represented as in fig. 1.5.

Looking at the integrands of eq. (1.70) is also now clear that the integrals over β and α converge,

$$\phi_{\text{up}}^{(a1)}(\beta, \underline{k}) + \phi_{\text{up}}^{(a1)}(-\beta, -\underline{k}) \sim \frac{1}{\beta^2}. \quad (1.71)$$

The contributions of all the diagrams are necessary to prove the convergence of the integrals over β .

We choose to integrate over the contour \mathcal{C}^- in the β - and α - complex planes shown in fig. 1.6, the integral

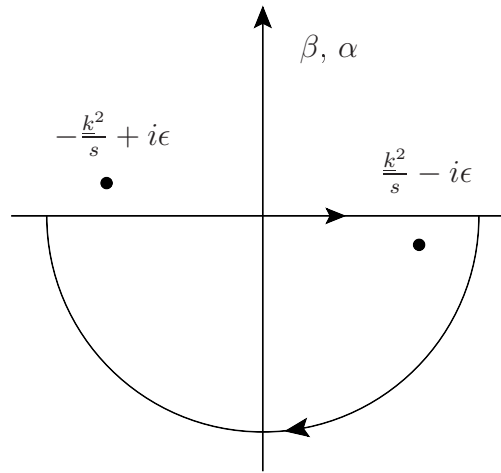
$$\begin{aligned} &\frac{1}{2} \left(\int_{\mathcal{C}^-} \frac{d\beta}{2\pi} (\phi(\beta, \underline{k}) + \phi(-\beta, -\underline{k})) \right) \frac{1}{2} \left(\int_{\mathcal{C}^-} \frac{d\alpha}{2\pi} (\phi(\alpha, \underline{k}) + \phi(-\alpha, -\underline{k})) \right) \\ &= \frac{1}{4} \int_{\mathcal{C}^-} \frac{d\beta}{2\pi} \phi(\beta, \underline{k}) \int_{\mathcal{C}^-} \frac{d\alpha}{2\pi} \phi(\alpha, \underline{k}) = \frac{1}{4} (2i(ig)^2)^2 (-i)(-i) = (4\pi\alpha_s)^2. \end{aligned} \quad (1.72)$$

After restoring the color factor, we get the same result than in the direct computation with the Cutkosky rules eq. (1.54)

$$\mathcal{Im} \mathcal{A} = \frac{N^2 - 1}{4N^2} 16\pi^2 \alpha_s^2 s \int \frac{d^2 \underline{k}_1}{(2\pi)^2} \frac{1}{(\underline{k}^2)^2}. \quad (1.73)$$

$$\begin{aligned}
& \frac{1}{2} \left(\begin{array}{c} \text{diagram 1} \\ \text{diagram 2} \end{array} + \begin{array}{c} \text{diagram 3} \\ \text{diagram 4} \end{array} \right)_{\text{up}} \\
& \times \left(\begin{array}{c} \text{diagram 5} \\ \text{diagram 6} \end{array} + \begin{array}{c} \text{diagram 7} \\ \text{diagram 8} \end{array} \right) \\
& \frac{1}{2} \left(\begin{array}{c} \text{diagram 9} \\ \text{diagram 10} \end{array} + \begin{array}{c} \text{diagram 11} \\ \text{diagram 12} \end{array} \right)_{\text{down}}
\end{aligned}$$

Figure 1.5: Decomposition of the total amplitude and combinatorial factors.

Figure 1.6: β - or α - complex planes, the poles of the $\phi(\pm\alpha, \pm\vec{k})$ function and the contour \mathcal{C}^- of integration.

Going back to eq. (1.70) we see that the amplitude reads

$$\mathcal{A} = \frac{is}{2} \int \frac{d^2 \underline{k}}{(2\pi)^2} \frac{2}{(\underline{k}^2)^2} \Phi_{\text{up}}^{ab}(\underline{k}) \Phi_{\text{down}}^{ab}(\underline{k}), \quad (1.74)$$

$$= is \int \frac{d^2 \underline{k}}{(2\pi)^2} \frac{1}{(\underline{k}^2)^2} \Phi_{\text{up}}^{ab}(\underline{k}) \Phi_{\text{down}}^{ab}(\underline{k}), \quad (1.75)$$

with,

$$\Phi_{\text{up}}^{ab}(\underline{k}) = \frac{\delta^{ab}}{2N} \frac{1}{2} \int \frac{d\beta}{2\pi} (\phi(\beta, \underline{k}) + \phi(-\beta, -\underline{k})) \quad (1.76)$$

$$= \frac{1}{2} \int \frac{d\beta}{2\pi} \varepsilon_{\mu}^{\text{NS}} \varepsilon_{\nu}^{\text{NS}} \mathcal{S}_{q(p_1)g(k_1,a) \rightarrow q(p_1)g(k_2,b)}^{\mu\nu}(\beta, \underline{k}), \quad (1.77)$$

the so-called *impact factor* for the upper part of the process, where $\mathcal{S}_{q(p_1)g(k_1,a) \rightarrow q(p_1)g(k_2,b)}^{\mu\nu}(\beta, \underline{k})$ is the \mathcal{S} -matrix element of the upper sub-process where the quark couples with gluons with "non-sense" polarizations ε^{NS} as defined in eq. (1.44) due to eikonal approximation.

Note that other conventions exist, for example in ref. [22], the impact factor is defined as $\Phi^{[22]} = 2\pi \Phi^{\text{Here}}$ and the amplitude reads

$$\mathcal{A}^{[22]} = is \int \frac{d^2 \underline{k}}{(2\pi)^4} \frac{\Phi^{[22]} \Phi^{[22]}}{(\underline{k}^2)^2},$$

or in ref. [32], $\Phi^{[32]} = 2\sqrt{\pi} \Phi^{\text{Here}}$ and the amplitude reads

$$\mathcal{A}^{[32]} = \frac{is}{2} \int \frac{d^2 \underline{k}}{(2\pi)^3} \frac{\Phi^{[32]} \Phi^{[32]}}{(\underline{k}^2)^2}.$$

Depending on the conventions, the color factor $\frac{\delta^{ab}}{2N}$ is included in the impact factor definition such as the color factor $\frac{N^2-1}{4N^2} = \left(\frac{\delta^{ab}}{2N}\right)_{\text{up}} \left(\frac{\delta^{ab}}{2N}\right)_{\text{down}}$ is recovered in the final amplitude.

Note that in the case of two quark scattering amplitude, the impact factors are constant and equal to $4\pi\alpha_s$. As a consequence the integral over \underline{k} is infra-red divergent. We will see that in the case where colorless particles are involved in the initial and final states of the impact factor, the gauge invariance forces the impact factor to cancel, preventing thus the infra-red divergence of the \underline{k} integral.

1.2.4 The k_T factorization scheme

We present how the k_T -factorization procedure is generalized for colorless states. Let us consider a more general process where two colorless probes scatter with an exchange of a pomeron in t -channel,

$$A(p_1) + B(p_2) \rightarrow A'(p_1 + \Delta) + B'(p_2 - \Delta).$$

Due to the fact that we are in the high energy limit there will be a large rapidity gap between A' and B' . The dominant contribution in powers of s to the amplitude is given by an exchange

of gluons in t -channel. Indeed the power behavior in s of the amplitude at high energy for N particles exchanged in t -channel depends on the spins σ_i of these particles,

$$\mathcal{A} \propto s^{\sum_i \sigma_i - N + 1}, \quad (1.78)$$

thus the leading contributions in powers of s involves only gluons. As a general principle, in the limit $s \rightarrow \infty$ the eikonal approximation for gluons leads to the finite terms that does not decrease as power of s .

One can replace the numerators of the gluon propagators by the non-sense polarizations thanks to the eikonal approximation in the upper and lower blob vertices. Then one can safely neglect the component of the gluon momenta along the dominant like-cone direction of the upper or lower blob compared to the component of the momenta of the particles of the blobs. The amplitude factorizes then as illustrated in fig. 1.7 where Φ_a^{up} and Φ_b^{up} are the s - and u -contributions to the sub-processes $A + g \rightarrow A' + g$. The 4-point Green function of the gluons G contains the energy dependence and as we define the impact factors as the sum of the s - and u - channel, we need to put a factor $1/2$ in the definition of the impact factor to avoid double counting when joining the gluonic lines as it was illustrated on the quark-quark scattering. One should not forget also the factor 2 coming from the Jacobian $s/2$ in the integral measure.

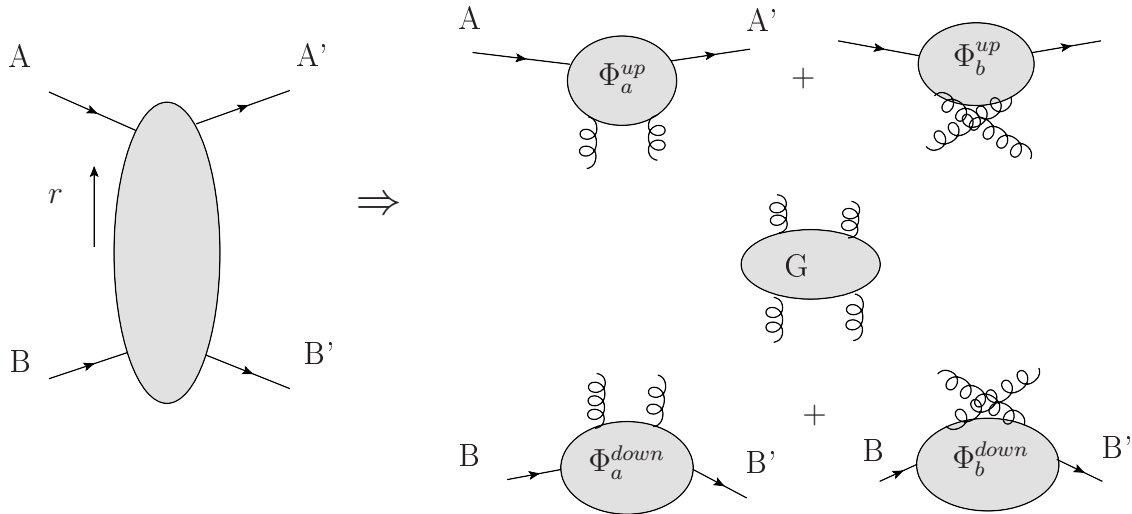


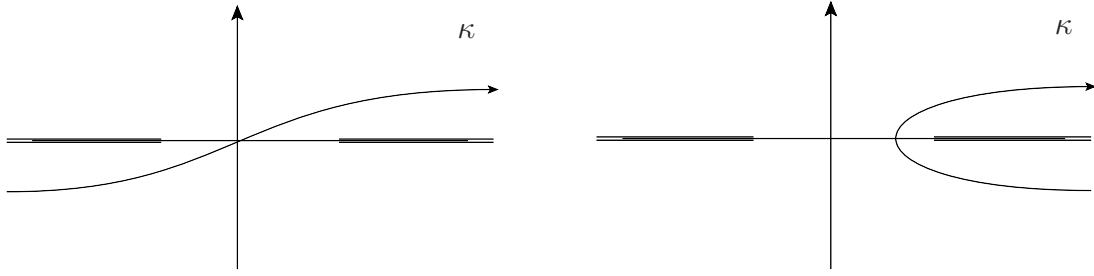
Figure 1.7: k_T -factorization of the process $A + B \rightarrow A' + B'$. The upper and lower impact factors are the sum of the s - and u -contributions $\Phi^{up(down)} = \frac{1}{2}(\Phi_a^{up(down)} + \Phi_b^{up(down)})$.

The 4-point Green function of the gluons at Born level G reads

$$\frac{2}{\underline{k}^2(\underline{k} - \underline{\Delta})^2},$$

where the factor 2 is due to the fact that there are two combinations to link the upper gluons to the lower ones as illustrated in fig. 1.5 and the amplitude reads

$$\mathcal{A} = i s \int \frac{d^2 \underline{k}}{(2\pi)^2} \frac{1}{\underline{k}^2(\underline{k} - \underline{\Delta})^2} \Phi_{up}^{ab}(\underline{k}, \underline{k} - \underline{\Delta}) \Phi_{down}^{ab}(\underline{k}, \underline{k} - \underline{\Delta}), \quad (1.79)$$

Figure 1.8: Deformation of the contour in the κ complex plane.

with

$$\Phi_{\text{up}}^{ab}(\underline{k}) = \frac{1}{2} \int \frac{d\beta}{2\pi} \varepsilon_{\mu}^{\text{NS}} \varepsilon_{\nu}^{\text{NS}} \mathcal{S}_{A g \rightarrow A' g}^{\mu\nu, ab}(\beta, \underline{k}). \quad (1.80)$$

Defining the s -channel Mandelstam variable κ of the system $A(p_A) + g(k_1)$, such as,

$$\kappa = (p_A + k_1)^2 \equiv \beta s + p_A^2 + k_1^2,$$

we can replace the integral over β by an integral over κ ,

$$\Phi_{\text{up}}^{ab}(\underline{k}) = \frac{1}{2s} \int \frac{d\kappa}{2\pi} \varepsilon_{\mu}^{\text{NS}} \varepsilon_{\nu}^{\text{NS}} \mathcal{S}_{A g \rightarrow A' g}^{\mu\nu, ab}(\kappa, \underline{k}). \quad (1.81)$$

The impact factor is then defined as the integral along the contour illustrated in fig. 1.8. This contour can be closed on the discontinuity of the right cut along the real axis, leading to the final expression

$$\Phi_{\text{up}}^{ab}(\underline{k}) = \frac{1}{2s} \int \frac{d\kappa}{2\pi} \varepsilon_{\mu}^{\text{NS}} \varepsilon_{\nu}^{\text{NS}} \mathcal{D}_{\text{isc}\kappa} \mathcal{S}_{A g \rightarrow A' g}^{\mu\nu, ab}(\kappa, \underline{k}). \quad (1.82)$$

The energy dependence of the gluon Green function can be worked out at the leading $\log(1/x)$ (LLx) accuracy by resumming the amplitude in the relevant parameter $\alpha_s \ln(s)$ as the large logarithm of s can compensate the small value of α_s . The large $\ln(s)$ are given at LLx in the multi-Regge kinematic where, considering A and B flying respectively almost along the light-cone vectors p_1 and p_2 , a ladder of gluons with momenta

$$k_i = \alpha_i p_1 + \beta_i p_2 + k_{\perp i},$$

is exchanged in t -channel with the following strong ordering,

$$\begin{aligned} 1 &\gg \alpha_1 \gg \alpha_i \gg \alpha_n, \\ \beta_1 &\ll \beta_i \ll \beta_n \ll 1, \\ k_{\perp 1}^2 &\sim k_{\perp i}^2 \sim s \alpha_i \beta_i. \end{aligned} \quad (1.83)$$

In this kinematic, the ladder of gluons can be resummed in two "reggeized" gluons which exchange usual gluons coupling with an effective vertex called Lipatov vertex [33]. Using

Mellin transformation to decouple the gluon ladder from the impact factors the amplitude reads

$$\begin{aligned} \mathcal{A}(s, t) = & \frac{is}{(2\pi)^2} \int \frac{d^2 \underline{k}}{\underline{k}^2} \Phi_1^{ab}(\underline{k}, \underline{\Delta} - \underline{k}) \int \frac{d^2 \underline{k}'}{\underline{k}'^2} \Phi_2^{ab}(-\underline{k}', -\underline{\Delta} + \underline{k}') \\ & \int_{\delta-i\infty}^{\delta+i\infty} \frac{d\omega}{2\pi i} \left(\frac{s}{s_0} \right)^\omega G_\omega(\underline{k}, \underline{k}', \underline{\Delta}), \end{aligned} \quad (1.84)$$

with the Mellin transform of the Green function $G_\omega(\underline{k}, \underline{k}', \underline{\Delta})$ is governed by the Balitsky, Fadin, Kuraev and Lipatov (BFKL) equation [34, 35, 36, 37] at LLx. The BFKL equation in terms of the rapidity $Y = \ln(1/x)$ reads

$$\frac{\partial}{\partial Y} \mathcal{F}(Y, \underline{k}') = \frac{\alpha_s N_c}{2\pi} \int d^2 \underline{k} K(\underline{k}', \underline{k}) \mathcal{F}(Y, \underline{k}) \quad (1.85)$$

with $\mathcal{F}(Y, \underline{k}, \underline{\Delta})$ the unintegrated gluon density which contains the 4-point gluon Green function Y -dependence and $K(\underline{k}', \underline{k})$ the BFKL kernel. The BFKL solution [38, 33] is of the form

$$\mathcal{F}(Y, \underline{k}) \sim (1/x)^{\frac{4N_c \alpha_s}{\pi} \ln(2)} \sim s^{\omega_0}. \quad (1.86)$$

This solution exhibits a value for the pomeron intercept of $\alpha_P = 1 + \omega_0 = 1 + \frac{4N_c \alpha_s}{\pi} \ln(2)$ which is slightly above one, leading to the violation of the Froissart bound as it was already expected from the Donnachie and Landshoff fits. We will see in section 1.3.4 some of the models proposed to solve this problem of unitarity violation.

Note that the impact factors do not depend on s and the whole s -dependence is included in the Green function of the gluons. This remark agrees with the discussion in part 1.1.2 on the universality of the t -channel reggeon exchange which contains the s -dependence of the amplitudes.

The QCD gauge invariance and the fact that the probes are colorless, require the cancellation of the impact factors in the limits $k_\perp \rightarrow 0$ or $(k_\perp - \Delta_\perp) \rightarrow 0$. Indeed this is due to the QCD Ward identities, assuming that the t -channel gluons are on-shell (which is the case in the limit $k_\perp^2 \approx k^2 \rightarrow 0$),

$$S_{\mu\nu}^{\gamma^* g \rightarrow \gamma^* g} k^\mu = S_{\mu\nu}^{\gamma^* g \rightarrow \gamma^* g} (\Delta - k)^\nu = 0. \quad (1.87)$$

eq. (1.87) implies that the impact factor proportional to

$$S_{\mu\nu}^{\gamma^* g \rightarrow \gamma^* g} \varepsilon^{\text{NS}\mu} \varepsilon^{\text{NS}\nu} = \frac{2}{s} S_{\mu\nu}^{\gamma^* g \rightarrow \gamma^* g} p_2^\mu p_2^\nu = -\frac{2}{s} S_{\mu\nu}^{\gamma^* g \rightarrow \gamma^* g} k_\perp^\mu (k_\perp - \Delta_\perp)^\nu,$$

vanishes when $k_\perp \rightarrow 0$ or $k_\perp - \Delta_\perp \rightarrow 0$. The fact that the probes are colorless is essential for the QCD Ward identity used here. For example, in the quark-quark scattering, we saw that the amplitude are not infra-red safe because they do not cancel when $k_\perp \rightarrow 0$, but the quarks are not colorless probes. Another way to see this gauge invariance requirement is that a colorless probe interacts with the t -channel gluons through a partonic system. For k_\perp of the order of the transverse size of the partonic system, the gluon can resolve the color

charges of the partons. When k_\perp vanishes, the transverse size resolved by the gluon becomes larger than the transverse size \underline{r} of the system and the color charges of the partons are then screening each other. As the probe is colorless, the whole partonic system is colorless and the coupling of the gluon to this system is then vanishing as the effective color charge resolved by the gluon vanishes, as illustrated in fig. 1.9.

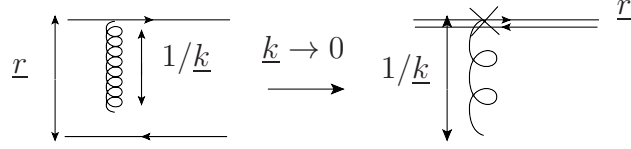


Figure 1.9: In the limit $\underline{k} \rightarrow 0$, the gluon cannot resolve anymore the colored quark as its color charge is shadowed by the color charge of the antiquark.

1.3 Deep inelastic scattering amplitude in the perturbative Regge kinematics

1.3.1 Introduction to DIS observables

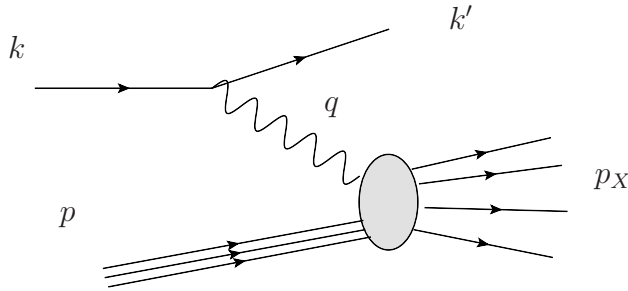


Figure 1.10: Deep inelastic scattering process $e^-(k) + p(p) \rightarrow e^-(k') + X(p_X)$ summed over all final states X .

We denote p , q and k the respective momenta of the proton, the virtual photon and the electron. The virtuality Q of the photon is defined as $q^2 = -Q^2$. Let us denote,

- $S = (k + p)^2$ the squared center of mass energy of the ep system,
- $W = (q + p)^2$ the squared center of mass energy of the γ^*p system,
- $x = \frac{Q^2}{2p \cdot q} = \frac{Q^2}{2\nu}$ with $\nu = p \cdot q$, the Bjorken variable of the process, which in the parton model is the fraction of proton momentum carried by the interacting parton and ν/M_p the virtual photon energy in the proton rest frame.
- $y = \frac{p \cdot q}{p \cdot k}$ the fraction of the electron energy transferred to the virtual photon in the proton rest frame.

In the high energy limit, (for a pedagogical book on high energy QCD see Ref. [39]), $s \gg Q^2 \gg (M_p^2, \Lambda_{QCD}^2)$ with Λ_{QCD} the QCD scale and M_p the mass of the proton, the variables x and y can be approximated by $x \approx \frac{Q^2}{W^2}$ and $y \approx \frac{Q^2}{xs}$. The differential cross-section reads

$$E' \frac{d\sigma^{e^-p}}{d^3k'} = \frac{e^2}{8\pi^2(s - M_p^2)q^4} L^{\mu\nu} W_{\mu\nu}, \quad (1.88)$$

with E' and k' the energy and the momentum of the scattered electron, $L_{\mu\nu}$ the leptonic part of the process associated to the leptonic current and $W_{\mu\nu}$ the hadronic tensor associated with the interaction between the probe (the virtual photon) and the hadron. Neglecting the mass of the electron

$$L^{\mu\nu} = 2(k^\mu k'^\nu + k^\nu k'^\mu - g^{\mu\nu} k \cdot k'). \quad (1.89)$$

The tensor $W_{\mu\nu}$ reads

$$\begin{aligned} 4\pi W_{\mu\nu} &= \sum_X \int d\Pi_X (2\pi)^4 \delta(p + q - p_X) \\ &\times \langle \langle p(p) | J_\nu^\dagger(0) | X(p_X) \rangle \langle X(p_X) | J_\mu(0) | p(p) \rangle \rangle_{spin} \\ &= \int d^4y e^{iq \cdot y} \langle \langle p(p) | J_\nu^\dagger(y) J_\mu(0) | p(p) \rangle \rangle_{spin} \end{aligned} \quad (1.90)$$

from the first line to the second we used first a translation of the matrix element

$$\langle p(p) | e^{-i\hat{P} \cdot y} e^{i\hat{P} \cdot y} J_\nu^\dagger(0) e^{-i\hat{P} \cdot y} e^{i\hat{P} \cdot y} | X(p_X) \rangle = e^{iy \cdot (p_X - p)} \langle p(p) | J_\nu^\dagger(y) | X(p_X) \rangle,$$

and then the completeness relation

$$\sum_X \int d\Pi_X |X(p_X)\rangle \langle X(p_X)| = 1.$$

Due to the optical theorem, the tensor $W_{\mu\nu}$ is related to the imaginary part of the forward Compton scattering amplitude $T_{\mu\nu}$ ($W_{\mu\nu} = 2\mathcal{I}m T_{\mu\nu}$) illustrated in fig. 1.11,

$$4\pi T_{\mu\nu} = i \int d^4y e^{iy \cdot q} \langle \langle p(p) | T \{ J_\nu^\dagger(y) J_\mu(0) \} | p(p) \rangle \rangle_{spin}. \quad (1.91)$$

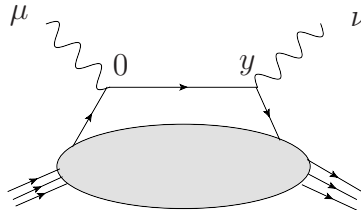


Figure 1.11: Forward Compton scattering amplitude.

The hadronic tensor cannot be computed perturbatively and have to be modeled by parameterizing it on the relevant Lorentz structures. Using the transformations under parity

and time reversal of the correlator and the gauge invariance conditions $q^\mu W_{\mu\nu} = q^\nu W_{\mu\nu} = 0$, the hadronic tensor $W_{\mu\nu}$ can be parameterized by two independent structure functions F_1 and F_2 such as,

$$W_{\mu\nu} = -(g_{\mu\nu} - \frac{q_\mu q_\nu}{q^2}) F_1(x, Q^2) + \frac{1}{\nu} (p_\mu - q_\mu \frac{p \cdot q}{q^2}) (p_\nu - q_\nu \frac{p \cdot q}{q^2}) F_2(x, Q^2). \quad (1.92)$$

Putting all together one finds for the differential cross-section of the DIS of the proton and the electron in the proton rest frame,

$$\frac{d\sigma_{tot}^{ep}}{dE'd\Omega} = \frac{\alpha^2}{4M_p E^2 \sin^4(\theta/2)} \left(2F_1 \sin^2(\theta/2) + \frac{M_p^2}{\nu} F_2 \cos^2(\theta/2) \right), \quad (1.93)$$

with Ω and θ the solid angle and the azimuthal angle of the scattered electron and $\alpha = e^2/4\pi$ the fine structure constant.

The parton model

In the so-called naive parton model proposed by Feynman and Bjorken [2, 40, 1], the proton is assumed to be constituted of point-like fermionic particles called partons. Comparing the result (1.93) with the differential cross-section of a spin 1/2 point-like particle, for example $e^- \mu^-$ cross-section,

$$\frac{d\sigma^{e^- \mu^-}}{dE'd\Omega} = \frac{\alpha^2 \delta(1-x)}{4m_\mu E^2 \sin^4(\theta/2)} \left(\sin^2(\theta/2) + \frac{m_\mu^2}{\nu} \cos^2(\theta/2) \right), \quad (1.94)$$

and assuming that a parton of mass m_f and momentum $p_f = x_f p$ interacts with the photon, leads to

$$2F_1 = \frac{M_p}{m_f} \delta(1-z_f) = \frac{M_p}{m_f} \delta(1-x/x_f)$$

and

$$F_2 = \frac{m_f}{M_p x_f} \delta(1-z_f) = \frac{m_f}{M_p x_f} \delta(1-x/x_f) = x_f \frac{M_p}{m_f} \delta(1-x/x_f) = 2x_f F_1,$$

with $z_f = Q^2/2q \cdot p_f = x/x_f$. Note that ν is replaced in (1.94) by $\nu_f = q \cdot p_f = x_f \nu$ and in the proton rest frame $\nu_f/\nu = m_f/M_p$. It implies that the structure functions are independent of Q^2 which could explain in the early experimental analysis at SLAC the fact that the measure of F_2 depends very weakly on Q^2 known as the Bjorken scaling. In the parton model, the hadronic tensor $W_{\mu\nu}$ is written as,

$$W_{\mu\nu} = \sum_f \int \frac{dx_f}{x_f} f_f(x_f) W_{\mu\nu}^f, \quad (1.95)$$

with f_f the parton distribution function and $W_{\mu\nu}^f$ the "partonic tensor",

$$\begin{aligned} 4\pi W_{\mu\nu}^f &= \int d^4p' 2\pi \delta(p'^2) (2\pi)^4 \delta(x_f p + q - p') \langle \langle x_f p | J_\nu^\dagger(y) J_\mu(0) | x_f p \rangle \rangle_{spin} \\ &= 2\pi x_f \delta(x_f - x) e_f^2 \left(-(g_{\mu\nu} - \frac{q_\mu q_\nu}{q^2}) + \frac{2x_f}{\nu} (p_\mu - q_\mu \frac{p \cdot q}{q^2}) (p_\nu - q_\nu \frac{p \cdot q}{q^2}) \right). \end{aligned} \quad (1.96)$$

This leads to the expressions

$$F_1 = \frac{1}{2} \sum_f e_f^2 f_f(x) \text{ and } F_2 = 2xF_1(x), \quad (1.97)$$

the second equality in (1.97) is known as the Callan-Gross relation [41], and could explain why the data for the longitudinal structure function defined as $F_L(x) = F_2(x) - 2xF_1(x)$ were small compared to the data of F_2 . Despite of these predictions, the main problem of the naive parton model is that it assumes that the partons are free inside the nucleon while they should be in the same time strongly interacting with each other to maintain themselves in the hadron bound state. This is of course explain by the asymptotic freedom in QCD, i.e. the coupling of the partons becomes weak at high energy scales $Q^2 \gg \Lambda_{QCD}^2$.

The parton picture in QCD

A hadron in the point of view of QCD contains fluctuations of partonic fields of space and time scale smaller than its hadronic size. The probe (virtual photon) can resolve the fluctuations in the hadrons that have typically larger sizes than the size of the probe and all smaller fluctuations only participate in the renormalization of the masses and the coupling constants. In the infinite momentum frame where the proton has the speed of light, the Lorentz dilatation of time scales implies that the fluctuations have a long life time compared to the time scale of the probe and they behave as if they were free. From this point of view we see that the number of fluctuations resolved by the probe becomes larger and larger with decreasing x because of the emission of gluons by bremsstrahlung. The fact that the probe resolves more and more partons as Q^2 increases is the source of the quantum corrections that violates the Bjorken scaling. So both x and Q^2 variations leads to quantum corrections to the observables. The x -evolution is given by the BFKL equation in the diluted regime where the partonic density is small and by the Balitsky-Kovchegov (BK) equation [42, 43] in the dense regime where the partonic interactions due to their overlapping leads to non-linear evolution equations. Both equations resum the large leading terms in $\alpha_s \int^{p^+} \frac{dk^+}{k^+} \sim \alpha_s \ln(1/x)$ due to the soft gluon emissions. The Q^2 evolution is given by the Dokshitzer-Gribov-Lipatov-Altarelli-Parisi (DGLAP) equation [44, 45, 46, 47] which resums the large $\ln(Q^2)$ leading terms that appear due to collinear singularities $\alpha_s \int^{Q^2} \frac{dk_\perp^2}{k_\perp^2} \sim \alpha_s \ln(Q^2)$.

In the Bjorken limit ($Q^2 \rightarrow \infty$, x fixed), the expression (1.90) of $W_{\mu\nu}$, the integral is dominated by the value of the correlator for $0 < y^2 < \frac{1}{Q^2}$. The way to compute these contributions is to use the operator product expansion (OPE) on the light-cone $y^2 \rightarrow 0$, the OPE technique was introduced in particle physics by Wilson in the 70's [6] and was then applied to DIS [7, 4] and later to exclusive processes [48]. It consists in expanding the product of the electromagnetic currents as

$$J(y)J(0) \stackrel{|y| \rightarrow 0}{=} \sum_{s,i} C_{\mu_1 \dots \mu_s}^{s,i}(y) \mathcal{O}_i^{\mu_1 \dots \mu_s}(0), \quad (1.98)$$

where the coefficients $C_{\mu_1 \dots \mu_s}^{s,i}(y) = y_{\mu_1} \dots y_{\mu_s} C^{s,i}(y^2)$ are the Wilson coefficients, the functions $C^{s,i}(y^2)$ contain the singularities when $|y| \rightarrow 0$. $\mathcal{O}_i^{\mu_1 \dots \mu_s}(0)$ are local operators of spin s that

have the same quantum numbers of the l.h.s. of (1.98). By dimensional analysis, the canonical dimension of the currents are $d_J = 3$ and then the Wilson coefficients behave as

$$C^{s,i}(y^2) \sim |y|^{d_{s,i}-s-6} = |y|^{t_i-6}, \quad (1.99)$$

where $d_{s,i}$ is the canonical dimension of the operator $\mathcal{O}_i^{\mu_1 \cdots \mu_s}$ and s is the spin and $t_i = d_{s,i} - s$ is the twist of the operator $\mathcal{O}_i^{\mu_1 \cdots \mu_s}$. Note that the difference between the OPE on the light-cone ($y^2 \rightarrow 0$) and the standard OPE ($y_\mu \rightarrow 0$), is that the hierarchy of the leading operators is not given by the canonical dimension of the operators but by their twists and thus there is an infinite set of operators of the same twist, as the dimension of the operators can be compensated by their spins. The singularities that drive the behavior of the non-local correlators are given by operators of twist $t_{s,i} < 6$ and the leading twist operators of QCD are of twist 2.

One can parameterize the correlators on the possible Lorentz structures as,

$$\langle \langle p(p) | \mathcal{O}_{s,i}^{\mu_1 \cdots \mu_s}(0) | p(p) \rangle \rangle_{spin} = p^\mu \cdots p^{\mu_s} \langle \mathcal{O}_{s,i}(0) \rangle + \cdots, \quad (1.100)$$

where " \cdots " stand for terms with trace. Replacing $J_\mu(y)J_\nu(0)$ in the definition (1.90) of $W_{\mu\nu}$ by the OPE leads to

$$\begin{aligned} 4\pi W_{\mu\nu} &= \sum_{s,i} \langle \mathcal{O}_{s,i}(0) \rangle \int d^4y e^{iq \cdot y} (y \cdot p)^s C^{s,i}(y^2) \\ &= \sum_s x^{-s} \sum_i \langle \mathcal{O}_{s,i}(0) \rangle (-iQ^2 \frac{\partial}{\partial Q^2})^s \tilde{C}^{s,i}(Q^2) \\ &\equiv \sum_s x^{-s} \sum_i \langle \mathcal{O}_{s,i}(0) \rangle D^{s,i}(Q^2), \end{aligned} \quad (1.101)$$

with $\tilde{C}^{s,i}(Q^2)$ the Fourier transform of $C^{s,i}(y^2)$. $D^{s,i}(Q^2)$ scales like $\sim (1/Q)^{t_i-2}$, so at leading twist the Bjorken scaling is verified. The coefficient functions $D^{s,i}(Q^2)$ are universal as the target dependence is contained in the initial and final states of $\langle \mathcal{O}_{s,i}(0) \rangle$ and they are calculable in pQCD. The structure functions take the forms

$$F_1(x, Q^2) = \sum_s x^{-s} \sum_i \langle \mathcal{O}_{s,i}(0) \rangle D_1^{s,i}(Q^2), \quad (1.102)$$

$$F_2(x, Q^2) = \sum_s x^{-s+1} \sum_i \langle \mathcal{O}_{s,i}(0) \rangle D_2^{s,i}(Q^2). \quad (1.103)$$

The leading twist QCD operators are,

$$\mathcal{O}_{s,q_f}^{\mu_1 \cdots \mu_s} = \bar{\psi}(0) \gamma^{\{\mu_1} \partial^{\mu_2} \cdots \partial^{\mu_s\}} \psi(0), \quad (1.104)$$

$$\mathcal{O}_{s,g}^{\mu_1 \cdots \mu_s} = F_\mu^{\{\mu_1} \partial^{\mu_2} \cdots \partial^{\mu_{s-1}} F^{\mu_s\}\mu}, \quad (1.105)$$

with " $\{\cdots\}$ " stands for the symmetrization of μ_1, \cdots, μ_s indices and the subtraction of the trace terms. Identifying the structure functions in (1.97) and (1.102, 1.103) leads to

$$\int \frac{dx}{x} x^s (f_f(x) + f_{\bar{f}}(x)) = \langle \mathcal{O}_{s,q_f} \rangle, \quad (1.106)$$

which relates the Mellin moments of the PDFs to the expected values on the hadronic state $\langle \mathcal{O}_{s,q_f} \rangle$.

Taking the average value of $\mathcal{O}_{s,q_f}^{\mu_1 \dots \mu_s}$ and $\mathcal{O}_{s,g}^{\mu_1 \dots \mu_s}$ on quark of flavor f' state, one can show that the corresponding $\langle \mathcal{O}_{s,q_f} \rangle = \delta_{ff'}$ and $\langle \mathcal{O}_{s,g} \rangle = 0$. Identifying the structure functions in (1.97) and (1.102, 1.103) leads to

$$\int \frac{dx}{x} (f_f(x) + f_{\bar{f}}(x)) = \langle \mathcal{O}_{s,q_f} \rangle. \quad (1.107)$$

The Callan-Symanzik renormalization group equations for the correlators $\langle J(y)J(0) \rangle$ and $\langle \mathcal{O}_{s,i} \rangle$ read

$$\left(\mu \frac{\partial}{\partial \mu} + \beta(g) \frac{\partial}{\partial \alpha_s} \right) \langle J(y)J(0) \rangle = 0, \quad (1.108)$$

$$\left(\left(\mu \frac{\partial}{\partial \mu} + \beta(\alpha_s) \frac{\partial}{\partial \alpha_s} \right) \delta_{ij} + \gamma_{s,ij}(\alpha_s) \right) \langle \mathcal{O}_{s,j} \rangle = 0, \quad (1.109)$$

with $\beta(\alpha_s) = \mu^2 \frac{d\alpha_s}{d\mu^2}$ and $\gamma_{s,ij}$ the element of the anomalous dimension matrix. The running of α_s at one loop approximation leads to

$$\alpha_s(Q) = \frac{8\pi^2}{\beta_0 \ln(Q/\Lambda_{QCD})}, \quad (1.110)$$

with $\beta_0 = \frac{11}{3}N_c - \frac{2}{3}n_f$. As the structure functions do not depend on the choice of μ^2 , the coefficient functions satisfy

$$\left(\left(\mu \frac{\partial}{\partial \mu} + \beta(\alpha_s) \frac{\partial}{\partial \alpha_s} \right) \delta_{ij} + \gamma_{s,ij} \right) D^{s,j} = 0, \quad (1.111)$$

The solutions of this equation is given by,

$$D^{s,i}(Q/\mu, \alpha_s) = D^{s,j}(Q_0/\mu, \alpha_s(Q)) \left(\left(\frac{\ln(Q/\Lambda_{QCD})}{\ln(Q_0/\Lambda_{QCD})} \right)^{\frac{8\pi^2 A(s)}{\beta_0}} \right)_{ji}.$$

The coefficients $A_{ij}(s) = \gamma_{s,ij}(\mu)/(4\pi\alpha_s(\mu))$ of the matrix A are calculable at one loop level from the counter terms that regularize the operator divergence. As a consequence the scaling violations at one loop are responsible for the Bjorken scaling and the mixing between the operator expectation values involves the gluon operators (fluctuations resolved when probing with a higher sensibility),

$$\int \frac{dx}{x} x^s \sum_f (f_f(x, Q^2) + f_{\bar{f}}(x, Q^2)) \propto \left(\left(\frac{\ln(Q/\Lambda_{QCD})}{\ln(Q_0/\Lambda_{QCD})} \right)^{\frac{8\pi^2 A}{\beta_0}} \right)_{fi} \langle \mathcal{O}_{s,i} \rangle_{Q_0}. \quad (1.112)$$

Deriving this equation with respect to $\ln(Q^2)$ leads to

$$Q^2 \frac{\partial \tilde{f}_f(s, Q^2)}{\partial Q^2} = -2\pi\alpha_s(Q) A_{fj}(s) \tilde{f}_j(s), \quad (1.113)$$

with \tilde{f} the Mellin moments of the PDFs. This equation is equivalent to the DGLAP equation in x -space,

$$\frac{\partial f_i(x, Q^2)}{\partial \ln(Q^2)} = \frac{\alpha_s(Q^2)}{2\pi} \int_x^1 \frac{dy}{y} P_{ij}(x/y) f_j(y, Q^2), \quad (1.114)$$

where the splitting functions $P_{ij}(x/y)$ are the Mellin moments of the elements $A_{ij}(s)$,

$$\int \frac{dx}{x} x^s P_{ij}(x) = -4\pi A_{ij}(s). \quad (1.115)$$

Note that the eigenvectors associated to the eigenvalue zero of the matrix A determine the sum rules. These eigenvectors, which are combinations of operators, are scale independent. For example the sum rule for $s = 1$ implies the conservation of the number of partons and for $s = 2$ the conservation of the longitudinal momentum carried by all the partons.

The physical picture is that the photon can resolve the parton structure inside the parton q_i . The splitting functions $P_{ij}(y)$ are the amplitudes of probability to get the parton j with fraction of momentum y of the momentum of the parton from the parton i . The DGLAP equation is currently known up to NNLO corrections [49].

1.3.2 Impact factors $\gamma_{L,T}^* \rightarrow \gamma_{L,T}^*$

In terms of the Lorentz invariant quantities x , y and Q^2 , the differential cross-section (1.93) in the infinite momentum frame reads

$$\frac{d\sigma_{tot}^{ep}}{dx dQ^2} = \frac{2\pi\alpha^2}{xQ^4} ((1 + (1 - y)^2)F_2(x, Q^2) - y^2 F_L(x, Q^2)). \quad (1.116)$$

These two structure functions are closely linked to the longitudinal and transverse polarized cross-sections σ_L and σ_T of the processes $\sum_X \gamma_{L,T}^* + p(p) \rightarrow X(p_X)$,

$$F_L(x, Q^2) = \frac{Q^2}{4\pi^2\alpha} \sigma_L(x, Q^2), \quad (1.117)$$

$$F_2(x, Q^2) = \frac{Q^2}{4\pi^2\alpha} (\sigma_T(x, Q^2) + \sigma_L(x, Q^2)). \quad (1.118)$$

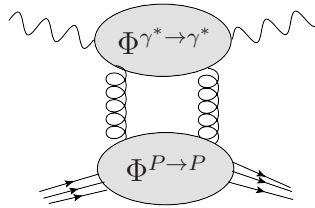


Figure 1.12: k_T -factorization of the forward Compton scattering amplitude.

We will focus in this part on the determination of the polarized cross-sections σ_L and σ_T defined in eqs. (1.117, 1.118) in the perturbative Regge limit. Using the optical theorem,

the polarized cross-sections $\sigma_{L,T}$ are related to the forward Compton scattering amplitudes $\mathcal{A}_{L,T}^{\text{el.}} \equiv \mathcal{A}_{\gamma_{L,T}^* p \rightarrow \gamma_{L,T}^* p}(s, t = 0)$,

$$\sigma_{L,T} = \frac{2}{F} \text{Im} \mathcal{A}_{L,T}^{\text{el.}}(s) = \frac{1}{s} \text{Im} \mathcal{A}_{L,T}^{\text{el.}}. \quad (1.119)$$

Using the impact factor representation for the Compton scattering amplitude, as illustrated in fig. 1.12 we get at Born level

$$\sigma_{L,T} = \int \frac{d^2 \underline{k}}{(2\pi)^2} \frac{1}{(\underline{k}^2)^2} \Phi^{\gamma_{L,T}^* \rightarrow \gamma_{L,T}^*}(\underline{k}, Q^2) \Phi^{P \rightarrow P}(\underline{k}, M^2), \quad (1.120)$$

where M is some non-perturbative scale of the transverse dynamics of the partons inside the proton.

In the region $Q^2 \gg \Lambda_{QCD}^2$, the impact factor $\Phi^{\gamma_{L,T}^* \rightarrow \gamma_{L,T}^*}$ can be computed within the perturbation theory. We will consider here the lowest order in perturbation theory where the photons interact with the gluons in t -channel by dissociating in a quark anti-quark pair. We neglect for simplicity the masses of the quark in this computation assuming $Q^2 \gg m_f^2$, where m_f is the mass of a quark of flavor f .

The vectors q , l and k are decomposed in the Sudakov basis of light-cone vectors p_1 and p_2 such as,

$$q = p_1 - \frac{Q^2}{s} p_2, \quad (1.121)$$

$$l = y p_1 + \beta p_2 + l_\perp, \quad (1.122)$$

$$k = \frac{\kappa + Q^2 + \underline{k}^2}{s} p_2 + k_\perp. \quad (1.123)$$

Note that we work in the infinite momentum frame where the proton and the virtual photon are moving respectively near the light-cone vectors p_2 and p_1 .

The longitudinal and transverse polarization vectors of the virtual photons are

$$\varepsilon_{\gamma_L}^\mu = \frac{1}{Q} (p_1^\mu + \frac{Q^2}{s} p_2^\mu), \quad \varepsilon^\pm = \frac{1}{\sqrt{2}} (0, \mp 1, -i, 0). \quad (1.124)$$

We define the euclidean polarization vectors in the transverse space as,

$$\underline{e}^\pm = \frac{1}{\sqrt{2}} (\mp 1, -i). \quad (1.125)$$

We use the Cutkosky rules to compute the discontinuity of the four diagrams shown in fig. 1.13 that contribute to the impact factors.

The contribution to the impact factor of the diagram (a) for a loop involving a quark of electric charge e ,

$$\Phi_{(a)}^{\gamma_L^* \rightarrow \gamma_L^*} = \frac{1}{2s} \int \frac{d\kappa}{(2\pi)} \mathcal{D}^{\text{isc}_\kappa} \mathcal{A}_{(a)} \quad (1.126)$$

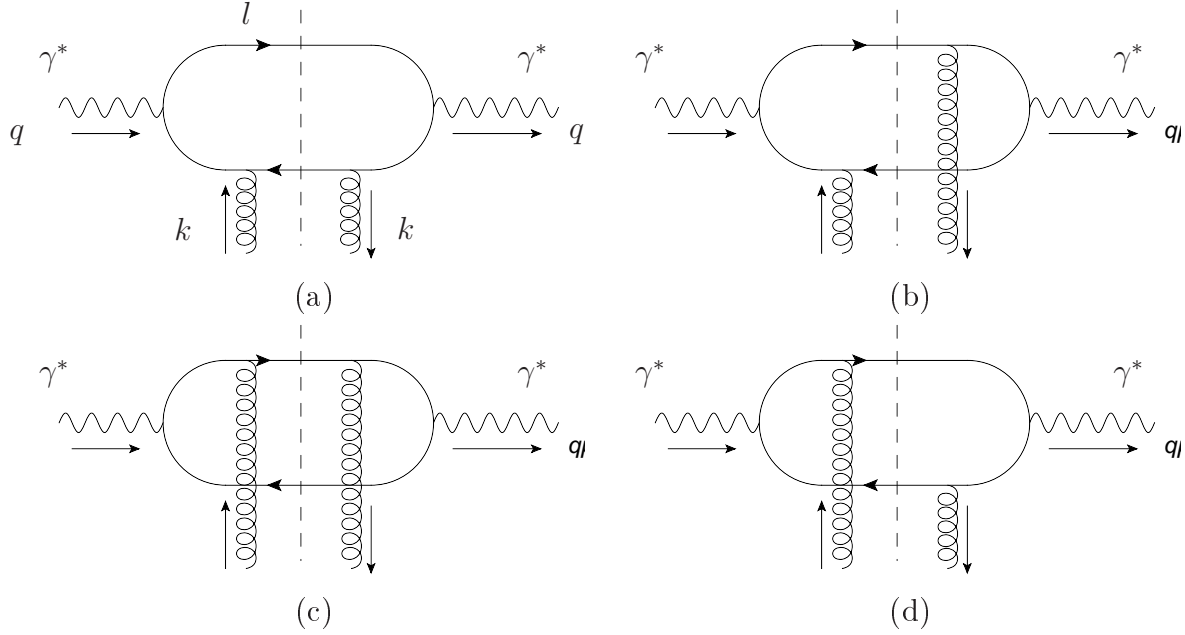


Figure 1.13: The four diagrams contributing to the $\gamma^* \rightarrow \gamma^*$ impact factors, the dashed lines are the cut in the diagrams.

and

$$\begin{aligned}
 \text{Disc}_\kappa \mathcal{A}_{(a)} &= \int \frac{d^4 l}{(2\pi)^2} \delta(l^2) \delta((l - q - k)^2) (4\pi\alpha) (4\pi\alpha_s) \\
 &\times \frac{-\text{Tr} \left(\not{\epsilon}_L^{\gamma^*} (\not{y} - \not{q}) \not{\epsilon}^{\text{NS}} (\not{y} - \not{q} - \not{k}) \not{\epsilon}^{\text{NS}} (\not{y} - \not{q}) \not{\epsilon}_L^{*\gamma^*} \not{l} \right)}{((l - q)^2)^2} \\
 &= \frac{s}{2} \int \frac{dy d\beta d^2 \underline{\ell}}{(2\pi)^2} \delta(y s (\beta - \frac{\underline{\ell}^2}{y s})) \delta(\bar{y}(\kappa - \kappa_0)) (4\pi\alpha) (4\pi\alpha_s) \\
 &\times \frac{-\text{Tr} \left(\not{\epsilon}_L^{\gamma^*} (\not{y} - \not{q}) \not{\epsilon}^{\text{NS}} (\not{y} - \not{q} - \not{k}) \not{\epsilon}^{\text{NS}} (\not{y} - \not{q}) \not{\epsilon}_L^{*\gamma^*} \not{l} \right)}{((l - q)^2)^2} \\
 &= \frac{s}{2} \int \frac{dy d^2 \underline{\ell}}{(2\pi)^2} \frac{1}{y s} \frac{\delta(\kappa - \kappa_0)}{\bar{y}} (4\pi\alpha) (4\pi\alpha_s) \\
 &\times \left(\frac{2Q}{s} \right)^2 \left(\frac{2}{s} \right) \frac{-\text{Tr} (\not{p}_2 (-\bar{y} \not{p}_1) \not{p}_2 (-\bar{y} \not{p}_1) \not{p}_2 (-\bar{y} \not{p}_1) \not{p}_2 (y \not{p}_1))}{(\frac{1}{y} (\underline{\ell}^2 + y \bar{y} Q^2))^2} \\
 &= 32 s \alpha \alpha_s \int dy d^2 \underline{\ell} \delta(\kappa - \kappa_0) \frac{\bar{y}^2 y^2 Q^2}{(\underline{\ell}^2 + y \bar{y} Q^2)^2}, \tag{1.128}
 \end{aligned}$$

with $\kappa_0 = \frac{1}{y \bar{y}} (\underline{\ell} - y \underline{k})^2$. Note that we use the Ward identity to simplify the computation by rewriting the longitudinal polarization of the virtual photon as

$$\varepsilon_L^{\gamma^*} = \frac{1}{Q} \left(q + \frac{2Q^2}{s} p_2 \right). \tag{1.129}$$

The Ward identity

$$q^\mu \mathcal{A}_\mu = 0, \tag{1.130}$$

with \mathcal{A}_μ such as $\mathcal{A} = \varepsilon^{\gamma^*\mu}(q)\mathcal{A}_\mu$, allows then to get rid of the terms in q^μ in the photon polarizations,

$$\varepsilon_L^* = \frac{1}{Q} \left(q^\mu + \frac{2Q^2}{s} p_2^\mu \right) \longrightarrow \frac{2Q}{s} p_2^\mu. \quad (1.131)$$

The contribution of the diagram (a) to the impact factor reads

$$\Phi_{(a)}^{\gamma_L^* \rightarrow \gamma_L^*} = \frac{8\alpha\alpha_s}{\pi} \int dy d^2\ell \frac{\bar{y}^2 y^2 Q^2}{(\ell^2 + y\bar{y}Q^2)^2}. \quad (1.132)$$

Computing the other contributions in the case of the longitudinally polarized photon, summing the contributions of all the flavors f of electric charge q_f and including the color factor $Tr(t^a t^b) = \frac{\delta^{ab}}{2}$ involved in the color singlet exchange, the total impact factor reads

$$\Phi^{\gamma_L^* \rightarrow \gamma_L^*} = \frac{\delta^{ab}}{2} \frac{8\alpha\alpha_s}{\pi} \sum_f q_f^2 \int dy d^2\ell \left(\frac{y\bar{y}Q}{D(\ell)} - \frac{y\bar{y}Q}{D(\ell + \underline{k})} \right)^2. \quad (1.133)$$

where $D(\ell) = \ell^2 + \mu^2$ with $\mu^2 = y\bar{y}Q^2 + m_f^2$. For completeness, we have restored in eq. (1.133) the masses of the quarks involved in the loop m_f .

The impact factor $\Phi^{\gamma_T^* \rightarrow \gamma_T^*}$ can be computed using the same techniques than we have presented for $\Phi^{\gamma_L^* \rightarrow \gamma_L^*}$. The result reads

$$\begin{aligned} \Phi^{\gamma_T^* \rightarrow \gamma_T^*} &= \frac{\delta^{ab}}{2} \frac{2\alpha_s\alpha}{\pi} \sum_f q_f^2 \int dy d^2\ell \\ &\times \left\{ -4y\bar{y} \underline{e}_i \cdot (\underline{L}(\ell) - \underline{L}(\ell - \underline{k})) (\underline{L}(\ell) - \underline{L}(\ell - \underline{k})) \cdot \underline{e}_j^* \right. \\ &\quad + \underline{e}_i \cdot \underline{e}_j^* (\underline{L}(\ell) - \underline{L}(\ell - \underline{k}))^2 \\ &\quad \left. + m_f^2 \underline{e}_i \cdot \underline{e}_j^* \left(\frac{1}{D(\ell)} - \frac{1}{D(\ell + \underline{k})} \right) \left(\frac{1}{D(\ell)} - \frac{1}{D(\ell - \underline{k})} \right) \right\}, \end{aligned} \quad (1.134)$$

with \underline{e}_i and \underline{e}_j^* the euclidean transverse polarization vectors of the ingoing and outgoing photons, and

$$\underline{L}(\ell) = \frac{\ell}{\ell^2 + \mu^2}.$$

It is easy to check that the impact factors vanish when $\underline{k}^2 \rightarrow 0$ as a consequence of the Ward identity as discussed in section. 1.2.4.

1.3.3 Color dipole picture

Introduction

The basic idea of the dipole picture for DIS, initiated by the works of Nikolaev, Zakharov [8, 9] and Mueller [10, 11], is that in the proton rest frame at low x , the photon dissociates into a partonic system that constitutes a collection of color anticolor pairs called "color dipoles" which have a long life time compared to the time of the interaction of the partons with the proton target. The sizes of the dipoles can then be assumed to be fixed during the scattering of the partons with the nucleon target. The dipole states parameterized in

terms of their transverse sizes are eigenstates of the scattering operators as the dipole size is preserved during the scattering with the target. The amplitude factorizes into, the overlap of the initial Ψ_i and final Ψ_f^* wave functions of the virtual photon in the case of DIS, which are the amplitude of probability to produce a configuration of dipoles with fixed transverse sizes, and the scattering amplitude T of these dipoles with the target.

The amplitude of the process $ip \rightarrow fp$, where p is the nucleon target and i and f the initial and final states, can be written symbolically [50, 51],

$$\mathcal{A} = \sum_{n, \mathcal{F}_n, \{\lambda_k\}} \int [d^{2n} \underline{r}_k] \int [dy_k] \Psi_f^*(n, \{y_k, \underline{r}_k, \lambda_k\}) T(\mathcal{F}_n) \Psi_i(n, \{y_k, \underline{r}_k, \lambda_k\}), \quad (1.135)$$

where n is the number of partons involved in the intermediate Fock state \mathcal{F}_n with longitudinal fraction of momentum $\{z_k\}_{k=1..n}$ and impact parameters $\{\underline{r}_k\}_{k=1..n}$, of helicities $\{\lambda_k\}_{k=1..n}$. The scattering operator $T(\mathcal{F}_n)$ being diagonal in the dipole states formed by the partonic system is independent of the initial and final states that have formed the dipoles and by consequence is a universal quantity that depends only on the nucleon target dynamics.

The simplest case is given by the lowest intermediate Fock state constituted by a quark (y, \underline{r}_1) antiquark (\bar{y}, \underline{r}_2) pair, where the couples (z, \underline{r}_k) denotes the longitudinal fraction of momentum and the transverse position (impact parameter) of the parton. Indeed the contribution of higher Fock states due to the emission of low energy gluons are important when the rapidity increases but they can be absorbed, in the large N_c limit, in the dipole scattering amplitude evolution governed by the BFKL evolution equation [52]. The dipole picture for DIS corresponds to the diagram shown in fig. 1.14, where we denote $\mathcal{N}(x, \underline{r}, \underline{b})$ the imaginary part of the $(T(\mathcal{F}_2))$, $\underline{r} = \underline{r}_2 - \underline{r}_1$ is the dipole vector and $\underline{b} = y\underline{r}_1 + \bar{y}\underline{r}_2$ is the impact parameter of the dipole, which is Fourier conjugate of the transverse momentum transfer $\underline{\Delta}$.

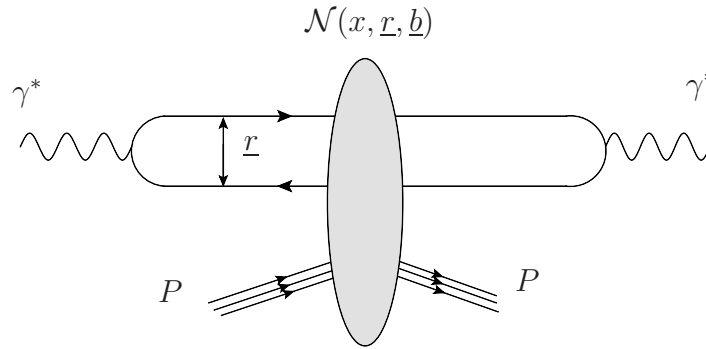


Figure 1.14: DIS within the color dipole picture

Let us stress a useful analogy pointed out by Susskind [53] between the parton kinematics and the two-body problem in quantum mechanics. The Poincaré group in the infinite momentum frame contains a sub-group that we denote F of transformations that leave invariant the hypersurface orthogonal to the dominant light-cone direction p_1 and whose algebra is isomorphic to the Galilean algebra of the transformations on a two-dimensional space. Among the transformations of the sub-group F are "Galilean boost"-like transformations on

the transverse space. In Ref. [53], a dictionary is established between the generators of the Galilean transformations of a two-dimensional system of non-relativistic particles of masses m_i , positions r_i and momenta ℓ_i , and the generators of the sub-group F of the system of particles of longitudinal fractions of momentum $y_i = \{y, \bar{y}\}$, transverse impact parameters $\underline{r}_i = \{\underline{r}_1, \underline{r}_2\}$ and transverse momenta $\underline{\ell}_i = \{\underline{\ell}_1, \underline{\ell}_2\}$. The analog of the masses m_1 and m_2 of the quark and the antiquark are proportional to the longitudinal components $2yp_1$ and $2\bar{y}p_1$ in our computation.

In the two-dimensional mechanics, the two-body problem can be simplified by splitting the system into the kinematic variables of its center of mass and of its reduced particle. Following the above analogy, we find that the transverse coordinate of the "center of mass" of the dipole is given by \underline{b} , and the vector of the reduced particle is given by \underline{r} , while the momentum of the reduced particle is,

$$\underline{\ell} = \bar{y}\underline{\ell}_1 - y\underline{\ell}_2,$$

and the effective mass is

$$M = \frac{m_1 m_2}{m_1 + m_2} = 2y\bar{y}p_1.$$

The imaginary part of the dipole amplitude can be related to the b -dependent dipole cross-section,

$$\frac{d\hat{\sigma}}{d^2\underline{b}} = 2\mathcal{N}(x, \underline{r}, \underline{b}). \quad (1.136)$$

In the case of DIS, the momentum exchanged in t -channel is zero which leads to the following dipole cross-section,

$$\hat{\sigma}(x, \underline{r}) = \int d^2\underline{b} \frac{d^2\hat{\sigma}}{d^2\underline{b}} = 2 \int d^2\underline{b} \mathcal{N}(\underline{r}, \underline{b}, x).$$

A usual assumptions is that the b -dependence factorizes in $\mathcal{N}(x, \underline{r}, \underline{b})$ as,

$$\mathcal{N}(x, \underline{r}, \underline{b}) = T(\underline{b})\mathcal{N}(x, \underline{r}).$$

The function $T(\underline{b})$ describes the gluon density inside the nucleon, it can be for example chosen as a step function which is one inside the nucleon and zero outside, giving after integration over \underline{b} ,

$$\int d^2\underline{b} \mathcal{N}(x, \underline{r}, \underline{b}) = \pi R^2 \mathcal{N}(x, \underline{r}),$$

where R is the radius of the nucleon. This integral over \underline{b} gives then an overall normalization to the dipole cross-section denoted σ_0 such as

$$\hat{\sigma}(x, \underline{r}) = \sigma_0 \mathcal{N}(x, \underline{r}), \quad (1.137)$$

with $\sigma_0 = 2 \int d^2\underline{b} T(\underline{b}) = 2\pi R^2$.

As we will see on the particular "saturation model", the dipole picture will be also convenient to implement saturation effects as one can define dense and diluted partonic systems depending on the size that the dipole can resolve compared to a so-called "saturation scale" that emerges from the non-linear equations that govern the x -dependence of the dipole scattering amplitude.

DIS: factorization of the wave functions

Coming back to the $\gamma_{L,T}^* \rightarrow \gamma_{L,T}^*$ impact factors eqs. (1.133, 1.134) for the DIS process, we will show that the results are consistent with the dipole picture of fig. 1.14 once expressed in the impact parameter representation. Let us introduce two identities¹,

$$\frac{1}{\underline{\ell}^2 + \mu^2} = \int \frac{d^2 \underline{r}}{2\pi} e^{i\mathbf{k} \cdot \underline{r}} K_0(\mu r), \quad (1.138)$$

$$\frac{\underline{\ell}}{\underline{\ell}^2 + \mu^2} = -i\mu \int \frac{d^2 \underline{r}}{2\pi} e^{i\mathbf{k} \cdot \underline{r}} \frac{\underline{r}}{r} K_1(\mu r). \quad (1.139)$$

where \underline{r} is a vector of the transverse coordinate space conjugated to the transverse momentum $\underline{\ell}$, $r = |\underline{r}|$ and $K_\alpha(x)$ are the modified Bessel functions of the second kind which obey the modified Bessel's equations,

$$x^2 K_\alpha''(x) + x K_\alpha'(x) - (x^2 + \alpha^2) K_\alpha(x) = 0.$$

Using these identities, we can get the following expressions for the impact factors

$$\begin{aligned} \Phi^{\gamma_L^* \rightarrow \gamma_L^*} &= \frac{\delta^{ab}}{2} \frac{8\alpha\alpha_s}{\pi} \sum_f^{n_f} q_f^2 \int dy d^2 \underline{\ell} \left(\frac{y\bar{y}Q}{D(\underline{\ell})} - \frac{y\bar{y}Q}{D(\underline{\ell} - \underline{k})} \right) \left(\frac{y\bar{y}Q}{D(\underline{\ell})} - \frac{y\bar{y}Q}{D(\underline{\ell} - \underline{k})} \right) \\ &= \frac{\delta^{ab}}{2} \frac{8\alpha\alpha_s}{\pi} \sum_f^{n_f} q_f^2 \int dy \int d^2 \underline{r} y\bar{y}Q K_0(\mu r) \int d^2 \underline{r}' y\bar{y}Q K_0(\mu r') \\ &\quad \times (1 - e^{-i\mathbf{k} \cdot \underline{r}}) (1 - e^{-i\mathbf{k} \cdot \underline{r}'}) \int \frac{d^2 \underline{\ell}}{(2\pi)^2} e^{i\mathbf{\ell} \cdot (\underline{r} + \underline{r}')} \\ &= \frac{\delta^{ab}}{2} \frac{8\alpha\alpha_s}{\pi} \sum_f^{n_f} q_f^2 \int dy \int d^2 \underline{r} (y\bar{y}Q K_0(\mu r)) (y\bar{y}Q K_0(\mu r)) \\ &\quad \times (1 - e^{-i\mathbf{k} \cdot \underline{r}}) (1 - e^{i\mathbf{k} \cdot \underline{r}}) \\ &= \int dy \int d^2 \underline{r} \sum_f^{n_f} \sum_{h, \bar{h}} \left| \Psi_{f, h\bar{h}}^{\gamma_L^*} \right|^2 \left[\frac{\delta^{ab}}{2} \frac{4\pi\alpha_s}{N} (1 - e^{-i\mathbf{k} \cdot \underline{r}}) (1 - e^{i\mathbf{k} \cdot \underline{r}}) \right], \end{aligned} \quad (1.140)$$

where $\Psi_{f, h\bar{h}}^{\gamma_L^*}$ is the amplitude of probability for the photon to dissociate into a quark and an antiquark of flavor f and of respective helicities h and \bar{h} and longitudinal fractions of momentum y and $\bar{y} = 1 - y$, which form a color dipole of size \underline{r} . $\Psi_{f, h\bar{h}}^{\gamma_L^*}$ is the wave function of the longitudinally polarized virtual photon computed in the first order of the light-cone perturbation theory [54],

$$\Psi_{f, h\bar{h}}^{\gamma_L^*}(y, \underline{r}; Q^2) = \delta_{\bar{h}, -h} \frac{eq_f}{2\pi} \sqrt{\frac{N_c}{\pi}} (y\bar{y}Q) K_0(\mu |\underline{r}|). \quad (1.141)$$

In eq. (1.140), the part between the square brackets corresponds to the interaction of the dipole with the two t -channel gluons. The factorization of the amplitude into the wave functions of the virtual photon and the dipole interaction is valid even at low Q^2 , it is only

¹Note that we got a overall minus sign in (1.139) compared to [32].

a consequence of the high energy limit. Coming back to the expressions of the polarized cross-sections eq. (1.120) and replacing the impact factor of the proton by the unintegrated gluon density $\mathcal{F}(x, \underline{k})$ defined as $\Phi^{P \rightarrow P}/(2\pi)^2$ at Born order, the polarized cross-sections read

$$\sigma_{L,T} = \int d^2 \underline{k} \frac{1}{(\underline{k}^2)^2} \Phi^{\gamma_{L,T}^* \rightarrow \gamma_{L,T}^*}(\underline{k}, Q^2) \mathcal{F}(x, \underline{k}). \quad (1.142)$$

Note that the gluon density $g(x, Q^2)$ is given by

$$g(x, Q^2) = \frac{1}{\pi} \int^{Q^2} \frac{d^2 \underline{k}}{\underline{k}^2} \mathcal{F}(x, \underline{k}). \quad (1.143)$$

Inserting the result of eq. (1.140) in the expression of the polarized cross-sections eq. (1.142) leads to the formula,

$$\sigma_L = \sum_f^{n_f} \int dy \int d^2 \underline{r} \sum_{h, \bar{h}} \left| \Psi_{f, h\bar{h}}^{\gamma_L^*} \right|^2 \hat{\sigma}(x, \underline{r}), \quad (1.144)$$

with the dipole cross-section

$$\hat{\sigma}(x, \underline{r}) = \frac{N^2 - 1}{4} \frac{4\pi\alpha_s}{N} \int d^2 \underline{k} \frac{1}{(\underline{k}^2)^2} \mathcal{F}(x, \underline{k}) (1 - e^{-i\vec{k} \cdot \underline{r}}) (1 - e^{i\vec{k} \cdot \underline{r}}). \quad (1.145)$$

Similarly the polarized cross-section σ_T reads

$$\sigma_T = \sum_f^{n_f} \int dy \int d^2 \underline{r} \sum_{h, \bar{h}} \left| \Psi_{f, h\bar{h}}^{\gamma_T^*} \right|^2 \hat{\sigma}(x, \underline{r}), \quad (1.146)$$

where the wave function $\Psi_{f, h\bar{h}}^{\gamma_T^*}$ of the virtual transversely polarized photon is,

$$\Psi_{f, h, \bar{h}}^{\gamma_T^* (\lambda_\gamma)}(y, \underline{r}; Q^2) = \delta_{\bar{h}, -h} \frac{ieq_f}{2\pi} \sqrt{\frac{N_c}{\pi}} (y\delta_{h, \lambda_\gamma} + \bar{y}\delta_{h, -\lambda_\gamma}) \frac{(\underline{r} \cdot \underline{e}^{(\lambda_\gamma)})}{|\underline{r}|} \mu K_1(\mu |\underline{r}|). \quad (1.147)$$

Note that the expressions of the wave functions of the virtual photon become in the non-forward limit [32] where a momentum Δ is exchanged in the t -channel,

$$\Psi_{h\bar{h}}^{\gamma_L^*}(q + \Delta) = \delta_{\bar{h}, -h} \frac{eq_f}{2\pi} \sqrt{\frac{N}{\pi}} y\bar{y} Q K_0(\mu r) e^{i\bar{y}\Delta \cdot \underline{r}}, \quad (1.148)$$

$$\begin{aligned} \Psi_{h\bar{h}}^{\gamma_T^*}(q + \Delta) &= \delta_{\bar{h}, -h} \frac{ieq_f}{2\pi} \sqrt{\frac{N}{\pi}} (y\delta_{h, \lambda_\gamma} - \bar{y}\delta_{h, -\lambda_\gamma}) \frac{\underline{e}^{(\lambda_\gamma)} \cdot \underline{r}}{r} \mu K_1(\mu r) e^{i\bar{y}\Delta \cdot \underline{r}} \\ &+ \delta_{\bar{h}, h} \delta_{h, \lambda_\gamma} m_f \frac{eq_f}{2\pi} \sqrt{\frac{N}{2\pi}} K_0(\mu r) e^{i\bar{y}\Delta \cdot \underline{r}}. \end{aligned} \quad (1.149)$$

Let us now sketch how the light-cone wave functions naturally emerge from the eikonal limit. The eikonal limit $s \rightarrow \infty$ can be seen as an infinite boost of the incoming and outgoing states along their longitudinal direction z ,

$$S_{\alpha\beta} = \text{Lim}_{\omega \rightarrow \infty} \langle \beta | e^{i\omega K^-} U(\infty, -\infty) e^{-i\omega K^-} | \alpha \rangle, \quad (1.150)$$

with $K^- = -K^z$ the Lorentz boost generator along z . Splitting the S -matrix as,

$$U(-\infty, \infty) = U(-\infty, -L)U(-L, L)U(L, \infty), \quad (1.151)$$

where $U(-L, L)$ contains the interactions $eA^\mu(x)J_\mu(x)$ with an external potential $A^\mu(x)$ for $x^+ \in [-L, L]$, and inserting the infinite boost along z leads to

$$\begin{aligned} S_{\alpha\beta} &= \langle \beta | U_0(+\infty, 0) \\ &\quad \times T_+ \{ e^{ie \int d^2x_\perp (\int dx^+ A^-(x^+, 0, x_\perp)) (\int dx^- J^+(0, x^-, x_\perp))} \} \\ &\quad \times U_0(0, -\infty) | \alpha \rangle, \end{aligned} \quad (1.152)$$

where $U_0(t_1, t_2)$ is the evolution operator that contains only the self interaction of the fields. The expression (1.152) can be projected on all intermediate Fock states $|\gamma\rangle$ and $|\beta\rangle$ as,

$$\begin{aligned} S_{\alpha\beta} &= \sum_{\gamma, \delta} \langle \beta | U_0(+\infty, 0) | \gamma \rangle \langle \gamma | \\ &\quad \times T_+ \{ e^{ie \int d^2x_\perp (\int dx^+ A^-(x^+, 0, x_\perp)) (\int dx^- J^+(0, x^-, x_\perp))} \} \\ &\quad \times | \delta \rangle \langle \delta | U_0(0, -\infty) | \alpha \rangle, \end{aligned} \quad (1.153)$$

with T_+ the light-cone time ordered product. In our case, the sums over γ and δ are restricted to the lowest Fock state, i.e. a quark antiquark pair. The photon light-cone wave function for a given intermediate state $\langle \delta |$ containing n particles with coordinate $\{y_i, r_{\perp i}\}$ is defined as the amplitude of probability to get from the initial photon state at $x^+ = -\infty$ the state δ at the light-cone time $x^+ = 0$,

$$\Psi(\{y_i, r_{\perp i}\}) = \langle \delta | U_0(0, -\infty) | \alpha \rangle. \quad (1.154)$$

In the case $\delta = q(p_1, h)\bar{q}(p_2, \bar{h})$, the Fourier transform in k_\perp -space of light-cone wave function of the photon $\gamma^*(q, \lambda_\gamma)$ reads

$$\tilde{\Psi}_{h\bar{h}}^\lambda(\{y_i, k_{\perp i}\}) = \int \frac{d^2k_{\perp i}}{(2\pi)^2} e^{-ik_{\perp i} \cdot r_{\perp i}} \langle \delta | U_0(0, -\infty) | \alpha \rangle, \quad (1.155)$$

which is the amplitude of a photon to split as $\gamma^*(q, \lambda_\gamma) \rightarrow q(\ell_1, h)\bar{q}(\ell_2, \bar{h})$. We keep the conventions

$$\ell_1 = yp_1 + \frac{\ell^2}{ys}p_2 + \ell_\perp, \quad \ell_2 = \bar{y}p_1 + \frac{\ell^2}{\bar{y}s}p_2 - \ell_\perp \quad (1.156)$$

$$q = p_1 - \frac{Q^2}{s}p_2, \quad (1.157)$$

and we denote the energy $E_i = k_i^-$ with $k_i^-/\sqrt{s} \equiv p_1 \cdot k$. We define also the plus component as $k_i^+/\sqrt{s} \equiv p_2 \cdot k$. The light-cone wave function can be computed in light-cone perturbation theory (Feynman rules can be found in [55]). It reads

$$\tilde{\Psi}_{h\bar{h}}^\lambda(y, \ell_\perp) = \int_{-\infty}^0 dt e^{-it(E_\gamma - E_1 - E_2 + i\epsilon)} \frac{1}{\sqrt{s}} \frac{\bar{u}_h(\ell_1)}{\sqrt{y}} (e_q(-\not{\epsilon}^{(\lambda_\gamma)})) \frac{v_{\bar{h}}(\ell_2)}{\sqrt{\bar{y}}} \quad (1.158)$$

$$= \frac{i}{E_\gamma - E_1 - E_2} \frac{1}{\sqrt{s}} \frac{\bar{u}_h(\ell_1)(e_q\delta_{ab}(-\not{\epsilon}^{(\lambda_\gamma)}))v_{\bar{h}}(\ell_2)}{\sqrt{y\bar{y}}} \quad (1.159)$$

$$= \frac{i2\sqrt{y\bar{y}}}{\underline{\ell}^2 + \mu^2} \bar{u}_h(\ell_1)(e_q\delta_{ab}(-\not{\epsilon}^{(\lambda_\gamma)}))v_{\bar{h}}(\ell_2). \quad (1.160)$$

Note that in the standard way to calculate Feynman diagrams, the wave function can be obtained by replacing the conservation of energy factor $2\pi\delta(E_\gamma - E_1 - E_2)$ in the expression of the T -matrix, by the integral

$$\int_{-\infty}^0 dx^+ e^{-ix^+(E_\gamma - E_1 - E_2 + i\epsilon)} = \frac{i}{E_\gamma - E_1 - E_2},$$

and by adding the phase space factor $\frac{1}{\sqrt{y\bar{y}s}}$. This space factor $\frac{1}{\sqrt{y\bar{y}s}}$ should be omitted for external spinor fields but as we are interested in the case when the quark antiquark pair interacts at $x^+ = 0$, we keep this factor in the definition of the wave function.

The explicit computation of the currents $\bar{u}\not{\epsilon}v$ can be done using the chiral representation for the Dirac spinors,

$$u_h(p) = \frac{\not{p} + m}{\sqrt{E + m}} \begin{pmatrix} \chi_h(p) \\ 0 \end{pmatrix} \quad (1.161)$$

and

$$v_h(p) = \frac{-\not{p} + m}{\sqrt{E + m}} \begin{pmatrix} 0 \\ \chi_{-h}(p) \end{pmatrix}, \quad (1.162)$$

with $\chi_{1/2}(p) = (1, 0)$ and $\chi_{-1/2} = (0, 1)$ and using the expressions (1.138) and (1.139) to Fourier transform the results, allows to come back to the results for the photon wave function $\Psi_{h\bar{h}}^{\lambda_\gamma}(y, \underline{x})$ given by eqs. (1.141, 1.147) up to a normalization factor that depends on the quantum numbers of the quark antiquark pair.

Let us now make a brief remark on the role of the eikonal approximation in the factorization of the photon wave functions following the derivation in Ref. [56] in "usual" Feynman diagrams. Let us consider the diagram illustrated in fig. 1.15.

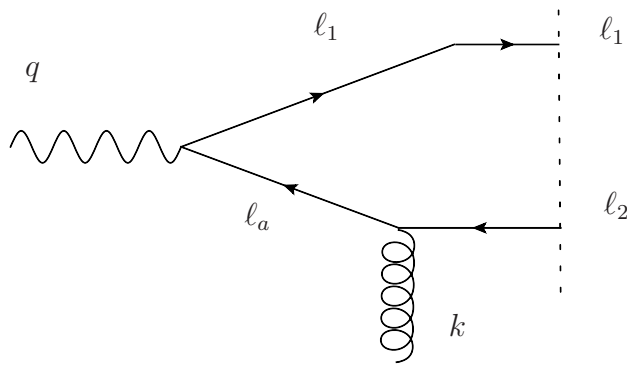


Figure 1.15: One part of the cut diagrams.

The diagram gives the contribution,

$$\mathcal{A} = -e \frac{\bar{u}^{(h)}(\ell_1) \not{\epsilon}^{(\lambda)}(q) \not{\epsilon}_a^{\text{NS}} v^{(\bar{h})}(\ell_2)}{\ell_a^2 + i\epsilon} \quad (1.163)$$

$$= e \frac{y}{\underline{\ell}^2 + y\bar{y}Q^2} \bar{u}^{(h)}(\ell_1) \not{\epsilon}^{(\lambda)}(q) \not{\epsilon}_a^{\text{NS}} v^{(\bar{h})}(\ell_2), \quad (1.164)$$

where

$$\ell_1 = yp_1 + \frac{\underline{\ell}^2}{ys}p_2 + \ell_\perp, \quad \ell_2 = \bar{y}p_1 + \frac{\underline{\ell}^2}{\bar{y}s}p_2 - \ell_\perp, \quad (1.165)$$

$$q = p_1 - \frac{Q^2}{s}p_2, \quad k = \frac{\kappa + Q^2 + \underline{k}^2}{s}p_2 + k_\perp, \quad (1.166)$$

$$\ell_a = \ell_1 - q = -\bar{y}p_1 + \frac{\underline{\ell}^2 + yQ^2}{ys}p_2 + \ell_\perp. \quad (1.167)$$

Due to the eikonal approximation in the gluonic vertex, the polarization of the t -channel gluon is along p_2 . We can then safely change in the numerator $\ell_a \rightarrow \ell_a + \beta p_2$, with β an arbitrary number as

$$(\ell_a + \beta p_2)\not{p}_2 = \not{\ell}_a p_2,$$

to change in the numerator $\ell_a \rightarrow \tilde{\ell}_a$ with $\tilde{\ell}_a$ on the mass shell,

$$\tilde{\ell}_a = -\bar{y}p_1 - \frac{\underline{\ell}^2}{\bar{y}s}p_2 + \ell_\perp = -\ell_2.$$

Then we can rewrite

$$\not{\ell}_a \rightarrow \sum_{\tilde{h}} v^{(\tilde{h})}(\ell_2) \bar{v}^{(\tilde{h})}(\ell_2),$$

to get a factorized form of the amplitude,

$$\mathcal{A} = \sum_{\tilde{h}} y \left(e \frac{\bar{u}^{(h)}(\ell_1) \not{\epsilon}^{(\lambda)}(q) v^{(\tilde{h})}(\ell_2)}{\underline{\ell}^2 + y\bar{y}Q^2} \right) \bar{v}^{(\tilde{h})}(\ell_2) \not{\epsilon}^{\text{NS}} v^{(\tilde{h})}(\ell_2) \quad (1.168)$$

$$= \frac{s}{(2\pi)^2} \sum_{\tilde{h}} \tilde{\Psi}_{h, -\tilde{h}}^{\gamma_\lambda^*}(y, \underline{\ell}) \delta_{\tilde{h}, \tilde{h}}. \quad (1.169)$$

1.3.4 Models for the dipole target interactions

Under the assumption that the b -parameter dependence of the dipole scattering amplitude factorizes, we saw that the dipole cross-section reads

$$\hat{\sigma}(x, \underline{r}) = \sigma_0 \mathcal{N}(x, \underline{r}) \equiv \sigma_0 \mathcal{N}(Y, \underline{r}), \quad (1.170)$$

with Y the rapidity $Y = \ln(1/x)$. Note that the assumption that the b dependence factorizes, even though used in most of dipole models, is not supported by the data on exclusive diffractive processes at HERA.

The dipole cross-section $\hat{\sigma}(x, \underline{r})$ involves the dynamics of the gluons inside the proton. At small- x one can expect saturation effects which appear when the partonic density of the nucleon becomes large. In the infinite momentum frame, we can interpret saturation effects as the saturation of the number of gluons of transverse size $1/Q$ in the wave function of the nucleon target. This growth of the gluon density could be responsible for a unitarity problem (violation of the Froissart bound by the hard QCD pomeron exchange) of the theory but we can expect that at some point the number of gluons stops growing, i.e. saturates, due

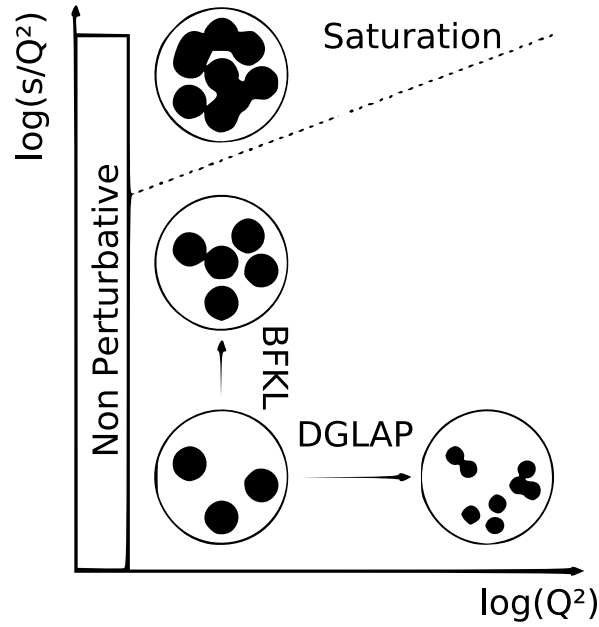


Figure 1.16: Saturation and diluted regimes.

to recombinations of the partons following the idea of Gribov, Levin and Ryskin [57]. Two regimes can be then defined as illustrated in fig. 1.16, the diluted regime where the nucleon is not saturated by the partons and the saturation regime where the gluon transverse areas start to overlap. The so-called critical line between the two regimes is given by $Q^2 = Q_s^2(x)$, with $Q_s^2(x)$ the inverse transverse area where the probability to find more than one gluon is of order one.

To take into account these saturation effects inside the proton, a first saturation model was introduced by Golec-Biernat and Wüsthoff in 1998, where the dipole cross-section is parameterized by a Gaussian ansatz which saturates at a value σ_0 ,

$$\hat{\sigma}(x, r) = \sigma_0 \left\{ 1 - \exp \left(-\frac{r^2}{4R_0^2(x)} \right) \right\}, \quad (1.171)$$

where $R_0(x)$ is the saturation radius

$$R_0^2(x) = \frac{1}{\text{GeV}^2} \left(\frac{x}{x_0} \right)^\lambda, \quad (1.172)$$

and the saturation regime is given for

$$Q^2 \lesssim \frac{1}{R_0^2(x)} \sim Q_s^2(x). \quad (1.173)$$

The success of this model was to describe all the contemporary HERA data [58, 59, 60, 61] for inclusive as well as diffractive cross-sections. The main feature of this model [62] is that it provides a dipole cross-section that gives back the pomeron trajectory in the diluted regime $1/Q \ll R_0(x)$,

$$F_2 \sim x^{-\lambda},$$

while for dense partonic systems $1/Q \gg R_0(x)$ the Froissart condition is recovered,

$$F_2 \sim Q^2 \sigma_0 \ln(1/x).$$

In the limit $r \rightarrow 0$ the dipole cross-section vanishes like $\hat{\sigma}(x, \underline{r}) \sim r^2$, this is known as the property of "color transparency" [63, 64] due to the screening of the quark and the antiquark colors when the $r \rightarrow 0$. Note that the Taylor expansion of eq. (1.145) around $r = 0$ shows this behavior of the dipole cross-section. To make contact with the photoproduction regime, it is customary [65] to make the following modification in the definition of the Bjorken variable x

$$x \rightarrow x \left(1 + \frac{4m_f^2}{Q^2}\right) = \frac{Q^2}{W^2 + Q^2} \left(1 + \frac{4m_f^2}{Q^2}\right) \xrightarrow{Q^2 \rightarrow 0} \frac{4m_f^2}{W^2}, \quad (1.174)$$

where m_f is an effective quark mass which depends on the flavor f and of the model used to fit the data. The values of the best fit parameters of the original saturation model are shown in tab. 1.1. Note that the inclusion of the charm contribution, with $m_c = 1.5$ GeV has also been performed in Ref. [65]. In fig. 1.17 are compared the fits with and without mass m_f to HERA data.

Fits	σ_0 (mb)	λ	x_0
No charm	23.03	0.288	3.04×10^{-4}
With charm	29.12	0.277	0.41×10^{-4}

Table 1.1: Values of the parameters entering the GBW dipole cross-section.

Another important feature of the saturation model which is well reproduced by the data is the geometric scaling [66]. The geometric scaling can be seen as a consequence of the scaling of the dipole cross-section in the variable $\hat{r} = r/R_0(x)$. As wave functions scale in $rQ = \hat{r}QR_0(x)$, one can show that after integration over \hat{r} , the cross-section does not depend on Q^2 and x but on a single scaling variable $\tau = Q^2 R_0^2(x)$. In fig. 1.18 the data for $\sigma_{tot}^{\gamma^*p}$ versus τ , are all lying on the same line, showing clearly that the variables Q^2 and x are not independent variables. It was shown that the geometric scaling still holds in the diluted regime in the region governed by the BFKL equation up to $Q^2 \sim Q_s^4/\Lambda_{QCD}^2$ [67].

With the increasing precision of data [68, 69, 70], the original saturation model failed to describe the new set of data, as it has been checked in Ref. [71] but it inspired many studies [72, 71, 73, 74, 75, 76, 77]. A way to improve the large Q^2 behavior of the old GBW model, is inspired from the connection at large Q^2 between the gluon density $g(x, \mu^2)$ and the dipole cross-section [78],

$$\hat{\sigma}(x, r) = \frac{\pi^2}{3} r^2 \alpha_s x g(x, C/r^2), \quad (1.175)$$

with $xg(x, \mu^2)$ driven by the DGLAP evolution. The model proposed in Ref. [71] by Bartels, Golec-Biernat and Kowalski for the dipole cross-section is,

$$\hat{\sigma}(x, r) = \sigma_0 \left(1 - \exp\left(-\frac{\pi^2 r^2 \alpha_s (\mu_g^2) x g(x; \mu_g^2)}{3\sigma_0}\right)\right), \quad (1.176)$$

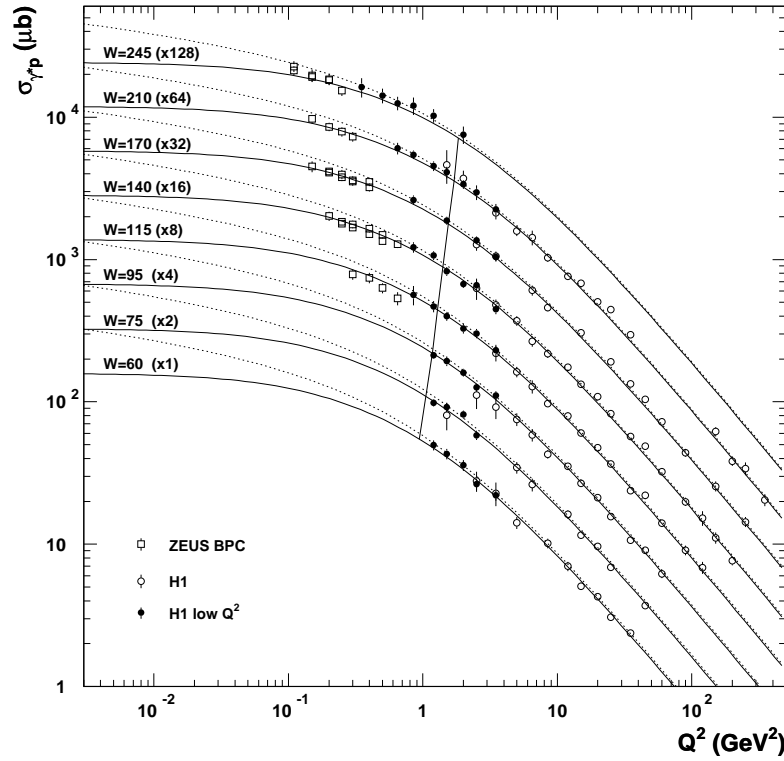


Figure 1.17: The saturation model compared to H1 and ZEUS data, [62]. The solid and dotted lines are respectively the results with $m_f = 140$ MeV and $m_f = 0$.

where the scale $\mu_g^2 = \frac{C}{r^2} + \mu_0^2$. The gluon density $g(x, \mu_g^2)$ evolves with the LO-DGLAP equation, neglecting the quark distributions as we are in the low x regime, and obeys the initial condition at $Q_0^2 = 1$ GeV²

$$xg(x, Q_0^2) = A_g x^{-\lambda_g} (1-x)^{5.6}. \quad (1.177)$$

Two sets of the parameters $\{m_f, A_g, \lambda_g, C, \mu_0^2\}$ were found to give a good description of the DIS data as shown in the table 1.2.

Fits	m_f (GeV)	A_g	σ_0 (mb)	λ_g	C	μ_0^2 (GeV ²)	χ^2/N_{df}
1	0.14	1.20	23.0	0.28	0.26	0.52	1.17
2	0	13.71	23.8	-0.41	11.10	1.00	0.97

Table 1.2: Values of the parameters entering the BGBK dipole cross-section.

The extension of this model with b -parameter dependence "b-sat" model [74, 76], for non-forward scattering amplitudes, reads

$$\mathcal{N}(x, r, b) = 1 - \exp\left(-\frac{\pi^2}{2N_c} r^2 \alpha_s(\mu_g^2) xg(x, \mu^2) T(b)\right), \quad (1.178)$$

where the proton shape in the transverse plane $T(b)$ is assumed to have a Gaussian shape. This model assumes that multiple dipoles scatter independently and the models based on this

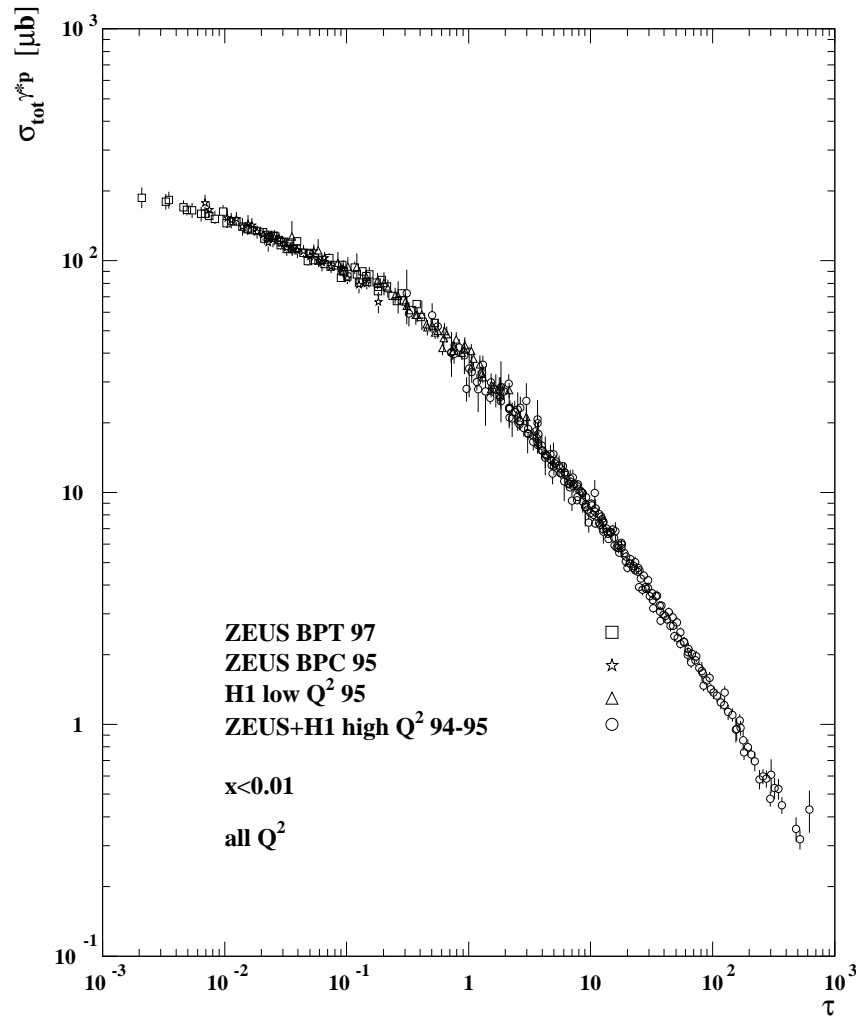


Figure 1.18: Exhibition of the geometric scaling by HERA data [66].

assumption, using the kind of parameterization of the dipole cross-section as in eq. (1.178), are referred as Glauber-Mueller models. Exclusive processes in the high energy limit offer a good opportunity to probe the gluon density shape $T(b)$ in the hadrons. The results obtained with a Gaussian shape from the electroproduction of vector mesons at HERA, give the value $\sqrt{\langle b \rangle^2} = 0.56$ fm which is slightly smaller than the proton radius charge 0.87 fm.

The saturation scale Q_s at the energies of HERA collider is of the order $Q_s(x) \sim 1$ GeV which allows a perturbative treatment of the evolution equations of the dipole scattering amplitude. In the diluted regime, the scattering amplitude is driven by the BFKL equation in the regime $Q_s^2 < Q^2 < Q_s^4/\Lambda_{QCD}^2$ [67]. In the saturation regime, the recombinations of gluons are responsible for non-linear terms in the evolution equations that describe the small- x evolution of the hadronic wave function. In the color glass condensate (CGC) formalism, the JIMWLK equation, based on the study of renormalization (a la Wilson) group equation for Wilson line correlators gives the gluon density evolution in dense partonic regime accounting for saturation effects. The JIMWLK equation is equivalent in principle to an infinite set of

coupled equations on correlators of Wilson lines known as the Balitsky hierarchy. This is due to the fact that one needs to average over the target configurations during the collisions, leading then to coupled equations between different Wilson line correlators. In the large N_c -limit, this set of infinite coupled equations involves only dipole operators T and under the assumption that $\langle TT \rangle \approx \langle T \rangle^2$, the evolution equation on $\langle T \rangle$ is given by the BK equation on $\mathcal{N} \equiv T$ the forward dipole scattering amplitude which reads at LO in the impact parameter space,

$$\begin{aligned} \frac{\partial \mathcal{N}(Y, r_{12})}{\partial Y} &= \frac{\alpha_s N_c}{2\pi^2} \int d^2 r_{0\perp} \frac{r_{12}^2}{r_{10}^2 r_{02}^2} \\ &\times (\mathcal{N}(Y, r_{01}) + \mathcal{N}(Y, r_{02}) - \mathcal{N}(Y, r_{12}) - \mathcal{N}(Y, r_{01})\mathcal{N}(Y, r_{02})) , \end{aligned} \quad (1.179)$$

with $r_{ij} = |r_{i\perp} - r_{j\perp}|$. In the CGC formalism, it was shown [79] that in the weakly coupled regime ($\mathcal{N}(Y, r) \ll 1$), one gets back the BFKL equation,

$$\frac{\partial \mathcal{N}(Y, r_{12})}{\partial Y} = \frac{\alpha_s N_c}{2\pi^2} \int d^2 r_{0\perp} \frac{r_{12}^2}{r_{10}^2 r_{02}^2} (\mathcal{N}(Y, r_{01}) + \mathcal{N}(Y, r_{02}) - \mathcal{N}(Y, r_{12})) , \quad (1.180)$$

which is the linearized version of the BK-equation where the quadratic term $\mathcal{N}(Y, r_{01})\mathcal{N}(Y, r_{02})$ is neglected as the partonic density is small. Note that the BFKL equation leads to unbound solutions related to the gluon density and responsible for the violation of the unitarity while the BK equation leads to bound solutions.

A parameterization for the dipole scattering amplitude known as the CGC model [73] comes from an approximation of the solution to the LO-BFKL equation in the vicinity of the saturation regime. The LO-BFKL solution using the Mellin moments representation of the dipole scattering amplitude reads

$$\mathcal{N}(Y, r) = \int_c \frac{d\gamma}{2i\pi} (r^2 Q_0^2)^\gamma e^{h(Y)\chi(\gamma)} \tilde{\mathcal{N}}_0(\gamma) = \int_c \frac{d\gamma}{2i\pi} \exp(h(Y)\chi(\gamma) - \gamma\rho) \tilde{\mathcal{N}}_0(\gamma) , \quad (1.181)$$

where

$$\begin{aligned} h(Y) &= \frac{\alpha_s(Q_s(Y))N_c}{\pi} Y , \quad \rho = \ln(1/r^2 Q_0^2) , \\ \chi(\gamma) &= 2\psi(1) - \psi(\gamma) - \psi(1 - \gamma), \text{ with } \psi(\gamma) = \frac{d \ln \Gamma(\gamma)}{d\gamma} , \end{aligned}$$

with Γ the Euler function. The integral over γ is evaluated by using the saddle point approximation expanding to the second order around the saturation saddle point $\gamma_0(Y) = \rho/h(Y)$. This leads to a solution of the form,

$$\mathcal{N}(Y, r) \approx \mathcal{N}_0 \exp \left(-\gamma_s(\rho - \rho_s) - \frac{\mathcal{R}_s}{2\chi''(\gamma_s)\rho_s} (\rho - \rho_s)^2 \right) \quad (1.182)$$

where $\rho_s(Y) = \ln(Q_s^2(Y)/Q_0^2)$ and $\mathcal{R}_s = \rho_s(Y)/h(Y)$. One finds back the geometric scaling when the first term " $\gamma_s(\rho - \rho_s)$ " dominates for $\rho \sim \rho_s$. The second term which is analogous to a diffusion term violates the geometric scaling.

Note that an analogy exists between the BK equation and the equation in reaction-diffusion processes in statistical physics governed by the equation of Fisher, Kolmogorov, Petrov and Piscounov (FKPP),

$$\partial_t N = \partial_z^2 N + N - N^2. \quad (1.183)$$

This analogy found by Munier and Peschanski [80, 81, 82, 83] by rescaling the BK equation [84] for the quantity

$$N(Y, k) = \int \frac{d^2 r_\perp}{2\pi r_\perp^2} \mathcal{N}(Y, r_\perp) e^{ik_\perp \cdot r_\perp},$$

was used in order to get information on the universal properties of the BK solutions which are related to traveling wave solutions.

The CGC model assumes that the approximated solution is of order $\mathcal{N}(Y, r) = \mathcal{N}_0 \sim 1$ when $r = 1/Q_s$, in order to take into account the vicinity with the saturation regime. The solution in the forward limit proposed by Iancu, Itakura and Munier in Ref. [73] is,

$$\begin{aligned} \mathcal{N}(x, r) &= \mathcal{N}_0 \left(\frac{rQ_s}{2} \right)^{2(\gamma_s + \frac{\ln(2/rQ_s)}{9.9\lambda \ln(1/x)})} \quad \text{if } rQ_s \leq 2, \\ &= 1 - \exp(-a \ln^2(brQ_s)) \quad \text{if } rQ_s \geq 2. \end{aligned} \quad (1.184)$$

where γ_s is the saddle point in the vicinity of the saturation regime. The solution for $rQ_s \geq 2$ corresponds to the functional form of solutions expected from BK- equation and the a and b are determined in order that there is no discontinuity of $\mathcal{N}(x, r)$ and its derivative. This model was extended to include the impact parameter b dependence in order to describe the exclusive diffractive processes at HERA. The first extension by Marquet, Peschanski and Soyez [85], includes the b dependence through the saturation scale, $Q_s^2(Y, \underline{\Delta}) = Q_0^2(1 + c\underline{\Delta}^2)e^{\lambda Y}$, and a multiplicative non-perturbative form factor $f(\underline{\Delta}) = e^{-B\underline{\Delta}^2}$, with $t = -\underline{\Delta}^2$. A second approach called the "b-CGC" model in Ref. [76] by Kowalski, Motyka and Watt, consists only in replacing

$$Q_s(x, b) = Q_s(x) \left(e^{-\frac{b^2}{2B_{CGC}}} \right)^{\frac{1}{2\gamma_s}}.$$

Recently, the dipole scattering amplitude has been worked out by numerical resolution of the BK equation with running coupling correction, the rcBK equation [86, 87], taking different initial conditions close to the GBW saturation model and to the McLerran-Venugopalan (MV) model [88]. We will denote these numerical solutions for the dipole scattering amplitudes as the Albacete-Armesto-Milhano-Quiroga-Salgado (AAMQS)-model. Indeed the solution of LO-BK does not work so well as it predicts a growth of the saturation scale way to fast when rapidity is increasing [67, 89]. It was shown [90, 91] that the main correction that allows to solve the discrepancy between the predictions and the data is the running coupling correction of the kernel of the BK- equation.

The rcBK equation reads

$$\begin{aligned} \frac{\partial \mathcal{N}(Y, r_{12})}{\partial Y} = & \int d^2 r_{0\perp} \frac{N_c \alpha_s(r_{12}^2)}{2\pi^2} \left[\frac{r_{12}^2}{r_{01}^2 r_{02}^2} + \frac{1}{r_{01}^2} \left(\frac{\alpha_s(r_{01}^2)}{\alpha_s(r_{02}^2)} - 1 \right) + \frac{1}{r_{02}^2} \left(\frac{\alpha_s(r_{02}^2)}{\alpha_s(r_{01}^2)} - 1 \right) \right] \\ & \times \{ \mathcal{N}(Y, r_{01}) + \mathcal{N}(Y, r_{02}) - \mathcal{N}(Y, r_{12}) - \mathcal{N}(Y, r_{01}) \mathcal{N}(Y, r_{02}) \} . \end{aligned} \quad (1.185)$$

The coupling constant in the evolution kernel of the rcBK equation (1.185) depends on the number of active quark flavors n_f ,

$$\alpha_{s,n_f}(r^2) = \frac{4\pi}{\beta_{0,n_f} \ln \left[\frac{4C^2}{r^2 \Lambda_{n_f}^2} \right]}, \quad (1.186)$$

where $\beta_{0,n_f} = 11 - \frac{2}{3}n_f$, Λ_{n_f} is the QCD scale and C is one of the free parameters of the model. The scales Λ_{n_f} are determined by the matching condition $\alpha_{s,n_f-1}(r_\star^2) = \alpha_{s,n_f}(r_\star^2)$ at $r_\star^2 = 4C^2/m_f^2$ and an experimental value of α_s . The coupling constant is frozen to a value $\alpha_{fr} \sim 1$ that it cannot exceed to avoid infra-red divergences.

The initial conditions are inspired by the GBW model $\mathcal{N}^{GBW}(Y_0, r)$ and the MV model $\mathcal{N}^{MV}(Y_0, r)$ reads

$$\mathcal{N}^{GBW}(Y_0, r) = \sigma_0^{GBW} \left\{ 1 - \exp \left[- \left(\frac{r^2 Q_{s0}^2}{4} \right)^\gamma \right] \right\}, \quad (1.187)$$

$$\mathcal{N}^{MV}(Y_0, r) = \sigma_0^{MV} \left\{ 1 - \exp \left[- \left(\frac{r^2 Q_{s0}^2}{4} \right)^\gamma \ln \left(\frac{r}{\Lambda_3} + e \right) \right] \right\}, \quad (1.188)$$

with Y_0 the rapidity that corresponds to $x_0 = 0.01$, Q_{s0} the initial saturation scale at $x = x_0$ and γ the anomalous dimension. The free parameters involved in the AAMQS model are fitted on the structure function $F_2(x, Q^2)$ and the x -dependence is completely driven by the rcBK equation.

The solutions for the dipole cross-sections are given with and without the heavy quarks charm and beauty contributions. For further use in chap. 3 we denote the solutions as follows,

- AAMQS set (a), with the initial condition given by (1.187) a la GBW, with the contribution of light quarks (u, d, s) only,
- AAMQS set (e), with the initial condition given by (1.188) a la MV, with the contribution of light quarks (u, d, s) only,
- AAMQS set (b), with the initial condition given by (1.187) a la GBW, with the contribution of light and heavy quarks (u, d, s, c, b),
- AAMQS set (f), with the initial condition given by (1.188) a la MV, with the contribution of light and heavy quarks (u, d, s, c, b).

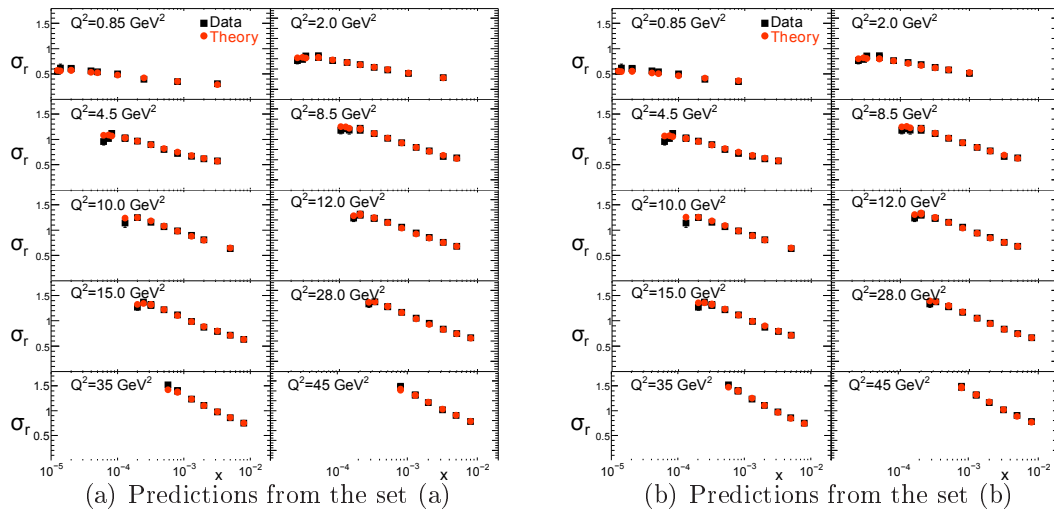


Figure 1.19: Comparison of the results for the reduced cross-section σ_r with the data, figure from ref. [87]. In (a) the results are obtained with the GBW initial condition and only the contribution of light quarks. In (b), the contribution of heavy quarks charm and beauty is included.

It turns out that the results are very weakly dependent on the choice of the initial conditions and one can restrict its choice to the sets (a) and (b). The polarized cross-sections read

$$\sigma_{L,T;\text{set(a)}}^{\gamma^*p} = \sigma_0 \sum_{f=u,d,s} \int d^2\underline{r} \int dy \left| \Psi_f^{\gamma_{L,T}^*}(y, \underline{r}; Q, m_f, e_f) \right|^2 \mathcal{N}^l(x, \underline{r}), \quad (1.189)$$

$$\begin{aligned} \sigma_{L,T;\text{set(b)}}^{\gamma^*p} &= \sigma_0^l \sum_{f=u,d,s} \int d^2\underline{r} \int dy \left| \Psi_f^{\gamma_{L,T}^*}(y, \underline{r}; Q, m_f, e_f) \right|^2 \mathcal{N}^l(x, \underline{r}) \\ &+ \sigma_0^h \sum_{f=c,b} \int d^2\underline{r} \int dy \left| \Psi_f^{\gamma_{L,T}^*}(y, \underline{r}; Q, m_f, e_f) \right|^2 \mathcal{N}^h(x, \underline{r}). \end{aligned} \quad (1.190)$$

where $\sigma_0^l \mathcal{N}^l(x, \underline{r})$ and $\sigma_0^h \mathcal{N}^h(x, \underline{r})$ are respectively the dipole cross-section contributions of light and heavy quarks.

We present in tabs. 1.3 and 1.4 values of the parameters of the fits obtained in ref. [87].

Fits	Q_{s0}^2	σ_0 (mb)	γ	C	χ^2/N_{df}
(a)	0.241	32.357	0.971	2.46	1.226
(e)	0.165	32.895	1.135	2.52	1.171

Table 1.3: Values of the parameters entering the AAMQS sets (a) and (e) dipole cross-sections.

Another kind of dipole cross-sections models [92, 93] exist based on the Regge theory, where the universal trajectories of hard and soft pomerons are fitted from HERA data. The hard pomeron exchange is involved for small dipole size $r < r_0$ and the soft pomeron exchange for large dipole size $r > r_1$. The so-called FS04 model parameterizes the dipole cross-section

Fits	Q_{s0}^2	$Q_{s0}^{(c,b)2}$	σ_0^l (mb)	σ_0^h (mb)	γ	$\gamma^{(c,b)}$	C	χ^2/N_{df}
(b)	0.2386	0.2329	35.465	18.430	1.263	0.883	3.902	1.231
(f)	0.1687	0.1417	35.449	19.066	1.369	1.035	4.079	1.244

Table 1.4: Values of the parameters entering the AAMQS sets (b) and (f) dipole cross-sections.

as,

$$\hat{\sigma}(x, r) = A_H r^2 x^{-\lambda_H} \quad \text{if } r < r_0 \quad (1.191)$$

$$= A_S x^{-\lambda_S} \quad \text{if } r > r_1, \quad (1.192)$$

combining the color transparency behavior for small r with the soft pomeron exchange behavior at large r . A linear interpolation is performed in the region of intermediate r ($r_0 < r < r_1$). An improved version of the FS04 Regge model was proposed to include saturation effects by allowing the parameter r_0 to vary in order that the dipole cross-section satisfies the condition,

$$\sigma(x, r_0)/\sigma(x, r_1) = f, \quad (1.193)$$

where the parameter f is fitted.

A general remark about the amplitudes of the exclusive diffractive processes computed within the dipole model approach, is that two kinds of corrections can be taken into account in these treatments. The first one is a correction due to the non-zero skewness involved in the process. At small x , the skewness ξ is of the order $\xi \sim \frac{x}{2}$ and it was shown that the effect of the skewness result in a multiplicative factor R_g in front of the gluon density [94],

$$R_g(\lambda) = \frac{2^{2\lambda+3}}{\sqrt{\pi}} \frac{\Gamma(\lambda + 5/2)}{\Gamma(\lambda + 4)}, \quad \text{with} \quad \lambda \equiv \frac{\partial \ln x g(x, \mu^2)}{\partial \ln(1/x)}. \quad (1.194)$$

The second one is that in the high energy limit, the imaginary part of the amplitude dominates the real part but one can evaluate the real part by using dispersion techniques. The ratio of the real and imaginary parts of the amplitude \mathcal{A} reads

$$\beta = \mathcal{R}e \mathcal{A} / \mathcal{I}m \mathcal{A} = \tan(\pi\lambda/2), \quad \text{with} \quad \lambda \equiv \frac{\partial \ln \mathcal{A}}{\partial \ln(1/x)}.$$

Chapter 2

Light-Cone Collinear Factorization applied to the ρ –meson production

2.1 Introduction

2.1.1 Diffractive exclusive vector electroproduction

In the chap. 1 we have introduced the k_T –factorization scheme that holds in the high energy limit $s \gg |t|$. In this context, we introduced the concept of hard pomeron exchange in hadronic processes and we presented color dipole models that include the idea of partonic density saturation that could restore the unitarity of the theory.

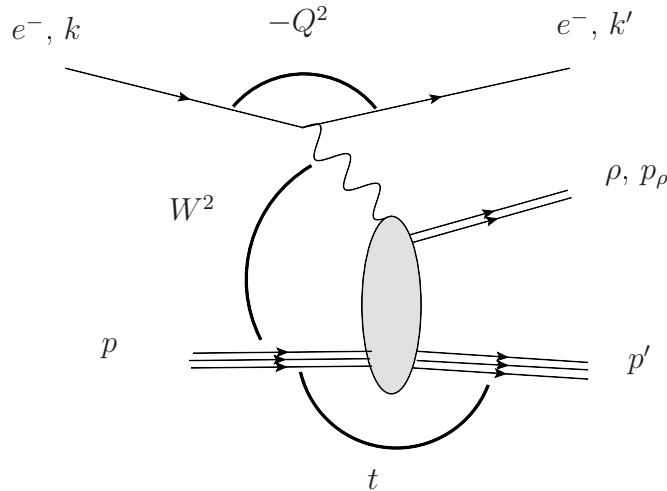


Figure 2.1: The diffractive electroproduction of the ρ –meson and Lorentz invariant kinematic variables.

The two forthcoming chapters are devoted to the study of helicity amplitudes of the diffractive leptonproduction of the ρ –meson in the high energy limit illustrated in fig. 2.1,

$$\gamma^*(q, \lambda_\gamma) p(p_p) \rightarrow \rho(p_\rho, \lambda_\rho) p(p'_p),$$

with λ_γ and λ_ρ the polarizations of the virtual photon and the ρ –meson.

The diffractive vector meson production (DVMP) at HERA as well as the deeply virtual Compton scattering (DVCS) are excellent processes to probe the hadronic content in pQCD regime. Contrary to inclusive processes, exclusive processes allows to get information on additional degrees of freedom such as the skewness dependence or the transverse distributions of gluons at small $-x$ inside the nucleon target.

A proof of the factorization theorem for the electroproduction of vector mesons was given by Collins, Frankfurt and Strikman in [95]. This theorem states that the leading twist amplitude is given by,

$$\mathcal{A} = \sum_{i,j} (f_{i/p} \otimes H_{ij} \otimes \phi_j^V)_\mu + \text{power suppressed terms}. \quad (2.1)$$

where the three main amplitude pieces are, $f_{i/p}$ the distribution function of the parton i inside the hadron p (transversity distribution if transversely polarized vector meson), H_{ij} the hard scattering amplitude and Φ_j^V the light cone wave function of the vector meson. The parameter μ is the renormalization-factorization scale which should be chosen of the order of the virtuality Q of the photon in order to compute the coefficient function H_{ij} using perturbative theory at a finite order of the expansion. It was also shown by power counting argument that the production from a transversely polarized virtual photon is suppressed by $1/Q$ compared to the production from a longitudinal photon.

The DVMP has been the subject of many experiments. The pioneering experiments on small $-x$ diffractive muon-production of vector mesons were analyzed on deuterium, calcium and carbon targets down to $x \sim 5 \cdot 10^{-3}$ by the NMC collaboration [96] and on proton target down to $x \sim 2 \cdot 10^{-4}$ by the E665 collaboration [97], for a wide range of virtualities. The HERA collaborations ZEUS and H1 have provided very precise data with respectively integrated luminosity of 120 pb^{-1} and 51 pb^{-1} on the spin density matrix elements of the diffractive ρ^0 and ϕ mesons production in a small $-x$, for a wide range of energies W in the center of mass γ^*p and photon virtualities Q . The recent analysis provided by ZEUS in 2007 [98] and by H1 in 2009 [99] are a motivating experimental background to investigate the helicity amplitudes of the vector meson production at small $-x$. These analysis supersede the former analysis already performed by these collaborations in late 90's [100, 101, 102]. The data of H1 and ZEUS are precious to access such important universal quantities as the pomeron trajectory, through the energy dependence and the t -dependence of the differential cross-section. One usually uses ansatz for the vector meson wave functions based on the dipole configuration inside the vector meson constituted by the valence quarks. The data allows to investigate the factorization procedure as well as the content of the ρ -meson wave function.

The DVMP was also analyzed by HERMES [103, 104, 105], JLab [106] and COMPASS [107] in other kinematic range of lower energies in the center of mass, i.e. higher x , essential to understand the pQCD approaches based on collinear factorization and GPDs.

There are many models derived from mostly three theoretical approaches (we will not make here a review of all the models). Two of the approaches are equivalent approaches, the k_T -factorization approach and the color dipole approach, the third is the collinear factorization approach. As we saw in the chap. 1, k_T -factorization allows to regroup the particles into

sub-processes involving the incoming and outgoing particles of approximately same rapidities leading to two impact factors exchanging reggeized gluons which resum the gluons exchanged in t -channel. In the case of the DVMP the helicity amplitudes as illustrated in fig. 2.2 read,

$$T_{\lambda_V \lambda_\gamma} \propto is \int \frac{d^2 k_\perp}{k_\perp^4} \Phi^{\gamma_{\lambda_\gamma}^* \rightarrow V_{\lambda_V}}(Q^2, k_\perp), \quad (2.2)$$

with $\mathcal{F}(x, k_\perp)$ the unintegrated gluon density.

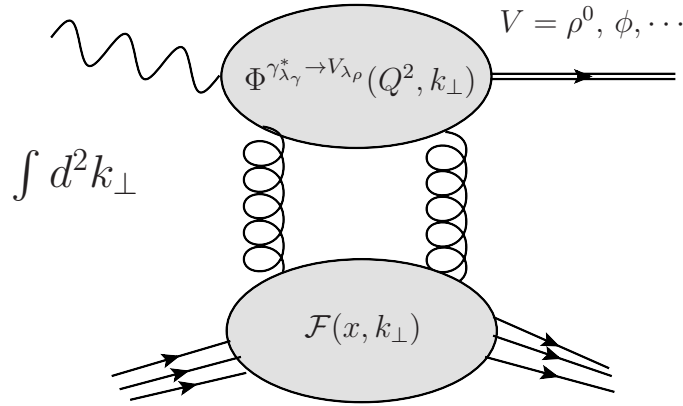


Figure 2.2: k_T -factorization of the DVMP.

The energy dependence of the process is then given by the BFKL evolution for the unintegrated gluons density known at LLx [34, 35, 36, 37] and NLLx [108, 109, 110, 111].

This approach needs a model for the proton impact factor at Born order or a model for the unintegrated gluon density of the nucleon target. It is the approach we will use in the second part of this chapter to get a model for the helicity amplitude $T_{\lambda_\rho \lambda_\gamma}$. Let us describe some of the applications of this approach.

Martin, Ryskin and Teubner (MRT) [112] have pointed out that the diffractive ρ -meson production data from HERA indicates that it should be treated within pQCD. They proposed a model based on the parton-hadron duality, to express the ρ -meson production cross-section as

$$\sigma_{\gamma^* p \rightarrow \rho p} \approx 0.9 \sum_{q=u,d} \int dM^2 \frac{d\sigma_{\gamma^* p \rightarrow (q\bar{q})p}}{dM^2}, \quad (2.3)$$

with M^2 the invariant mass of the $q\bar{q}$ system. Using k_T -factorization approach and a gluon density ansatz $xg(x, Q^2) \sim x^{-\lambda}(Q^2)^\gamma$, with γ the effective anomalous dimension of the gluon density, leads to the ratio of polarized cross-sections

$$\frac{\sigma_L}{\sigma_T} = \frac{Q^2}{M^2} \left(\frac{\gamma}{\gamma + 1} \right)^2. \quad (2.4)$$

More recent models based on the k_T -factorization and model of gluon density exist, e.g. the model from Ivanov, Nikolaev and Savin [113], which allows predictions for all spin density matrix elements for the electroproduction of ρ -meson.

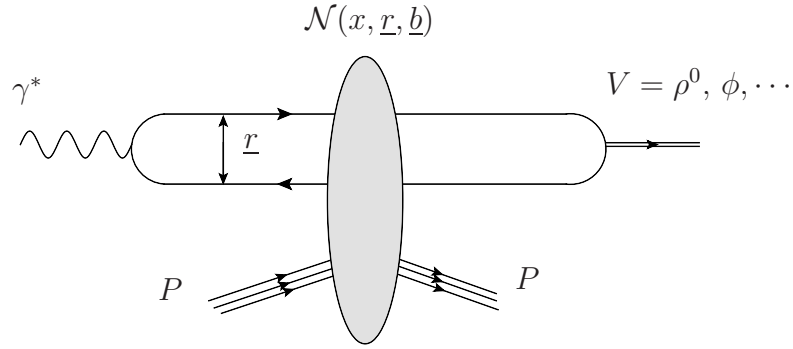


Figure 2.3: DVMP within the color dipole picture.

The color dipole approach of DVMP illustrated in fig. 2.3, is equivalent to the k_T -factorization scheme but in impact parameter space where the convolution of the wave functions of the initial projectile and final state can be factorized even at low Q^2 , from the dipole target scattering amplitude. Like in the k_T -factorization scheme the dipole target cross-section has to be modeled and contains the x -dependence of the process. This x -dependence is linked to the behavior the gluon density $xg(x, Q^2) \sim x^{-\lambda}$. The amplitude takes the form

$$T_{\lambda_\rho \lambda_\gamma} = \int_0^1 dy \int d^2 \underline{r} \left(\Psi_{\lambda_\rho}^{\rho*} \Psi_{\lambda_\gamma}^\gamma \right) (y, \underline{r}) \mathcal{A}_{(q\bar{q})p \rightarrow (q\bar{q})p'}(x, \underline{r}), \quad (2.5)$$

where y and \underline{r} are respectively the fraction of longitudinal momentum and the transverse size of the dipole. In the previous chapter we have already mentioned some of the models that exist for the dipole cross-section. Note that another type of approach exists based on the generalized vector dominance to get the DVMP amplitudes, see e.g. [114] where predictions are made for the ratios of helicity amplitudes. The ρ -meson wave functions are unknown but many models have been proposed. Some of them assume the factorization of the transverse degrees of freedom from the longitudinal ones. For example the model of Dosch, Gousset, Kulzinger and Pirner (DGKP) model [115], where the transverse size dependence is assumed to be independent from y and to have a Gaussian shape. Other models, for example the Nemchik, Nikolaev, Predazzi and Zakharov (NNPZ) model [116, 117, 113] or models proposed by Forshaw, Sandapen and Shaw [118, 119, 120], assume a dynamics of the constituent quark antiquark pair that is in agreement with the size of the meson suggested by spectroscopic models in the rest frame of the meson. The light-cone meson wave functions are then obtained by applying a "relativization procedure" which allows to get their expressions in the infinite momentum frame. In general the dynamics of the $q\bar{q}$ pair assumed in the rest frame is given by an harmonic oscillator potential for the large distance dynamics and the short distance dynamics is driven by a Coulombic potential term.

Another approach close to the MRT model, based on the k_T -factorization scheme in the impact parameter space, is followed in ref. [121] by Ivanov and Kirschner to factorize the wave functions of the virtual photon and the vector meson. The vector meson wave function and the dipole scattering amplitude are then expanded around small dipole size and the end-point divergences when $y \rightarrow \{0, 1\}$ are regularized by the scale dependence of the gluon

density. This model allows to get predictions for the full set of helicity amplitudes.

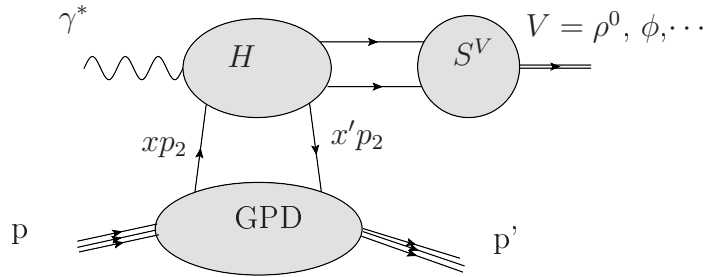


Figure 2.4: Leading hand bag diagrams in the collinear factorization approach.

The collinear factorization approach initiated in [122, 123] by Brodsky, Frankfurt, Gunion, Koepf, Mueller and Strikman, based on the collinear factorization scheme eq. (2.1) [95, 124] where the amplitude is factorized as illustrated in fig. 2.4 into GPDs, distributions amplitudes (DAs) of the ρ -meson and a hard process calculable using pQCD.

The longitudinally polarized amplitude reads

$$T_{00} \propto \int dy \int dx f_i(x, x') H_{ij}(y, x, x') \Psi_j^V(y), \quad (2.6)$$

with y the usual fraction of photon longitudinal momentum carried by one of the quark, $f_i(x, x')$ represents GPDs, which are the probability to find the parton i inside the proton that carries x fraction of its longitudinal momentum and comes back inside the proton with the fraction x' . GPDs are a generalization of PDF to the non-forward limit $x \neq x'$ allowing to take into account skewness effects. H_{ij} is the hard sub-process where the parton i gives a parton j that hadronizes into the meson with integrated wave function Ψ_j^V . The collinear factorization scheme have been improved to remove end-point singularities that appear for the transversely polarized cross-section using Sudakov factors [125], which allows to overcome end-point singularity problems, and has been applied to ρ -electroproduction through the VGG model [126] and the Kroll and Goloskokov model [127, 128, 129]. In practice the end-point singularities are regularized by keeping the transverse momenta of the $q\bar{q}$ pair that forms the vector meson and by assuming that they are distributed by a Gaussian distribution that prevents large dipole size configurations. Note that this approach is valid not only in the large energy limit but also for $W \sim Q$. The GPDs are not known and have to be modeled starting from the PDFs forms and implementing the skewness and t -dependencies.

2.1.2 The underlying ideas of our approach

In the approach presented below, we use at a first level the k_T -factorization to factorize the $\gamma^*(\lambda_\gamma) \rightarrow \rho(\lambda_\rho)$ impact factor in the amplitude. Using the fact that the virtuality of the photon is large, we can apply the collinear factorization scheme to factorize the soft part associated to the ρ -meson production from the partons produced in the hard part. Note that the notion of twist here is defined as the twist of the operators involved in the $(q\bar{q}) \rightarrow \rho$ and $(q\bar{q}g) \rightarrow \rho$ meson production and not in the sense of the twist of the operators of the

$\gamma^*p \rightarrow \rho p$ amplitude. This approach was performed a long time ago by Ginzburg, Panfil and Serbo [130] up to twist 2 for the $\gamma_L^* \rightarrow \rho_L$ and $\gamma_T^* \rightarrow \rho_L$ transitions and was recently derived by Anikin, Ivanov, Pire, Szymanowski and Wallon [131] for the $\gamma_T^* \rightarrow \rho_T$ transition up to twist 3 in the forward limit. The presence of the k_\perp of the t -channel gluons, regularizes the end-point divergences as it gives a finite size of the order $r \sim 1/k_\perp$ to the $q\bar{q}$ pair. The quark and the antiquark, after the interaction with the t -channel gluons, are flying collinearly and hadronize into a ρ -meson. A little deviation from the collinear direction aligned on the ρ -meson momentum will give higher twist corrections and we will present how to take into account these higher twist corrections up to twist 3.

The chapter can be divided in two parts. The first part is the description of the so-called light-cone collinear factorization (LCCF) procedure [132, 133, 134], inspired from the initial Ellis–Furmanski–Petronzio (EFP) factorization [135, 136, 137, 138, 139, 140], generalized for exclusive processes. This factorization scheme uses the Taylor expansion of the hard part around the dominant light-cone direction in the light cone gauge to get the higher twist contributions. We will present the LCCF on the calculation of the impact factors $\gamma^* \rightarrow \rho$, following the approach of Ref. [131]. This approach being gauge invariant, a connection between the LCCF results and the results obtained within another approach called the covariant collinear factorization (CCF) approach can be established. The relations between the CCF DAs and the LCCF DAs were derived in [131]. A model developed by Ball, Braun, Koike and Tanaka in [141, 142], based on the conformal symmetry of the non-local correlators in the CCF approach, is then used to get a model for the LCCF DAs.

In the second part of the chapter we will present a model [18] using an impact factor model [143] for the proton, based on the results of the first part. At the end we compare the predictions to HERA data.

2.2 Light-cone collinear factorization up to twist 3 accuracy

2.2.1 Soft parts and hard parts

We consider the \mathcal{S} -matrix element of the lepton production of the ρ -meson involving a hard part where a highly virtual photon dissociates into the constituent partons involved in the ρ -meson final state wave function and a soft part which describes the hadronization of these partons into the ρ -meson. Up to twist 3, one needs to consider the two $(q\bar{q})$ and three $(q\bar{q}g)$ parton intermediate Fock states and we will denote respectively $\mathcal{A}_{q\bar{q}}$ and $\mathcal{A}_{q\bar{q}g}$ the associated amplitudes. The partons interact at Born order with two t -channel gluons with non-sense polarizations as illustrated in fig. 2.5.

The main idea is to separate the process into the hard sub-process involving the small distance physics that can be treated in the pQCD approach and the soft sub-process involving the long distance interactions between the partons in the hadronic state. The hard sub-

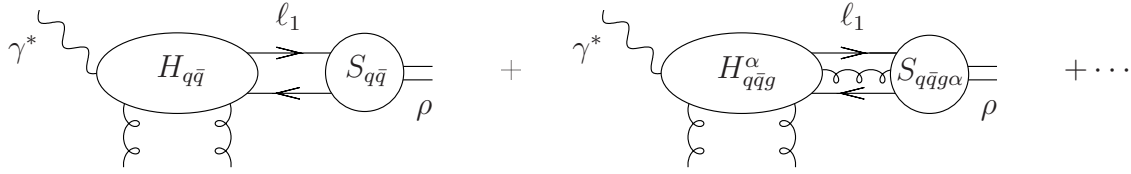


Figure 2.5: 2- and 3-parton correlators attached to a hard scattering amplitude in the specific case of the $\gamma^* \rightarrow \rho$ impact factor, where vertical lines are hard t -channel gluons in the color singlet state.

process corresponds to the Feynman diagrams where the partons are propagating the hard scale which is the virtuality of the photon Q , this hard part is then related to the photon vertex. The soft part of the process cannot be described in terms of free field operators due to the interactions with other partons in the non-perturbative regime, and one ends up with soft parts expressed in terms of interacting fields in the Heisenberg picture operators. In order to get gauge invariant operators in the soft parts, one needs also to include the gluonic radiations into the final state due to the motion of the partons, which in practice results in the presence of Wilson lines linking the coordinates of the partonic fields.

The amplitudes read

$$i\mathcal{A}_{q\bar{q}} = \int \frac{d^4\ell_1}{(2\pi)^4} \text{Tr} (H_{q\bar{q}}(\ell) S_{q\bar{q}}(\ell)) , \quad (2.7)$$

$$i\mathcal{A}_{q\bar{q}g} = \int \frac{d^4\ell_1}{(2\pi)^4} \frac{d^4\ell_g}{(2\pi)^4} \text{Tr} (H_{q\bar{q}g}^\alpha(\ell_1, \ell_g) S_{q\bar{q}g\alpha}(\ell_1, \ell_g)) , \quad (2.8)$$

where we explicitly put the integral over ℓ_1 and ℓ_g , the momenta of the quark and the gluon involved in the loops. The hard parts of these processes are denoted with $H_{q\bar{q}}$ and $H_{q\bar{q}g}^\alpha$ and the soft parts by $S_{q\bar{q}}$ and $S_{q\bar{q}g\alpha}$. The traces are over spinor and color indices of the hard and soft parts. More explicitly the soft parts are given by the Fourier transforms of the non-local correlators of the partonic fields¹ between the vacuum and the ρ -meson states

$$S(\ell) = \int d^4z \langle \rho(p_\rho) | \psi(0)[0, z] \bar{\psi}(z) | 0 \rangle_{\mu_F^2} e^{-i\ell \cdot z} , \quad (2.9)$$

$$\begin{aligned} S_\alpha(\ell_1, \ell_g) &= \int d^4z_1 d^4z_g e^{-i\ell_g \cdot z_g - i\ell_1 \cdot z_1} \\ &\times \langle \rho(p_\rho) | \psi(0)[0, z_g] g A_\alpha^T(z_g)[z_g, z_1] \bar{\psi}(z_1) | 0 \rangle_{\mu_F^2} , \end{aligned} \quad (2.10)$$

where the brackets are Wilson lines defined by the path-ordered product

$$[z_1, z_2] \equiv \mathcal{P} \exp \left(ig \int_0^1 dt (z_1 - z_2)^\nu A_\nu(t z_1 + (1-t) z_2) \right) .$$

In the following parts we will omit to write Wilson lines in the correlators, we will see that they reduce to a factor one in a specific axial gauge in which we will choose to work. The

¹The flavor of the $q\bar{q}$ pairs involved in the ρ^0 -meson wave function $|\rho^0\rangle = \frac{1}{\sqrt{2}}(|\bar{u}u\rangle - |\bar{d}d\rangle)$, is restored by considering a flavorless $q\bar{q}$ pair of electric charge $\frac{e}{\sqrt{2}}$. The fields $\bar{\psi}$ and ψ here are then associated to a flavorless $q\bar{q}$ pair with an electric charge $\frac{e}{\sqrt{2}}$.

scale μ_F is the factorization scale under which the internal momenta of the partons inside the hadron are integrated over. This scale allows to separate the large distance physics inside the hadron from the small distance physics.

The hard sub-process is described by Feynman diagrams shown in fig. 2.7 for the $q\bar{q}$ intermediate state amplitude, and in figs. 2.8, 2.9 and 2.10, for respectively the "abelian", the "non-abelian with one triple gluon vertex" and the "non-abelian with two triple gluons vertices" diagrams for the $q\bar{q}g$ intermediate state amplitude. Let us emphasize the fact that in all these diagrams the external partonic legs are amputated.

Let us illustrate how one can decompose the amplitude into in one hand the Fourier transform of a space coordinate correlator and on the other hand the usual momentum space representation amplitude given by Feynman diagrams. We choose a very simple example; the amplitude of a photon decaying into a $q\bar{q}$ pair, as shown in fig. 2.6.

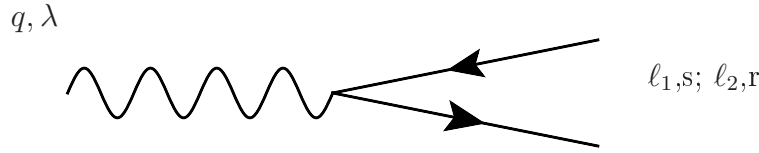


Figure 2.6: $\gamma \rightarrow q\bar{q}$, decomposition in two pieces of the amplitude.

The amplitude can be written as follows,

$$\begin{aligned}
 i\mathcal{A} &= \langle \ell_1, s; \ell_2, r | -ie \int d^4z \bar{\psi}(z) \not{A}(z) \psi(z) | q, \lambda \rangle \\
 &= \varepsilon_\mu(q, \lambda) \langle \ell_1, s; \ell_2, r | -ie \int d^4z \bar{\psi}_s(z) \gamma_{sr}^\mu \psi_r(z) | 0 \rangle \\
 &= (-ie \not{\varepsilon}(q, \lambda))_{rs} \int d^4z \langle \ell_1, s; \ell_2, r | \bar{\psi}_s(z) \psi_r(z) | 0 \rangle .
 \end{aligned} \tag{2.11}$$

In the last line we see that the amplitude reads as the trace of a hard part $(-ie \not{\varepsilon}(q, \lambda))_{rs}$ amputated of the external $q\bar{q}$ external legs, multiplied by the local correlator

$$\int d^4z \langle \ell_1, s; \ell_2, r | \bar{\psi}_s(z) \psi_r(z) | 0 \rangle .$$

In this simple example, the correlator is local as it involves only one vertex and it reduces to $\bar{u}_s(\ell_1)v_r(\ell_2)$ as the final state is a $q\bar{q}$ state contrary to our case where the final state is a hadronic state with complicated interactions between the external fields. The eqs. (2.7) and (2.8) are obtained in the same way, the final correlators cannot be calculated within pQCD and have to be parameterized as we will see later after applying the light-cone collinear factorization procedure which allows to fully separate the hard parts from the soft parts which are still linked by color, spinor indices and the 4-momentum integrals over the intermediate parton momenta.

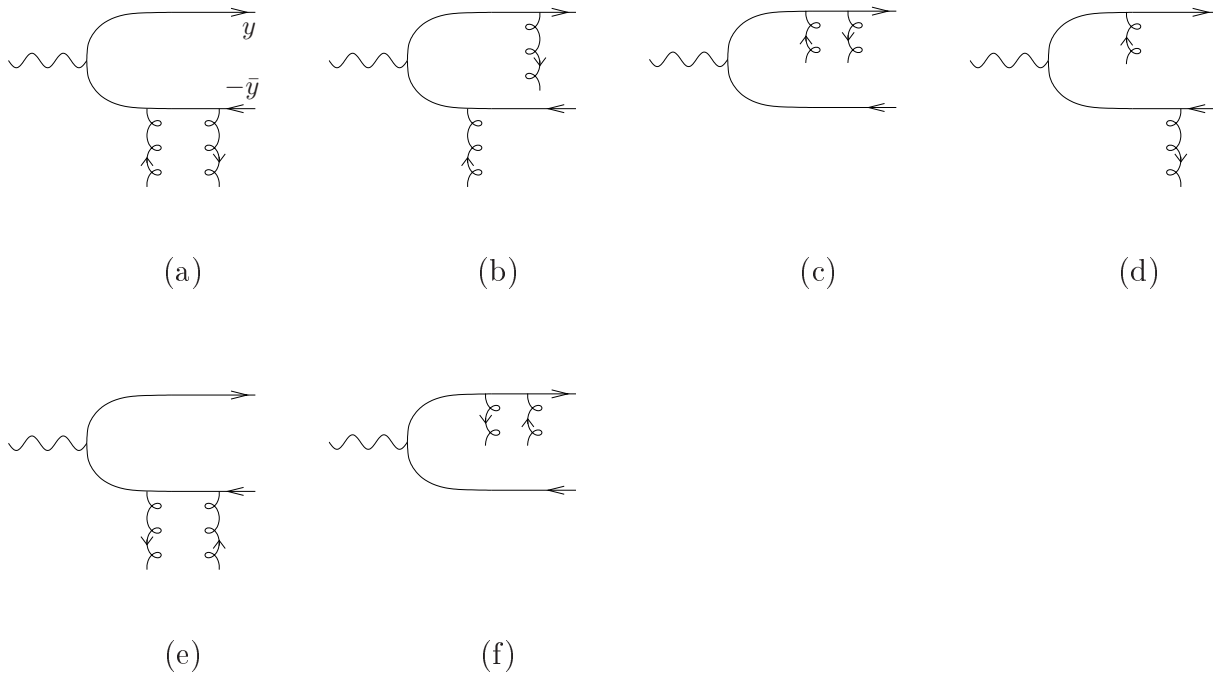


Figure 2.7: The 6 hard diagrams attached to the 2-parton correlators, which contribute to the $\gamma^* \rightarrow \rho$ impact factor.

2.2.2 Factorization of the spinor indices

Let us introduce very helpful identities called Fierz identity in the spinor space, which is a decomposition on the basis of the sixteen Dirac matrices²

$$\begin{array}{ccccc}
 \Gamma_S & \Gamma_V^\mu & \Gamma_T^{\mu\nu} & \Gamma_A^\mu & \Gamma_P \\
 I & \gamma^\mu & \sigma^{\mu\nu} = \frac{i}{2}[\gamma^\mu, \gamma^\nu] & \gamma^5 \gamma^\mu & i \gamma^5
 \end{array}$$

We denote the inverse of the Dirac matrix

$$\Gamma_\alpha \equiv (\Gamma^\alpha)^{-1}. \quad (2.12)$$

The inverse matrix are explicitly given by

$$\begin{aligned}
 (\gamma^\mu)^{-1} &= \gamma_\mu \equiv \Gamma_{V\mu}, & (\sigma^{\mu\nu})^{-1} &= \sigma_{\mu\nu} \equiv \Gamma_{T\mu\nu}, \\
 (\gamma^5 \gamma^\mu)^{-1} &= \gamma_\mu \gamma^5 \equiv \Gamma_{A\mu}, & (i \gamma^5)^{-1} &= -i \gamma^5 \equiv \Gamma_P^{-1}.
 \end{aligned} \quad (2.13)$$

The Fierz identity in spinor space reads

$$\delta_{b\bar{b}} \delta_{a\bar{a}} = \frac{1}{4} \Gamma_{\alpha \bar{b}a} \Gamma_{ab}^\alpha. \quad (2.14)$$

Any matrix of the spinor space can be decomposed as

$$X = x_\alpha \Gamma^\alpha = \frac{1}{4} \Gamma^\alpha \text{Tr}(X \Gamma_\alpha) = \frac{1}{4} \Gamma_\alpha \text{Tr}(X \Gamma^\alpha), \quad (2.15)$$

²The convention taken is $\gamma_5 = i \gamma^0 \gamma^1 \gamma^2 \gamma^3$.

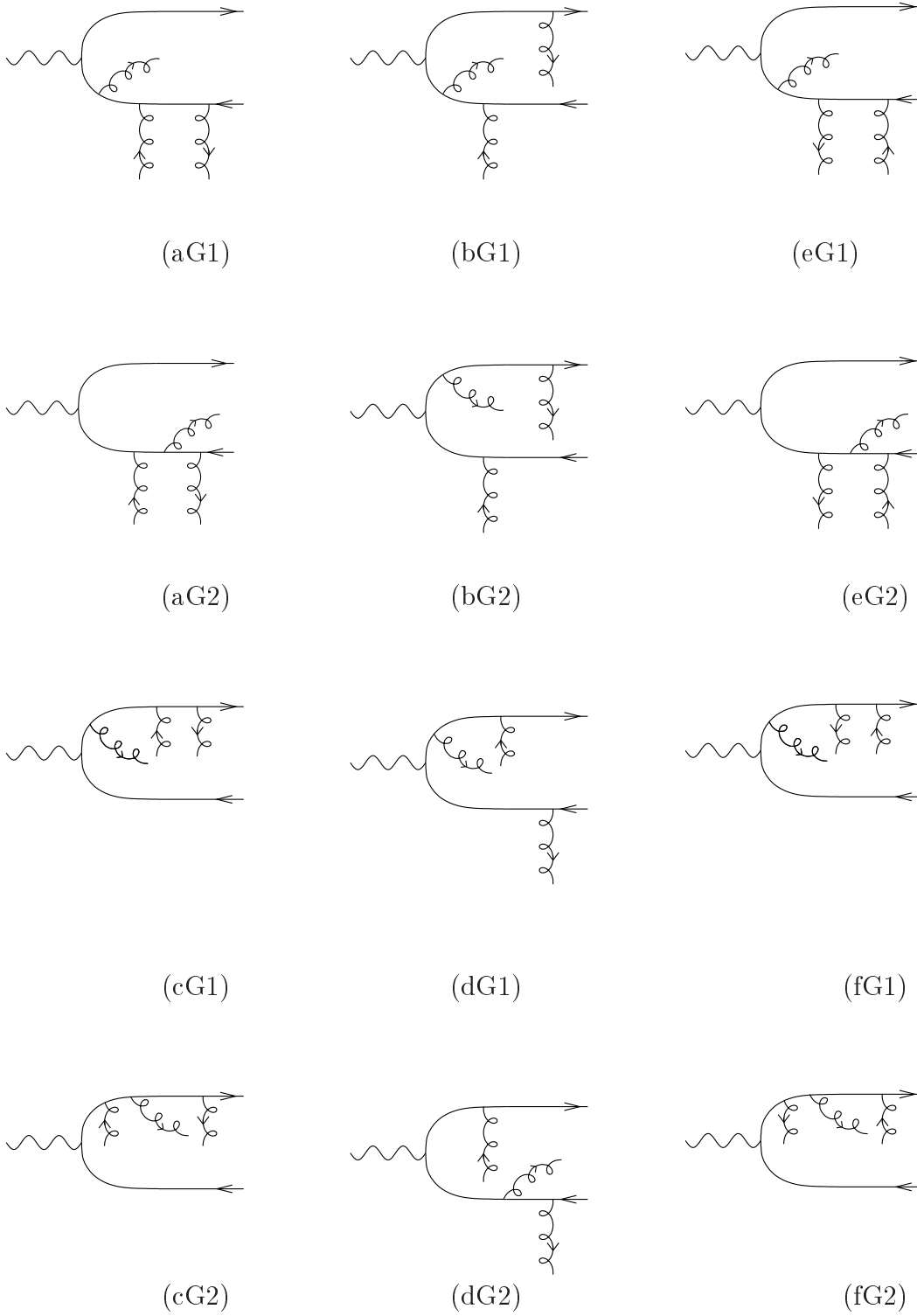


Figure 2.8: The 12 "Abelian" (i.e. without triple gluon vertex) type contributions from the hard scattering amplitude attached to the 3-parton correlators for the $\gamma^* \rightarrow \rho$ impact factor.

based on the identity,

$$\text{Tr } \Gamma^\alpha \Gamma_\beta = 4\delta_\beta^\alpha. \quad (2.16)$$

The Fierz identity can be illustrated as in fig. 2.11. We use this identity to factorize the

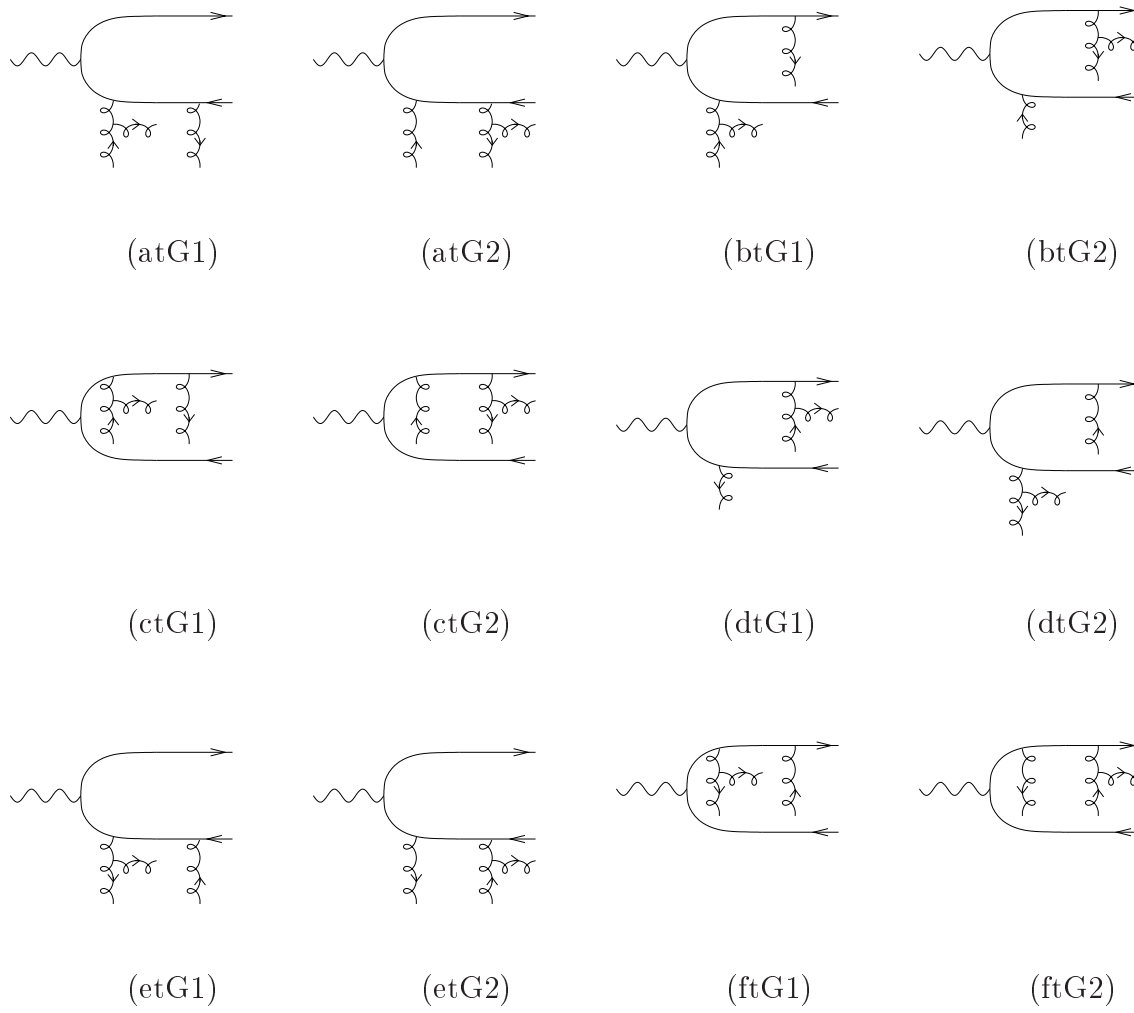


Figure 2.9: The 12 "non-Abelian" -(with one triple gluon vertex) contributions from the hard scattering amplitude attached to the 3-parton correlators, for the $\gamma^* \rightarrow \rho$ impact factor.

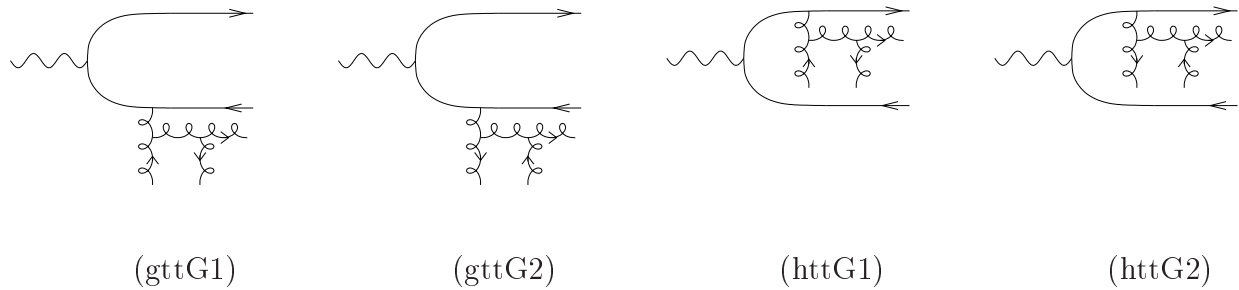


Figure 2.10: The 4 "non-Abelian" -(with two triple gluon vertices) contributions from the hard scattering amplitude attached to the 3-parton correlators, for the $\gamma^* \rightarrow \rho$ impact factor.

spinor indices of the hard and soft parts,

$$\begin{aligned}
 \text{Tr}(H S) &= H_{ij} S_{ij} = H_{rs} \delta_{ir} \delta_{js} S_{ij} = \frac{1}{4} \sum_{\Gamma} H_{rs} S_{ij} \Gamma_{rs}^{\mu} \Gamma_{\mu ij} \\
 &= \frac{1}{4} \sum_{\Gamma} \text{Tr}(H \Gamma^{\mu}) (S \Gamma_{\mu}) .
 \end{aligned} \tag{2.17}$$

Figure 2.11: Fierz identity in spinor space.

In our case, a minus sign comes from the Wick theorem, one has to commute the spinor fields,

$$-\langle \psi_r \bar{\psi}_s \rangle = \frac{1}{4} \langle \bar{\psi} \gamma_\mu \psi \rangle \gamma_{rs}^\mu + \frac{1}{4} \langle \bar{\psi} \gamma_5 \gamma_\mu \psi \rangle (\gamma^\mu \gamma_5)_{rs} + \dots \quad (2.18)$$

where we have put explicitly the spinor indices r and s of the fermionic fields.

Note that the spinor indices factorization only involves the fermionic fields, and consequently the Fierz decomposition goes the same way for the $q\bar{q}$ and the $q\bar{q}g$ intermediate states.

2.2.3 Factorization of the color indices

The Fierz identity can be also derived in color space. Assuming the normalization of the generators t

$$\text{Tr}(t^a t^b) = \frac{1}{2} \delta^{ab}, \quad (2.19)$$

one can show the Fierz identity for the generators of $SU(N_c)$,

$$t_{ij}^a t_{kl}^a = \frac{1}{2} \left(\delta_{il} \delta_{jk} - \frac{1}{N_c} \delta_{ij} \delta_{kl} \right), \quad (2.20)$$

which graphically reads

In the case of the $q\bar{q}$ exchange, we can use this identity as

with i, j are the hard part indices and k, l are soft part indices. Then we see that the first term of the r.h.s. will give zero once projected on a color singlet state because of the gluon coupling to the fermionic fields involved in the soft part. Hence the trace over the color indices of the hard and soft part can be written as

$$\text{Tr}(H_{q\bar{q}} S_{q\bar{q}}) = \frac{1}{N_c} \text{Tr}(H_{q\bar{q}}) \text{Tr}(S_{q\bar{q}}).$$

The normalization of the $q\bar{q}g$ singlet state in color space is $2/(N_c^2 - 1)$ leading to the factorized expression

$$\text{Tr}(H_{q\bar{q}g} S_{q\bar{q}g}) = \frac{2}{N_c^2 - 1} \text{Tr}(H_{q\bar{q}g}) \text{Tr}(S_{q\bar{q}g}),$$

for the $q\bar{q}g$ amplitude.

2.2.4 Factorization in the momentum space around the light cone direction p

The amplitude $i\mathcal{A}_{q\bar{q}}$ after factorization of the spinor and color indices³ reads

$$i\mathcal{A}_{q\bar{q}} = -\frac{1}{4} \sum_{\{\Gamma\}} \int \frac{d^4\ell}{(2\pi)^4} \text{Tr} (H_{q\bar{q}}(\ell)\Gamma^\mu) S_{q\bar{q}}^{\Gamma^\mu}(\ell), \quad (2.23)$$

$$i\mathcal{A}_{q\bar{q}g} = -\frac{1}{4} \sum_{\{\Gamma\}} \int \frac{d^4\ell_1}{(2\pi)^4} \int \frac{d^4\ell_g}{(2\pi)^4} \text{Tr} (H_{q\bar{q}g}^\alpha(\ell_1, \ell_g)\Gamma^\mu) S_{q\bar{q}g\alpha}^{\Gamma^\mu}(\ell_1, \ell_g), \quad (2.24)$$

with

$$S_{q\bar{q}}^{\Gamma^\mu}(\ell) \equiv \int d^4z \langle \rho(p_\rho) | \bar{\psi}(z)\Gamma_\mu\psi(0) | 0 \rangle e^{-i\ell \cdot z}, \quad (2.25)$$

$$S_{q\bar{q}g\alpha}^{\Gamma^\mu}(\ell_1, \ell_g) \equiv \int d^4z_1 d^4z_g \langle \rho(p_\rho) | \bar{\psi}(z_1) g\Gamma_\mu A_\alpha^T(z_g)\psi(0) | 0 \rangle e^{-i\ell_1 \cdot z_1 - i\ell_g \cdot z_g}. \quad (2.26)$$

The factorization in momentum space around the dominant light cone vector requires that we define a basis of light-cone vectors on which the partonic momenta can be decomposed in order then to Taylor expand the hard part around the dominant light cone vector. We define then two light like vectors p and n , which satisfy $p \cdot n = 1$ and such as p is the dominant light cone direction, p and n are denoted usually the "plus" and "minus" light cone vectors. The dominant light cone direction in our case is given naturally by the direction of the ρ -meson

$$p_\rho = p + \frac{m_\rho^2}{2} n \stackrel{\text{twist } 3}{=} p,$$

as the mass term of the vector meson leads to kinematic twist corrections starting at twist 4 which is beyond the scope of this study. Note that the choice of the light cone vector n is not unique. The amplitude at the end should not depend on the particular choice of this vector and this will give additional constraints on the DAs as we will see in the section 2.4.2.

The momenta of the quark ℓ_1 and the antiquark ℓ_2 in the two-parton amplitude are decomposed as

$$\ell_1 = yp + \beta_1 n + \ell_\perp \quad \text{and} \quad \ell_2 = \bar{y}p + \beta_2 n - \ell_\perp. \quad (2.27)$$

Following [144, 138], in this approach the partons are on the mass-shell leading to

$$\beta_1 = \frac{\ell^2}{2y} \quad \text{and} \quad \beta_2 = \frac{\ell^2}{2\bar{y}},$$

For the three-parton amplitude, the quark ℓ_1 , antiquark ℓ_2 and gluon ℓ_g momenta are decomposed as

$$\ell_1 = y_1 p + \beta_1 n + \ell_{1\perp}, \quad (2.28)$$

$$\ell_2 = \bar{y}_2 p + \beta_2 n + \ell_{2\perp}, \quad (2.29)$$

$$\ell_g = y_g p + \beta_g n + \ell_{g\perp}. \quad (2.30)$$

³The Fierz coefficients from color space factorization $1/N_c$ and $2/(N_c^2 - 1)$ are implicitly put in the hard part expressions for conciness of the formulas.

the momentum conservation and the on-shellness of the partons, imply that

$$y_g = y_2 - y_1, \quad \ell_{g\perp} = -(\ell_{1\perp} + \ell_{2\perp}), \quad 2(\beta_1 + \beta_2 + \beta_g) = \frac{\ell_1^2}{y_1} + \frac{\ell_2^2}{y_2} + \frac{\ell_g^2}{y_g}.$$

We decompose the Fourier conjugate in coordinate space z_i of the momentum ℓ_i as

$$z_i = \gamma_i p + \lambda_i n + z_{i\perp}.$$

Let us focus on the two-parton contribution. The leading twist contribution to the amplitude is given by assuming that the quark and the antiquark are flying collinearly to the direction of the ρ -meson

$$H_{q\bar{q}}(\ell_1) \equiv H_{q\bar{q}}(y, \beta_1, \ell_\perp) \approx H_{q\bar{q}}(y), \quad (2.31)$$

which correspond to the zero order term of the Taylor expansion of the hard part around the dominant light cone direction p .

The contributions in each order in $1/Q$, are given by the Taylor expansion of the hard part around the dominant light cone direction p [144, 138]. Up to twist 3, this expansion can be interpreted as the emission from the hard part of a $q\bar{q}$ pair with a very small relative transverse momentum justifying the Taylor expansion around the collinear direction. The relevant terms of the Taylor expansion up to twist 3 are

$$\begin{aligned} H_{q\bar{q}}^{\Gamma\mu}(\ell_1) &= H_{q\bar{q}}^{\Gamma\mu}(y) + H_{q\bar{q}}^{\nu,\Gamma\mu}(y) (\ell_1 - yp)_\nu + \cdots \\ &\stackrel{\text{twist } 3}{\approx} H_{q\bar{q}}^{\Gamma\mu}(y) + H_{q\bar{q}}^{\nu,\Gamma\mu}(y) \ell_{1\perp\nu}. \end{aligned} \quad (2.32)$$

where, for conciseness, we use the notations

$$H_{q\bar{q}}^{\Gamma\mu} \equiv \text{Tr}(H_{q\bar{q}}\Gamma^\mu), \quad H_{q\bar{q}}^{\nu,\Gamma\mu} \equiv \frac{\partial}{\partial \ell_{1\nu}} \text{Tr}(H_{q\bar{q}}\Gamma^\mu).$$

The term of n -th order of this Taylor expansion reads

$$\frac{\partial^n}{\partial \ell_{1\nu_1} \cdots \partial \ell_{1\nu_n}} \text{Tr}(H_{q\bar{q}}\Gamma^\mu) (\ell_1 - yp)_{\nu_1} \cdots (\ell_1 - yp)_{\nu_n},$$

where $(\ell_1 - yp)_{\nu_1} \cdots (\ell_1 - yp)_{\nu_n}$ acting on the soft part, will give transverse derivatives of the correlator, leading to the moments of the wave function of the hadron. Note that the insertions of transverse gluons and transverse derivatives $((\ell_1 - yp)_{\nu_1} \sim \ell_{1\perp\nu_1})$ increase the twist of the operators in the soft part.

We will treat separately the convolutions of the two terms of the last line of eq. (2.32) with the soft part. The first term (zero-th order of the Taylor expansion) is

$$\begin{aligned} i\mathcal{A}_{q\bar{q}}^{(0)} &= -\frac{1}{4} \int \frac{dy}{2\pi} H_{q\bar{q}}^{\Gamma\mu}(y) \int \frac{d\beta_1}{2\pi} \frac{d\ell_\perp}{(2\pi)^2} \int d\gamma d\lambda dz_\perp e^{-i(y\lambda + \beta_1\gamma + \ell_\perp \cdot z_\perp)} \\ &\times \langle \rho(p) | \bar{\psi}(\gamma p + \lambda n + z_\perp) \Gamma_\mu \psi(0) | 0 \rangle \\ &= -\frac{1}{4} \int dy H_{q\bar{q}}^{\Gamma\mu}(y) \int \frac{d\lambda}{2\pi} e^{-iy\lambda} \langle \rho(p) | \bar{\psi}(\lambda n) \Gamma_\mu \psi(0) | 0 \rangle_{\mu_F^2}. \end{aligned} \quad (2.33)$$

In eq. (2.33), the subscript μ_F^2 is the factorization scale up to which the fluctuations in the transverse momentum space are integrated,

$$\langle \rho(p) | \bar{\psi}(\lambda n) \Gamma_\mu \psi(0) | 0 \rangle_{\mu_F^2} \equiv \int_{\ell_\perp^2 \leq \mu_F^2} \frac{d\ell_\perp dz_\perp}{(2\pi)^2} e^{-i\ell_\perp \cdot z_\perp} \langle \rho(p) | \bar{\psi}(\lambda n + z_\perp) \Gamma_\mu \psi(0) | 0 \rangle. \quad (2.34)$$

Let us give now a more precise interpretation of the presence of this cut-off on the transverse momenta. In the rest frame of the meson, its size is of order μ_0^{-1} in all directions with $\mu_0 \sim m_\rho$, and in this frame a cut-off at $\mu_F^{-1} \sim Q^{-1}$ GeV allows to get most of the internal dynamics which is not resolved by the system of partons. In the rest frame of the partons created by the virtual photon and propagating with the hard scale Q , the partonic system has a typical spatial extension of the order Q^{-1} . The boost to go from the meson rest frame to the partonic system rest frame induces a contraction of the longitudinal size of the meson by a factor Q/μ_0 , leading to a longitudinal size of the order of Q^{-1} . Hence we see that the fluctuations along the longitudinal size can be always resolved even for very large virtualities, while the fluctuations in the transverse direction are not boosted and remains of the order μ_0^{-1} . Thus these transverse fluctuations are part on the long distance dynamics of the meson and have to be integrated over up to the scale $\mu_F \sim Q$. Choosing the renormalization scale to be equal to the factorization scale, the dependence of the DAs on the scale μ_F is given by the renormalization equations of the operators in the correlators.

Note that for the case of the $q\bar{q}$ pair intermediate state, the transverse size of the pair is of the order $\sqrt{y\bar{y}}Q$ instead of Q due to the fact that the photon is split in two constituents. In a symmetric jet configuration ($y \sim 1/2$), a reasonable choice for μ_F is

$$\mu_F = \sqrt{\langle y\bar{y}Q^2 \rangle} \sim \frac{Q}{2}.$$

For aligned jet configurations ($y \sim 0$ or $\bar{y} \sim 0$) which are expected to dominate the transversely polarized ρ -meson production, this choice has to be justified depending on the average values of y and \bar{y} given by the distribution of dipoles, i.e. the overlaps of the wave functions of the transverse virtual photon and the ρ -meson.

After the momentum factorization, the operators in the correlation functions are a product of fields on the light cone direction n , $z^2 = (\lambda n)^2 = 0$. Restoring the Wilson line, the gauge invariant correlator reads

$$\langle \rho(p) | \bar{\psi}(\lambda n) [\lambda n, 0] \Gamma_\alpha \psi(0) | 0 \rangle. \quad (2.35)$$

We choose to work in the light-cone gauge $A \cdot n = 0$ which allows to simplify the Wilson line to a factor one

$$[\lambda n, 0] \equiv \mathcal{P} \exp \left(ig \int_0^1 dt \lambda n^\nu A_\nu(t \lambda) \right) = 1.$$

The second term of the Taylor expansion (2.32), i.e. the first order in ℓ_\perp of the Taylor

$$\begin{aligned}
i\mathcal{A}_{q\bar{q}}^{(1)} &= -\frac{1}{4} \int \frac{dy}{2\pi} H_{q\bar{q}}^{\nu, \Gamma^\mu}(y) \int \frac{d\beta_1}{2\pi} \int \frac{d\ell_\perp}{(2\pi)^2} \ell_{\perp\nu} \int d\gamma d\lambda dz_\perp \\
&\times e^{-i(y\lambda + \beta_1\gamma + \ell_\perp \cdot z_\perp)} \langle \rho(p) | \bar{\psi}(\gamma p + \lambda n + z_\perp) \Gamma_\mu \psi(0) | 0 \rangle \\
&= -\frac{1}{4} \int dy H_{q\bar{q}}^{\nu, \Gamma^\mu}(y) \int \frac{d\lambda}{2\pi} e^{-iy\lambda} \\
&\times \int dz_\perp \int \frac{d\ell_\perp}{(2\pi)^2} \ell_{\perp\nu} e^{-i\ell_\perp \cdot z_\perp} \langle \rho(p) | \bar{\psi}(\lambda n + z_\perp) \Gamma_\mu \psi(0) | 0 \rangle. \tag{2.36}
\end{aligned}$$
$$\begin{aligned}
i\mathcal{A}_{q\bar{q}}^{(1)} &= -\frac{1}{4} \int dy H_{q\bar{q}}^{\nu,\Gamma^\mu}(y) \int \frac{d\lambda}{2\pi} e^{-iy\lambda} \int \frac{d\ell_\perp}{(2\pi)^2} dz_\perp (i\partial_{\perp\nu} e^{-i\ell_\perp \cdot z_\perp}) \\
&\times \langle \rho(p) | \bar{\psi}(\lambda n + z_\perp) \Gamma_\mu \psi(0) | 0 \rangle \\
&= \frac{i}{4} \int dy H_{q\bar{q}}^{\nu,\Gamma^\mu}(y) \int \frac{d\lambda}{2\pi} e^{-iy\lambda} \int \frac{d\ell_\perp}{(2\pi)^2} \int dz_\perp e^{-i\ell_\perp \cdot z_\perp} \\
&\times \frac{\partial}{\partial z_{\perp\nu}} \langle \rho(p) | \bar{\psi}(\gamma p + \lambda n + z_\perp) \Gamma_\mu \psi(0) | 0 \rangle \\
&= \frac{i}{4} \int dy H_{q\bar{q}}^{\nu,\Gamma^\mu}(y) \int \frac{d\lambda}{2\pi} e^{-i\lambda y} \frac{\partial}{\partial z_{\perp\nu}} \langle \rho(p) | \bar{\psi}(\lambda n) \Gamma_\mu \psi(0) | 0 \rangle_{\mu_F^2}. \tag{2.37}
\end{aligned}$$
$$\frac{\partial}{\partial z_{|\nu}} \langle \rho(p) | \bar{\psi}(\lambda n + 0_{\perp}) \Gamma_{\alpha} \psi(0) | 0 \rangle_{\mu_F^2} = - \langle \rho(p) | \bar{\psi}(\lambda n + 0_{\perp}) \Gamma_{\alpha} \overset{\longleftrightarrow}{\partial_{\nu}^{\perp}} \psi(0) | 0 \rangle_{\mu_F^2}, \quad (2.38)$$
$$i\mathcal{A}_{q\bar{q}}^{(1)} = \frac{-1}{4} \int dy H_{q\bar{q}}^{\nu,\Gamma^\mu}(y) \int \frac{d\lambda}{2\pi} e^{-i\lambda y} \langle \rho(p) | \bar{\psi}(\lambda n) \Gamma_\mu i \overset{\leftrightarrow}{\partial}_\nu^\perp \psi(0) | 0 \rangle_{\mu_F^2}. \quad (2.39)$$

The diagram illustrates the renormalization of the Higgs self-energy. On the left, the bare self-energy is shown as a loop with a fermion line labeled ℓ and a scalar line labeled ρ . On the right, the renormalized self-energy is shown as the sum of two diagrams. The first diagram is the same as the bare one but with the fermion line labeled yp and the scalar line labeled ρ . The second diagram is a new loop diagram with a fermion line labeled ℓ and a scalar line labeled ρ , and a fermion line labeled yp and a scalar line labeled ρ . The diagrams are connected by a plus sign.

The derivative term of the hard part $H_{q\bar{q}}^{\nu_i\Gamma^\mu}(y)$ in the expression of $\mathcal{A}_{q\bar{q}}^{(1)}$ can be computed using the following identity,

$$\frac{\partial}{\partial p_\mu} \text{---}\text{>}\text{---} = \text{---}\text{>}\text{---} \bullet \text{---}\text{>}\text{---} \quad \text{where} \quad \text{---}\text{>}\text{---} = \frac{1}{m - \not{p} - i\epsilon}. \quad (2.40)$$

The hard part $H_{q\bar{q}}^{\nu,\Gamma^\mu}(y)$ corresponds then to the computation of the 12 diagrams shown in fig. 2.13. Indeed the derivative of each of the 6 diagrams of fig. 2.7 involves the sum of the derivatives of each propagators of the diagram leading to

$$\frac{\partial}{\partial \ell^\nu} \left(\text{diagram} \right) = \text{diagram with dashed line on left} + \text{diagram with dashed line on right} . \quad (2.41)$$

where the dashed lines are only here to indicate with respect to which propagator we are deriving.

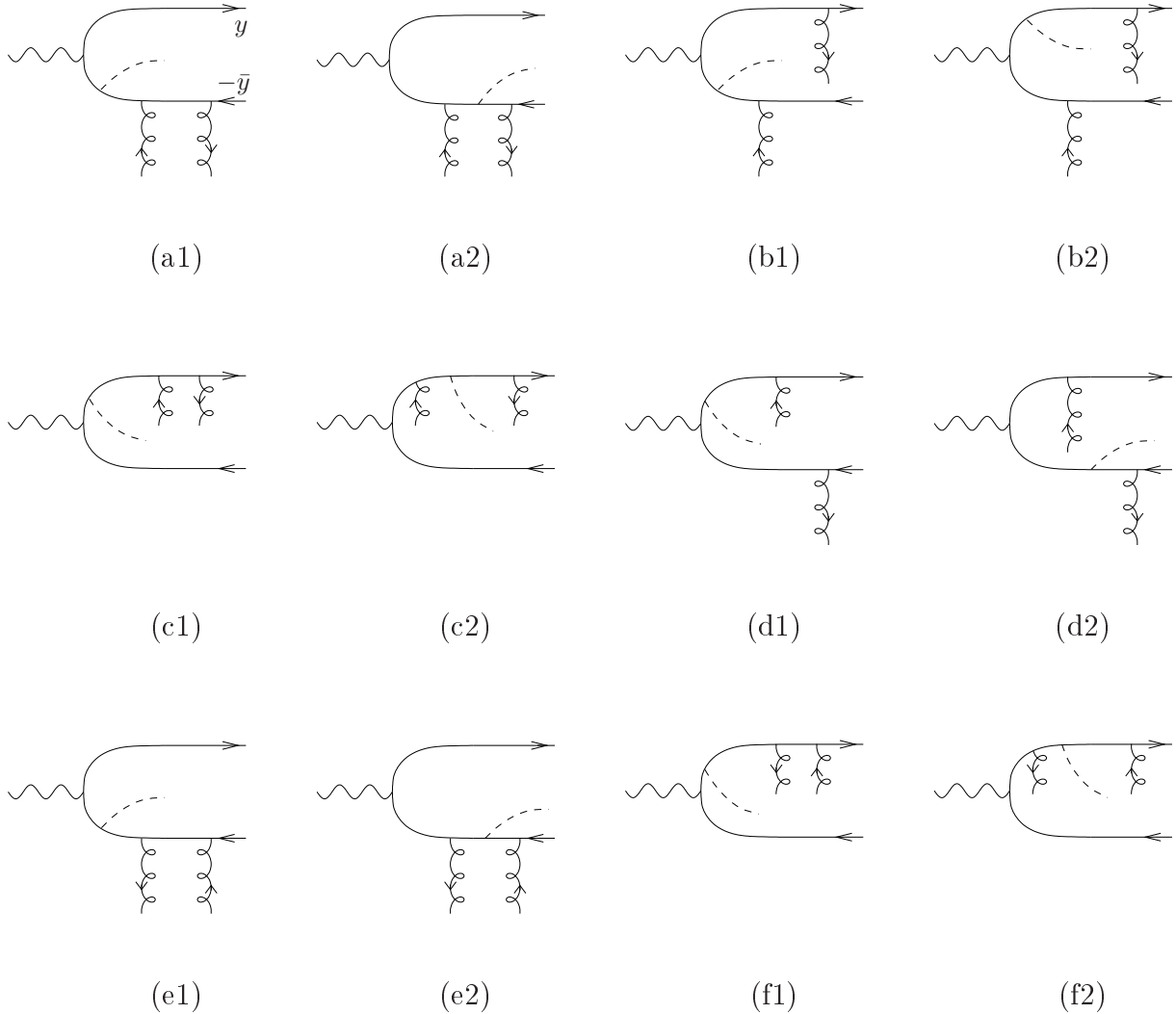


Figure 2.13: The 12 contributions arising from the first derivative of the 6 hard diagrams attached to the 2-parton correlators, which contribute to the $\gamma^* \rightarrow \rho$ impact factor, with momentum flux of external line, along p_1 direction.

At the twist 3 level, we need to consider also the non-minimal parton configuration where there is an additional gluon. Contrary to a covariant gauge treatment, the choice of the axial light-cone gauge ($n \cdot A = 0$) allows to get rid of the longitudinal component of the gluon polarization.

We now focus on the $q\bar{q}g$ intermediate state amplitude. In the case of three-parton exchange contribution, only the zero-th order of the Taylor expansion of the hard part is needed up to twist 3 with a transversely polarized gluon,

$$\begin{aligned}
 i\mathcal{A}_{q\bar{q}g} &= -\frac{1}{4} \int \frac{dy_1 d\beta_1 d^2\ell_{1\perp}}{(2\pi)^4} \int \frac{dy_g d\beta_g d^2\ell_{g\perp}}{(2\pi)^4} \int d\gamma_1 d\lambda_1 d^2z_{1\perp} \int d\gamma_g d\lambda_g d^2z_{g\perp} \\
 &\times H_{q\bar{q}g}^{\alpha,\Gamma^\mu}(y_1, y_g) \langle \rho(p) | \bar{\psi}(z_1) \Gamma_\mu g A_\alpha^\perp(z_g) \psi(0) | 0 \rangle e^{-i\ell_1 \cdot z_1} e^{-i\ell_g \cdot z_g} \\
 &= -\frac{1}{4} \int dy_1 \int dy_g H_{q\bar{q}g}^{\alpha,\Gamma^\mu}(y_1, y_g) \\
 &\times \int \frac{d\lambda_1 d\lambda_g}{(2\pi)^2} e^{-iy_1 \lambda_1} e^{-iy_g \lambda_g} \langle \rho(p) | \bar{\psi}(\lambda_1 n) \Gamma_\mu g A_\alpha^\perp(\lambda_g n) \psi(0) | 0 \rangle_{\mu_F^2}, \tag{2.42}
 \end{aligned}$$

where we denote $Tr(H_{q\bar{q}g}^\alpha \Gamma^\mu) = H_{q\bar{q}g}^{\alpha,\Gamma^\mu}$. The factorization for the three-parton contribution is illustrated in fig. 2.14.

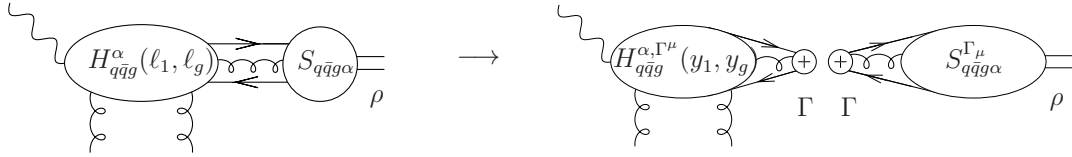


Figure 2.14: Factorization of 3-parton contributions in the example of the $\gamma^* \rightarrow \rho$ impact factor.

Note that the sum of the first order term of the Taylor expansion in ∂^\perp for the $q\bar{q}$ intermediate state contribution given by eq. (2.39) and the $q\bar{q}g$ intermediate state contribution given by eq. (2.42), corresponds to the first order term of a Taylor expansion with respect to the transverse covariant derivative $D_\mu^\perp(z) = \partial_\mu^\perp - igA_\mu^\perp(z)$ of the hard part around the dominant light-cone direction, it reads

$$\begin{aligned}
 i\mathcal{A}_{qD\bar{q}}^{(1)} &= \frac{-1}{4} \int dy_1 \int dy_g H_{q\bar{q}g}^{\nu,\Gamma^\mu}(y_1, y_g) \int \frac{d\lambda_1}{2\pi} e^{-i\lambda_1 y_1} \int \frac{d\lambda_g}{2\pi} e^{-i\lambda_g y_g} \\
 &\times \langle \rho(p) | \bar{\psi}(\lambda_1 n) \Gamma_\mu i \overleftrightarrow{D}_\nu^\perp(\lambda_g) \psi(0) | 0 \rangle_{\mu_F^2}. \tag{2.43}
 \end{aligned}$$

2.3 Parameterizing the vacuum to rho-meson matrix elements

The goal of this part is to parameterize the vacuum to ρ -meson matrix elements that appear in eqs. (2.33), (2.39) and (2.42) and contains the twist 2 and twist 3 contributions to the $\gamma^* g \rightarrow \rho g$ amplitude. We will first introduce the notion of DA, then we will show how considering the quantum numbers of the ρ -meson state, the equations of motion (EOMs) of QCD and another condition called n -independence, allows to restrict ourselves to a minimal set of DAs. We finally describe how one can find explicit expressions for these DAs using conformal expansion, renormalization equations and QCD sum rules techniques.

2.3.1 Light-cone wave functions and distribution amplitudes

Let us introduce the lowest Fock state light-cone wave function of the ρ -meson $\Psi_{h\bar{h}}^{(\lambda\rho)}(y, \underline{\ell})$ and its connection with the DAs. Note that in our notation the usual "+" and "-" components of a vector $z = \alpha_z p_1 + \gamma p_2 + z_\perp$ are respectively given by projecting on p_2 and p_1 , $z^+ \sqrt{s} \equiv z \cdot p_2 = \alpha_z$ and $z^- \sqrt{s} \equiv z \cdot p_1 = \gamma$.

The wave function in momentum space is the Fourier transform of the Bethe-Salpeter wave function of positive energy at the fixed light-cone time $z^+ \equiv \gamma = 0$. This object is the amplitude of probability to find a $q\bar{q}$ pair with respective helicities h and \bar{h} , fractions of longitudinal momentum y and \bar{y} , and transverse momenta $\underline{\ell}$ and $-\underline{\ell}$, in the ρ -meson state. Following the conventions of [120], the mode expansion of the quark field with z laying on the light-cone direction $z = \lambda n$ is

$$\psi(\lambda n) = \int \frac{dy d^2 \ell}{(2\pi)^3 (2y)} \sum_h [u^{(h)}(y, \underline{\ell}) \hat{b}_h(y, \underline{\ell}) e^{-iy\lambda} + v^{(h)}(y, \underline{\ell}) \hat{d}_h^\dagger(y, \underline{\ell}) e^{iy\lambda}]. \quad (2.44)$$

The ρ -meson state is defined at lowest order of the Fock expansion by

$$|\rho(p_\rho, \lambda_\rho)\rangle = \sqrt{4\pi N_c} \sum_{h, \bar{h}} \int \frac{dy d^2 \ell_\perp}{(2\pi)^3 \sqrt{(2y)(2\bar{y})}} \Psi_{h, \bar{h}}^{\lambda_\rho}(y, \underline{\ell}) \hat{b}_h^\dagger(y, \underline{\ell}) \hat{d}_{\bar{h}}^\dagger(\bar{y}, -\underline{\ell}) |0\rangle, \quad (2.45)$$

where the anticommutation relations at equal light-cone time ($z^+ \equiv \gamma$) are,

$$\left\{ \hat{b}_h^\dagger(y, \underline{\ell}), \hat{b}_{h'}(y', \underline{\ell}') \right\}_{\gamma=0} = (2\pi)^3 \delta(y - y') \delta^{(2)}(\underline{\ell} - \underline{\ell}') (2yp) \delta_{h, h'}. \quad (2.46)$$

Assuming that the $q\bar{q}$ state saturates the ρ -meson state, then the probability $P_{q\bar{q}}$ to find a $q\bar{q}$ in the ρ -meson state is one, leading to the normalization condition [55, 145]

$$P_{q\bar{q}} = \sum_{h, \bar{h}} \int dy \int d^2 \underline{r} \left| \Psi_{h, \bar{h}}^{\lambda_\rho}(y, \underline{r}) \right|^2 = 1, \quad (2.47)$$

with $\Psi_{h, \bar{h}}^{\lambda_\rho}(y, \underline{r})$ the Fourier transform in the transverse space, \underline{r} is the transverse size of the $q\bar{q}$ pair. Considering the electronic decay of the ρ -meson in terms of the wave functions of a virtual photon $\Psi_{h, \bar{h}}^{\lambda_\gamma}$, and of the ρ -meson gives the additional relation [115, 145]

$$ef_\rho m_\rho (e_\gamma^* \cdot e_\rho) = \sum_{h, \bar{h}} \int dy \int d^2 \underline{r} \Psi_{h, \bar{h}}^{\lambda_\rho}(y, \underline{r}) \Psi_{h, \bar{h}}^{\lambda_\gamma}(y, \underline{r}). \quad (2.48)$$

The vacuum to ρ -meson matrix elements that are involved in $\mathcal{A}^{(0)}$ are

$$\begin{aligned} \langle \rho(p, \lambda_\rho) | \bar{\psi}(\lambda n) \Gamma_\mu \psi(0) | 0 \rangle &= \sqrt{4\pi N_c} \sum_{h, \bar{h}} \int \frac{dy d^2 \ell}{(2\pi)^3 \sqrt{(2y)(2\bar{y})}} e^{iy\lambda} \\ &\quad \Psi_{h, \bar{h}}^{*\lambda_\rho}(y, \underline{\ell}) [\bar{u}^{(h)}(y, \underline{\ell}) \Gamma_\mu v^{(\bar{h})}(y, -\underline{\ell})]. \end{aligned} \quad (2.49)$$

By definition, the DAs parameterize the Fourier transforms of the vacuum to ρ -meson matrix elements. We can write as a generic definition of the DA $\varphi_i(y, \mu_F)$,

$$\begin{aligned}
 m_\rho f_\rho \varphi_i(y, \mu_F^2) &= \int \frac{d\lambda}{2\pi} e^{-iy\lambda} \langle \rho(p) | \bar{\psi}(\lambda n) (L \cdot \Gamma) \psi(0) | 0 \rangle_{\mu_F^2} \\
 &= \sqrt{4\pi N_c} \sum_{h\bar{h}} \int_{\underline{\ell}^2 < \mu_F^2} \frac{d^2 \underline{\ell}}{(2\pi)^3 \sqrt{(2y)(2\bar{y})}} e^{iy\lambda} \\
 &\times \Psi_{h\bar{h}}^{*(\lambda_\rho)}(y, \underline{\ell}) [\bar{u}^{(h)}(y, \underline{\ell}) L \cdot \Gamma v^{(\bar{h})}(y, -\underline{\ell})], \tag{2.50}
 \end{aligned}$$

with L_μ the relevant Lorentz structure associated to φ_i on which is projected the correlator. The wave function is not known but it is customary to parameterize it as a spinor part $S_{h\bar{h}}^{\lambda_\rho}$ which is similar to the coupling to the $q\bar{q}$ pair to a photon, and a scalar part ϕ_{λ_ρ} which has to be modeled and which is constrained by the relations (2.47, 2.48). In this case the wave function takes the form

$$\Psi_{h\bar{h}}^{(\lambda_\rho)} = \sqrt{\frac{N_c}{4\pi}} S_{h\bar{h}}^{\lambda_\rho} \phi_{\lambda_\rho}, \tag{2.51}$$

with $S_{h\bar{h}}^{\lambda_\rho} = \bar{u}_h(y, \underline{\ell}) \not{\epsilon}^{(\lambda_\rho)} v_{\bar{h}}(\bar{y}, -\underline{\ell})$. The computation of the DA with the wave function defined in (2.51) leads to interpret the DAs in the asymptotic limit $\mu_F^2 \rightarrow \infty$ as the moments of the scalar function $\phi_{\lambda_\rho}(y, \underline{\ell})$ in the transverse momentum space.

2.3.2 Lorentz decomposition and parity analysis

We will now investigate the set of DAs we need to parameterize the matrix elements of the twist 2 and twist 3 operators.

The role of chirality conservation

We first restrict the sum over the Γ^μ matrices to the sum of γ^μ and $\gamma^\mu \gamma_5$ as they are chirality-conserving matrices. Indeed, as we have neglected the quark masses, the conservation of helicity implies then the conservation of the chirality in the QED and QCD vertices. The conservation of chirality at each vertices of the hard part and the fact that the quantum number exchanged in t -channel are those of the vacuum, i.e. chiral even, impose that the Γ^μ matrices must be chiral even. One can readily check that the chirality-violating matrices like $1, \sigma_{\mu\nu}, \dots$ are giving vanishing contributions in the two t -channel gluon approximation. The consequence of the chirality conserving condition is that the chiral odd DAs [142] such as the leading twist DA for a transversely vector meson or the twist 3 DAs for a longitudinally polarized meson, decouple from the hard parts. As a consequence, the twist expansion starts at twist 3 for the production of a ρ_T and the next term of the twist expansion for the production of a ρ_L is of twist 4. Let us give an exhaustive list of the Fourier transforms of the vacuum to ρ -meson matrix elements that we have to parameterize given the two chiral

even structure $\{\gamma_\mu, \gamma_5 \gamma_\mu\}$,

$$S_{q\bar{q}}^{\gamma_\mu}(y, \mu_F^2) \equiv \int \frac{d\lambda}{2\pi} e^{-i\lambda y} \langle \rho(p) | \bar{\psi}(\lambda n) \gamma_\mu \psi(0) | 0 \rangle_{\mu_F^2}, \quad (2.52)$$

$$S_{q\bar{q}}^{\gamma_5 \gamma_\mu}(y, \mu_F^2) \equiv \int \frac{d\lambda}{2\pi} e^{-i\lambda y} \langle \rho(p) | \bar{\psi}(\lambda n) \gamma_5 \gamma_\mu \psi(0) | 0 \rangle_{\mu_F^2}, \quad (2.53)$$

$$S_{q\bar{q}}^{\gamma_\mu, \perp}(y, \mu_F^2) \equiv \int \frac{d\lambda}{2\pi} e^{-i\lambda y} \langle \rho(p) | \bar{\psi}(\lambda n) \gamma_\mu i \overleftrightarrow{\partial}_\alpha^\perp \psi(0) | 0 \rangle_{\mu_F^2}, \quad (2.54)$$

$$S_{q\bar{q}}^{\gamma_5 \gamma_\mu, \perp}(y, \mu_F^2) \equiv \int \frac{d\lambda}{2\pi} e^{-i\lambda y} \langle \rho(p) | \bar{\psi}(\lambda n) \gamma_5 \gamma_\mu i \overleftrightarrow{\partial}_\alpha^\perp \psi(0) | 0 \rangle_{\mu_F^2}, \quad (2.55)$$

$$S_{q\bar{q}g}^{\gamma_\mu, \alpha}(y_1, y_2, \mu_F^2) \equiv \int \frac{d\lambda_1}{2\pi} e^{-i\lambda_1 y_1} \int \frac{d\lambda_g}{2\pi} e^{-i\lambda_g(y_2 - y_1)} \\ \times \langle \rho(p) | \bar{\psi}(\lambda_1 n) \gamma_\mu g A_\alpha^\perp(\lambda_g n) \psi(0) | 0 \rangle_{\mu_F^2}, \quad (2.56)$$

$$S_{q\bar{q}g}^{\gamma_5 \gamma_\mu, \alpha}(y_1, y_2, \mu_F^2) \equiv \int \frac{d\lambda_1}{2\pi} e^{-i\lambda_1 y_1} \int \frac{d\lambda_g}{2\pi} e^{-i\lambda_g(y_2 - y_1)} \\ \times \langle \rho(p) | \bar{\psi}(\lambda_1 n) \gamma_5 \gamma_\mu g A_\alpha^\perp(\lambda_g n) \psi(0) | 0 \rangle_{\mu_F^2}. \quad (2.57)$$

Decomposition on Lorentz structures

The idea is to decompose on Lorentz structures the non-local correlators and to keep the structures which will give contributions up to a given twist. The Lorentz structures have to be built from the relevant momenta p, n and the polarization of the outgoing ρ -meson e^* . To understand which are the relevant Lorentz structures to keep up to a given twist, let us give a power counting argument in the infinite momentum frame where $p \sim Q \rightarrow \infty$. We directly see in this frame that the scalar product $p \cdot n = 1$ implies that $n \sim \frac{1}{Q}$ and $e_\perp^* \sim 1$. This scaling of the momenta, gives the power behavior in $1/Q$ for each term of the decomposition. The twist 2 $\mathcal{O}(1)$ and twist 3 $\mathcal{O}(1/Q)$ Lorentz structures that we can build are then,

$$(n \cdot e^*) p_\mu = \frac{1}{m_\rho} p_\mu \sim Q \Rightarrow \text{Twist 2, longitudinal polarization, (vector)}, \quad (2.58)$$

$$(n \cdot p) e_{\perp\mu}^* = e_{\perp\mu}^* \sim 1 \Rightarrow \text{Twist 3, transverse polarization, (vector)}, \quad (2.59)$$

$$R_{\perp\mu}^* \sim 1 \Rightarrow \text{Twist 3, transverse polarization,} \\ \text{(axial vector)}, \quad (2.60)$$

where⁴

$$R_{\perp\mu}^* \equiv \varepsilon_{\mu\alpha\beta\gamma} e_{\perp}^{*\alpha} p^\beta n^\gamma.$$

Other Lorentz structures exist but they can be expressed in terms of these ones or they are of twist 4 like for example $(p \cdot e^*) n_\mu \sim \frac{1}{Q}$. We see from the power counting that the correlators with two Lorentz indices associated to the production of a transversely polarized ρ -meson can be only,

$$p_\alpha e_{\perp\mu}^* \Rightarrow \text{Twist 3, transverse polarization, (vector)}, \quad (2.61)$$

$$p_\alpha R_{\perp\mu}^* \Rightarrow \text{Twist 3, transverse polarization, (axial vector)}. \quad (2.62)$$

⁴The convention taken for the Levi-Civita tensor is $\varepsilon^{0123} = -\varepsilon_{0123} = 1$.

Note that another way to perform the power counting in twist [146] is to decompose the fields in their "+" and "-" components, which are also called good and bad components, leading to the definitions of quasipartonic operators (only constituted of "+" fields) and non-quasipartonic operators containing "-" components. For spinor fields of dimension d and spin s , these components correspond to the spin projection of the field ψ , $\psi_+ = \Pi_+ \psi \equiv \frac{1}{2} \gamma_- \gamma_+ \psi$ has spin $s = 1/2$ and $\psi_- = \Pi_- \psi \equiv \frac{1}{2} \gamma_+ \gamma_- \psi$ has spin $s = -1/2$, with Π_{\pm} the spin projection operators. The conformal spin of the primary field ψ , $j = \frac{d+s}{2}$ and its so-called collinear twist $t = d - s$, are different for ψ_+ and ψ_- components which have respectively twist 1 and 2. To illustrate the twist counting of the operators, let us focus on the operator $\bar{\psi} \gamma_{\mu} \psi$. The quasipartonic operator $\bar{\psi}_+ \gamma_+ \psi_+$ is a leading twist operator while $\bar{\psi}_+ \gamma_{\perp} \psi_- + \bar{\psi}_- \gamma_{\perp} \psi_+$ is a twist 3 operator and $\bar{\psi}_- \gamma_- \psi_-$ is a twist 4 operator. The role of the conformal spin of the operators will be discussed in section 2.5.

Let us now focus on the parameterization of the $S_{q\bar{q}}^{\gamma\mu}$, which a priori involves three unknown functions $\varphi_1(y)$, $\varphi_3(y)$ and $\tilde{\varphi}_A(y)$,

$$S_{q\bar{q}}^{\gamma\mu} = \int \frac{d\lambda}{2\pi} e^{-i\lambda y} \langle \rho(p) | \bar{\psi}(\lambda n) \gamma_{\mu} \psi(0) | 0 \rangle \quad (2.63)$$

$$= m_{\rho} f_{\rho} \left(\varphi_1(y) (e^* \cdot n) p_{\mu} + i \tilde{\varphi}_A(y) R_{\perp\mu}^* + \varphi_3(y) (p \cdot n) e_{\perp}^* \right). \quad (2.64)$$

The normalization $m_{\rho} f_{\rho}$ contains the information on the large distance physics. The decay constant f_{ρ} is defined as

$$\langle 0 | \bar{\psi}(0) \gamma_{\mu} \psi(0) | \rho(p, \lambda) \rangle = m_{\rho} f_{\rho} e_{\mu}^{\lambda}, \quad (2.65)$$

and it has been measured: $f_{\rho} \sim 200$ MeV.

In practice one has to define non-perturbative coupling constants ($f_{3,\rho}^V, \dots$) in order that the DAs have proper normalizations. We will see in section 2.6 the determination of such non perturbative inputs, using QCD sum rules techniques. Let us now investigate how the parity analysis will constrain the set of unknown functions, on the particular case of $S_{q\bar{q}}^{\gamma\mu}$.

Parity constraints

Under parity, the light cone vectors p , n and e_{\perp}^* transform as

$$\mathcal{P}_{\mu}^{\nu} p_{\nu} = n_{\mu}, \quad \mathcal{P}_{\mu}^{\nu} n_{\nu} = p_{\mu}, \quad \mathcal{P}_{\mu}^{\nu} e_{\nu}^*(-\vec{p}, \lambda) = -e_{\mu}^*(\vec{p}, \lambda), \quad (2.66)$$

and the operator $\bar{\psi}(z) \gamma_{\mu} \psi(0)$ transforms as

$$\bar{\psi}(z) \gamma_{\mu} \psi(0) \longrightarrow \mathcal{P}_{\mu}^{\nu} \bar{\psi}(\mathcal{P}_{\beta}^{\alpha} z^{\beta}) \gamma_{\nu} \psi(0), \quad (2.67)$$

where $\mathcal{P} = \text{diag}(1, -1, -1, -1)$ is the parity matrix on the Lorentz vector representation. The proofs are quite straightforward except for the transformation of e_{ν}^* where one needs to boost by $L_{\mu}^{\nu}(p)$ the vector in the rest frame of the ρ -meson where $\vec{p} = \vec{0}$,

$$e^{\mu}(\mathcal{P}p, \lambda) = L_{\nu}^{\mu}(\mathcal{P}p) e^{\nu}(\vec{0}, \lambda) = \mathcal{P}_{\alpha}^{\mu} L_{\beta}^{\alpha}(p) \mathcal{P}_{\nu}^{\beta} e^{\nu}(\vec{0}, \lambda) = -\mathcal{P}_{\nu}^{\mu} e^{\nu}(p, \lambda), \quad (2.68)$$

where we use the fact that in the rest frame

$$\mathcal{P}_\nu^\beta e^\nu(\vec{0}, \lambda) = -e^\beta(\vec{0}, \lambda),$$

as $e^0(\vec{0}, \lambda) = 0$.

Inserting the identity $1 = PP^\dagger$ between the operator and the states, the matrix element transforms as

$$\langle \rho(p, \lambda) | PP^\dagger \bar{\psi}(z) \gamma_\mu \psi(0) PP^\dagger | 0 \rangle = \eta_\rho \mathcal{P}_\mu^\nu \langle \rho(\mathcal{P}p, \lambda) | \bar{\psi}(\mathcal{P}z) \gamma_\mu \psi(0) | 0 \rangle, \quad (2.69)$$

with $\eta_\rho = -1$ the intrinsic parity of the ρ -state. This equality in terms of DAs reads

$$\begin{aligned} & \int dy (\varphi_1(y)(e^*(\vec{p}, \lambda) \cdot n) p_\mu + \varphi_3(y) e_\perp^*(p, \lambda) + i\tilde{\varphi}_A(y) R_{\perp\mu}^*) e^{iyp \cdot z} \\ &= \eta_\rho \mathcal{P}_\mu^\nu \int dy e^{iy(\mathcal{P}p) \cdot (\mathcal{P}z)} (\varphi_1(y) (e_\alpha^*(\mathcal{P}p, \lambda) (\mathcal{P}n)^\alpha) (\mathcal{P}p)_\nu + \varphi_3(y) e_{\perp\nu}^*(\mathcal{P}p, \lambda) \\ &+ i\tilde{\varphi}_A(y) \varepsilon_{\nu\alpha\beta\gamma} e_\perp^{*\alpha}(\mathcal{P}p, \lambda) (\mathcal{P}p)^\beta \mathcal{P}n^\gamma). \end{aligned} \quad (2.70)$$

The first term that multiplies $\varphi_1(y)$, simplifies as

$$\begin{aligned} \eta_\rho \mathcal{P}_\mu^\nu \mathcal{P}_\nu^\beta p_\beta (e_\alpha^*(\mathcal{P}p, \lambda) \mathcal{P}_\sigma^\alpha n^\sigma) &= \eta_\rho p_\mu (-\mathcal{P}_\alpha^\sigma e_\sigma^*(p, \lambda) p^\alpha) \\ &= -\eta_\rho (e_\sigma^*(p, \lambda) \cdot n) p_\mu. \end{aligned} \quad (2.71)$$

The term multiplying $\varphi_3(y)$ simplifies as

$$\eta_\rho \mathcal{P}_\mu^\nu e_{\perp\nu}^*(\mathcal{P}p, \lambda) = -\eta_\rho \mathcal{P}_\mu^\nu \mathcal{P}_\nu^\sigma e_{\perp\sigma}^*(p, \lambda) = -\eta_\rho e_{\perp\mu}^*(p, \lambda) \quad (2.72)$$

and finally the term multiplying $\tilde{\varphi}_A(y)$ reads

$$\begin{aligned} & \eta_\rho \mathcal{P}_\mu^\nu \varepsilon_{\nu\alpha\beta\gamma} e_\perp^{*\alpha}(\mathcal{P}p, \lambda) \mathcal{P}_\lambda^\beta p^\lambda \mathcal{P}_\rho^\delta n^\rho \\ &= -\eta_\rho \mathcal{P}_\mu^\nu \varepsilon_{\nu\alpha\beta\gamma} \mathcal{P}_\sigma^\alpha e_\perp^{*\sigma}(\mathcal{P}p, \lambda) \mathcal{P}_\lambda^\beta p^\lambda \mathcal{P}_\rho^\delta n^\rho \\ &= -\eta_\rho \left(\varepsilon_{\nu\alpha\beta\gamma} \mathcal{P}_\nu^\mu \mathcal{P}_\sigma^\alpha \mathcal{P}_\lambda^\beta \mathcal{P}_\rho^\gamma \right) e_\perp^{*\sigma}(p, \lambda) p^\lambda n^\rho \\ &= -\eta_\rho \det(\mathcal{P}) \varepsilon_{\mu\sigma\lambda\rho} e_\perp^{*\sigma}(p, \lambda) p^\lambda n^\rho \\ &= \eta_\rho \varepsilon_{\mu\sigma\lambda\rho} e_\perp^{*\sigma}(p, \lambda) p^\lambda n^\rho, \end{aligned} \quad (2.73)$$

where we use the fact that $\mathcal{P}_\mu^\nu = \mathcal{P}_\nu^\mu$, $\varepsilon_{\mu\alpha\beta\gamma} \mathcal{P}_\nu^\mu \mathcal{P}_\sigma^\alpha \mathcal{P}_\lambda^\beta \mathcal{P}_\rho^\gamma = \det(\mathcal{P}) \varepsilon_{\nu\sigma\lambda\rho}$ by definition of the determinant, and $\det(\mathcal{P}) = -1$. The relation given in eq. (2.70) leads to

$$\begin{aligned} & \int dy (\varphi_1(y)(e^* \cdot n) p_\mu + \varphi_3(y) e_\perp^*(p, \lambda) + i\tilde{\varphi}_A(y) R_{\perp\mu}^*) e^{iyp \cdot z} \\ &= \int dy (\varphi_1(y)(e^* \cdot n) p_\mu + \varphi_3(y) e_\perp^*(p, \lambda) - i\tilde{\varphi}_A(y) R_{\perp\mu}^*) e^{iyp \cdot z}. \end{aligned} \quad (2.74)$$

The conditions given by the parity analysis are then

$$\varphi_1(y) = \varphi_1(y), \quad \varphi_3(y) = \varphi_3(y), \quad \tilde{\varphi}_A(y) = -\tilde{\varphi}_A(y) \Rightarrow \tilde{\varphi}_A(y) = 0. \quad (2.75)$$

C-parity constraints

The transformation under C-parity of the operator $\bar{\psi}(z)\gamma^\mu\psi(0)$ is

$$C^\dagger \bar{\psi}(z)\gamma^\mu\psi(0)C = -\bar{\psi}(0)\gamma^\mu\psi(z).$$

The correlator reads

$$\begin{aligned} \langle \rho(p, \lambda) | CC^\dagger \bar{\psi}(z)\gamma_\mu\psi(0)CC^\dagger | 0 \rangle &= -\eta_\rho^c \langle \rho(p, \lambda) | \bar{\psi}(0)\gamma_\mu\psi(z) | 0 \rangle \\ &= -\eta_\rho^c \langle \rho(p, \lambda) | e^{i\hat{P}\hat{Z}} e^{-i\hat{P}\hat{Z}} \bar{\psi}(0) e^{i\hat{P}\hat{Z}} e^{-i\hat{P}\hat{Z}} \gamma_\mu\psi(z) e^{i\hat{P}\hat{Z}} e^{-i\hat{P}\hat{Z}} | 0 \rangle \\ &= -\eta_\rho^c \langle \rho(p, \lambda) | e^{i\hat{P}\hat{Z}} \bar{\psi}(-z)\gamma_\mu\psi(0) e^{-i\hat{P}\hat{Z}} | 0 \rangle, \end{aligned} \quad (2.76)$$

where we have inserted the translation operators $e^{-i\hat{P}\hat{Z}}$. The intrinsic C-parity of the ρ^0 -meson is $\eta_\rho^c = -1$. The vacuum state is invariant under translation while the ρ -meson state gives the eigenvalue $\exp(ip \cdot z)$. We get then the equality

$$\langle \rho(p, \lambda) | CC^\dagger \bar{\psi}(z)\gamma_\mu\psi(0)CC^\dagger | 0 \rangle = -\eta_\rho^c e^{ip \cdot z} \langle \rho(p, \lambda) | \bar{\psi}(-z)\gamma_\mu\psi(0) | 0 \rangle. \quad (2.77)$$

Parameterizing the correlator in terms of the $\varphi_1(y)$ and $\varphi_3(y)$ gives the relation

$$\begin{aligned} m_\rho f_\rho \int dy e^{iyp \cdot z} [\varphi_1(y)(e^* \cdot n)p_\mu + \varphi_3(y)e_\perp^*] &= -\eta_\rho e^{ip \cdot z} m_\rho f_\rho \\ &\times \int dy e^{-iyp \cdot z} [\varphi_1(y)(e^* \cdot n)p_\mu + \varphi_3(y)e_\perp^*]. \end{aligned} \quad (2.78)$$

Changing the integration variable y by $\tilde{y} = 1 - y$, leads to

$$\begin{aligned} m_\rho f_\rho \int dy e^{iyp \cdot z} [\varphi_1(y)(e^* \cdot n)p_\mu + \varphi_3(y)e_\perp^*] \\ = m_\rho f_\rho \int d\tilde{y} e^{i\tilde{y}p \cdot z} [\varphi_1(1 - \tilde{y})(e^* \cdot n)p_\mu + \varphi_3(1 - \tilde{y})e_\perp^*]. \end{aligned} \quad (2.79)$$

We can now identify the different terms, and the constraints given by the C-parity transformation of the correlator are

$$\varphi_1(y) = \varphi_1(1 - y) \quad \text{and} \quad \varphi_3(y) = \varphi_3(1 - y). \quad (2.80)$$

Time reversal constraints

The ρ -meson state transforms under T -parity as

$$T |\rho(p, \lambda)\rangle = \zeta_\rho^*(-1)^{1-\lambda} |\rho(\mathcal{P}p, -\lambda)\rangle. \quad (2.81)$$

One can prove also the relation

$$e_\mu^*(\mathcal{P}p, -\lambda) = (-1)^{1+\lambda} \mathcal{P}_\mu^\nu e_\nu(p, \lambda), \quad (2.82)$$

which will be useful in the transformations. The operator $\bar{\psi}(z)\gamma_\mu\psi(0)$ transforms under time reversal as,

$$T^{-1} \bar{\psi}(z)\gamma_\mu\psi(0)T = \mathcal{P}_\mu^\nu \bar{\psi}(-\mathcal{P}z)\gamma_\nu\psi(0).$$

The correlator after inserting the operators TT^{-1} reads

$$\begin{aligned}
 & \langle \rho(p, \lambda) | TT^{-1} \bar{\psi}(z) \gamma_\mu \psi(0) TT^{-1} | 0 \rangle \\
 &= \zeta_\rho(-1)^{1-\lambda} (\langle \rho(\mathcal{P}p, -\lambda) | \bar{\psi}(-\mathcal{P}z) \mathcal{P}_\mu^\nu \gamma_\nu \psi(0) | 0 \rangle)^* \\
 &= \zeta_\rho(-1)^{1-\lambda} \left(\int dy e^{-iy(\mathcal{P}p) \cdot (\mathcal{P}n)} [\varphi_1(y) (e^*(\mathcal{P}p, -\lambda) \cdot \mathcal{P}n) \mathcal{P}_\mu^\nu (\mathcal{P}p)_\nu \right. \\
 & \quad \left. + \varphi_3(y) \mathcal{P}_\mu^\nu e_{\perp\nu}^*(\mathcal{P}p, -\lambda)] \right)^* .
 \end{aligned} \tag{2.83}$$

The fact that the correlator is conjugated is due to the fact that time reversal exchanges the *in*-state with the *out*-state. The scalar product $e^*(\mathcal{P}p, -\lambda) \cdot \mathcal{P}n$ simplifies,

$$e^*(\mathcal{P}p, -\lambda) \cdot \mathcal{P}n = (-1)^{1+\lambda} (\mathcal{P}e(p, \lambda)) \cdot (\mathcal{P}n) = (-1)^{1+\lambda} e(p, \lambda) \cdot n .$$

We get then,

$$\begin{aligned}
 &= \zeta_\rho(-1)^{1-\lambda} \left(\int dy e^{-iy(\mathcal{P}p) \cdot (\mathcal{P}n)} [\varphi_1(y) (e^*(\mathcal{P}p, -\lambda) \cdot \mathcal{P}n) \mathcal{P}_\mu^\nu (\mathcal{P}p)_\nu \right. \\
 & \quad \left. + \varphi_3(y) \mathcal{P}_\mu^\nu e_{\perp\nu}^*(\mathcal{P}p, -\lambda)] \right)^* \\
 &= \zeta_\rho(-1)^2 \left(\int dy e^{-iyp \cdot n} [\varphi_1(y) (e(p, \lambda) \cdot n) p_\mu + \varphi_3(y) e_{\perp\mu}(p, \lambda)] \right)^* \\
 &= \zeta_\rho \int dy e^{iyp \cdot n} [\varphi_1^*(y) (e^*(p, \lambda) \cdot n) p_\mu + \varphi_3^*(y) e_{\perp\mu}^*(p, \lambda)] .
 \end{aligned} \tag{2.84}$$

By identification we have the following relations

$$\varphi_1^*(y) = \varphi_1(y) , \quad \varphi_3^*(y) = \varphi_3(y) , \tag{2.85}$$

which show that the DAs are real functions.

The full set of distribution amplitudes

The same procedure can be applied to the other correlators and one finds at the end that the parameterization of the correlators involves two DAs (φ_1, φ_3) for the $S_{q\bar{q}}^\mu(y, \mu_F)$, one (φ_A) for the axial vector correlator $S_{q\bar{q}}^{\gamma_5 \gamma_\mu}$, one for the vector (φ_1^T) and axial vector (φ_A^T) correlators with transverse derivative, and one for the vector (B) and for the axial vector (D) correlators with three partons,

$$S_{q\bar{q}}^\mu(y; \mu_F^2) = m_\rho f_\rho [\varphi_1(y; \mu_F^2) (e^* \cdot n) p_\mu + \varphi_3(y; \mu_F^2) e_{\perp\mu}^*] , \tag{2.86}$$

$$S_{q\bar{q}}^{\gamma_5 \gamma_\mu}(y; \mu_F^2) = m_\rho f_\rho i \varphi_A(y; \mu_F^2) R_{\perp\mu}^* , \tag{2.87}$$

$$S_{q\bar{q}}^{\gamma_\mu, \perp}(y; \mu_F^2) = m_\rho f_\rho \varphi_1^T(y; \mu_F^2) p_\mu e_{\perp\alpha}^* , \tag{2.88}$$

$$S_{q\bar{q}}^{\gamma_5 \gamma_\mu, \perp}(y; \mu_F^2) = i m_\rho f_\rho \varphi_A^T(y; \mu_F^2) p_\mu R_{\perp\alpha}^* , \tag{2.89}$$

$$S_{q\bar{q}g}^{\gamma_\mu, \alpha}(y_1, y_2; \mu_F^2) = m_\rho f_\rho \zeta_{3\rho}^V(\mu_F^2) B(y_1, y_2; \mu_F^2) p_\mu e_{\perp\alpha}^* , \tag{2.90}$$

$$S_{q\bar{q}g}^{\gamma_5 \gamma_\mu, \alpha}(y_1, y_2; \mu_F^2) = m_\rho f_\rho \zeta_{3\rho}^A(\mu_F^2) i D(y_1, y_2; \mu_F^2) p_\mu R_{\perp\alpha}^* , \tag{2.91}$$

where $\zeta_{3\rho}^V(\mu_F^2)$ and $\zeta_{3\rho}^A(\mu_F^2)$ are dimensionless coupling constants:

$$\zeta_{3\rho}^V(\mu_F^2) = \frac{f_{3\rho}^V(\mu_F^2)}{f_\rho} , \quad \zeta_{3\rho}^A(\mu_F^2) = \frac{f_{3\rho}^A(\mu_F^2)}{f_\rho} . \tag{2.92}$$

We remind that, for the $q\bar{q}g$ amplitude, the quark, the antiquark and the gluon fractions of longitudinal momentum are respectively denoted y_1 , $\bar{y}_2 = 1 - y_2$ and y_g , and verify the relation $y_1 + \bar{y}_2 + y_g = 1$. Note that for the $q\bar{q}g$ DAs B and D , the gluon fraction of momentum is positive $0 \leq y_g \leq 1$ which constrains the integral over y_1 and y_2 by the condition $y_1 \leq y_2 \leq 1$,

$$\int_0^1 dy_1 \int_0^1 dy_2 \longrightarrow \int_0^1 dy_2 \int_0^{y_2} dy_1.$$

The constraints obtained from the parity relations are,

$$\begin{aligned} \varphi_1(y) &= \varphi_1(\bar{y}), & \varphi_3(y) &= \varphi_3(\bar{y}), & \varphi_A(y) &= -\varphi_A(-\bar{y}) \\ \varphi_1^T(y) &= -\varphi_1^T(\bar{y}), & \varphi_A^T(y) &= \varphi_A^T(\bar{y}) \\ B(y_1, y_2) &= -B(\bar{y}_2, \bar{y}_1), & D(y_1, y_2) &= D(\bar{y}_2, \bar{y}_1). \end{aligned}$$

Inserting in eqs. (2.33), (2.39), (2.96) the previous parameterization of the correlators and using the shorthand notations,

$$\begin{aligned} H_{q\bar{q}}^{\Gamma^\mu a_\mu}(y) &\equiv H_{q\bar{q}}^{\Gamma^\mu}(y) a_\mu, & H_{q\bar{q}}^{b, \Gamma^\mu a_\mu}(y) &\equiv H_{q\bar{q}}^{\alpha, \Gamma^\mu}(y) a_\mu b_\alpha, \\ H_{q\bar{q}g}^{b, \Gamma^\mu a_\mu}(y_1, y_2) &\equiv H_{q\bar{q}}^{\alpha, \Gamma^\mu}(y_1, y_2) a_\mu b_\alpha, \end{aligned}$$

we get the convolutions

$$i\mathcal{A}_{q\bar{q}}^{(0)} = -\frac{m_\rho f_\rho}{4} \int dy H_{q\bar{q}}^b(y) \varphi_1(y; \mu_F^2) (e_\rho^* \cdot n), \quad (2.93)$$

for a longitudinally polarized ρ -meson,

$$i\mathcal{A}_{q\bar{q}}^{(0)} = -\frac{m_\rho f_\rho}{4} \int dy \left[H_{q\bar{q}}^{\not{e}_\rho^* T}(y) \varphi_3(y; \mu_F^2) + i H_{q\bar{q}}^{R_\perp^* \gamma_5}(y) \varphi_A(y; \mu_F^2) \right], \quad (2.94)$$

$$i\mathcal{A}_{q\bar{q}}^{(1)} = -\frac{m_\rho f_\rho}{4} \int dy \left[H_{q\bar{q}}^{e_\rho^* T, \not{p}}(y) \varphi_1^T(y; \mu_F^2) + i H_{q\bar{q}}^{R_\perp^*, \not{p} \gamma_5}(y) \varphi_A^T(y; \mu_F^2) \right], \quad (2.95)$$

for the two-parton contributions and

$$\begin{aligned} i\mathcal{A}_{q\bar{q}g} &= -\frac{m_\rho f_\rho}{4} \int dy_1 dy_2 \left[H_{q\bar{q}g}^{e_\rho^* T, \not{p}}(y_1, y_2) \zeta_3^V(\mu_F^2) B(y_1, y_2; \mu_F^2) \right. \\ &\quad \left. + H_{q\bar{q}g}^{R_\perp^*, \not{p} \gamma_5}(y_1, y_2) \zeta_3^A(\mu_F^2) i D(y_1, y_2; \mu_F^2) \right], \end{aligned} \quad (2.96)$$

for the three-parton contribution of the transversely polarized ρ -meson. The DAs satisfy the normalization conditions

$$\int_0^1 dy \varphi_1(y) = 1, \quad \int_0^1 dy \varphi_3(y) = 1, \quad \int_0^1 dy (y - \bar{y}) \varphi_A(y) = \frac{1}{2}, \quad (2.97)$$

by definition of the associated coupling constants.

2.4 Reduction to a minimal set of DAs

The set of DAs defined above is over-complete, first the DAs are related by the EOMs of QCD (sec. 2.4.1) [138] and second their parameterizations depend on an arbitrary vector n and the amplitude has to be invariant under the transformations that preserve $p \cdot n = 1$ and $n^2 = 0$, leading to additional relations among DAs (sec. 2.4.2). These relations can be solved and lead to two sets of independent solutions (sec. 2.4.3), the first set corresponds to the so-called Wandzura-Wilczek (WW) solutions [147] $\{\varphi_3^{WW}, \varphi_A^{WW}, \varphi_1^{TWW}, \varphi_A^{TWW}\}$ which only depend on φ_1 the leading twist two-parton DA and the second set of solutions are called "genuine" solutions $\{\varphi_3^{gen}, \varphi_A^{gen}, \varphi_1^{Tgen}, \varphi_A^{Tgen}\}$, they depend only on the twist 3 three-parton DAs. The genuine twist 3 solutions can be interpreted as the higher Fock state contribution to the amplitude. The relations between the DAs have been derived independently of the hard sub-process in [142] in the covariant approach using exact operators identities that relate the non-local operators [148, 149]. We will follow here the approach of [131]. In the last part (sec. 2.155) we show how the three independent DAs $\{\varphi_1, B, D\}$ and the analogous DAs of Ref. [142] $\{\phi_{\parallel}, \mathcal{V}, \mathcal{A}\}$ in the covariant approach, are related, as it was shown in Ref. [131].

2.4.1 DA relations from the equations of motion of QCD

The Dirac equation on the spinor fields allows to derive relations between the DAs. Let us insert the Dirac equation inside the correlator $\langle \psi_r(0) \bar{\psi}_s(z) \rangle$, where r and s are the spinor indices of the fields, such as

$$\left\langle i \vec{D}_{ur}^x \psi_r(x) \bar{\psi}_s(z) \right\rangle_{x=0} = 0, \quad (2.98)$$

with \vec{D}_r^x is the covariant derivative with respect to the coordinate x . Another constraint can be similarly obtained by acting on $\bar{\psi}(z)$,

$$\left\langle \psi_r(0) \bar{\psi}_r(z) i \overleftarrow{D}_{st}^z \right\rangle = 0. \quad (2.99)$$

Let first focus on the $\vec{\partial}_r$ part of the covariant derivative, and split it into its longitudinal component $\vec{\partial}_L$ and its transverse component $\vec{\partial}_{\perp}$. Then the Fourier transform of the correlator reads

$$\int d^4 z e^{-iyp \cdot z - i\bar{y}p \cdot x} \left(\left\langle i \vec{\partial}_L^x \psi(x) \bar{\psi}(z) \right\rangle + \left\langle i \vec{\partial}_{\perp}^x \psi(x) \bar{\psi}(z) \right\rangle \right)_{x=0}. \quad (2.100)$$

The first term of eq. 2.100 involving the longitudinal derivative can be simplified as

$$\begin{aligned} & \int d^4 z e^{-iyp \cdot z - i\bar{y}p \cdot x} \left\langle i \vec{\partial}_L^x \psi(x) \bar{\psi}(z) \right\rangle_{x=0} \\ &= -\bar{y} \not{p} \int d^4 z e^{-iyp \cdot z - i\bar{y}p \cdot x} \left\langle \psi(x) \bar{\psi}(z) \right\rangle_{x=0}. \end{aligned} \quad (2.101)$$

The result of eq. (2.101) is obtained by first translating the correlator by $-z$, then performing an integration by part and translating back by $+z$ the correlator. Using the Fierz identity

$$-\langle \varphi_r \bar{\varphi}_s \rangle = \frac{1}{4} (\langle \bar{\varphi} \gamma_{\mu} \varphi \rangle \gamma_{rs}^{\mu} + \langle \bar{\varphi} \gamma_5 \gamma_{\mu} \varphi \rangle (\gamma^{\mu} \gamma_5)_{rs}), \quad (2.102)$$

and the parametrization of the correlators given in eqs.(2.86, 2.87), the contribution of the longitudinal derivative reads

$$\frac{m_\rho f_\rho}{4} \bar{y} (\not{p} \not{\epsilon}_\perp^* \varphi_3(y; \mu_F^2) + i \not{p} \not{R}_\perp^* \gamma_5 \varphi_A(y; \mu_F^2)) = -\frac{im_\rho f_\rho}{4} \bar{y} \sigma_{p, e_\perp^*} (\varphi_3(y; \mu_F^2) + \varphi_A(y; \mu_F^2)) , \quad (2.103)$$

where in the r.h.s.

$$\sigma_{p, e_\perp^*} = \frac{i}{2} [\not{p}, \not{\epsilon}_\perp^*] .$$

The longitudinal derivative contribution is then

$$\begin{aligned} & \int d^4 z e^{-iyp \cdot z - i\bar{y}p \cdot x} \left\langle i \vec{\partial}_L^x \psi(x) \bar{\psi}(z) \right\rangle_{x=0} \\ &= \frac{-im_\rho f_\rho}{4} \sigma_{p, e_\perp^*} (\bar{y} \varphi_3(y; \mu_F^2) + \bar{y} \varphi_A(y; \mu_F^2)) . \end{aligned} \quad (2.104)$$

The contribution from the transverse derivative ∂_\perp^x

$$\int d^4 z e^{-iyp \cdot z - i\bar{y}p \cdot x} \left\langle i \vec{\partial}_\perp^x \psi(x) \bar{\psi}(z) \right\rangle_{x=0} , \quad (2.105)$$

is directly parameterized by DAs of eqs. (2.88, 2.89) after using the Fierz identity. The transverse derivative contribution reads

$$\begin{aligned} & \int d^4 z e^{-iyp \cdot z - i\bar{y}p \cdot x} \left\langle i \vec{\partial}_\perp^x \psi(x) \bar{\psi}(z) \right\rangle_{x=0} \\ &= \frac{m_\rho f_\rho}{4} (\not{p} \varphi_1^T(y) + i \not{p} \not{R}_\perp^* \gamma_5 \varphi_A^T(y)) \end{aligned} \quad (2.106)$$

$$= -i \frac{m_\rho f_\rho}{4} \sigma_{p, e_\perp^*} (\varphi_1^T(y; \mu_F^2) + \varphi_A^T(y; \mu_F^2)) . \quad (2.107)$$

Adding the two contributions, the derivative term ∂ of the covariant derivative D reads

$$\begin{aligned} & \int d^4 z e^{-iyp \cdot z - i\bar{y}p \cdot x} \left(\left\langle i \vec{\partial}_L^x \psi(x) \bar{\psi}(z) \right\rangle + \left\langle i \vec{\partial}_\perp^x \psi(x) \bar{\psi}(z) \right\rangle \right)_{x=0} \\ &= -i \frac{m_\rho f_\rho}{4} \sigma_{p, e_\perp^*} [\bar{y} \varphi_3(y; \mu_F^2) + \bar{y} \varphi_A(y; \mu_F^2) + \varphi_1^T(y; \mu_F^2) + \varphi_A^T(y; \mu_F^2)] . \end{aligned} \quad (2.108)$$

The interaction term with the gluon field of the covariant derivative reads

$$\int d^4 z e^{-iyp \cdot z} \langle g \mathcal{A}(0) \psi(0) \bar{\psi}(z) \rangle , \quad (2.109)$$

which after using the Fierz identity, reads

$$\begin{aligned} & \int d^4 z e^{-iyp \cdot z} \langle g \mathcal{A}^\perp(0) \psi(0) \bar{\psi}(z) \rangle \\ &= -\frac{1}{4} \gamma_\rho \int d^4 z e^{-iyp \cdot z} [\langle \bar{\psi}(z) \gamma_\mu g A^{\perp\rho}(0) \psi(0) \rangle \gamma^\mu \\ &+ \langle \bar{\psi}(z) \gamma_5 \gamma_\mu g A^{\perp\rho}(0) \psi(0) \rangle \gamma^\mu \gamma_5] . \end{aligned} \quad (2.110)$$

Using the parameterization eqs.(2.90, 2.91), we get

$$\begin{aligned} & \int d^4 z e^{-iyp \cdot z} \langle g \mathcal{A}^\perp(0) \psi(0) \bar{\psi}(z) \rangle \\ &= \frac{m_\rho f_\rho}{4} \int_{y_1}^1 dy_2 [\zeta_3^V B(y_1, y_2) \not{p} \not{\epsilon}_\perp^* + i \zeta_3^A D(y_1, y_2) \not{p} \not{R}_\perp^* \gamma_5] \\ &= -i \frac{m_\rho f_\rho}{4} \sigma_{p, e_\perp^*} \int_{y_1}^1 dy_2 [\zeta_3^V B(y_1, y_2) + \zeta_3^A D(y_1, y_2)] . \end{aligned} \quad (2.111)$$

We finally obtain that the Dirac equation inserted in the correlator as

$$\int d^4 z e^{-i y p \cdot z} \left\langle \vec{\mathcal{D}}(0) \psi(0) \bar{\psi}(z) \right\rangle = 0, \quad (2.112)$$

leads to

$$\begin{aligned} & \bar{y} \varphi_3(y; \mu_F^2) + \bar{y} \varphi_A(y; \mu_F^2) + \varphi_1^T(y; \mu_F^2) + \varphi_A^T(y; \mu_F^2) \\ &= - \int_{y_1}^1 dy_2 \left[\zeta_3^V(\mu_F^2) B(y_1, y_2; \mu_F^2) + \zeta_3^A(\mu_F^2) D(y_1, y_2; \mu_F^2) \right]. \end{aligned} \quad (2.113)$$

The second equation given by the Dirac equation applied to the second fermionic field gives the following condition,

$$\begin{aligned} & y \varphi_3(y; \mu_F^2) - y \varphi_A(y; \mu_F^2) - \varphi_1^T(y; \mu_F^2) + \varphi_A^T(y; \mu_F^2) \\ &= - \int_{y_1}^1 dy_2 \left[-\zeta_3^V(\mu_F^2) B(y_1, y_2; \mu_F^2) + \zeta_3^A(\mu_F^2) D(y_1, y_2; \mu_F^2) \right]. \end{aligned} \quad (2.114)$$

Finally we see that the EOMs of QCD lead to two relations on the DAs, mixing the twist 2 and twist 3 DAs.

2.4.2 Equations from the n -independence condition

The basis of light cone vector chosen to perform the expansion of the hard part around the dominant light cone direction p , is not unique as n is not fixed by a physical direction. The amplitude should then be independent of this arbitrary choice, leading to an additional set of equations on the DAs which is independent of the associated hard scattering amplitude, as it relies on Ward identities. We will see that separating the axial vector from the vector contributions of the amplitudes and demanding the n -independence of these contributions, one can simplify these conditions thanks to the Ward identities. At the end, the n -independence conditions are the convolutions of a common hard part (involving only the quark and antiquark pair exchange) with the following combinations of DAs

$$\begin{aligned} & \frac{d\varphi_1^T}{dy}(y; \mu_F^2) + \varphi_1(y; \mu_F^2) - \varphi_3(y; \mu_F^2) \\ & + \zeta_3^V(\mu_F^2) \int_0^1 dy_2 \frac{B(y, y_2) + B(y_2, y)}{y_2 - y} = 0, \end{aligned} \quad (2.115)$$

for the vector contribution and

$$\begin{aligned} & \frac{d\varphi_A^T}{dy}(y; \mu_F^2) - \varphi_A(y; \mu_F^2) + \\ & \zeta_3^A(\mu_F^2) \int_0^1 dy_2 \frac{D(y, y_2) + D(y_2, y)}{y_2 - y} = 0, \end{aligned} \quad (2.116)$$

for the axial vector contribution.

The conditions that we require to get a Sudakov basis on the vector n are,

- n is light-like,
- $p \cdot n = 1$.

Starting from a basis of reference with a fixed light-cone reference vector n^0 satisfying these conditions, we can decompose on this basis any vector n satisfying the same conditions as

$$n^\mu = -\frac{n_\perp^2}{2}p^\mu + n_0^\mu + n_\perp^\mu.$$

Hence only the transverse degrees of freedom parameterize the n -vectors and the n -independence of the amplitude reads

$$\frac{d}{dn_\perp^\mu} \mathcal{A} = 0. \quad (2.117)$$

The total derivative can be written as

$$\begin{aligned} \frac{d}{dn_\perp^\mu} \mathcal{A} &= \frac{\partial n^\nu}{\partial n_\perp^\mu} \frac{\partial}{\partial n^\nu} + \frac{\partial(e^* \cdot n)}{\partial n_\perp^\mu} \frac{\partial}{\partial(e^* \cdot n)} \mathcal{A} \\ &= [-n_{\perp\mu} p^\nu + g_{\perp\mu}^\nu] \frac{\partial \mathcal{A}}{\partial n^\nu} + e_\perp^* \frac{\partial \mathcal{A}}{\partial(e^* \cdot n)} = 0, \end{aligned} \quad (2.118)$$

as the amplitude dependence on n is partially due to the parameterization of the polarization e^* . The n -independence condition applies separately for the vector $\mathcal{A}^{\text{vector}}$ and the axial vector $\mathcal{A}^{\text{axial}}$ parts of the amplitudes, due to their different parity properties. The dependence on n of $\mathcal{A}^{\text{vector}}$ and $\mathcal{A}^{\text{axial}}$ comes respectively from the factor $e^* \cdot n$ as

$$e_T^\mu = e^\mu - (e^* \cdot n)p_\mu,$$

and $R_{\perp\mu}^* = \varepsilon_{\mu e^* p n}$ where the vector n can only be contracted with p so that the dependence is in $p \cdot n$ then,

$$\frac{\partial n^\nu}{n_\perp^\mu} \frac{d\mathcal{A}^{\text{axial}}}{dn^\nu} = 0 \quad \Rightarrow \quad \frac{\partial \mathcal{A}^{\text{axial}}}{\partial n_\perp^\mu} = 0, \quad (2.119)$$

$$\frac{d\mathcal{A}^{\text{vector}}}{dn_\perp^\mu} = 0 \quad \Rightarrow \quad \frac{\partial \mathcal{A}^{\text{vector}}}{\partial(e^* \cdot n_\perp)} = 0. \quad (2.120)$$

The equation of n -independence of the vector amplitude $\mathcal{A}^{\text{vector}}$ (2.120) involves the terms proportional to φ_1 , φ_3 , φ_1^T and B . The associated Fierz structure closing the spinor indices of the partonic fields of the hard "vector" scattering is γ_μ . The term proportional to φ_1 reads diagrammatically as,

$$\begin{aligned} \frac{\partial}{\partial(e^* \cdot n)} \mathcal{A}_{q\bar{q}}^{(0)} &= -\frac{m_\rho f_\rho}{4} \frac{\partial}{\partial(e^* \cdot n)} \int dy \varphi_1(y) (e^* \cdot n) \text{ [diagram: wavy line to a loop with two vertical gluon lines, then a dashed line to } \not{p} \text{]} \\ &= -\frac{m_\rho f_\rho}{4} \int dy \varphi_1(y) \text{ [diagram: wavy line to a loop with two vertical gluon lines, then a dashed line to } \not{p} \text{]}. \end{aligned} \quad (2.121)$$

The term in φ_3 is

$$\begin{aligned}
 \frac{\partial}{\partial(e^* \cdot n)} \mathcal{A}_{q\bar{q}}^{(1), \varphi_3} &= -\frac{m_\rho f_\rho}{4} \frac{\partial}{\partial(e^* \cdot n)} \int dy \varphi_3(y) (e_\mu^* - (e^* \cdot n) p_\mu) \text{ (diagram)} \gamma^\mu \\
 &= \frac{m_\rho f_\rho}{4} \int dy \varphi_3(y) \text{ (diagram)} \not{p}.
 \end{aligned} \tag{2.122}$$

The term in φ_1^T involves the derivative of the hard part $H_{q\bar{q}}^{\nu, \gamma^\mu}$, which formally reads

$$\frac{\partial}{\partial(e^* \cdot n)} \left(-\frac{m_\rho f_\rho}{4} \int dy H_{q\bar{q}}^{e^* - (e^* \cdot n) p, \not{p}}(y) \varphi_1^T(y; \mu_F^2) \right) \tag{2.123}$$

$$\begin{aligned}
 &= \frac{m_\rho f_\rho}{4} \int dy \varphi_1^T(y; \mu_F^2) \left(\text{diagram 1} + \text{diagram 2} \right) \\
 &= -\frac{m_\rho f_\rho}{4} \int dy_1 \int dy_2 \delta(y_2 - y_1) \frac{\varphi_1^T(y_1; \mu_F^2)}{y_2 - y_1} \left(\text{diagram 3} - \text{diagram 4} \right) \\
 &= -\frac{m_\rho f_\rho}{4} \int dy \left(\text{diagram 5} \right) \frac{d}{dy} \varphi_1^T(y; \mu_F^2),
 \end{aligned} \tag{2.124}$$

where we used the following Ward identity in the collinear limit [150],

$$p_\mu \xrightarrow{y_1 p} \bullet \xrightarrow{\gamma^\mu} y_2 p = \frac{1}{y_2 - y_1} \left[\text{diagram 6} - \text{diagram 7} \right]. \tag{2.125}$$

We see that it is some kind of integration by part in order that the derivative acting on the hard part finally acts on the DA.

One can show that the three-parton contribution to eq. (2.120) that will mix with the previous terms is associated to the abelian diagrams of fig. 2.8. These diagrams have the

same color structure than the two-parton diagrams and the term in B reads

$$\begin{aligned}
 & \frac{\partial}{\partial(e^* \cdot n)} \left(\frac{-m_\rho f_\rho}{4} \int dy_1 dy_2 H_{q\bar{q}g}^{e^*-(e^* \cdot n)p, \not{p}}(y_1, y_2) \zeta_3^V(\mu_F^2) B(y_1, y_2; \mu_F^2) \right) \\
 &= \frac{m_\rho f_\rho}{4} \int dy_1 dy_2 \zeta_3^V(\mu_F^2) B(y_1, y_2; \mu_F^2) \left(\text{Diagram 1} + \text{Diagram 2} \right) \\
 &= -\frac{m_\rho f_\rho}{4} \zeta_3^V(\mu_F^2) \int dy_1 \int dy_2 \frac{B(y_1, y_2; \mu_F^2)}{y_2 - y_1} \left(\text{Diagram 3} - \text{Diagram 4} \right) \\
 &= -\frac{m_\rho f_\rho}{4} \zeta_3^V(\mu_F^2) \int dy_1 \int dy_2 \left(\text{Diagram 5} \right) \\
 & \quad \times \frac{B(y_1, y_2; \mu_F^2) + B(y_2, y_1; \mu_F^2)}{y_2 - y_1}, \tag{2.126}
 \end{aligned}$$

where we used the Ward identity (2.125), and the symmetry property

$$B(y_1, y_2; \mu_F^2) = -B(\bar{y}_2, \bar{y}_1; \mu_F^2).$$

Finally, the sum of these terms gives the hard sub-process independent relation coming from eq. (2.120),

$$\begin{aligned}
 & \frac{d\varphi_1^T}{dy}(y; \mu_F^2) + \varphi_1(y; \mu_F^2) - \varphi_3(y; \mu_F^2) \\
 & + \zeta_3^V(\mu_F^2) \int_0^1 dy_2 \frac{B(y, y_2) + B(y_2, y)}{y_2 - y} = 0. \tag{2.127}
 \end{aligned}$$

The axial vector n -independence condition can be derived with the same techniques and gives the relation

$$\begin{aligned}
 & \frac{d\varphi_A^T}{dy}(y; \mu_F^2) - \varphi_A(y; \mu_F^2) + \\
 & \zeta_3^A(\mu_F^2) \int_0^1 dy_2 \frac{D(y, y_2) + D(y_2, y)}{y_2 - y}. \tag{2.128}
 \end{aligned}$$

The equations (2.127) and (2.128) are the results of the n -independence conditions.

2.4.3 Wandzura-Wilczek and genuine solutions

As we saw in the two previous sections, the seven DAs involved in the chiral even process are not independent. They are related by four equations, namely two equations from the EOMs of QCD and two equations coming from the n -independence conditions. This means that four of the seven DAs, denoted " φ_i " = $\{\varphi_3, \varphi_A, \varphi_1^T, \varphi_A^T\}$, can be expressed in terms of three independent DAs chosen to be $\{\varphi_1, B, D\}$. The solutions for φ_i can be split into a

solution depending only on the twist 2 DA φ_1 , by putting B and D to zero which consists in forgetting about the correlators with an additional transverse gluon, these solutions are called Wandzura-Wilczek (WW) solutions [147, 151] and are denoted φ_i^{WW} , and genuine solutions denoted φ_i^{gen} which only depend on B and D . The decomposition of the solutions φ_i is a linear decomposition in φ_i^{gen} and φ_i^{WW} ,

$$\varphi_i(y; \mu_F^2) = \varphi_i^{WW}(y; \mu_F^2) + \varphi_i^{gen}(y; \mu_F^2).$$

The WW-solutions

Putting the contributions of B and D to zero, the EOMs for the WW DAs are⁵

$$\bar{y}\varphi_3^{WW}(y) + \bar{y}\varphi_A^{WW}(y) + \varphi_1^{TWW}(y) + \varphi_A^{TWW}(y) = 0, \quad (2.129)$$

$$y\varphi_3^{WW}(y) - y\varphi_A^{WW}(y) - \varphi_1^{TWW}(y) + \varphi_A^{TWW}(y) = 0. \quad (2.130)$$

The n -independence relations read

$$\frac{d}{dy}\varphi_1^{TWW}(y) = -\varphi_1(y) + \varphi_3^{WW}(y), \quad \frac{d}{dy}\varphi_A^{TWW}(y) = \varphi_A^{WW}(y). \quad (2.131)$$

From the previous equations, one can deduce a set of equations relating φ_3 and φ_A to φ_1 ,

$$\frac{d}{dy}\varphi_3^{WW}(y) = -(\bar{y} - y)\frac{d}{dy}\varphi_A^{WW}(y), \quad 2\varphi_1(y) = \frac{d}{dy}\varphi_A^{WW}(y) + (\bar{y} - y)\frac{d}{dy}\varphi_3^{WW}(y). \quad (2.132)$$

The solutions of these equations are [147, 151]

$$\varphi_A^{WW}(y) = \frac{1}{2} \left[\int_0^y \frac{dv}{v} \varphi_1(v) - \int_y^1 \frac{dv}{v} \varphi_1(v) \right], \quad (2.133)$$

$$\varphi_3^{WW}(y) = \frac{1}{2} \left[\int_0^y \frac{dv}{v} \varphi_1(v) + \int_y^1 \frac{dv}{v} \varphi_1(v) \right], \quad (2.134)$$

they satisfy the normalization conditions

$$\int_0^1 dy \varphi_3^{WW}(y) = 1 \quad \text{and} \quad \int_0^1 dy \varphi_A^{WW}(y) = 1. \quad (2.135)$$

Inserting these solutions in the eqs. (2.129, 2.130) gives the solutions for φ_1^T and φ_A^T ,

$$\varphi_A^{TWW}(y) = \frac{1}{2} \left[-\bar{y} \int_0^y \frac{dv}{v} \varphi_1(v) - y \int_y^1 \frac{dv}{v} \varphi_1(v) \right], \quad (2.136)$$

$$\varphi_1^{TWW}(y) = \frac{1}{2} \left[-\bar{y} \int_0^y \frac{dv}{v} \varphi_1(v) + y \int_y^1 \frac{dv}{v} \varphi_1(v) \right]. \quad (2.137)$$

The WW-solutions (2.134, 2.133) were already derived in Ref. [152] for the computation of the transition form factors $B_{u,d} \rightarrow V + \gamma$ with $V = \{K^*, \rho\}$, $B_d \rightarrow \omega + \gamma$ and $B_s \rightarrow V + \gamma$ $V = \{\phi, K^*\}$.

Let us emphasize that the WW solutions are not intrinsic twist 3 distributions, they only depend on the leading twist DA φ_1 associated to the production of a longitudinal meson.

⁵For the sake of conciseness, we will omit the dependence in μ_F^2 of the DAs as it is not needed in this part.

Genuine solutions

The genuine solutions obey the full EOMs and n -independence relations,

$$\begin{aligned} \bar{y}_1 \varphi_3^{gen}(y_1) + \bar{y}_1 \varphi_A^{gen}(y_1) + \varphi_1^{Tgen}(y_1) + \varphi_A^{Tgen}(y_1) \\ = - \int_0^1 dy_2 [\zeta_3^V B(y_1, y_2) + \zeta_3^A D(y_1, y_2)] , \end{aligned} \quad (2.138)$$

$$\begin{aligned} y_1 \varphi_3^{gen}(y_1) - y_1 \varphi_A^{gen}(y_1) - \varphi_1^{Tgen}(y_1) + \varphi_A^{Tgen}(y_1) \\ = - \int_0^1 dy_2 [-\zeta_3^V B(y_2, y_1) + \zeta_3^A D(y_2, y_1)] , \end{aligned} \quad (2.139)$$

$$\frac{d}{dy_1} \varphi_1^{Tgen}(y_1) = \varphi_3^{gen}(y_1) - \zeta_3^V \int_0^1 \frac{dy_2}{y_2 - y_1} (B(y_1, y_2) + B(y_2, y_1)) , \quad (2.140)$$

$$\frac{d}{dy_1} \varphi_A^{Tgen}(y_1) = \varphi_A^{gen}(y_1) - \zeta_3^A \int_0^1 \frac{dy_2}{y_2 - y_1} (D(y_1, y_2) + D(y_2, y_1)) . \quad (2.141)$$

Isolating the distributions φ_3^{gen} and φ_A^{gen} , one finds the equations,

$$\begin{aligned} \frac{d}{dy_1} \varphi_3^{gen}(y_1) + (\bar{y}_1 - y_1) \frac{d}{dy_1} \varphi_A^{gen}(y_1) = 4 \zeta_3^A \int_0^1 \frac{dy_2}{y_2 - y_1} D^{(+)}(y_1, y_2) \\ - 2 \zeta_3^V \frac{d}{dy_1} \int_0^1 dy_2 B^{(-)}(y_1, y_2) - 2 \zeta_3^A \frac{d}{dy_1} \int_0^1 dy_2 D^{(+)}(y_1, y_2) , \end{aligned} \quad (2.142)$$

$$\begin{aligned} \frac{d}{dy_1} \varphi_A^{gen}(y_1) + (\bar{y}_1 - y_1) \frac{d}{dy_1} \varphi_3^{gen}(y_1) = 4 \zeta_3^V \int_0^1 \frac{dy_2}{y_2 - y_1} B^{(+)}(y_1, y_2) \\ - 2 \zeta_3^V \frac{d}{dy_1} \int_0^1 dy_2 B^{(+)}(y_1, y_2) - 2 \zeta_3^A \frac{d}{dy_1} \int_0^1 dy_2 D^{(-)}(y_1, y_2) , \end{aligned} \quad (2.143)$$

where we denote,

$$B^{(\pm)}(y_1, y_2) = B(y_1, y_2) \pm B(y_2, y_1) \text{ and } D^{(\pm)}(y_1, y_2) = D(y_1, y_2) \pm D(y_2, y_1) . \quad (2.144)$$

From the system of equations (2.142, 2.143), we can deduce the following equation on φ_3^{gen} ,

$$\begin{aligned} \frac{d}{dy_1} \varphi_3^{gen}(y_1) = -\frac{1}{2} \left(\frac{1}{y_1} + \frac{1}{\bar{y}_1} \right) \left\{ \zeta_3^V \left[y_1 \int_{y_1}^1 dy_2 \frac{d}{dy_1} B(y_1, y_2) - \bar{y}_1 \int_0^{y_1} \frac{d}{dy_1} B(y_2, y_1) \right. \right. \\ \left. \left. + (\bar{y}_1 - y_1) \left(\int_{y_1}^1 dy_2 \frac{B(y_1, y_2)}{y_2 - y_1} + \int_0^{y_1} dy_2 \frac{B(y_2, y_1)}{y_2 - y_1} \right) \right] \right. \\ \left. + \zeta_3^A \left[y_1 \int_{y_1}^1 dy_2 \frac{d}{dy_1} D(y_1, y_2) + \bar{y}_1 \int_0^{y_1} \frac{d}{dy_1} D(y_2, y_1) \right. \right. \\ \left. \left. - \int_{y_1}^1 dy_2 \frac{D(y_1, y_2)}{y_2 - y_1} - \int_0^{y_1} dy_2 \frac{D(y_2, y_1)}{y_2 - y_1} \right] \right\} . \end{aligned} \quad (2.145)$$

The normalized solution for φ_3^{gen} is obtained by integrating over y_1 . The solution is expected to be of the form,

$$\varphi_3^{gen}(y) = \frac{1}{2} \left(- \int_y^1 \frac{dy_1}{y_1} + \int_0^1 \frac{dy_1}{\bar{y}_1} \right) \{ \dots \} . \quad (2.146)$$

Finding the right combination between the brackets gives the following solution for φ_3^{gen} ,

$$\begin{aligned} \varphi_3^{gen}(y) = & \\ & -\frac{1}{2} \int_y^1 \frac{du}{u} \left[\int_0^u dy_2 \frac{d}{du} (\zeta_3^V B - \zeta_3^A D)(y_2, u) - \int_u^1 \frac{dy_2}{y_2 - u} (\zeta_3^V B - \zeta_3^A D)(u, y_2) \right. \\ & \quad \left. - \int_0^u \frac{dy_2}{y_2 - u} (\zeta_3^V B - \zeta_3^A D)(y_2, u) \right] \\ & -\frac{1}{2} \int_0^{y_1} \frac{du}{\bar{u}} \left[\int_u^1 dy_2 \frac{d}{du} (\zeta_3^V B + \zeta_3^A D)(u, y_2) - \int_u^1 \frac{dy_2}{y_2 - u} (\zeta_3^V B + \zeta_3^A D)(u, y_2) \right. \\ & \quad \left. - \int_0^u \frac{dy_2}{y_2 - u} (\zeta_3^V B + \zeta_3^A D)(y_2, u) \right]. \end{aligned} \quad (2.147)$$

We will denote,

$$S(y_1, y_2; \mu_F^2) = \zeta_3^V(\mu_F^2) B(y_1, y_2; \mu_F^2) + \zeta_3^A(\mu_F^2) D(y_1, y_2; \mu_F^2), \quad (2.148)$$

$$M(y_1, y_2; \mu_F^2) = \zeta_3^V(\mu_F^2) B(y_1, y_2; \mu_F^2) - \zeta_3^A(\mu_F^2) D(y_1, y_2; \mu_F^2). \quad (2.149)$$

They transform under the exchange of the quark and the antiquark roles as

$$S(\bar{y}_2, \bar{y}_1; \mu_F^2) = -M(y_1, y_2; \mu_F^2). \quad (2.150)$$

The solution φ_3^{gen} can be written in the form analogously to the expression of the WW solution (2.134),

$$\varphi_3^{gen}(y) = \frac{1}{2} \left[\int_{\bar{y}}^1 du \frac{A(u)}{u} + \int_y^1 du \frac{A(u)}{u} \right], \quad (2.151)$$

where

$$A(u) = \int_0^u dy_2 \left[\frac{1}{y_2 - u} - \partial_u \right] M(y_2, u) + \int_u^1 dy_2 \frac{1}{y_2 - u} M(u, y_2). \quad (2.152)$$

the quantity $A(u)$ satisfies the constraints,

$$\int_0^1 du A(u) = 0 \quad \text{and} \quad \int_0^1 du \bar{u} A(u) = 0. \quad (2.153)$$

Inserting the solution (2.147) in eq. (2.140), the genuine solution for φ_1^T is

$$\varphi_1^{Tgen} = \int_0^y du \varphi_3^{gen}(u) - \zeta_3^V \int_0^y dy_1 \int_y^1 dy_2 \frac{B(y_1, y_2)}{y_2 - y_1}. \quad (2.154)$$

Similarly, the genuine solutions for φ_A and φ_A^T can be obtained from the solutions φ_3^{gen} and φ_1^{Tgen} by exchanging the role of $\zeta_3^V B$ and $\zeta_3^A D$. In terms of the combinations $S(y_2, y_1)$ and $M(y_2, y_1)$, this corresponds to exchange

$$S(y_1, y_2) \rightarrow S(y_1, y_2) \text{ and } M(y_1, y_2) \rightarrow -M(y_1, y_2).$$

2.4.4 The dictionary

In Ref. [131], the equivalence between the covariant collinear approach (CCF), which is developed in Refs. [141, 142, 153, 154, 155] and the LCCF parameterization of the DAs is shown on the example of the $\gamma^* \rightarrow \rho$ impact factor. The dictionary between the two sets of DAs is

$$\begin{aligned} B(y_1, y_2) &= -\frac{\mathcal{V}(y_1, \bar{y}_2)}{y_2 - y_1}, \quad D(y_1, y_2) = -\frac{\mathcal{A}(y_1, \bar{y}_2)}{y_2 - y_1}, \\ \varphi_1(y) &= \phi_{\parallel}(y), \quad \varphi_3(y) = g_{\perp}^{(v)}(y), \quad \varphi_A(y) = -\frac{1}{4} \frac{\partial g_{\perp}^{(a)}(y)}{\partial y}. \end{aligned} \quad (2.155)$$

The higher twist contributions come from the deviation from the light-cone direction $z^2 \rightarrow 0$ due to the non-zero meson mass m_{ρ} . In our approach we neglected the mass term in the definitions of the momentum $p_{\rho} \sim p$ and the parton separation z , justifying that it would lead to twist 4 terms at least. The two-parton chiral-even DAs up to twist 3 accuracy, neglecting the quark mass terms, are defined as

$$\begin{aligned} \langle 0 | \bar{u}(z) \gamma_{\mu} [z, -z] d(-z) | \rho(p, \lambda) \rangle &= m_{\rho} f_{\rho} \left(p_{\mu} \frac{e^{(\lambda)} \cdot z}{p \cdot z} \int_0^1 dy e^{i\xi p \cdot z} \Phi_{\parallel}(y, \mu^2) \right. \\ &\quad \left. + e_{\perp \mu}^{(\lambda)} \int_0^1 dy e^{i\xi p \cdot z} g_{\perp}^{(v)}(y, \mu^2) \right), \end{aligned} \quad (2.156)$$

$$\langle 0 | \bar{u}(z) \gamma_{\mu} \gamma_5 [z, -z] d(-z) | \rho(p, \lambda) \rangle = \frac{1}{2} m_{\rho} f_{\rho} \varepsilon_{\mu e_{\perp}^{(\lambda)}} p_z \int dy e^{i\xi p \cdot z} g_{\perp}^{(a)}, \quad (2.157)$$

with $\xi = y - \bar{y}$, where the twist 2 DA is ϕ_{\parallel} and where $g_{\perp}^{(a)}$, $g_{\perp}^{(v)}$ are the twist 3 DAs. The chiral-even three parton DAs are defined as

$$\begin{aligned} \langle 0 | \bar{u}(z) \gamma_{\alpha} [z, vz] g G_{\mu\nu}(vz) [vz, -z] d(-z) | \rho(p, \lambda) \rangle &= im_{\rho} f_{\rho} \zeta_3^V \\ &\quad \times p_{\alpha} (p_{\mu} e_{\perp \nu}^{(\lambda)} - p_{\nu} e_{\perp \mu}^{(\lambda)}) \mathcal{V}(v, pz), \end{aligned} \quad (2.158)$$

$$\begin{aligned} \langle 0 | \bar{u}(z) \gamma_{\alpha} \gamma_5 [z, vz] g \tilde{G}_{\mu\nu}(vz) [vz, -z] d(-z) | \rho(p, \lambda) \rangle &= m_{\rho} f_{\rho} \zeta_3^A \\ &\quad \times p_{\alpha} (p_{\mu} e_{\perp \nu}^{(\lambda)} - p_{\nu} e_{\perp \mu}^{(\lambda)}) \mathcal{A}(v, pz), \end{aligned} \quad (2.159)$$

with

$$\mathcal{F}(v, pz) = \int \mathcal{D}[\underline{y}] e^{-ipz(\bar{y}_2 - y_1 + vy_g)} \mathcal{F}(y_1, \bar{y}_2, y_g), \quad (2.160)$$

and $\int \mathcal{D}[\underline{y}] \equiv \int_0^1 dy_1 \int_0^1 dy_2 \int_0^1 dy_g \delta(1 - y_1 - \bar{y}_2 - y_g)$. The dual of the strength tensor being defined as $\tilde{G}_{\mu\nu} = -\frac{1}{2} \varepsilon_{\mu\nu\rho\sigma} G^{\rho\sigma}$.

Writing the two-parton matrix elements appearing in the soft parts of our process in

terms of the previous DAs, leads to

$$\begin{aligned} \langle \rho(p) | \bar{\psi}(z)[z, 0] \gamma_\mu \psi(0) | 0 \rangle &= m_\rho f_\rho \int_0^1 dy e^{iyp \cdot z} \left(\phi_\parallel(y) \frac{e^* \cdot z}{p \cdot z} p_\mu \right. \\ &\quad \left. + e_{\perp\mu}^* g_\perp^{(v)}(y) \right), \end{aligned} \quad (2.161)$$

$$\begin{aligned} \langle \rho(p) | \bar{\psi}(z)[z, 0] \gamma_5 \gamma_\mu \psi(0) | 0 \rangle &= -\frac{m_\rho f_\rho}{4} \int_0^1 dy e^{iyp \cdot z} g_\perp^{(a)}(y) \varepsilon_{\mu e_\perp^* p z} \\ &= im_\rho f_\rho \int_0^1 dy e^{iyp \cdot z} \left[-\frac{1}{4} \frac{dg_\perp^{(a)}(y)}{dy} \right] \frac{\varepsilon_{\mu e_\perp^* p z}}{p \cdot z}. \end{aligned} \quad (2.162)$$

Identifying the coordinate z with the light cone direction $z = \lambda n$ and choosing the axial gauge $n \cdot A = 0$, the identification of the DAs is straightforward and leads to the dictionary (2.155) for φ_1 , φ_3 , φ_A .

The three particle correlators reads

$$\langle \rho(p) | \bar{\psi}(z)[z, tz] \gamma_\mu g G_{\alpha\beta}(tz) [tz, 0] \psi(0) | 0 \rangle \quad (2.163)$$

$$= -im_\rho f_\rho \zeta_3^V p_\mu (p_\alpha e_{\perp\beta}^* - p_\beta e_{\perp\alpha}^*) \int \mathcal{D}[y] \mathcal{V}(y_1, \bar{y}_2) e^{iy_1 p \cdot z + iy_g p \cdot (tz)},$$

$$\langle \rho(p) | \bar{\psi}(z)[z, tz] \gamma_5 \gamma_\mu g \tilde{G}_{\alpha\beta}(tz) [tz, 0] \psi(0) | 0 \rangle \quad (2.164)$$

$$= m_\rho f_\rho \zeta_3^A p_\mu (p_\alpha e_{\perp\beta}^* - p_\beta e_{\perp\alpha}^*) \int \mathcal{D}[y] \mathcal{A}(y_1, \bar{y}_2) e^{iy_1 p \cdot z + iy_g p \cdot (tz)}.$$

In the axial gauge $n \cdot A = 0$, the Wilson lines drop off and the gluon field is expressed in terms of the field-strength tensor as

$$A_\alpha(y) = \int_0^\infty d\sigma e^{-\epsilon\sigma} n^\beta G_{\alpha\beta}(y + \sigma n). \quad (2.165)$$

Multiplying (2.163, 2.167) by n^β , integrating over σ i.e. over t after a change of variable, one gets

$$\langle \rho(p) | \bar{\psi}(z) \gamma_\mu g A_\alpha(tz) \psi(0) | 0 \rangle \quad (2.166)$$

$$= -m_\rho f_\rho \zeta_3^V p_\mu p_\alpha e_{\perp\beta}^* \int \mathcal{D}[y] \frac{\mathcal{V}(y_1, \bar{y}_2)}{y_g} e^{iy_1 p \cdot z + iy_g p \cdot (tz)},$$

$$\langle \rho(p) | \bar{\psi}(z) \gamma_5 \gamma_\mu g A_\alpha(tz) \psi(0) | 0 \rangle \quad (2.167)$$

$$= -im_\rho f_\rho \zeta_3^A p_\mu \frac{\varepsilon_{\alpha e_\perp^* p z}}{p \cdot z} \int \mathcal{D}[y] \frac{\mathcal{A}(y_1, \bar{y}_2)}{y_g} e^{iy_1 p \cdot z + iy_g p \cdot (tz)}. \quad (2.168)$$

The identification in $z = \lambda n$ gives the relations in (2.155) for the three-parton DAs.

In [131] the equivalence of the DAs (2.155) was carefully checked on the results for the spin flip and spin non-flip impact factor calculations. The fact that both results in covariant gauge and light-cone gauge are the same is also an explicit check on the gauge invariance of the impact factor results.

2.5 Conformal expansion and scale dependence of DAs

Now, having established a connection between the DAs of the LCCF approach [131] and the DAs of the CCF approach [142], we can use the models for the DAs that was presented in [142] using

- first conformal expansion terms of the DAs,
- factorization/renormalization scale dependence driven by renormalization group equations of the conformal operator expansion,
- QCD sum rules for the values of the coupling constants at a initial scale $\mu_0 = 1$ GeV

to get explicit expressions for $\phi_{\parallel}(y; \mu^2)$, $\mathcal{V}(y; \mu^2)$, $\mathcal{A}(y; \mu^2)$.

2.5.1 Goal of the conformal expansion

Let us first motivate the conformal expansion of the light-cone wave functions by considering an analogous problem; the problem of one particle in a spherical potential in quantum mechanics. In this case, the invariance under rotation of the spherical potential allows to decouple the radial dependence from the angular dependence by performing a partial wave expansion of the wave function in the basis of the spherical harmonics. This decomposition allows to put all the angular dependence into these harmonics, and then the radial dependence is driven by the one-dimensional Schrödinger equation.

In our case, the massless QCD is invariant under the transformations of the collinear subgroup of the conformal group $SL(2, \mathbb{R})$ that describes Möbius transformations on the light-cone. The conformal invariance is broken by quantum corrections but it is valid at the level of leading logarithm accuracy. The Efremov-Radyushkin-Brodsky-Lepage (ERBL) equation [156, 157] that governs the Q^2 -dependence of the DA $\varphi(y; Q^2)$, reads

$$Q^2 \frac{\partial}{\partial Q^2} \varphi(y; Q^2) = \frac{\alpha_s(Q^2)}{4\pi} \int_0^1 [dz] V(z, y) \varphi(z; Q^2), \quad (2.169)$$

where the kernel V can be computed in pQCD for large Q^2 . Note that the ERBL evolution is currently known at NLO [158, 159, 160, 161]. The eigenfunctions φ_n that diagonalize the Brodsky-Lepage potential are given by the representations of the conformal group $P_n(y)$ labeled by a conformal spin n

$$\varphi_n(y, Q^2) \propto a_n(Q^2) P_n(y). \quad (2.170)$$

For example, the leading twist DA longitudinal y dependence is expanded on the basis of the Gegenbauer orthogonal polynomials $C_n^{3/2}$

$$\varphi_1(y; \mu^2) \equiv \Phi_{\parallel}(y) = 6y\bar{y} \sum_{n=0}^{\infty} a_n^{\parallel}(\mu_F^2) C_n^{3/2}(y - \bar{y}), \quad (2.171)$$

like in quantum mechanics the wave function angular dependence is expanded on Legendre orthogonal polynomials labeled by the orbital quantum numbers. In this expansion, the n -th term has a conformal spin $n + 2$. At the LL accuracy, the coefficients $a_n(Q^2)$ evolution is driven by the renormalization group (RG) equation of the operators \mathcal{O}_n of same conformal spin,

$$\left(\mu \frac{\partial}{\partial \mu} + \beta(g) \frac{\partial}{\partial g} \right) \mathcal{O}_n^{(i)}(x; \mu^2) = -\frac{\alpha_s}{2\pi} \Gamma_{ij}^n \mathcal{O}_n^{(j)}(x; \mu^2). \quad (2.172)$$

There is no operator mixing under renormalization between operators of different conformal spins, which means in other words that in the basis of these operators the anomalous dimension matrix Γ_n is block diagonal. Indeed the matrices Γ_n is diagonal for leading twist operators but the representation of twist 3 operators are degenerate as we will see. The solutions have the form,

$$\varphi(y; \mu^2) = N \sum_n a_n(\mu^2) P_n(y), \quad (2.173)$$

with N a normalization factor. The scale evolution of $a_n(\mu^2)$ is of the form

$$a_n^{(i)}(\mu^2) = [L^{\frac{\Gamma_n}{\beta_0}}(\mu^2, \mu_0^2)]_{ij} a_n^{(j)}(\mu_0^2),$$

where $L(\mu^2, \mu_0^2) = (\alpha_s(\mu^2)/\alpha_s(\mu_0^2))$.

The conformal spin of a constituent primary field is equal to $j = \frac{1}{2}(d + s)$ with d the canonical dimension and s the spin projection of the field onto the light-cone. The multi-particle states can be expanded in terms of conformal spin and its lowest spin is the sum of the spin of the constituent primary fields. This lowest spin state is called "asymptotic DA", and is the only surviving state in the large energy limit due to the fact that it has the lowest anomalous dimension. The asymptotic DA for a multi-particle state takes the form [162, 149]

$$\phi^{AS}(\alpha_1, \alpha_2, \dots, \alpha_n) = \frac{\Gamma(2j_1 + \dots + 2j_n)}{\Gamma(2j_1)\Gamma(2j_2)\dots\Gamma(2j_n)} \alpha_1^{2j_1-1} \alpha_2^{2j_2-1} \dots \alpha_n^{2j_n-1}, \quad (2.174)$$

with α_k the longitudinal fraction of the momentum ($\sum_1^n \alpha_k = 1$) carried by the primary constituent field f_k (quark antiquark or gluon field) of conformal spin j_k . The asymptotic DA $\varphi_1(y, \mu_F^2)$ with $\mu_F^2 \sim Q^2 \rightarrow \infty$, denoted $\varphi_1^{AS}(y)$ is then given by

$$\varphi_1^{AS}(y) = 6y\bar{y}. \quad (2.175)$$

In the production of the ρ -meson up to twist 3 we neglect the masses of the quarks which are fairly small compared to the scales of the problem but if one would be interested in the ϕ -meson production for example, one should be more careful and take into account SU(3)-flavor breaking symmetry. The introduction of mass effects breaks explicitly the conformal invariance.

Nevertheless, the masses do not affect the transverse evolution of DAs as it is given by the scale evolution of the operators governed by the anomalous dimensions which does not depend on the masses as long as they can be neglected compared to the scale of the process. Keeping the quark masses, the higher twist DAs when expressed in terms of a minimal

set of DAs through the relations such as EOMs of QCD or n -independence, exhibit terms proportional to the quark masses. These terms mix the chiral even and chiral odd sectors. For example the twist 3 DAs φ_1^T would get a dependence from the twist 2 DA of the chiral odd sector proportional to the sum of quark masses $m_u + m_d$. As the masses of the quarks are inside multiplicative factors in these terms, the conformal expansion can still be used to study the DA evolutions.

2.5.2 Conformal expansion of the DAs

The twist 2 DA $\varphi_1(y; \mu^2)$ conformal partial wave expansion is already given in eq. (2.171). The first coefficient a_0^\parallel is constant due to the normalization condition

$$\int_0^1 dy \varphi_1(y; \mu^2) = 1.$$

The invariance of the ρ -meson state under G-parity implies that the n -odd terms are vanishing.

The conformal expansion can be performed on operators with definite spin projection on the light-cone. The spin projectors on the light-cone are $P_+ = \frac{1}{2}\gamma_*\gamma$ and $P_- = \frac{1}{2}\gamma\gamma_*$ with the notations $a \cdot = a \cdot z$ and $a_* = \frac{a \cdot p}{p \cdot z}$. The twist 3 DAs operators are

$$\langle 0 | \gamma \cdot \gamma_\mu^\perp \gamma_* [z, -z] d(-z) | \rho^-(p, \lambda) \rangle = -m_\rho f_\rho e_{\perp\mu}^{(\lambda)} \int_0^1 dy e^{i\xi p \cdot z} g^{\uparrow\downarrow}(y), \quad (2.176)$$

$$\langle 0 | \gamma_* \gamma_\mu^\perp \gamma [z, -z] d(-z) | \rho^-(p, \lambda) \rangle = -m_\rho f_\rho e_{\perp\mu}^{(\lambda)} \int_0^1 dy e^{i\xi p \cdot z} g^{\downarrow\uparrow}(y), \quad (2.177)$$

with,

$$g^{\uparrow\downarrow} = g_\perp^{(v)} + \frac{1}{4} \frac{d}{du} g_\perp^{(a)} \equiv \varphi_3 - \varphi_A, \quad (2.178)$$

$$g^{\downarrow\uparrow} = g_\perp^{(v)} - \frac{1}{4} \frac{d}{du} g_\perp^{(a)} \equiv \varphi_3 + \varphi_A. \quad (2.179)$$

The conformal expansion for the DAs $g^{\uparrow\downarrow}, g^{\downarrow\uparrow}$ reads

$$g^{\uparrow\downarrow}(y) = 2\bar{y} \sum_{n=0}^{\infty} g_n^{\uparrow\downarrow} P_n^{(1,0)}(\xi), \quad (2.180)$$

$$g^{\downarrow\uparrow}(y) = 2y \sum_{n=0}^{\infty} g_n^{\downarrow\uparrow} P_n^{(0,1)}(\xi), \quad (2.181)$$

with $P_n^{(i,j)}$ the Jacobi polynomials. The term labeled with n has a conformal spin $n + 3/2$. This leads to the following expressions for $g_\perp^{(v,a)}$,

$$g_\perp^{(v)} = \sum_{n \text{ even}} (G_n - G_{n-1}) C_n^{1/2}(\xi) + \sum_{n \text{ odd}} (g_n - g_{n-1}) C_n^{1/2}(\xi), \quad (2.182)$$

$$g_\perp^{(a)} = 8y\bar{y} \left(\sum_{n \text{ even}} \frac{G_n - G_{n+1}}{(n+1)(n+2)} C_n^{3/2}(\xi) + \sum_{n \text{ odd}} \frac{g_n - g_{n+1}}{(n+1)(n+2)} C_n^{3/2}(\xi) \right), \quad (2.183)$$

with,

$$G_n = \frac{1}{2} (g_n^{\uparrow\downarrow} + (-1)^n g_n^{\downarrow\uparrow}) , \quad (2.184)$$

$$g_n = \frac{1}{2} (g_n^{\uparrow\downarrow} - (-1)^n g_n^{\downarrow\uparrow}) . \quad (2.185)$$

It is interesting that the expansion of $g_{\perp}^{(v,a)}$ are involving coefficients of different conformal spin. However we do not have to worry about this mixing of conformal spin terms as $g_{\perp}^{(v,a)}$ can be expressed in terms of $\varphi_1(y) \equiv \phi_{\parallel}$ and $B(y_1, y_2) \equiv -\frac{V(y_1, \bar{y}_2)}{y_2 - y_1}$ and $D(y_1, y_2) \equiv -\frac{A(y_1, \bar{y}_2)}{y_2 - y_1}$ where there is no such mixing.

The conformal expansion of the twist 3 $q\bar{q}g$ correlators reads

$$\mathcal{V}(y_1, \bar{y}_2, y_g) = 360 y_1 \bar{y}_2 y_g^2 \sum_{k,l=0}^{\infty} \omega_{k,l}^V J_{k,l}(y_1, \bar{y}_2) , \quad (2.186)$$

$$\mathcal{A}(y_1, \bar{y}_2, y_g) = 360 y_1 \bar{y}_2 y_g^2 \sum_{k,l=0}^{\infty} \omega_{k,l}^A J_{k,l}(y_1, \bar{y}_2) , \quad (2.187)$$

where $J_{k,j}(y_1, \bar{y}_2) \equiv J_{k,l}(6, 2, 2, y_1, \bar{y}_2)$ are Appell polynomials and $y_g = 1 - (y_1 + \bar{y}_2)$ the gluon fraction of momentum. The conformal spin of the term labeled by the couple $\{k, l\}$ is $n = l + k + 7/2$, hence the conformal representation of spin n is degenerate as the operators with $l + k = n - 7/2$ have same conformal spins. Note also that the number of degeneracy increases with n . They can mix with each other explaining why the anomalous dimension matrix is only block diagonal at twist 3. The G-parity invariance of the DAs implies the following relations between the coefficients $\omega^{V,A}$,

$$\omega_{k,l}^V = -\omega_{l,k}^V , \quad \omega_{k,l}^A = \omega_{l,k}^A .$$

We denote $\omega_{[k,l]}^V = (\omega_{k,l}^V - \omega_{l,k}^V)/2$ and $\omega_{\{k,l\}}^A = (\omega_{k,l}^A + \omega_{l,k}^A)/2$. The normalization condition implies that

$$\omega_{[0,1]}^V = 28/3 , \quad \omega_{\{0,0\}}^A = 1 . \quad (2.188)$$

2.5.3 Scale dependence of the DAs

The different terms of the conformal expansion are associated to conformal operators \mathcal{O}_n whose evolution is given by the Callan-Symanzik equation (2.172). To find which are these operators, the technique is to use the orthogonality of the polynomials to isolate the terms of definite conformal spin in the conformal expression of the DA and then to reverse the expressions of the type (2.156, 2.157) in order to get the normalizations as a function of the relevant operators. Let us clarify this procedure on the example of a_n^{\parallel} for the leading twist DA $\varphi_1(y, \mu^2)$.

Using the orthogonality relation of the Gegenbauer polynomials

$$\int_{-1}^1 d\xi (1 - \xi^2)^{\alpha-1/2} C_n^{\alpha}(\xi) C_m^{\alpha}(\xi) = \delta_{m,n} \frac{\pi 2^{1-2\alpha} \Gamma(n+2\alpha)}{n!(n+\alpha)\Gamma(\alpha)^2} , \quad (2.189)$$

to extract a_n^\parallel , leads to

$$\begin{aligned} a_n^\parallel &= \frac{2(2n+3)}{3(n+1)(n+2)} \int_0^1 dy C^{3/2}(\xi) \phi_\parallel(y, \mu^2), \\ &= \frac{2(2n+3)}{3(n+1)(n+2)} \int_0^1 dy C_n^{3/2}(\xi) \end{aligned} \quad (2.190)$$

$$\times \frac{1}{m_\rho f_\rho} \int \frac{d^4 z}{(2\pi)^4} e^{-i\xi p \cdot z} \frac{1}{e^{(\lambda)} \cdot z} \langle 0 | \bar{u}(z) z^\mu \gamma_\mu [z, -z] d(-z) | \rho^-(p, \lambda) \rangle, \quad (2.191)$$

where we used the relation (2.156) multiplied by z^μ to isolate the DA ϕ_\parallel . One can show that the result can be put in the form,

$$a_n^\parallel = \frac{2(2n+3)}{3(n+1)(n+2)m_\rho f_\rho (e^{(\lambda)} \cdot z)} \frac{1}{(p \cdot z)^n} \langle 0 | \mathcal{O}_n(0; \mu^2) | \rho^-(p, \lambda) \rangle, \quad (2.192)$$

with the conformal operator,

$$\mathcal{O}_n(x) = \langle 0 | (i\partial)^n \bar{u}(x) \gamma C_n^{3/2}(\overleftrightarrow{D} \cdot \partial) d(x) | \rho^-(p, \lambda) \rangle, \quad (2.193)$$

where the notations used here are

$$\partial \cdot \left(\frac{\overleftrightarrow{D}}{\partial} \right)^k \equiv \partial^{(n-k)} \overleftrightarrow{D}^k = (z \cdot \partial)^{n-k} (z \cdot \frac{\overrightarrow{D} - \overleftarrow{D}}{2})^k,$$

with $\overleftrightarrow{D} = \frac{\overrightarrow{D} - \overleftarrow{D}}{2}$, and the total derivative $\partial_\alpha \equiv \frac{\overrightarrow{D} + \overleftarrow{D}}{2}$ is defined as,

$$\partial_\alpha (\bar{u}(x) \Gamma[x, -x] d(-x)) \equiv \frac{\partial}{\partial \epsilon_\alpha} (\bar{u}(x + \epsilon) \Gamma[x + \epsilon, -x + \epsilon] d(-x + \epsilon))_{\epsilon \rightarrow 0}. \quad (2.194)$$

The conformal spin of \mathcal{O}_n is the same than a_n that is $n+2$. The scale dependence of the operator \mathcal{O}_n is determined up to the LL accuracy by the one-loop anomalous dimension computation of the operator γ_n^\parallel [48, 156, 157],

$$\gamma_n^\parallel = 4C_F \left(\psi(n+2) + \gamma_E - \frac{3}{4} - \frac{1}{2(n+1)(n+2)} \right), \quad (2.195)$$

with $\psi(n) = -\gamma_E + \sum_{k=1}^{n+1} 1/k$, and γ_E the Euler constant. The scale dependence of a_n^\parallel is then given by

$$a_n^\parallel(\mu^2) = L(\mu^2, \mu_0^2)^{\gamma_n^\parallel/\beta_0} a_n^\parallel(\mu_0^2), \quad (2.196)$$

where $L(\mu^2, \mu_0^2)$ reads explicitly for $\mu_0 = 1 \text{ GeV}^2$,

$$L(\mu^2) \equiv L(\mu^2, 1 \text{ GeV}^2) = \frac{\alpha_s(\mu^2)}{\alpha_s(1 \text{ GeV}^2)} = \frac{1}{1 + \frac{\beta_0}{\pi} \alpha_s(1 \text{ GeV}^2) \ln(\mu^2)}. \quad (2.197)$$

For the three-particle DAs, steps are similar except that the conformal group representations are degenerate. The first step being to isolate the $\{k, l\}^{-th}$ terms of conformal spin $j = k + l + 7/2 \equiv (n-2) + 7/2$ using the orthogonality relations of Jacobi polynomials. We prefer to work with fix n instead of j , which is equivalent, as one can match the genuine solution for the two-parton twist 3 DAs label n with the conformal spin j as $j = n + 3/2$.

The definition (2.158) multiplied by $z^\alpha \varepsilon^{\perp \cdot \mu\nu}$ we obtain the relation,

$$\langle 0 | \bar{u}(z) \gamma.[z, vz] g \tilde{G}_\perp.(vz)[vz, -z] d(-z) | \rho(p, \lambda) \rangle = im_\rho f_\rho \zeta_3^V \quad (2.198)$$

$$\times \varepsilon_{\perp \cdot p \varepsilon_\perp^{(\lambda)}} \int \mathcal{D}[\underline{y}] \mathcal{V}(y_1, \bar{y}_2, y_g) e^{-ip \cdot z (w y_1 + t \bar{y}_2 + v y_g)}. \quad (2.199)$$

By acting on both sides of the eq. (2.198) with the operator

$$\frac{\partial^n}{\partial t^{n-k-2} \partial w^k},$$

and taking the limit $t, w \rightarrow 0$, we see that the r.h.s. will give

$$im_\rho f_\rho \zeta_3^V \varepsilon_{\perp \cdot p \varepsilon_\perp^{(\lambda)}} (p \cdot z)^{n-1} \int \mathcal{D}[\underline{y}] y_1^k \bar{y}_2^{n-k-2} \mathcal{V}(y_1, \bar{y}_2, y_g),$$

while on the l.h.s it will give the operator,

$$\langle 0 | \bar{u}(0) (i \overleftarrow{D})^{n-k-2} \gamma. g \tilde{G}_\perp.(0) (i \overrightarrow{D})^k d(0) | \rho^-(p, \lambda) \rangle.$$

The r.h.s can be simplified

$$\begin{aligned} & im_\rho f_\rho \zeta_3^V \varepsilon_{\perp \cdot p \varepsilon_\perp^{(\lambda)}} (p \cdot z)^{n-1} \int \mathcal{D}[\underline{y}] y_1^k \bar{y}_2^{n-k-2} \mathcal{V}(y_1, \bar{y}_2, y_g) \\ &= im_\rho f_\rho \zeta_3^V \varepsilon_{\perp \cdot p \varepsilon_\perp^{(\lambda)}} (p \cdot z)^{n-1} \\ &\times \int \mathcal{D}[\underline{y}] y_1^k \bar{y}_2^{n-k-2} (360 y_1 \bar{y}_2 y_g^2) \sum_{k', l'} \omega_{k', l'}^V J_{k', l'}(y_1, \bar{y}_2) \\ &= im_\rho f_\rho \zeta_3^V \varepsilon_{\perp \cdot p \varepsilon_\perp^{(\lambda)}} (p \cdot z)^{n-1} \left(\frac{360 (-1)^n k! (n-k-2)!}{2^{n+1} (n+1) (2n+1)!!} \omega_{k, n-k-2}^V \right. \\ &\quad \left. + \text{terms in } \omega_{l, r-l-2} \text{ with } r < n \right). \end{aligned} \quad (2.200)$$

The last line in the above equation was obtained with the help of the Jacobi polynomial relation

$$\int \mathcal{D}[\underline{y}] y_1^{m+1} \bar{y}_2^{n+1} y_g^2 J_{k, l}(y_1, \bar{y}_2) = \delta_{m, k} \frac{(-1)^{k+l} k! l!}{2^{k+l+3} (k+l+3) (2k+2l+5)!!}, \quad (2.201)$$

for $m+n = k+l$, otherwise the result is zero for $m+n < k+l$ and nonzero for $m+n > k+l$. The remaining terms in $\omega_{l, r-l-2}^V$ correspond to total derivatives of lower conformal operators, then the relevant conformal operator corresponding to $\omega_{k, n-k-2}^V$ is,

$$\mathcal{O}_{k, n-k-2}^V(0) \equiv \bar{u}(0) (i \overleftarrow{D})^{n-k-2} \gamma. g \tilde{G}_\perp.(0) (i \overrightarrow{D})^k d(0) + \text{total derivatives}, \quad (2.202)$$

the "total derivative terms" coming from other higher conformal terms remaining $\omega_{l, r-l-2}^V$ terms with $r = n$. Note that in the DIS case, the total derivative operators sandwiched between the proton state vanish due to the fact that they are proportional to the difference of the momenta of the initial and final states. In our case the matrix element is non-forward, so the total derivatives of the operators contribute to the matrix element. The relation on the coupling constants finally reads

$$(m_\rho f_\rho \zeta_3^V \omega_{k, n-k-2}^V) (\mu^2) = \frac{(-1)^n N_n}{90 k! (n-k-2)!} \langle 0 | \mathcal{O}_{k, n-k-2}^V(0) | \rho^-(p, \lambda) \rangle, \quad (2.203)$$

with the k independent normalization

$$N_n = \frac{2^{n-1}(2n+1)!!(n+1)}{i\varepsilon_\perp \cdot p\varepsilon_\perp^{(\lambda)}(p \cdot z)^{n-1}}.$$

We need now to get the scale dependence of the operators $(\mathcal{O}_{k,n-k-2}^V)_{k=0..n-2}$ that can mix with each others under renormalization. Moreover we can apply the same treatment for the axial-vector three-parton operators leading to

$$(m_\rho f_\rho \zeta_3^A \omega_{k,n-k-2}^A)(\mu^2) = \frac{(-1)^n N_n}{90k!(n-k-2)!} \langle 0 | \mathcal{O}_{k,n-k-2}^A(0) | \rho^-(p, \lambda) \rangle, \quad (2.204)$$

with,

$$\mathcal{O}_{k,n-k-2}^A(0) \equiv \bar{u}(0)(i \overleftarrow{D})^{n-k-2} i\gamma_5 g\tilde{G}_\perp(0)(i \overrightarrow{D})^k d(0) + \text{total derivatives}, \quad (2.205)$$

and the operators $(\mathcal{O}_{k,n-k-2}^A)_{k=0..n-2}$ and $(\mathcal{O}_{k,n-k-2}^V)_{k=0..n-2}$ can also mix with each other as they have the same conformal spin $j = n + 3/2$.

It is useful to consider then the sum and the difference of the operators,

$$R_{n,k}^{V(A)\pm}(0, \mu^2) = \mathcal{O}_{k,n-k-2}^{V(A)}(0, \mu^2) \pm \mathcal{O}_{n-k-2,k}^{V(A)}(0, \mu^2), \quad (2.206)$$

as the operators with different parity numbers don't mix under renormalization. $R_{n,k}^{V(A)+}$ and $R_{n,k}^{V(A)-}$ have respectively G-parity numbers $(-1)^{n+1}$ and $(-1)^n$. The relevant combinations of operators that satisfy the RG equation and which mix under renormalization are

$$R_{n,k}^\pm(0, \mu^2) = R_{n,k}^{V\pm}(0, \mu^2) \mp R_{n,k}^{A\mp}(0, \mu^2). \quad (2.207)$$

The solutions read,

$$R_{n,k}^\pm(0, \mu^2) = \sum_{l=0}^{n-2} \left(L^{\Gamma_n^\pm/\beta_0} \right)_{k,l} R_{n,l}^\pm(0, \mu_0^2), \quad (2.208)$$

and they lead to the scale evolution of the form

$$\begin{aligned} & f_{3\rho}^V \omega_{[k,n-k-2]}^V \pm f_{3\rho}^A \omega_{\{k,n-k-2\}}^A(\mu^2) \\ &= \sum_{l=0}^{n-2} \left(L^{\Gamma_n^\mp/\beta_0} \right)_{k,l} (f_{3\rho}^V \omega_{[l,n-l-2]}^V(\mu_0^2) \pm f_{3\rho}^A \omega_{\{l,n-l-2\}}^A(\mu_0^2)), \end{aligned} \quad (2.209)$$

with $f_{3\rho}^V = f_\rho \zeta_3^V$ and $f_{3\rho}^A = f_\rho \zeta_3^A$. The renormalization of the operators $R_{n,k}^\pm$ are known for the forward matrix elements [163, 164] as they are relevant for the evolution of the structure function g_2 . In [164] the explicit solutions for the computation is performed in the covariant approach.

For our purpose we will use the models of ref. [142] for the leading twist DA ϕ^\parallel , and the twist 3 DAs \mathcal{V} and \mathcal{A} . In this model the leading twist DA and the twist 3 DAs are

respectively expanded up to the conformal spins $j = 4$ and $j = 9/2$. The DAs truncated conformal expansions read,

$$\phi^{\parallel}(y; \mu^2) = 6y\bar{y} \left(1 + 3a_1^{\parallel}(\mu^2)\xi + \frac{3}{2}(5\xi^2 - 1)a_2^{\parallel}(\xi) \right), \quad (2.210)$$

$$\mathcal{V}(y_1, \bar{y}_2, y_g) = 5040(y_1 - \bar{y}_2)y_1\bar{y}_2y_g^2, \quad (2.211)$$

$$\mathcal{A}(y_1, \bar{y}_2, y_g) = 360y_1\bar{y}_2y_g^2 \left(1 + \frac{1}{2}(7y_g - 3)\omega_{1,0}^A(\mu^2) \right), \quad (2.212)$$

which is equivalent, according to (2.155), to

$$\varphi_1(y, \mu^2) = 6y\bar{y} \left(1 + a_2^{\parallel}(\mu^2)\frac{3}{2}(5(y - \bar{y})^2 - 1) \right), \quad (2.213)$$

$$B(y_1, y_2; \mu^2) = -5040y_1\bar{y}_2(y_1 - \bar{y}_2)(y_2 - y_1), \quad (2.214)$$

$$D(y_1, y_2; \mu^2) = -360y_1\bar{y}_2(y_2 - y_1) \left(1 + \frac{\omega_{\{1,0\}}^A(\mu^2)}{2}(7(y_2 - y_1) - 3) \right). \quad (2.215)$$

Note that $a_1^{\parallel} = 0$ due to the G-parity invariance of the ρ -meson in the vanishing quark masses limit. This model is valid under the hypothesis that the conformal expansion converges. This is indeed ensured by the scale dependence of the operators at large enough ratio μ/μ_0 with μ_0 the reference scale, as the higher is the conformal spin the faster the term decreases with μ^2/μ_0^2 .

The reference scale used here is $\mu_0 = 1$ GeV. The values of the coupling constants [142] displayed in the tab. 2.1 are determined at this scale by QCD sum rules (cf. next part).

α_s	0.52
$\omega_{\{1,0\}}^A$	-2.1
$\omega_{[0,1]}^V$	28/3
$a_{2,\rho}^{\parallel}$	0.18 ± 0.10
$m_\rho f_{3\rho}^A$	$0.5 - 0.6 \cdot 10^{-2} \text{ GeV}^2$
$m_\rho f_{3\rho}^V$	$0.2 \cdot 10^{-2} \text{ GeV}^2$
ζ_3^A	0.032
ζ_3^V	0.013

Table 2.1: Coupling constants and Gegenbauer coefficients entering the ρ -meson DAs, at the scale $\mu = 1$ GeV. Note that in Ref. [142] the normalizations are such that $f_{3\rho}^{V,A}[142] = m_\rho f_{3\rho}^{V,A}[\text{here}]$.

We need then the scale dependence of the following quantities,

$$a_2^\parallel(\mu^2), \quad (f_{3\rho}^V \omega_{[0,1]}^V)(\mu^2) = 28/3 f_{3\rho}^V(\mu^2) \quad \text{and} \quad (f_{3\rho}^A \omega_{1,0}^A)(\mu^2).$$

The evolutions of $a_2^\parallel(\mu^2)$ is given explicitly by

$$a_2^\parallel(\mu^2) = a_{2,0}^\parallel L(\mu^2)^{\gamma_2/\beta_0}. \quad (2.216)$$

The $f_{3\rho}^A$ coupling constant evolution reads

$$f_{3\rho}^A(\mu^2) = f_{3\rho}^A(1\text{GeV}^2) L(\mu^2)^{\Gamma_2^-/\beta_0}, \quad (2.217)$$

with $\Gamma_2^- = -\frac{C_F}{3} + 3C_g$ with $C_g = N_c$. Defining the vector

$$V(\mu^2) = \begin{pmatrix} \omega_{[0,1]}^V f_{3\rho}^V(\mu^2) - \omega_{\{0,1\}}^A(\mu^2) f_{3\rho}^A(\mu^2) \\ \omega_{[0,1]}^V f_{3\rho}^V(\mu^2) + \omega_{\{0,1\}}^A(\mu^2) f_{3\rho}^A(\mu^2) \end{pmatrix}, \quad (2.218)$$

the evolution of $V(\mu^2)$ is given by the matrix evolution equation

$$V(\mu^2) = L(\mu^2)^{\Gamma_3^+/\beta_0} V(1\text{ GeV}^2), \quad (2.219)$$

with Γ_3^+ given by

$$\Gamma_3^+ = \begin{pmatrix} \frac{8}{3}C_F + \frac{7}{3}C_g & \frac{2}{3}C_F - \frac{2}{3}C_g \\ \frac{5}{3}C_F - \frac{4}{3}C_g & \frac{1}{6}C_F + 4C_g \end{pmatrix}. \quad (2.220)$$

Hence we get the dependence of $f_{3\rho}^V$ and $\omega_{\{0,1\}}^A$ by solving this matrix equation in the eigenvectors basis of the matrix Γ_3^+ . In fig. 2.15 we display the three independent DAs φ_1 (left), S (center), M (right). The fig. 2.16 shows the DAs φ_3 (left) and φ_A (right) and fig. 2.17 shows the DAs φ_1^T (left) and φ_A^T (right) as a function of their longitudinal variables.

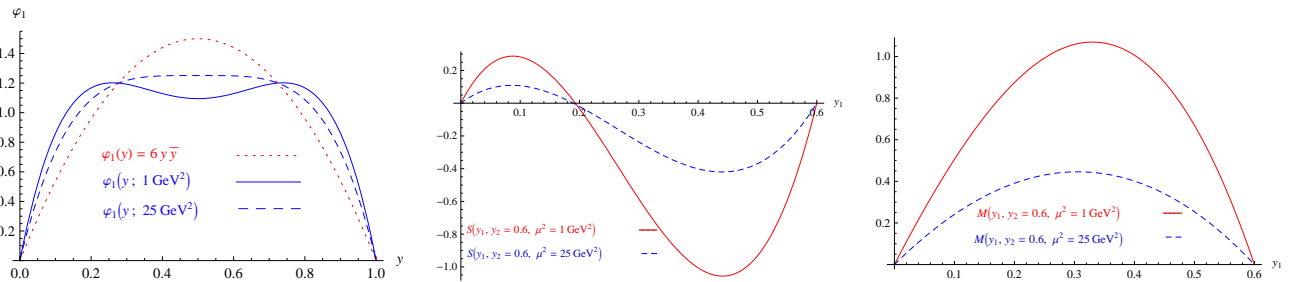


Figure 2.15: The three independent DAs. Left: $\varphi_1(y; \mu^2)$ as a function of y ; in red (dotted) asymptotic DA, in blue (solid) $\mu^2 = 1 \text{ GeV}^2$, in blue (dashed) $\mu^2 = 25 \text{ GeV}^2$. Center: $S(y_1, y_2 = 0.6; \mu^2)$ as a function of y_1 ; in red (solid) $\mu^2 = 1 \text{ GeV}^2$, in blue (dashed) $\mu^2 = 25 \text{ GeV}^2$. Right: $M(y_1, y_2 = 0.6; \mu^2)$ as a function of y_1 ; in red (solid) $\mu^2 = 1 \text{ GeV}^2$, in blue (dashed) $\mu^2 = 25 \text{ GeV}^2$.

These figures exhibit the non-negligible effects of QCD evolution on DAs, in particular for the genuine twist 3 contributions.

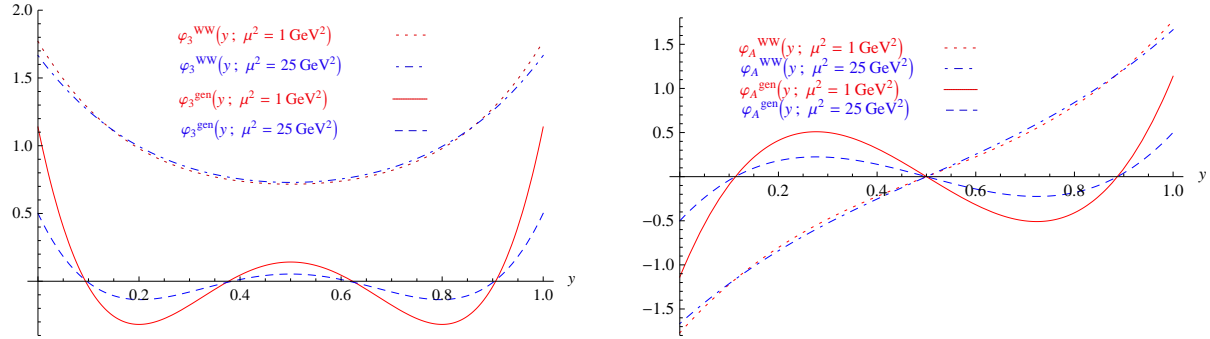


Figure 2.16: The two DAs φ_3 (left) and φ_A (right) as a function of y . In red (dotted) WW contribution with $\mu^2 = 1 \text{ GeV}^2$; in blue (dash-dotted) WW contribution with $\mu^2 = 25 \text{ GeV}^2$; in red (solid) genuine contribution with $\mu^2 = 1 \text{ GeV}^2$; in blue (dashed) genuine contribution with $\mu^2 = 25 \text{ GeV}^2$.

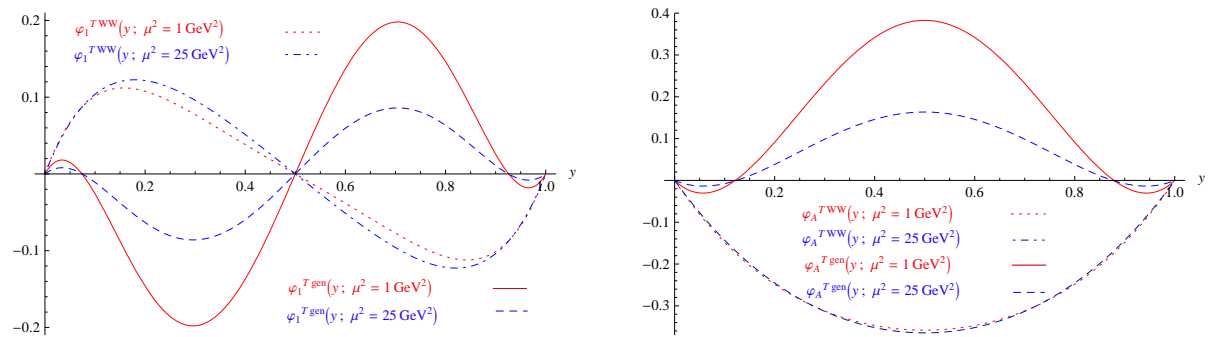


Figure 2.17: The two DAs φ_1^T (left) and φ_A^T (right) as a function of y . In red (dotted) WW contribution with $\mu^2 = 1 \text{ GeV}^2$; in blue (dash-dotted) WW contribution with $\mu^2 = 25 \text{ GeV}^2$; in red (solid) genuine contribution with $\mu^2 = 1 \text{ GeV}^2$; in blue (dashed) genuine contribution with $\mu^2 = 25 \text{ GeV}^2$.

2.6 QCD sum rules

Let us briefly sketch the main idea of the QCD sum rules method [165] to get access to the nonperturbative inputs, on the example of the twist 2 pion DA φ_π^A [166, 167] which parameterizes the bilocal correlator such as,

$$\langle 0 | \bar{d}(z) \not{z} \gamma_5 [z, -z] u(-z) | \pi^+(p) \rangle = iz \cdot p f_\pi \int_{-1}^1 d\xi e^{i\xi(z \cdot p)} \varphi_\pi^A(y). \quad (2.221)$$

This non-local correlator can be Taylor expanded as a sum of local operators,

$$\langle \bar{d}(z) \not{z} \gamma_5 [z, -z] u(-z) \rangle = \sum_n \frac{i^n}{n!} \langle \bar{d}(0) \not{z} \gamma_5 (iz \cdot \overleftrightarrow{D})^n u(0) \rangle. \quad (2.222)$$

Note that the pion decay constant f_π is defined as

$$\langle 0 | \bar{d}(0) \gamma_\mu \gamma_5 u(0) | \pi^+(p) \rangle = ip_\mu f_\pi, \quad (2.223)$$

which taking the limit $z \rightarrow 0$ in (2.221), gives the normalization of the DA,

$$\int_{-1}^1 d\xi \varphi_\pi^A(\xi) = 1.$$

Each terms of the expansion can be written as,

$$\begin{aligned} \langle \bar{d}(0) \not{z} \gamma_5 (iz \cdot \overleftrightarrow{D})^n u(0) \rangle &= z_\alpha z_{\mu_1} \cdots z_{\mu_n} \langle \bar{d}(0) \gamma^\alpha \gamma_5 (i \overleftrightarrow{D}^{\mu_1} \cdots i \overleftrightarrow{D}^{\mu_n}) u(0) \rangle \\ &= (z \cdot p)^{n+1} C_n. \end{aligned} \quad (2.224)$$

The coefficients C_n can now be identified with the Taylor coefficients by expanding the r.h.s of (2.221)

$$iz \cdot p f_\pi \int_{-1}^1 d\xi e^{i\xi(z \cdot p)} \varphi_\pi^A(y) = iz \cdot p f_\pi \int_{-1}^1 d\xi \sum_n \frac{(i\xi(z \cdot p))^n}{n!} \varphi_\pi^A(y), \quad (2.225)$$

leading to

$$C_n = \int_{-1}^1 d\xi \xi^n \varphi_\pi^A(\xi) = \langle \xi^n \rangle,$$

where $\langle \xi^n \rangle$ is the n -th moment of the wave function along the light-cone direction p . The goal now is to derive equations (sum rules) between the nonperturbative inputs such f_π that we want to evaluate and quantities that we can calculate or evaluate in the asymptotic regime where the hard scale $Q^2 \rightarrow \infty$.

Let us consider the following correlator,

$$I_{n,0}(z, q) = i \int dx e^{iq \cdot x} \langle 0 | T \mathcal{O}_n(x) \mathcal{O}_0(0) | 0 \rangle, \quad (2.226)$$

where we denote the operator $\mathcal{O}_m(y)$,

$$\mathcal{O}_m(y) = \bar{d}(y) \not{z} \gamma_5 (iz \cdot \overleftrightarrow{D})^m u(y). \quad (2.227)$$

The intermediate state

$$\mathcal{O}_0(0) |0\rangle = \bar{d}(0) \not{x} \gamma_5 u(0) |0\rangle ,$$

has the same quantum numbers as the $|\pi\rangle$ state. The operators $O_n(x)$ are the operators involved between the $|\pi\rangle$ state and the vacuum state in Eq. (2.224) so they are related to the values of $\langle \xi^n \rangle$. The momentum q is the momentum exchanged between the two local currents projected on the coordinate z as in Eq. (2.221). We can express $I_{n,0}(z, q)$ as a z -independent quantity $I_{n,0}(q^2)$,

$$I_{n,0}(z, q) = i \int dx e^{iq \cdot x} \langle 0 | \bar{d}(x) \not{x} \gamma_5 (iz \cdot \overleftrightarrow{D})^n u(x) \bar{d}(0) \not{x} \gamma_5 u(0) | 0 \rangle \quad (2.228)$$

$$= (z \cdot q)^{n+2} I_{n,0}(q^2) . \quad (2.229)$$

In the asymptotic limit $q^2 \rightarrow \infty$, the main contribution is given by pQCD. Then the

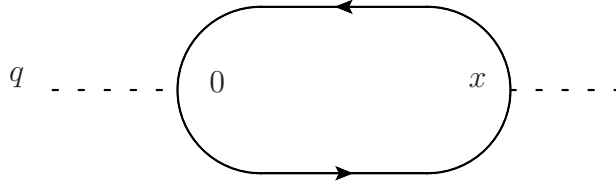


Figure 2.18: pQCD loop contribution to $I_{n,0}(q^2)$

asymptotically dominant contribution is given by the loop diagram in fig. 2.18, which gives [166, 167],

$$I_{n,0}^{AS}(q^2) = -\frac{\ln(Q^2)}{4\pi^2} \int d\xi \xi^n \frac{3}{4} (1 - \xi^2) = -\frac{\ln(Q^2)}{4\pi^2} \frac{3}{(n+1)(n+3)} . \quad (2.230)$$

The nonperturbative corrections to this result are given by considering the operator expansion of the external fields. These corrections involve the diagrams of fig. 2.19, where operators of lowest dimensions are $G_{\mu\nu}^2$ for the left diagram and $\bar{u}u$ for the right diagram. $I_{n,0}(q^2)$, with

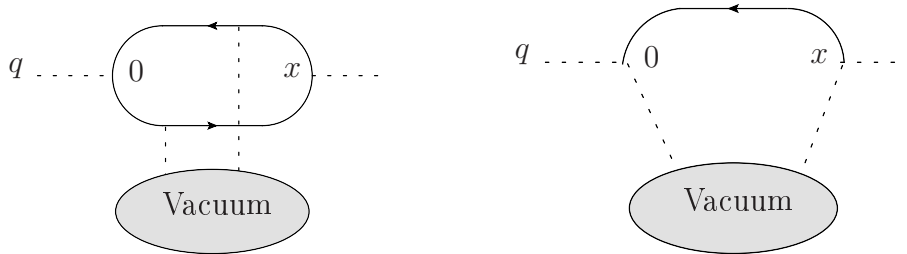


Figure 2.19: Nonperturbative corrections from the vacuum. Diagram on the left involves the vacuum expectation value $\langle 0 | G_{\mu\nu}^2 | 0 \rangle$, the right diagram involves $\langle 0 | \bar{u}u | 0 \rangle$.

the corrective contributions of this operator product expansion, takes the form,

$$\begin{aligned} I_{n,0}(q^2) &= I_{n,0}^{AS}(q^2) + \frac{\langle 0 | \frac{\alpha_s}{\pi} G^2 | 0 \rangle}{12q^4} - \frac{32\pi}{81} (11 + 4n) \frac{\langle 0 | \sqrt{\alpha_s} \bar{u}u | 0 \rangle}{q^6} \\ &+ \dots + C_k \frac{\langle 0 | \mathcal{O}_k | 0 \rangle}{q^{2k}} + \dots \end{aligned} \quad (2.231)$$

The technique is then to use an integral Borel transform of $I_{n,0}(q^2)$, defined as,

$$\begin{aligned} \frac{1}{\pi M^2} \int_0^\infty dS e^{-S/M^2} \mathcal{I}m I_{n,0}(S) &= \frac{1}{4\pi^2} \frac{3}{(n+1)(n+3)} + \frac{\langle 0 | \frac{\alpha_s}{\pi} G^2 | 0 \rangle}{12M^4} \\ &\quad - \frac{16\pi}{81} (11+4n) \frac{\langle 0 | \sqrt{\alpha_s} \bar{u}u | 0 \rangle}{M^6} \\ &\quad + \dots + \frac{(-1)^k}{(k-1)!} C_k \frac{\langle 0 | \mathcal{O}_k | 0 \rangle}{M^{2k}} + \dots \end{aligned} \quad (2.232)$$

This manipulation, called "borelization", has two important consequences, the first is that on the r.h.s. of (2.232), the operators of higher dimensions are suppressed, the second is that on the l.h.s the intermediate states with $S > M^2$ that could contribute to the spectral density $\mathcal{I}m I_{n,0}$ are also suppressed.

The sum rule given by eq. (2.232) allows to get nonperturbative inputs. Indeed we know that for large $S > S_n \gg \mu_0^2$ the pQCD gives for the spectral density,

$$\mathcal{I}_{n,0}(S) = \theta(S - S_n) \mathcal{I}_{n,0}^{AS}(S) = \theta(S - S_n) \frac{3}{4\pi^2(n+1)(n+3)}, \quad (2.233)$$

where S_n is the threshold under which we have to take into account nonperturbative corrections. These non-perturbative corrections to the spectral density is given by the lowest energy resonances among the bound states with the good quantum numbers. In this case the π^+ -meson state is the lowest energy resonance and the next one is the A_1 -meson, leading to

$$\mathcal{I}_{n,0}(S) = \theta(S - S_n) \mathcal{I}_{n,0}^{AS}(S) + f_\pi^2 \langle \xi^n \rangle_\pi \delta(S - m_\pi^2) + f_A^2 \langle \xi^n \rangle_A \delta(S - m_A^2). \quad (2.234)$$

Inserting (2.234) in the l.h.s of (2.232), we get a relation between the free parameters f_π , f_A , $\langle \xi^n \rangle_\pi$, $\langle \xi^n \rangle_A$ and S_n . The vacuum expectation values are assumed to be known as $\langle 0 | \sqrt{\alpha_s} \bar{u}u | 0 \rangle$ and $\langle 0 | \frac{\alpha_s}{\pi} G^2 | 0 \rangle$ can be determined phenomenologically [168, 169]. The best fit of the free parameters allows then to evaluate the nonperturbative input parameters.

2.7 Impact factors $\gamma^*(\lambda_\gamma) \rightarrow \rho(\lambda_\rho)$

In this part we will present the computation of the impact factors $\gamma^*(\lambda_\gamma) \rightarrow \rho(\lambda_\rho)$, denoted $\Phi^{\gamma_{\lambda_\gamma}^* \rightarrow \rho_{\lambda_\rho}}$ for the transitions $\gamma_L^* \rightarrow \rho_L$, $\gamma_T^* \rightarrow \rho_L$ and $\gamma_T^* \rightarrow \rho_T$.

Let us recall the formulas (2.93-2.96) for the amplitudes related to the impact factors as convolutions of DAs and hard sub-processes. For the transition $\gamma_L^* \rightarrow \rho_L$ it reads

$$i\mathcal{A}_{q\bar{q}}^{(0)} = -\frac{f_\rho}{4} \int dy H_{q\bar{q}}^\rho(y) \varphi_1(y; \mu_F^2), \quad (2.235)$$

and for the $\gamma_T^* \rightarrow \rho_T$,

$$\begin{aligned}
 i\mathcal{A} = & -\frac{m_\rho f_\rho}{4} \left(\int dy \left[H_{q\bar{q}}^{\rho^*T}(y) \varphi_3(y; \mu_F^2) + i H_{q\bar{q}}^{R^* \perp \gamma_5}(y) \varphi_A(y; \mu_F^2) \right. \right. \\
 & \left. \left. + H_{q\bar{q}}^{e^*T \not{p}}(y) \varphi_1^T(y; \mu_F^2) + i H_{q\bar{q}}^{R^* \perp \not{p} \gamma_5}(y) \varphi_A^T(y; \mu_F^2) \right] \right. \\
 & \left. - i \int dy_1 dy_2 \left[H_{q\bar{q}g}^{e^*T \not{p}}(y_1, y_2) \zeta_3^V(\mu_F^2) B(y_1, y_2; \mu_F^2) \right. \right. \\
 & \left. \left. + H_{q\bar{q}g}^{R^* \perp \not{p} \gamma_5}(y_1, y_2) \zeta_3^A(\mu_F^2) i D(y_1, y_2; \mu_F^2) \right] \right). \quad (2.236)
 \end{aligned}$$

In order to get the impact factor from (2.235, 2.236), one has to use the impact factor definition in our conventions defined in the sec. 1.2.4 of the chap. 1,

$$\Phi^{\gamma_{\lambda\gamma}^* \rightarrow \rho_{\lambda\rho}} = \frac{1}{2s} \int \frac{d\kappa}{2\pi} \text{Disc}_\kappa \left(S_{\mu\nu}^{\gamma^* g \rightarrow \rho g} p_2^\mu p_2^\nu \frac{2}{s} \right), \quad (2.237)$$

with $\kappa = (q + k_1)^2$ the Mandelstam variable associated to the hard sub-process.

We will present in this section the calculations of the impact factors for the different types of diagrams.

2.7.1 Kinematics

We choose the frame where the ρ -meson is along the dominant light-cone direction $p = p_1 \sim p_\rho$ (up to a factor m_ρ^2/s), as the amplitude is independent of the choice of the light-cone vector n , we choose to fix it along the dominant direction of the nucleon impact factor p_2 to compute the hard part. We recall that p_2 satisfies the relation $p_2 \cdot p_1 = \frac{s}{2}$ and is proportional to the vector n . In the forward kinematic $t = (q - p_\rho)^2 = -\underline{\Delta}^2 \rightarrow 0$ presented in fig. 2.20,

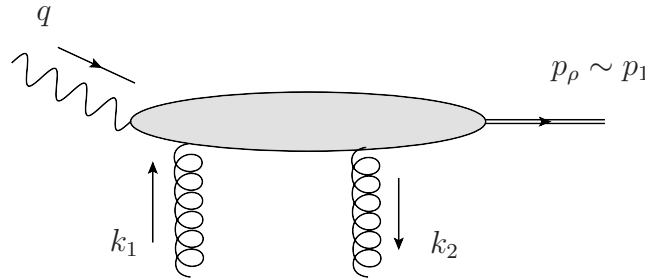


Figure 2.20: Kinematics of the process $\gamma^*(q)g(k_1) \rightarrow g(k_2)\rho(p_\rho)$.

the momenta can be expanded on the Sudakov basis as,

$$q = p_1 - \frac{Q^2}{s} p_2 \quad (2.238)$$

$$k_1 = \frac{\kappa + Q^2 + \underline{k}^2}{s} p_2 + k_\perp \quad (2.239)$$

$$k_2 = \frac{\kappa - m_\rho^2 + \underline{k}^2}{s} p_2 + k_\perp \sim \frac{\kappa + \underline{k}^2}{s} p_2 + k_\perp \quad (2.240)$$

and the polarizations

$$e_{\perp}^{(\lambda)} = \varepsilon^{(\lambda)} \quad (2.241)$$

$$e_L(q) = \frac{1}{Q} \left(q + \frac{2Q^2}{s} p_2 \right). \quad (2.242)$$

where $\varepsilon^{\pm} = \frac{1}{\sqrt{2}} (0, \mp 1, -i, 0)$, as defined by Eq. (1.124) in sec.1.3.2 of the chap. 1.

2.7.2 The $\gamma_L^* \rightarrow \rho_L$ transition

The impact factor $\Phi^{\gamma_L^* \rightarrow \rho_L}$ is computed from the expression of the amplitude $\mathcal{A}_{q\bar{q}}^{(0)}$ given in eq. (2.235) and from the definition eq. (2.237). The longitudinal polarization of the ρ -meson is given by,

$$e_L = \frac{1}{m_{\rho}} \left(p_1 - \frac{m_{\rho}^2}{s} p_2 \right). \quad (2.243)$$

The hard part $H_{q\bar{q}}^{\rho}(y)$ is given by the six diagrams presented in fig. 2.7. Let us derive the

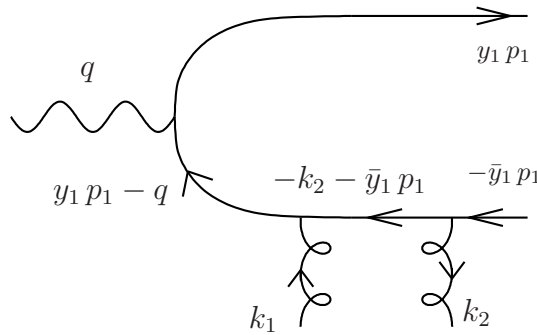


Figure 2.21: The detailed structure of the diagram (a), one of the six diagrams of the hard scattering.

contribution to the impact factor of the diagram (a) illustrated in fig. 2.21. It reads

$$\Phi_a = -\frac{e}{\sqrt{2}} \frac{1}{4} \frac{2}{s} (-i) f_{\rho} m_{\rho} g^2 \frac{\delta^{ab}}{2N} \frac{1}{s} \int_0^1 dy \int \frac{d\kappa}{2\pi} \frac{\text{Tr}[\not{\epsilon}_{\gamma_L} (y \not{p}_1 - \not{q}) \not{p}_2 (\not{k}_2 + \bar{y} \not{p}_1) \not{p}_2 \not{p}_1]}{[(y p_1 - q)^2 + i\epsilon][(k_2 + \bar{y} p_1)^2 + i\epsilon]} \varphi_1(y; \mu_F^2). \quad (2.244)$$

The computation is similar to the computations of the impact factors $\Phi^{\gamma_{L,T}^* \rightarrow \gamma_{L,T}^*}$ presented in the chap. 1. It is instructive to track the origin of the different factors in eq. (2.244). $\frac{1}{4}$ comes from Fierz identity, $\frac{2}{s}$ from the normalization of the non-sense polarizations of the t -channel gluons, $\frac{\delta^{ab}}{2}$ from the projection on the color singlet state in t -channel, $1/N$ from the Fierz factorization of the color indices of the ρ -meson. We remind that $\frac{e}{\sqrt{2}}$ stands for the electric charge of the $q\bar{q}$ content of the ρ -meson wave function $\frac{1}{\sqrt{2}}(\bar{u}u - \bar{d}d)$.

The poles in the κ -plane are given by the propagators. We recall that the six diagrams are needed to prove the convergence of the integral over κ on the infinite semi-circle. We

can then compute the integral with the residue method by choosing the lower contour for example. Among the six diagrams, only four of them give a contribution due to their κ -pole structure for a given contour choice.

The result for the impact factor is,

$$\begin{aligned}\Phi^{\gamma_L^* \rightarrow \rho_L} &= \frac{2eg^2 f_\rho}{\sqrt{2}Q} \frac{\delta^{ab}}{2N} \int dy \varphi_1(y) \mu^2 \left(\frac{1}{\mu^2} - \frac{1}{\underline{k}^2 + \mu^2} \right) \\ &= \frac{2eg^2 f_\rho}{\sqrt{2}Q} \frac{\delta^{ab}}{2N} \int dy \varphi_1(y) \frac{\underline{k}^2}{\mu^2 + \underline{k}^2},\end{aligned}\quad (2.245)$$

where according to the notation introduced in the DIS case in Sec. 1.3.2, $\mu^2 = y\bar{y}Q^2$. The result can be extended to the non-forward kinematic $\Delta \neq 0$, taking the momenta of the quark ℓ_1 and of the antiquark ℓ_2 as,

$$\ell_1 = yp_1 + \frac{(\underline{\ell} + y\underline{\Delta})^2}{ys} p_2 + \ell_\perp + y\Delta_\perp \quad (2.246)$$

$$\ell_2 = \bar{y}p_1 + \frac{(\underline{\ell} + \bar{y}\underline{\Delta})^2}{\bar{y}s} p_2 - (\ell_\perp - \bar{y}\Delta_\perp). \quad (2.247)$$

The result reads [130],

$$\Phi^{\gamma_L^* \rightarrow \rho_L}(\underline{k}, \underline{\Delta}, Q) = 4\pi\alpha_s \frac{ef_\rho}{\sqrt{2}Q} \frac{\delta_{ab}}{2N_c} \int_0^1 dy \mu^2 \varphi_1(y; Q^2) P_P(y, \underline{k}, \underline{\Delta}, Q) \quad (2.248)$$

with

$$\begin{aligned}P_P(y, \underline{k}, \underline{\Delta}, Q) &= \frac{1}{(y\underline{\Delta})^2 + y\bar{y}Q^2} + \frac{1}{(\bar{y}\underline{\Delta})^2 + y\bar{y}Q^2} \\ &- \left(\frac{1}{(\underline{k} - y\underline{\Delta})^2 + y\bar{y}Q^2} + \frac{1}{(\underline{k} - \bar{y}\underline{\Delta})^2 + y\bar{y}Q^2} \right).\end{aligned}\quad (2.249)$$

2.7.3 The $\gamma_T^* \rightarrow \rho_L$ impact factor

Using the same techniques, the first term of the expansion in twist of the impact factor $\gamma_T^* \rightarrow \rho_L$ is of twist 2. The twist 2 contribution to the $\gamma_T^* \rightarrow \rho_L$ impact factor is power suppressed by a kinematic factor \sqrt{t}/Q compared to the twist 2 contribution of the $\gamma_L^* \rightarrow \rho_L$ impact factor. It reads [130]:

$$\Phi^{\gamma_T^* \rightarrow \rho_L}(\underline{k}, \underline{\Delta}, Q) = 2\pi\alpha_s \frac{e}{\sqrt{2}} f_\rho \frac{\delta_{ab}}{2N_c} \int_0^1 dy (y - \bar{y}) \varphi_1(y; Q^2) \underline{e} \cdot \underline{Q}_P(y, \underline{k}, \underline{\Delta}, Q) \quad (2.250)$$

with

$$\begin{aligned}\underline{Q}_P(y, \underline{k}, \underline{\Delta}, Q) &= \frac{y\underline{\Delta}}{(y\underline{\Delta})^2 + y\bar{y}Q^2} - \frac{\bar{y}\underline{\Delta}}{(\bar{y}\underline{\Delta})^2 + y\bar{y}Q^2} \\ &+ \frac{\underline{k} - y\underline{\Delta}}{(\underline{k} - y\underline{\Delta})^2 + y\bar{y}Q^2} - \frac{\underline{k} - \bar{y}\underline{\Delta}}{(\underline{k} - \bar{y}\underline{\Delta})^2 + y\bar{y}Q^2}.\end{aligned}\quad (2.251)$$

2.7.4 The $\gamma_T^* \rightarrow \rho_T$ impact factor

The $\gamma_T^* \rightarrow \rho_T$ impact factor is technically more complicated as it involves many types of diagrams. We will give here the result for each of the different types of diagrams which are represented in figs. 2.13, 2.8, 2.9, 2.10. We skip the diagram of the type fig. 2.7 as the computation goes the same way than for $\Phi^{\gamma_L^* \rightarrow \rho_L}$.

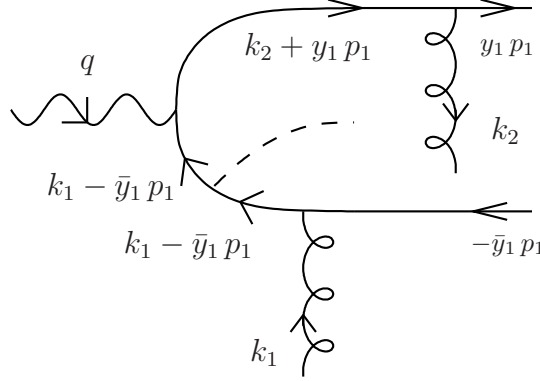


Figure 2.22: The detailed structure of the diagram (b1).

Let us focus on the diagram of fig. 2.22. We recall that there are two contributions, the vector and the axial vector contributions where the spinor indices of the diagram are respectively closed on the Fierz structures \not{p}_1 and $\not{p}_1 \gamma_5$. The vector contribution to the impact factor reads

$$\begin{aligned} \Phi_{b1}^V &= -\frac{e}{\sqrt{2}} \frac{1}{4} \frac{2}{s} (-i) g^2 f_\rho m_\rho \frac{\delta^{ab}}{2 N_c} \frac{1}{2s} \int_0^1 dy \int \frac{d\kappa}{2\pi} \\ &\times \frac{\text{Tr}[\not{\epsilon}_\gamma (\not{k}_1 - \bar{y} \not{p}_1) \not{\epsilon}_T^* (\not{k}_1 - \bar{y} \not{p}_1) \not{p}_2 \not{p}_1 \not{p}_2 (\not{k}_2 + y \not{p}_1)]}{[(k_1 - \bar{y} p_1)^2 + i\eta]^2 [(k_2 + \bar{y} p_1)^2 + i\eta]} \varphi_1^T(y). \end{aligned} \quad (2.252)$$

Computing the trace and integrating over κ leads to

$$\begin{aligned} \Phi_{b1}^V &= -\frac{e_q g^2}{2} f_\rho m_\rho \frac{\delta^{ab}}{2 N_c} \\ &\times \int_0^1 dy y \frac{-e_T^* \cdot e_\gamma (y \bar{y} Q^2 + \underline{k}^2) + 2 e_T^* \cdot k e_T^* \cdot k (1 - 2y)}{(Q^2 y \bar{y} + \underline{k}^2)^2} \varphi_1^T(y). \end{aligned} \quad (2.253)$$

The axial vector contribution reads

$$\begin{aligned} \Phi_{b1}^A &= -e_q \frac{i}{4} \frac{2}{s} (-i) g^2 f_\rho m_\rho \frac{\delta^{ab}}{2 N_c} \frac{1}{2s} \int_0^1 dy \int \frac{d\kappa}{2\pi} \\ &\times \frac{\text{Tr}[\not{\epsilon}_\gamma (\not{k}_1 - \bar{y} \not{p}_1) \gamma_\alpha (\not{k}_1 - \bar{y} \not{p}_1) \not{p}_2 \not{p}_1 \gamma_5 \not{p}_2 (\not{k}_2 + y \not{p}_1)]}{[(k_1 - \bar{y} p_1)^2 + i\eta]^2 [(k_2 + \bar{y} p_1)^2 + i\eta]} \epsilon_{e_T p n}^\alpha \varphi_A^T(y), \end{aligned} \quad (2.254)$$

which gives,

$$\begin{aligned} \Phi_{b1}^A &= -\frac{e_q g^2}{2} f_\rho m_\rho \frac{\delta^{ab}}{2 N_c} \\ &\times \int_0^1 dy y \frac{-e_T^* \cdot e_\gamma (y \bar{y} Q^2 - \underline{k}^2) + 2 e_T^* \cdot k e_T^* \cdot k}{(Q^2 y \bar{y} + \underline{k}^2)^2} \varphi_A^T(y). \end{aligned} \quad (2.255)$$

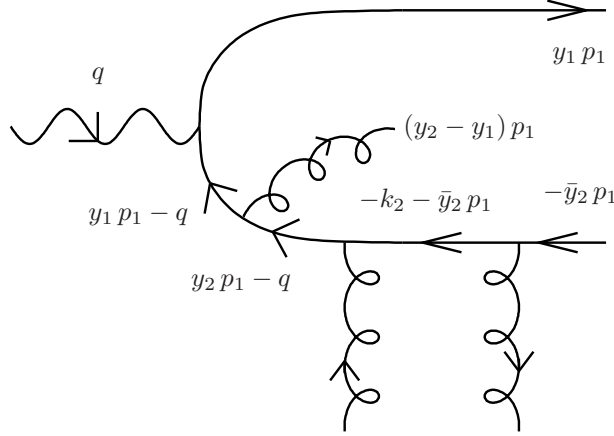


Figure 2.23: The detailed structure of the diagram (aG1).

Let us consider now the abelian three-parton contribution diagrams shown in fig. 2.23. Two different color factors can be obtained depending of where the gluon is attached,

$$\begin{aligned} \frac{2}{(N_c^2 - 1)} \text{Tr}(t^c t^a t^b t^c) &= \frac{\delta^{ab}}{2 N_c} : (\text{aG1}), (\text{cG1}), (\text{eG1}), (\text{fG1}) \\ \frac{2}{(N_c^2 - 1)} \text{Tr}(t^c t^a t^c t^b) &= \frac{1}{2} \left(2 - \frac{N_c}{C_F} \right) \frac{\delta^{ab}}{2 N_c} : (\text{bG1}), (\text{dG1}), (\text{aG2}), \\ &(\text{cG2}), (\text{bG2}), (\text{dG2}), (\text{eG2}), (\text{fG2}), \end{aligned} \quad (2.256)$$

where the $2/(N_c^2 - 1)$ comes from the Fierz coefficient when factorizing the $q\bar{q}g$ state in color space.

The vector contribution of the diagram aG1 reads

$$\begin{aligned} \Phi_{aG1}^V &= -e_q \frac{1}{4} \frac{2}{s} (i) g^2 f_\rho m_\rho \frac{\delta^{ab}}{2 N_c} \frac{1}{2s} \int_0^1 dy_1 dy_2 \int \frac{d\kappa}{2\pi} B(y_1, y_2) \\ &\times \frac{\text{Tr}[\not{\epsilon}_\gamma (y_1 \not{p}_1 - \not{q}) \not{\epsilon}_T^* (y_2 \not{p}_1 - \not{q}) \not{p}_2 (\not{k}_2 + \bar{y}_2 \not{p}_1) \not{p}_2 \not{p}_1]}{[(y_1 p_1 - q)^2 + i\eta][(y_2 p_1 - q)^2 + i\eta][(k_2 + \bar{y}_2 p_1)^2 + i\eta]}, \end{aligned} \quad (2.257)$$

$$= -\frac{e_q g^2}{2} f_\rho m_\rho \frac{\delta^{ab}}{2 N_c} \int_0^1 dy_1 dy_2 \frac{e_T^* \cdot e_\gamma}{\bar{y}_1 Q^2} B(y_1, y_2). \quad (2.258)$$

The axial-vector contribution of aG1 reads

$$\Phi_{aG1}^A = -e_q \frac{i}{4} \frac{2}{s} (i) g^2 f_\rho m_\rho \frac{\delta^{ab}}{2 N_c} \frac{1}{2s} \int_0^1 dy_1 dy_2 \int \frac{d\kappa}{2\pi} \varepsilon_{e_T^{*pn}}^\alpha D(y_1, y_2) \quad (2.259)$$

$$\begin{aligned} & \times \frac{\text{Tr}[\not{\epsilon}_\gamma (y_1 \not{p}_1 - \not{q}) \gamma_\alpha (y_2 \not{p}_1 - \not{q}) \not{p}_2 (\not{k}_2 + \bar{y}_2 \not{p}_1) \not{p}_2 \not{p}_1]}{[(y_1 p_1 - q)^2 + i\eta][(y_2 p_1 - q)^2 + i\eta][(k_2 + \bar{y}_2 p_1)^2 + i\eta]}, \\ & = -\frac{e_q g^2}{2} f_\rho m_\rho \frac{\delta^{ab}}{2 N_c} \int_0^1 dy_1 dy_2 \frac{e_T^* \cdot e_\gamma}{\bar{y}_1 Q^2} D(y_1, y_2). \end{aligned} \quad (2.260)$$

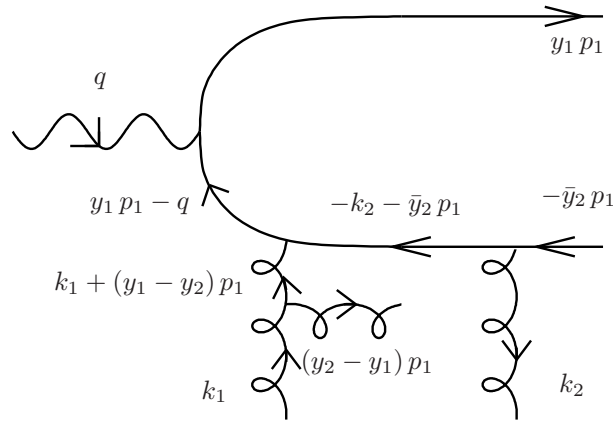


Figure 2.24: The detailed structure of the "non-Abelian" (with one triple gluon vertex) diagram (atG1).

The non-abelian diagram with one gluon triple vertex involves also two kinds of color factors,

$$\begin{aligned} & \frac{2}{N_c^2 - 1} (-i) \text{Tr}(t^c t^b t^d) f^{cad} = \frac{N_c}{2} \frac{1}{C_F} \frac{\delta^{ab}}{2 N_c} : \\ & \quad (\text{atG1}), (\text{dtG1}), (\text{etG1}), (\text{btG2}), (\text{ctG2}), (\text{ftG2}) \quad (2.261) \\ & \frac{2}{N_c^2 - 1} (-i) \text{Tr}(t^c t^d t^b) f^{cad} = -\frac{N_c}{2} \frac{1}{C_F} \frac{\delta^{ab}}{2 N_c} : \\ & \quad (\text{ctG1}), (\text{btG1}), (\text{ftG1}), (\text{atG2}), (\text{dtG2}), (\text{etG2}). \end{aligned}$$

Let us consider the diagram (atG1) illustrated in fig.2.24. We denote as

$$d^{\nu\rho}(k) = g^{\nu\rho} - \frac{k^\nu n^\rho + k^\rho n^\nu}{k \cdot n} \quad (2.262)$$

the numerator of the gluon propagator in axial gauge, and

$$V_{\mu_1 \mu_2 \mu_3}(k_1, k_2, k_3) = (k_1 - k_2)_{\mu_1} g_{\mu_1 \mu_2} + \dots \quad (2.263)$$

the momentum part of the 3-gluon vertex, where k_i are incoming, labeled in the counter-clockwise direction. The contribution of the diagram (atG1) proportional to the vector DA,

reads

$$\begin{aligned} \Phi_{atG1}^V = & -e_q \frac{1}{4} \frac{2}{s} \frac{(-i)N_c}{2C_F} g^2 m_\rho f_\rho \frac{\delta^{ab}}{2N_c} \frac{1}{2s} \int_0^1 dy_1 dy_2 \int \frac{d\kappa}{2\pi} p_2^\lambda e_T^{*\alpha} B(y_1, y_2) \\ & \times Tr[\not{\epsilon}_\gamma (y_1 \not{p}_1 - \not{q}) \gamma_\nu (\not{k}_2 + \bar{y}_2 \not{p}_1) \not{p}_2 \not{p}_1] \\ & \times \frac{d^{\nu\rho}(k_1 + (y_1 - y_2)p_1) V_{\rho\lambda\alpha}(-k_1 - (y_1 - y_2)p_1, k_1, (y_1 - y_2)p_1)}{[(y_1 p_1 - q)^2 + i\eta][(k_1 + (y_1 - y_2)p_1)^2 + i\eta][(k_2 + \bar{y}_2 p_1)^2 + i\eta]}. \end{aligned} \quad (2.264)$$

Note that for this diagram, as well as for all "non-Abelian" diagrams, one can easily check that only the $g^{\nu\rho}$ part of (2.262) contributes.

Closing the κ contour above or below gives for the vector DA part of the diagram (atG1) the result

$$\Phi_{atG1}^V = -\frac{e_q g^2}{2} m_\rho f_\rho \frac{\delta^{ab}}{2N_c} \frac{N_c}{C_F} \int_0^1 dy_1 dy_2 \frac{(y_1 - y_2) \bar{y}_2}{\bar{y}_1 (\bar{y}_1 \underline{k}^2 + \bar{y}_2 (y_2 - y_1) Q^2)} e_T^* \cdot e_\gamma B(y_1, y_2). \quad (2.265)$$

Similarly, the contribution of the diagram (atG1) proportional to the axial vector DA, reads

$$\begin{aligned} \Phi_{atG1}^A = & -e_q \frac{i}{4} \frac{2}{s} \frac{(-i)N_c}{2C_F} g^2 m_\rho f_\rho \frac{\delta^{ab}}{2N_c} \frac{1}{2s} \int_0^1 dy_1 dy_2 \int \frac{d\kappa}{2\pi} p_2^\lambda \epsilon_{e_T^{*pn}}^\alpha D(y_1, y_2) \\ & \times Tr[\not{\epsilon}_\gamma (y_1 \not{p}_1 - \not{q}) \gamma_\nu (\not{k}_2 + \bar{y}_2 \not{p}_1) \not{p}_2 \not{p}_1 \gamma_5] \\ & \times \frac{d^{\nu\rho}(k_1 + (y_1 - y_2)p_1) V_{\rho\lambda\alpha}(-k_1 - (y_1 - y_2)p_1, k_1, (y_1 - y_2)p_1)}{[(y_1 p_1 - q)^2 + i\eta][(k_1 + (y_1 - y_2)p_1)^2 + i\eta][(k_2 + \bar{y}_2 p_1)^2 + i\eta]}, \end{aligned} \quad (2.266)$$

and closing the κ contour above or below gives

$$\begin{aligned} \Phi_{atG1}^A = & -\frac{e_q g^2}{2} m_\rho f_\rho \frac{\delta^{ab}}{2N_c} \frac{N_c}{C_F} \\ & \times \int_0^1 dy_1 dy_2 \frac{(y_1 - y_2) \bar{y}_2}{\bar{y}_1 (\bar{y}_1 \underline{k}^2 + \bar{y}_2 (y_2 - y_1) Q^2)} e_T^* \cdot e_\gamma D(y_1, y_2). \end{aligned} \quad (2.267)$$

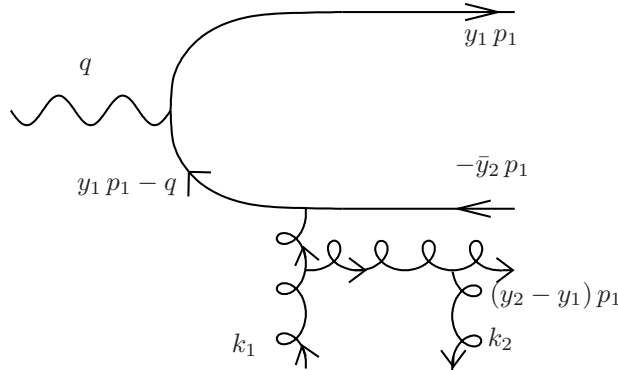


Figure 2.25: The detailed structure of the diagram (gttG1).

We consider now the "non-Abelian" diagrams of the type of gttG1 illustrated in fig.2.25, involving two triple gluon vertices. They all involve the color structure

$$-\frac{2}{N_c^2 - 1} \text{Tr}[t^c t^d] f^{cea} f^{edb} = \frac{N_c}{C_F} \frac{\delta^{ab}}{2 N_c}. \quad (2.268)$$

The vector contribution of gttG1 reads

$$\begin{aligned} \Phi_{gttG1}^V &= -e_q \frac{1}{4} \frac{2}{s} \frac{(-i)N_c}{C_F} g^2 m_\rho f_\rho \frac{\delta^{ab}}{2 N_c} \frac{1}{2s} \int_0^1 dy_1 dy_2 \int \frac{d\kappa}{2\pi} p_2^\lambda p_2^\tau e_T^{*\delta} B(y_1, y_2) \\ &\times \text{Tr}[\not{\epsilon}_\gamma (y_1 \not{p}_1 - \not{q}) \gamma_\nu \not{p}_1] d^{\nu\rho} (-q + (1 + y_1 - y_2) p_1) \\ &\times \frac{V_{\rho\lambda\alpha} (q - (1 + y_1 - y_2) p_1, k_1, -k_2 + (y_1 - y_2) p_1) d^{\alpha\beta} (k_2 + (y_2 - y_1) p_1)}{[(y_1 p_1 - q)^2 + i\eta][(-q + (1 + y_1 - y_2) p_1)^2 + i\eta][(k_2 + (y_2 - y_1) p_1)^2 + i\eta]} \\ &\times V_{\beta\tau\delta} (k_2 + (y_2 - y_1) p_1, -k_2, (y_1 - y_2) p_1). \end{aligned} \quad (2.269)$$

When closing the κ contour below on the single pole coming from the third propagator, it equals to

$$\Phi_{gttG1}^V = -\frac{e_q g^2}{2} m_\rho f_\rho \frac{\delta^{ab}}{2 N_c} \frac{N_c}{C_F} \frac{1}{Q^2} \int_0^1 dy_1 dy_2 \frac{B(y_1, y_2)}{\bar{y}_1} e_T^* \cdot e_\gamma. \quad (2.270)$$

The axial DA contribution from the diagram (gttG1) reads

$$\begin{aligned} \Phi_{gttG1}^A &= -e_q \frac{i}{4} \frac{2}{s} \frac{(-i)N_c}{C_F} g^2 m_\rho f_\rho \frac{\delta^{ab}}{2 N_c} \frac{1}{2s} \int_0^1 dy_1 dy_2 \int \frac{d\kappa}{2\pi} p_2^\lambda p_2^\tau \epsilon_{Tpn}^\sigma D(y_1, y_2) \\ &\times \text{Tr}[\not{\epsilon}_\gamma (y_1 \not{p}_1 - \not{q}) \gamma_\nu \not{p}_1 \gamma_5] d^{\nu\rho} (-q + (1 + y_1 - y_2) p_1) \\ &\times \frac{V_{\rho\lambda\alpha} (q - (1 + y_1 - y_2) p_1, k_1, -k_2 + (y_1 - y_2) p_1) d^{\alpha\beta} (k_2 + (y_2 - y_1) p_1)}{[(y_1 p_1 - q)^2 + i\eta][(-q + (1 + y_1 - y_2) p_1)^2 + i\eta][(k_2 + (y_2 - y_1) p_1)^2 + i\eta]} \\ &\times V_{\beta\tau\sigma} (k_2 + (y_2 - y_1) p_1, -k_2, (y_1 - y_2) p_1). \end{aligned} \quad (2.271)$$

It equals, when closing the κ contour below on the single pole coming from the third propagator, to the expression

$$\Phi_{gttG1}^A = -\frac{e_q g^2}{2} m_\rho f_\rho \frac{\delta^{ab}}{2 N_c} \frac{N_c}{C_F} \frac{1}{Q^2} \int_0^1 dy_1 dy_2 \frac{D(y_1, y_2)}{\bar{y}_1} e_T^* \cdot e_\gamma. \quad (2.272)$$

All other diagrams of each class can be computed according to the previous examples.

Finally the result for $\Phi^{\gamma_T^* \rightarrow \rho_T}$ can be decomposed on the spin flip and spin non-flip tensors respectively denoted T_f and $T_{n.f}$,

$$\Phi^{\gamma_T^* \rightarrow \rho_T} = \Phi_{n.f}^{\gamma_T^* \rightarrow \rho_T} T_{n.f} + \Phi_f^{\gamma_T^* \rightarrow \rho_T} T_f, \quad (2.273)$$

with

$$\begin{aligned} T_{n.f} &= -e_{\rho\perp}^* \cdot e_{\gamma\perp} \\ &= \underline{e}_\rho^* \cdot \underline{e}_\gamma, \end{aligned} \quad (2.274)$$

$$\begin{aligned} T_f &= \frac{(e_{\rho\perp}^* \cdot k_\perp)(k_\perp \cdot e_{\gamma\perp})}{\underline{k}^2} + \frac{(e_{\rho\perp}^* \cdot e_{\gamma\perp})}{2} \\ &= \frac{(\underline{e}_\rho^* \cdot \underline{k})(\underline{k} \cdot \underline{e}_\gamma)}{\underline{k}^2} - \frac{(\underline{e}_\rho^* \cdot \underline{e}_\gamma)}{2}. \end{aligned} \quad (2.275)$$

The spin non-flip impact factor $\Phi_{n.f}^{\gamma_T^* \rightarrow \rho_T} T_{n.f}$ corresponds to transitions where the virtual photon and the ρ -meson have the same polarizations while for the spin flip impact factor $\Phi_f^{\gamma_T^* \rightarrow \rho_T} T_f$ the virtual photon and the ρ -meson have different polarizations. Denoting $\alpha = \frac{k^2}{Q^2}$, the results for the spin non-flip $\gamma_T^* \rightarrow \rho_T$ impact factor is

$$\begin{aligned} \Phi_{n.f.}^{\gamma_T^* \rightarrow \rho_T} &= C^{ab} \frac{1}{C_F} \int_0^1 dy_1 \int_0^1 dy_2 \\ &\times \left\{ \frac{y_1 \zeta_3^A D(y_1, y_2)}{\alpha + (1 - y_1) y_1} \left(\frac{\alpha (N_c - 2 C_F)}{(y_1 - y_2 + 1) \alpha + y_1 (1 - y_2)} + \frac{\alpha N_c (1 - y_1)}{y_2 \alpha + y_1 (y_2 - y_1)} \right) \right. \\ &\quad - \frac{y_1 \zeta_3^V B(y_1, y_2)}{\alpha + (1 - y_1) y_1} \left(\frac{\alpha (2 C_F - N_c) (2 y_1 - 1)}{(y_1 - y_2 + 1) \alpha + y_1 (1 - y_2)} + \frac{\alpha N_c (1 - y_1)}{y_2 \alpha + y_1 (y_2 - y_1)} \right) \\ &\quad + (\zeta_3^V B(y_1, y_2) + \zeta_3^A D(y_1, y_2)) \\ &\quad \times \left(\frac{2 C_F y_1}{\alpha + (1 - y_1) y_1} - \frac{1}{1 - y_1} \left[\frac{N_c (1 - y_2) (y_1 - y_2)}{(1 - y_1) \alpha + (1 - y_2) (y_2 - y_1)} + C_F + N_c \right] \right) \Bigg\} \end{aligned} \quad (2.276)$$

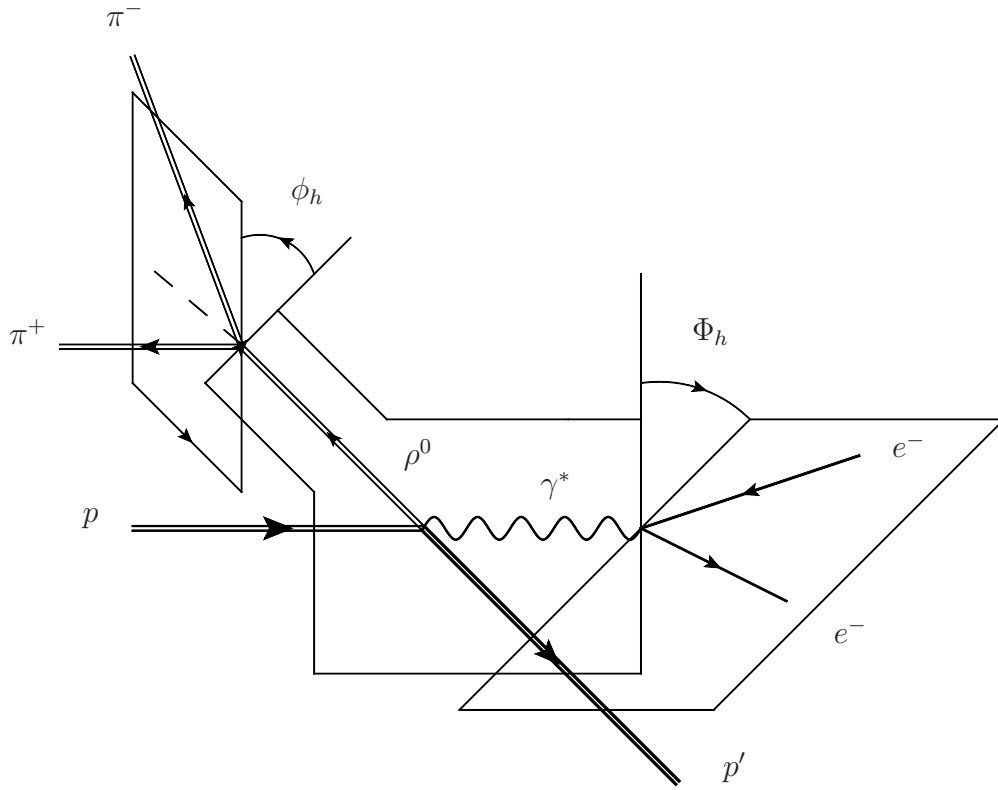
and the spin flip impact factor

$$\begin{aligned} \Phi_{f.}^{\gamma_T^* \rightarrow \rho_T}(\underline{k}^2) &= \frac{C^{ab}}{2} \left\{ 4 \int dy_1 \frac{\alpha}{(\alpha + y_1 (1 - y_1))^2} [\varphi_A^T(y_1) - (2 y_1 - 1) \varphi_1^T(y_1)] \right. \\ &\quad - 4 \int dy_1 dy_2 \frac{y_1 \alpha}{\alpha + y_1 (1 - y_1)} [\zeta_3^A D(y_1, y_2) (-y_1 + y_2 - 1) + \zeta_3^V B(y_1, y_2) (y_1 + y_2 - 1)] \\ &\quad \times \left[\frac{(2 - N_c / C_F)}{\alpha (y_1 - y_2 + 1) + y_1 (1 - y_2)} - \frac{N_c}{C_F} \frac{1}{y_2 \alpha + y_1 (y_2 - y_1)} \right] \Bigg\}. \end{aligned} \quad (2.277)$$

Note that to get the eq. (2.276) one has to use the EOMs given by eqs. (2.113, 2.114), in order to cancel the terms that are not vanishing in the limit $\underline{k}^2 \rightarrow 0$ and which would lead to end-point singularities. Thus the results have no end-point singularities and are vanishing when $\underline{k}^2 \rightarrow 0$, as imposed by the gauge invariance.

2.8 Helicity amplitudes

In this section, we build a phenomenological model of the ratios T_{11}/T_{00} in the forward limit and T_{01}/T_{00} as a function of $-t$, and we compare them to HERA data. But first let us make a brief remark on the determination of helicity amplitudes and spin matrix elements at HERA experiments.


 Figure 2.26: Kinematics of the ρ -production.

2.8.1 Measurement of helicity amplitudes and spin matrix elements

The motivation of this study is the analysis that was performed by ZEUS [98] and H1 [99] collaborations to extract the full set of spin density matrix elements r_{ij}^α of vector mesons diffractive electroproduction at small- x .

The kinematic range of energies in the center of mass, virtualities and t variable are displayed in tab. 2.8.1.

	Q^2 (GeV ²)	W (GeV)	$ t $ (GeV ²)
ZEUS	$2 < Q^2 < 160$	$32 < W < 180$	$-t < 1$
H1	$2.5 < Q^2 < 60$	$35 < W < 180$	$-t < 3$

In fig. 2.26 are shown the three different reaction planes and the angles Φ_h and ϕ_h between these planes. Φ_h is the angle between the plane of the virtual photon and the outgoing proton in the center of mass frame of the γ^*p system and the plane of the incoming and outgoing electrons. ϕ_h is the angle between the plane of the virtual photon and the outgoing proton in the center of mass frame of the γ^*p system and the plane of the pions momenta. Another important angle is θ_h , the angle in the ρ -meson rest frame between the direction of the outgoing proton and the pions direction.

The technique to extract the helicity amplitudes $T_{\lambda_\rho \lambda_\gamma}$ or the spin density matrix elements $r_{\lambda_\rho \lambda'_\rho}^\alpha$, is to expand the differential cross-section on the spherical harmonics $Y_{1\lambda_\rho}(\theta_h, \phi_h)$ leading

to

$$\frac{d\sigma}{d\cos\theta_h d\Phi_h d\phi_h} = \sigma \cdot W(\cos(\theta_h), \phi_h, \Phi_h) \quad (2.278)$$

$$= \sum_{\lambda_\gamma \lambda'_\gamma; \lambda_\rho \lambda'_\rho} T_{\lambda_\rho \lambda_\gamma} T_{\lambda'_\rho \lambda'_\gamma}^* \cdot Y_{1, \lambda_\rho}(\theta_h, \phi_h) Y_{1, \lambda'_\rho}^*(\theta_h, \phi_h) \cdot \rho_{\lambda_\gamma \lambda'_\gamma}, \quad (2.279)$$

where $\rho_{\lambda_\gamma \lambda'_\gamma}$ is the spin density matrix element associated to the production of the virtual photon from the scattering lepton. The quantities $\rho_{\lambda\lambda'}$ are defined by projecting the product of leptonic currents that appear at the cross-section level, on the polarizations λ and λ' of the virtual photons. The differential cross-section of $ep \rightarrow e'X$ with X an arbitrary final state, can be decoupled into,

$$\frac{d\sigma(ep \rightarrow e'X)}{dQ^2 dy} d\Pi_X = \frac{\alpha}{\pi Q^2 y} (1 - y + \frac{1}{2}y^2) \sum_{\lambda\lambda'} \rho_{\lambda\lambda'} d\sigma_{\lambda\lambda'}(\gamma^* p \rightarrow X), \quad (2.280)$$

with $\frac{d\sigma_{\gamma^* p \rightarrow X}}{d\Pi_X}$ the differential photoabsorption cross-section $\gamma^* p \rightarrow X$. The elements of the ρ -meson spin density matrix only depend on the angle Φ_h and the photon polarization parameter $\varepsilon \sim \frac{2(1-y)}{1+(1-y)^2}$ at small- x , which is different for H1 $\langle\varepsilon\rangle = 0.98$ and for ZEUS $\langle\varepsilon\rangle = 0.996$.

Following the analysis of Schilling and Wolf [170], in the s-channel helicity conserving (SCHC) approximation where only the transitions with $\lambda_\rho = \lambda_\gamma$ are allowed, the tensor $W(\cos(\theta_h), \phi_h, \Phi_h)$ can be parameterized by the following spin density matrix elements,

$$r_{00}^{04} = \frac{\varepsilon}{x_{11}^2 + \varepsilon}, \quad (2.281)$$

$$r_{1-1}^1 = -\mathcal{I}m(r_{1-1}^2) = \frac{1}{2} \frac{x_{11}^2}{x_{11}^2 + \varepsilon}, \quad (2.282)$$

$$\mathcal{R}e r_{10}^5 = -\mathcal{I}m r_{10}^6 = \frac{1}{2\sqrt{2}} \frac{\mathcal{R}e(T_{11} T_{00}^*)}{|T_{11}|^2 + \varepsilon |T_{00}|^2}, \quad (2.283)$$

with the notation $x_{ij} = |T_{ij}| / |T_{00}|$. The analysis of [170] goes beyond the SCHC approximation and involves the full set of the 15 spin density matrix elements.

Note that our calculations of impact factors $\gamma_T^* \rightarrow \rho_T$ are performed in the forward limit so we can access T_{11} only in this limit, while experimental data are integrated over some t range but are dominated by very small values of t . The t -dependence is given by an exponential falling functions

$$\frac{d\sigma_{L,T}}{dt} \sim \exp(-b_{L,T} |t|),$$

where b_L and b_T are fitted to HERA data. The difference $b_L - b_T$ being very small we can assume in a first approximation that the t -dependence in the ratios x_{11} cancels out. The influence of the SCHC helicity amplitudes due to the small but non-zero t -value can be estimated from the data. For $t \neq t_{min}$, r_{00}^{04} slightly depends on the s-channel helicity violating amplitudes T_{01} , T_{10} , and T_{1-1} . Experimental data are dominated by $|t - t_{min}| \leq 0.4 \text{ GeV}^2$, for which the significant amplitudes are $|T_{00}| > |T_{11}| > |T_{01}|$. The exact relation beyond SCHC

approximation reads

$$r_{00}^{04} = \frac{\varepsilon + x_{01}^2}{x_{11}^2 + \varepsilon + x_{01}^2 + x_{1-1}^2 + 2\varepsilon x_{10}^2}. \quad (2.284)$$

In the next section, we will make predictions for x_{11} and x_{01} based on the impact factor representation of the helicity amplitude using the results obtained in the LCCF scheme.

2.8.2 A proton impact factor model

The helicity amplitudes at Born level read,

$$T_{\lambda_\rho \lambda_\gamma} = is \int \frac{d^2 \underline{k}}{(2\pi)^2} \frac{1}{\underline{k}^2 (\underline{k} - \underline{\Delta})^2} \Phi^{\gamma_{\lambda_\gamma}^* \rightarrow \rho_{\lambda_\rho}}(\underline{k}, \underline{\Delta}) \Phi^{N \rightarrow N}(\underline{k}, \underline{\Delta}), \quad (2.285)$$

with $\underline{\Delta}$ the transverse momentum exchanged in t -channel. The nucleon impact factor $\Phi^{N \rightarrow N}(\underline{k}, \underline{k} - \underline{\Delta})$ is not calculable in pQCD and we have to use a model. A simple phenomenological model was provided for hadron-hadron scattering in Ref.[143] by Gunion and Soper (GS), of the form:

$$\Phi_{N \rightarrow N}(\underline{k}, \underline{\Delta}; M^2) = A \delta_{ab} \left[\frac{1}{M^2 + (\frac{\Delta}{2})^2} - \frac{1}{M^2 + (\underline{k} - \frac{\Delta}{2})^2} \right]. \quad (2.286)$$

A and M are free parameters that correspond to soft scales of the proton-proton impact factor. In order to get rid of the normalizations of the helicity amplitudes, we will focus on the descriptions of the ratios of helicity amplitudes. With the impact factor we have computed we can compare two ratios namely T_{11}/T_{00} in the forward limit and T_{01}/T_{00} as a function of $t = -\underline{\Delta}^2$.

The above model (2.286) that we will refer as the "GS model" can be interpreted as the interaction of color dipole configurations inside the nucleon with the two t -channel gluons. The scale M is then a internal hadronic transverse scale that governs the typical transverse momentum. Such a model was the basis of the dipole approach of high-energy scattering [10] and used successfully to describe DIS at small x [171].

2.8.3 Helicity amplitudes T_{11} and T_{00} at $t = t_{min}$ - Comparison of obtained predictions with H1 data

Inserting the impact factor results (2.248, 2.286) in the formula (2.285) for the helicity amplitudes leads to

$$T_{00} = \frac{is C_F 2AB}{(2\pi)Q^5} \int_0^1 dy \varphi_1(y, \mu^2) \int_{R_1^2}^\infty d\alpha \frac{1}{\alpha^2} \left(\frac{1}{R^2} - \frac{1}{\alpha + R^2} \right) \frac{\alpha}{\alpha + y\bar{y}}, \quad (2.287)$$

with $B = 2\pi\alpha_s \frac{e}{\sqrt{2}} f_\rho$, $R^2 = \frac{M^2}{Q^2}$ and $R_1^2 = \frac{\lambda^2}{Q^2}$ an infra-red cut-off on the integral over α . The infra-red cut-off is not necessary for the convergence of the integral but it allows to see how much the soft gluons contribute to the result. The helicity amplitude T_{11} is split in the WW contribution and the genuine contribution,

$$T_{11} = T_{11}^{WW} + T_{11}^{gen}.$$

The WW contribution contains only the two-parton ($q\bar{q}$) contribution to the impact factor and each WW DAs can be expressed as a function of $\varphi_1(y)$, as it was explicitly shown in Sec. 2.4.3. After interchanging the integrals over α , y and u in order to fix a specific model for DAs at the last step when performing the u integration, the WW contribution reads

$$T_{11}^{WW} = \frac{is C_F(\epsilon_\gamma \cdot \epsilon_\rho^*) m_\rho 2AB}{(2\pi)Q^6} \int_0^1 du \frac{\varphi_1(u; \mu^2)}{u} \int_0^u dy \int_{R_1^2}^\infty d\alpha$$

$$\times \frac{1}{\alpha^2} \left(\frac{1}{R^2} - \frac{1}{\alpha + R^2} \right) \frac{\alpha(\alpha + 2y\bar{y})}{(\alpha + y\bar{y})^2}, \quad (2.288)$$

The genuine ($q\bar{q}^{gen} + q\bar{q}g$) contribution involves two- and three-parton contributions. It reads

$$T_{11}^{gen} = \frac{is C_F(\epsilon_\gamma \cdot \epsilon_\rho^*) m_\rho AB}{(2\pi)Q^6} \int_{R_1^2}^\infty d\alpha \left\{ \frac{1}{R^2} - \frac{1}{\alpha + R^2} \right\}$$

$$\times \left\{ - \int_0^1 dy \frac{\alpha(\alpha + 2y\bar{y})}{y\bar{y}(\alpha + y\bar{y})^2} [(y - \bar{y})\varphi_{1T}^{gen}(y; \mu^2) + \varphi_{AT}^{gen}(y; \mu^2)] \right.$$

$$+ \int_0^1 dy_2 \int_0^{y_2} dy_1 M(y_1, y_2; \mu^2)$$

$$\times \frac{y_1\bar{y}_1\alpha}{\alpha + y_1\bar{y}_1} \left[\frac{2 - N_c/C_F}{\alpha(y_1 + \bar{y}_2) + y_1\bar{y}_2} - \frac{N_c}{C_F} \frac{1}{y_2\alpha + y_1(y_2 - y_1)} \right]$$

$$- \int_0^1 dy_2 \int_0^{y_2} dy_1 S(y_1, y_2; \mu^2)$$

$$\times \left[\frac{2 + N_c/C_F}{\bar{y}_1} + \frac{y_1}{\alpha + y_1\bar{y}_1} \left(\frac{(2 - N_c/C_F)y_1\alpha}{\alpha(y_1 + \bar{y}_2) + y_1\bar{y}_2} - 2 \right) \right.$$

$$\left. \left. - \frac{N_c}{C_F} \frac{(y_2 - y_1)\bar{y}_2}{\bar{y}_1} \frac{1}{\alpha\bar{y}_1 + (y_2 - y_1)\bar{y}_2} \right] \right\}. \quad (2.289)$$

We interchange the integrals over α and the longitudinal fractions of momentum and we define $I_1(y; R^2, R_1^2)$, $I_2(y_1, y_2; R^2, R_1^2)$ and $I_3(y_1, y_2; R^2, R_1^2)$ as the integrands after integration over α

$$I_1(y; R^2, R_1^2) = \int_{R_1^2}^\infty d\alpha \left(\frac{1}{R^2} - \frac{1}{\alpha + R^2} \right) \frac{\alpha(\alpha + 2y\bar{y})}{y\bar{y}(\alpha + y\bar{y})^2}, \quad (2.290)$$

$$I_2(y_1, y_2; R^2, R_1^2) = \int_{R_1^2}^\infty d\alpha \left\{ \frac{1}{R^2} - \frac{1}{\alpha + R^2} \right\}$$

$$\times \frac{y_1\bar{y}_1\alpha}{\alpha + y_1\bar{y}_1} \left[\frac{2 - N_c/C_F}{\alpha(y_1 + \bar{y}_2) + y_1\bar{y}_2} - \frac{N_c}{C_F} \frac{1}{y_2\alpha + y_1(y_2 - y_1)} \right], \quad (2.291)$$

$$I_3(y_1, y_2; R^2, R_1^2) = \int_{R_1^2}^\infty d\alpha \left\{ \frac{1}{R^2} - \frac{1}{\alpha + R^2} \right\} \quad (2.292)$$

$$\times \left[\frac{2 + N_c/C_F}{\bar{y}_1} + \frac{y_1}{\alpha + y_1\bar{y}_1} \left(\frac{(2 - N_c/C_F)y_1\alpha}{\alpha(y_1 + \bar{y}_2) + y_1\bar{y}_2} - 2 \right) \right.$$

$$\left. - \frac{N_c}{C_F} \frac{(y_2 - y_1)\bar{y}_2}{\bar{y}_1} \frac{1}{\alpha\bar{y}_1 + (y_2 - y_1)\bar{y}_2} \right],$$

leading to

$$T_{11}^{gen} = \frac{is C_F(\epsilon_\gamma \cdot \epsilon_\rho^*) m_\rho AB}{(2\pi)Q^6} \left\{ - \int_0^1 dy I_1(y) [(y - \bar{y}) \varphi_{1T}^{gen}(y; \mu^2) + \varphi_{AT}^{gen}(y; \mu^2)] \right. \\ \left. + \int_0^1 dy_2 \int_0^{y_2} dy_1 I_2(y_1, y_2) M(y_1, y_2; \mu^2) \right. \\ \left. - \int_0^1 dy_2 \int_0^{y_2} dy_1 I_3(y_1, y_2) S(y_1, y_2; \mu^2) \right\}, \quad (2.293)$$

where the variables R^2 and R_1^2 have been omitted for clarity. Using the symmetry property $S(y_1, y_2; \mu^2) = -M(\bar{y}_2, \bar{y}_1; \mu^2)$, this expression takes the form

$$T_{11}^{gen} = \frac{is C_F(\epsilon_\gamma \cdot \epsilon_\rho^*) m_\rho AB}{(2\pi)Q^6} \left\{ - \int_0^1 dy I_1(y) [(y - \bar{y}) \varphi_{1T}^{gen}(y; \mu^2) + \varphi_{AT}^{gen}(y; \mu^2)] \right. \\ \left. + \int_0^1 dy_2 \int_0^{y_2} dy_1 (I_2(y_1, y_2) + I_3(\bar{y}_2, \bar{y}_1)) M(y_1, y_2; \mu^2) \right\}, \quad (2.294)$$

with

$$I_2(y_1, y_2) + I_3(\bar{y}_2, \bar{y}_1) = \\ \left(2 - \frac{N_c}{C_F} \right) \int_{R_1^2}^\infty d\alpha \frac{1}{R^2(\alpha + R^2)(\alpha(y_1 + \bar{y}_2) + y_1 \bar{y}_2)} \left(\frac{\bar{y}_2^2}{\alpha + y_2 \bar{y}_2} + \frac{y_1 \bar{y}_1}{\alpha + y_1 \bar{y}_1} \right) \\ + \frac{N_c}{C_F} \int_{R_1^2}^\infty d\alpha \frac{1}{R^2(\alpha + R^2)(\alpha + y_1 \bar{y}_1)(\alpha y_2 + y_1(y_2 - y_1))} \\ + \frac{2}{y_2} \int_{R_1^2}^\infty d\alpha \frac{1}{R^2(\alpha + R^2)(\alpha + y_2 \bar{y}_2)}. \quad (2.295)$$

Combining the results (2.287) with (3.132) and (2.294), the ratios T_{11}^{WW}/T_{00} and T_{11}^{gen}/T_{00} read

$$\frac{T_{11}^{WW}}{T_{00}} = \quad (2.296) \\ - \frac{m_\rho \int_0^1 dv \varphi_1(v; \mu^2) \int_0^1 dx \int_{R_1^2}^\infty d\alpha \frac{\alpha + 2xv(1 - xv)}{\alpha(\alpha + xv(1 - xv))^2} \left(\frac{1}{R^2} - \frac{1}{\alpha + R^2} \right)}{Q \int_0^1 dy \varphi_1(y, \mu^2) \int_{R_1^2}^\infty \frac{d\alpha}{\alpha(\alpha + y\bar{y})} \left(\frac{1}{R^2} - \frac{1}{\alpha + R^2} \right)}$$

where we took into account that $\epsilon_\gamma \cdot \epsilon_\rho^* = -\underline{e}_\gamma \cdot \underline{e}_\rho^* = -1$, and

$$\frac{T_{11}^{gen}}{T_{00}} = \frac{m_\rho}{2Q} \quad (2.297) \\ \times \frac{\int_0^1 dy I_1(y) [(y - \bar{y}) \varphi_{1T}^{gen}(y; \mu^2) + \varphi_{AT}^{gen}(y; \mu^2)] - \int_0^1 dy_2 \int_0^{y_2} dy_1 (I_2(y_1, y_2) + I_3(\bar{y}_2, \bar{y}_1)) M(y_1, y_2)}{\int_0^1 dy \varphi_1(y; \mu^2) \int_{R_1^2}^\infty d\alpha \frac{1}{\alpha^2} \left(\frac{1}{R^2} - \frac{1}{\alpha + R^2} \right) \frac{\alpha}{\alpha + y\bar{y}}}.$$

The integration is performed analytically over α and numerically over remaining variables as for example y for T_{00} , x , v for T_{11}^{WW} and y_1 , y_2 for T_{11}^{gen} . The measured ratio T_{11}/T_{00} is

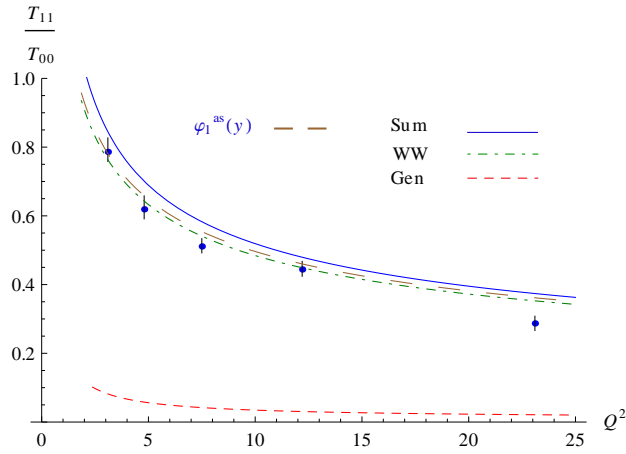


Figure 2.27: The WW contribution T_{11}^{WW}/T_{00} in green (dash-dotted line), the genuine contribution T_{11}^{gen}/T_{00} in red (dashed line), and the sum of the two contributions in blue (solid line), at $M = 1$ GeV and $\lambda = 0$ GeV, as functions of the virtuality of the photon. The brown (long-dashed) curve is the contribution based on the asymptotic DA of the ρ meson, $\varphi_1(y, \mu_F^2 = \infty) = \varphi_1^{as}(y) = 6y(1 - y)$. Our results are compared with the experimental data from H1 [99]. The experimental errors are taken to be the quadratic sum of statistical and systematical errors.

conventionally defined [105] to have an *opposite* sign with respect to eqs. (2.296) and (2.297), in order to ensure the usual matrix summation in the definition of the density matrix.

In fig. 2.27 we show the different contributions to the ratio T_{11}/T_{00} as a function of Q^2 and for the nonperturbative parameters $M = 1$ GeV and $\lambda = 0$ GeV. Unless specified, we take as a factorization scale $\mu_F^2 = Q^2$. Note that the factorization scale only appears in the ratios of the amplitudes through the DAs and the coupling constants. We see that the WW contribution dominates over the genuine one. For illustration, we also show the ratio T_{11}/T_{00} using the asymptotic $\varphi_1^{as} = 6y\bar{y}$ DA, which corresponds to $\mu_F^2 \rightarrow \infty$. In this limit, only the WW contribution survives since the three-parton coupling constants $\zeta_3^V(\mu_F^2)$ and $\zeta_3^A(\mu_F^2)$ vanish when $\mu_F^2 \rightarrow \infty$. The small difference between this asymptotic result and the total result (Sum) indicates a weak dependence of this ratio on the factorization scale μ_F .

The two parameters λ and M have different physical meanings. M is the typical nonperturbative hadronic scale, while λ is the minimal virtuality of gluons, which should be bigger than Λ_{QCD} for consistency of our perturbative approach. From fig. 2.28 (left panel), we see that our predictions are stable for M in the range 1-2 GeV. The data, when compared with our model, with $\mu = Q$, favor a value of M of the order of 1-2 GeV but exclude a very small value around Λ_{QCD} . From fig. 2.28 (right panel), we see that for λ around Λ_{QCD} , our results are very close to the experimental data and rather stable, whereas for $\lambda = 1$ GeV, i.e. significantly larger than $\Lambda_{QCD} \simeq 220$ MeV in the $\overline{\text{MS}}$ scheme, they notably deviate from the data. Let us stress the fact that our estimate provides the correct sign for the ratio T_{01}/T_{00} when compared to H1 data is a nontrivial success of our approach.

In figs. 2.29 and 2.30 we show the results of our calculations for the spin density matrix

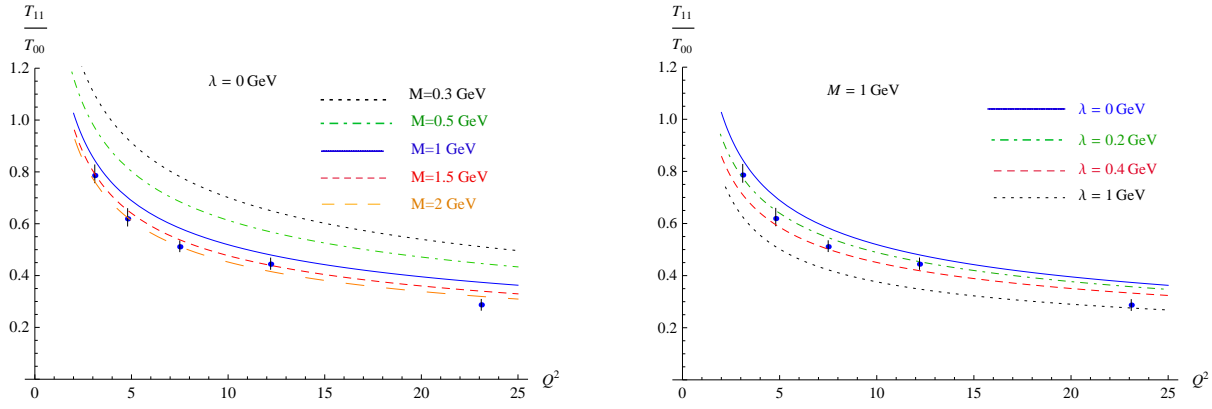


Figure 2.28: Predictions for the ratio T_{11}/T_{00} as a function of Q^2 , compared to the experimental data from H1 [99]. The experimental errors are taken to be the quadratic sum of statistical and systematical errors. Left panel: Fixed $\lambda = 0$ GeV cutoff and various values for M . Right panel: Fixed scale $M = 1$ GeV, and various values of the cutoff λ .

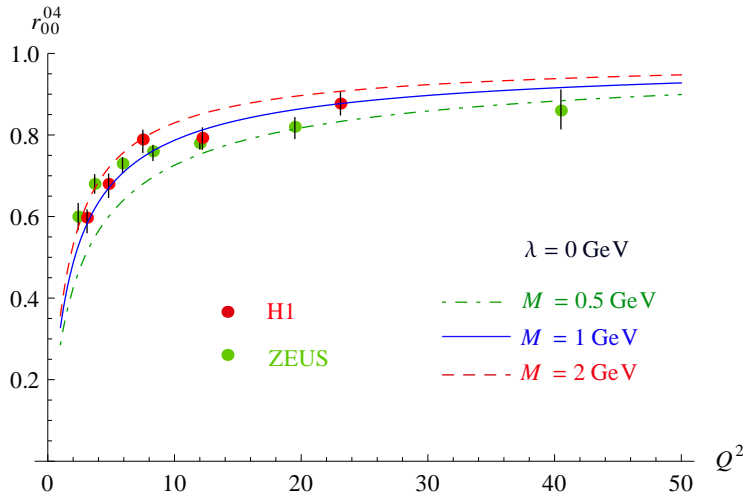


Figure 2.29: The spin density matrix element r_{00}^{04} as a function of Q^2 for $M = 0.5$ GeV in green (dash-dotted line), $M = 1$ GeV in blue (solid line), and $M = 2$ GeV in red (dashed line), and for $\lambda = 0$ GeV. Our results are compared with the experimental data from ZEUS [98] and H1 [99]. The experimental errors are taken to be the quadratic sum of statistical and systematical errors.

element r_{00}^{04} . In fig. 2.29 is shown r_{00}^{04} as a function of Q^2 for different values of the nonperturbative parameter M and for $\lambda = 0$ GeV. In fig. 2.30 is shown our predictions for $M = 1$ GeV and $\lambda = 0$ GeV as a function of W for several values of Q^2 compared to H1 and ZEUS data, of course our predictions are W -independent as our calculation is at the Born level. This observable allows a comparison of our predictions with the whole set of HERA data⁶.

⁶We predict ratios of amplitudes, while ZEUS made available the spin density matrix elements; H1 extracted both spin density matrix elements and ratios of amplitudes.

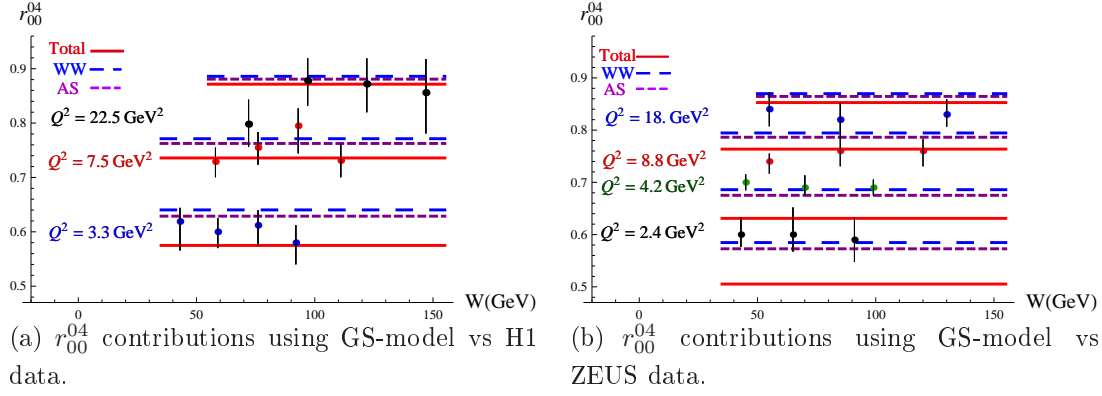


Figure 2.30: Predictions for r_{00}^{04} vs W and Q^2 compared respectively with H1[99] and ZEUS[98] data, the AS (purple dashed lines), WW (blue long dashed lines), Total (red solid lines) contributions are shown separately using the GS-model for $M = 1$ GeV and $\lambda = 0$ GeV.

2.8.4 Helicity amplitudes T_{00} and T_{01} for $t \neq t_{min}$

The H1 data show that the spin-flip amplitude T_{01} is nonzero, showing an explicit s -channel helicity violation. Besides, this amplitude vanishes when the squared momentum exchanged by the proton $t = -\underline{\Delta}^2$ is zero. We start with the generalization of eq. (2.287) for $t \neq t_{min}$,

$$\begin{aligned}
 T_{00} &= \frac{is C_F 2 Q A B}{(2\pi)^2 (M^2 + (\underline{\Delta}/2)^2)} \int_0^1 dy \, y \bar{y} \, \varphi_1(y; \mu^2) \\
 &\times \int \frac{d^2 \underline{k}}{\underline{k}^2 (\underline{k} - \underline{\Delta})^2} \frac{(\underline{k} - \underline{\Delta}/2)^2 - (\underline{\Delta}/2)^2}{(\underline{k} - \underline{\Delta}/2)^2 + M^2} \\
 &\times \left\{ \frac{1}{(y \underline{\Delta})^2 + y \bar{y} Q^2} + \frac{1}{(\bar{y} \underline{\Delta})^2 + y \bar{y} Q^2} - \frac{1}{(\underline{k} - y \underline{\Delta})^2 + y \bar{y} Q^2} - \frac{1}{(\underline{k} - \bar{y} \underline{\Delta})^2 + y \bar{y} Q^2} \right\}.
 \end{aligned} \tag{2.298}$$

Similarly,

$$\begin{aligned}
 T_{01} &= \frac{is C_F 2 Q A B}{(2\pi)^2 (M^2 + (\underline{\Delta}/2)^2)} \int_0^1 dy \, (y - \bar{y}) \, \varphi_1(y; \mu^2) \\
 &\times \int \frac{d^2 \underline{k}}{\underline{k}^2 (\underline{k} - \underline{\Delta})^2} \frac{(\underline{k} - \underline{\Delta}/2)^2 - (\underline{\Delta}/2)^2}{(\underline{k} - \underline{\Delta}/2)^2 + M^2} \\
 &\times \left\{ \frac{y \underline{\Delta} \cdot \underline{e}}{(y \underline{\Delta})^2 + y \bar{y} Q^2} - \frac{\bar{y} \underline{\Delta} \cdot \underline{e}}{(\bar{y} \underline{\Delta})^2 + y \bar{y} Q^2} + \frac{(\underline{k} - y \underline{\Delta}) \cdot \underline{e}}{(\underline{k} - y \underline{\Delta})^2 + y \bar{y} Q^2} - \frac{(\underline{k} - \bar{y} \underline{\Delta}) \cdot \underline{e}}{(\underline{k} - \bar{y} \underline{\Delta})^2 + y \bar{y} Q^2} \right\}.
 \end{aligned} \tag{2.299}$$

In eqs. (2.298, 2.299),

- the integrations over k_T are performed without infrared cutoff, partially analytically through a residue method,
- the integrations over k_T are performed with an infrared cutoff, fully numerically through triangulation coordinates centered at the pole of the two t -channel gluons.

In the next part we will detail the integration over \underline{k} with both methods.

Integration over \underline{k} for T_{00} and T_{01}

We describe the method used to evaluate the integrals over \underline{k} in eqs. (2.298, 2.299) when no infra-red cutoff is imposed. Let $(\underline{u}_1, \underline{u}_2)$ be the orthonormal basis such as $\underline{\Delta} = r \underline{u}_1$, and then $\underline{k} - \underline{\Delta} = (k_1 - r, k_2)$. In that case, a residue method, as described in Ref. [130], can be applied for the k_1 integration. In this basis, the amplitudes read

$$\begin{aligned}
 T_{00} = & \frac{is C_F 2QAB}{(2\pi)^2 (M^2 + (r/2)^2)} \int_0^1 dy \, y \bar{y} \varphi_1(y, \mu^2) \\
 & \times \int_{-\infty}^{\infty} dk_1 \int_{-\infty}^{\infty} dk_2 \frac{1}{k_1^2 + k_2^2} \frac{1}{(k_1 - r)^2 + k_2^2} \frac{(k_1 - r/2)^2 + k_2^2 - (r/2)^2}{(k_1 - r/2)^2 + k_2^2 + M^2} \\
 & \times \left\{ \frac{1}{(yr)^2 + y\bar{y} Q^2} + \frac{1}{(\bar{y}r)^2 + y\bar{y} Q^2} \right. \\
 & \left. - \frac{1}{(k_1 - yr)^2 + k_2^2 + y\bar{y} Q^2} - \frac{1}{(k_1 - \bar{y}r)^2 + k_2^2 + y\bar{y} Q^2} \right\}
 \end{aligned} \tag{2.300}$$

and

$$\begin{aligned}
 T_{01} = & \frac{is C_F AB}{(2\pi)^2 (M^2 + (r/2)^2)} \int_0^1 dy \, (y - \bar{y}) \varphi_1(y, \mu^2) \\
 & \times \int_{-\infty}^{\infty} dk_1 \int_{-\infty}^{\infty} dk_2 \frac{1}{k_1^2 + k_2^2} \frac{1}{(k_1 - r)^2 + k_2^2} \frac{(k_1 - r/2)^2 + k_2^2 - (r/2)^2}{(k_1 - r/2)^2 + k_2^2 + M^2} \\
 & \times \left\{ \frac{yr e_1}{(yr)^2 + y\bar{y} Q^2} - \frac{\bar{y}r e_1}{(\bar{y}r)^2 + y\bar{y} Q^2} \right. \\
 & \left. + \frac{e_1(k_1 - yr) + e_2 k_2}{(k_1 - yr)^2 + k_2^2 + y\bar{y} Q^2} - \frac{e_1(k_1 - \bar{y}r) + e_2 k_2}{(k_1 - \bar{y}r)^2 + k_2^2 + y\bar{y} Q^2} \right\},
 \end{aligned} \tag{2.301}$$

where e_1 and e_2 are the components of the transverse polarization of the γ^* in the basis $(\underline{u}_1, \underline{u}_2)$. We define the integrands F_{00} and F_{01} as

$$\begin{aligned}
 T_{00} = & \frac{is C_F 2QAB}{(2\pi)^2 (M^2 + (r/2)^2)} \int_0^1 dy \, y \bar{y} \varphi_1(y; \mu^2) \\
 & \times \int_{-\infty}^{\infty} dk_1 \int_{-\infty}^{\infty} dk_2 F_{00}(k_1, k_2, y),
 \end{aligned} \tag{2.302}$$

$$\begin{aligned}
 T_{01} = & \frac{is C_F AB}{(2\pi)^2 (M^2 + (r/2)^2)} \int_0^1 dy \, (y - \bar{y}) \varphi_1(y; \mu^2) \\
 & \times \int_{-\infty}^{\infty} dk_1 \int_{-\infty}^{\infty} dk_2 F_{01}(k_1, k_2, y).
 \end{aligned} \tag{2.303}$$

We perform a shift of the variables $\underline{k} \rightarrow (\underline{x} + \underline{u}_1) \frac{r}{2}$ i.e $k_1 \rightarrow x_1$, $k_2 \rightarrow x_2$. The shift symmetrizes and rescales the momenta of the gluons, which are zeros for $x_1 = \pm 1$ and $x_2 = 0$. The integrands then read

$$\begin{aligned}
 f_{00}(x_1, x_2, y) = & \frac{4}{r^2} \frac{1}{(x_1 + 1)^2 + x_2^2} \frac{1}{(x_1 - 1)^2 + x_2^2} \frac{x_1^2 + x_2^2 - 1}{g(M^2) + x_1^2} \\
 & \times \left\{ \frac{1}{(yr)^2 + y\bar{y} Q^2} + \frac{1}{(\bar{y}r)^2 + y\bar{y} Q^2} \right. \\
 & \left. - \frac{4}{r^2} \left[\frac{1}{(x_1 + (y - \bar{y}))^2 + g(y\bar{y} Q^2)} + \frac{1}{(x_1 - (y - \bar{y}))^2 + g(y\bar{y} Q^2)} \right] \right\}
 \end{aligned} \tag{2.304}$$

and

$$\begin{aligned}
 f_{01}(x_1, x_2, y) &= \frac{4}{r^2} \frac{1}{(x_1 + 1)^2 + x_2^2} \frac{1}{(x_1 - 1)^2 + x_2^2} \frac{x_1^2 + x_2^2 - 1}{g(M^2) + x_1^2} \\
 &\times \left\{ \frac{y r e_1}{(y r)^2 + y \bar{y} Q^2} + \frac{\bar{y} r e_1}{(\bar{y} r)^2 + y \bar{y} Q^2} \right. \\
 &\left. - \frac{2}{r} \left[\frac{x_1 + (y - \bar{y})}{(x_1 + (y - \bar{y}))^2 + g(y \bar{y} Q^2)} + \frac{x_1 - (y - \bar{y})}{(x_1 - (y - \bar{y}))^2 + g(y \bar{y} Q^2)} \right] \right\},
 \end{aligned} \tag{2.305}$$

with

$$g(v) = \frac{4v + r^2 x_2^2}{r^2} \tag{2.306}$$

and f_{00}, f_{01} being defined such that

$$\begin{aligned}
 T_{00} &= \frac{is C_F 2QAB}{(2\pi)^2 (M^2 + (r/2)^2)} \int_0^1 dy y \bar{y} \varphi_1(y, Q^2) \\
 &\times \int_{-\infty}^{\infty} dx_1 \int_{-\infty}^{\infty} dx_2 f_{00}(x_1, x_2, y),
 \end{aligned} \tag{2.307}$$

and

$$\begin{aligned}
 T_{01} &= \frac{is C_F AB}{(2\pi)^2 (M^2 + (r/2)^2)} \int_0^1 dy (y - \bar{y}) \varphi_1(y, Q^2) \\
 &\times \int_{-\infty}^{\infty} dx_1 \int_{-\infty}^{\infty} dx_2 f_{01}(x_1, x_2, y).
 \end{aligned} \tag{2.308}$$

Since the integrands in (2.307) and (2.308) oscillate quickly, we have used a method where the integration over x_1 can be analytically performed in order to avoid numerical integration issues for the case where there is no infra-red cut-off. We integrate over the variable x_1 using the residue method. The poles of the integrands are the same. The poles enclosed in the below contour line for $x_2 \geq 0$ are

$$x_1 = \pm(y - \bar{y}) - i\sqrt{g(Q^2 y \bar{y})}, \quad x_1 = \pm 1 - ix_2, \quad x_1 = -i\sqrt{g(M^2)}. \tag{2.309}$$

As the integrands are symmetric under $x_2 \leftrightarrow -x_2$, the result is the same for $x_2 \leq 0$. The remaining integrals over x_2 and y are then

$$\begin{aligned}
 T_{00}(r, Q, M) &= \frac{is C_F 2QAB}{(2\pi)^2 (M^2 + (r/2)^2)} \int_0^1 dy y \bar{y} \varphi_1(y, Q^2) \\
 &\times \int_{-\infty}^{\infty} dx_2 (-2i\pi) \sum_{i=1}^5 Res_i[f_{00}],
 \end{aligned} \tag{2.310}$$

$$\begin{aligned}
 T_{01}(r, Q, M) &= \frac{is C_F AB}{(2\pi)^2 (M^2 + (r/2)^2)} \int_0^1 dy (y - \bar{y}) \varphi_1(y, Q^2) \\
 &\times \int_{-\infty}^{\infty} dx_2 (-2i\pi) \sum_{i=1}^5 Res_i[f_{01}],
 \end{aligned} \tag{2.311}$$

where the explicit expressions for the residues $Res_i[f_{00}]$ and $Res_i[f_{01}]$ are too lengthy to be displayed here. We then integrate numerically over $x_2 \in [0, \infty]$ and y and finally multiply the result due to the symmetry of the pole structure by 2.

In the case where there is an infra-red cut-off, we cannot use anymore the residue method to simplify the integrals so the integration is performed only numerically but we have to change the variables to get stable numerical results. We will change the variables x_1 and x_2 by the distances of the point (x_1, x_2) from the singularities in $(-1, 0)$ and $(1, 0)$. Let b_1 and b_2 be these distances such that

$$b_1^2 = (x_1 + 1)^2 + x_2^2 \quad b_2^2 = (x_1 - 1)^2 + x_2^2. \quad (2.312)$$

We have two solutions for (x_1, x_2) , one restricted to the upper half-plane,

$$x_1 = \frac{1}{4}(b_1^2 - b_2^2), \quad x_2 = \frac{1}{4}\sqrt{(b_1 + b_2 + 2)(b_1 + b_2 - 2)(b_1 - b_2 + 2)(-b_1 + b_2 + 2)}, \quad (2.313)$$

and one restricted to the lower half-plane,

$$x_1 = \frac{1}{4}(b_1^2 - b_2^2), \quad x_2 = -\frac{1}{4}\sqrt{(b_1 + b_2 + 2)(b_1 + b_2 - 2)(b_1 - b_2 + 2)(-b_1 + b_2 + 2)}. \quad (2.314)$$

We can restrain the computations to the upper half-plane because the integrands of (2.308) and (2.307) are invariant in $x_2 \leftrightarrow -x_2$. The existence of both solutions requires that

$$(b_1 + b_2 + 2)(b_1 + b_2 - 2)(b_1 - b_2 + 2)(-b_1 + b_2 + 2) \geq 0, \quad (2.315)$$

or equivalently, at fixed b_1 , $b_2 \leq b_1 + 2$ and $b_2 \geq |b_1 - 2|$. This is the condition for the two circles centering in $(-1, 0)$ and $(1, 0)$ and of radius b_1 and b_2 , respectively, to cross each other. The Jacobian of the transformation is

$$\frac{2b_1b_2}{\sqrt{(b_1 + b_2 + 2)(b_1 + b_2 - 2)(b_1 - b_2 + 2)(-b_1 + b_2 + 2)}} \geq 0. \quad (2.316)$$

The infrared cutoff is included by a representation of the Heaviside distribution

$$\theta(b_1 - \beta_{cut}; k) = \frac{1}{1 + e^{-2k(b_1 - \beta_{cut})}}, \quad (2.317)$$

where β_{cut} is the cutoff for b_1 and b_2 . The link with the infra-red cutoff in GeV is $\lambda = \beta_{cut} \frac{r}{2}$. This ensures the stability of the numerical evaluation of the b_1 and b_2 integrations. Then the amplitudes read

$$T_{00}(\lambda; k) = \frac{is C_F 2QAB}{(2\pi)^2 (M^2 + (r/2)^2)} \int_0^1 dy y \bar{y} \varphi_1(y; \mu^2) \quad (2.318)$$

$$\times \int_0^\infty db_1 \int_{|b_1-2|}^{b_1+2} db_2 \theta(b_1 - \beta_{cut}(\lambda); k) \theta(b_2 - \beta_{cut}(\lambda); k)$$

$$\times \frac{2b_1b_2}{\sqrt{(b_1 + b_2 + 2)(b_1 + b_2 - 2)(b_1 - b_2 + 2)(-b_1 + b_2 + 2)}} \times f_{00}(y, x_1(b_1, b_2), x_2(b_1, b_2)),$$

$$T_{01}(\lambda; k) = \frac{is C_F 2QAB}{(2\pi)^2 (M^2 + (r/2)^2)} \int_0^1 dy (y - \bar{y}) \varphi_1(y; \mu^2) \quad (2.319)$$

$$\times \int_0^\infty db_1 \int_{|b_1-2|}^{b_1+2} db_2 \theta(b_1 - \beta_{cut}(\lambda); k) \theta(b_2 - \beta_{cut}(\lambda); k)$$

$$\times \frac{2b_1b_2}{\sqrt{(b_1 + b_2 + 2)(b_1 + b_2 - 2)(b_1 - b_2 + 2)(-b_1 + b_2 + 2)}} \times f_{01}(y, x_1(b_1, b_2), x_2(b_1, b_2)).$$

The integrations are performed numerically over b_1 , b_2 , and y . The constant k is chosen to be equal to 10. The width of model (2.317) of the Heaviside distribution equals $r \times \frac{1}{k} = \frac{r}{10}$ GeV. This ensures the stability of the computation without significantly affecting our results.

Comparison of the results for T_{01}/T_{00} with HERA data

Fig. 2.31 shows the dependence of the ratio T_{01}/T_{00} on the choice of the factorization scale μ for $M = 1$ GeV and $\lambda = 0$ GeV. For completeness, we also show the predictions based on the asymptotic DAs. We see that for factorization scales around $\mu^2 = Q^2$ our results are rather insensitive to its values. Nevertheless, the ratio T_{01}/T_{00} seems to be more sensitive to this scale than the ratio T_{11}/T_{00} .

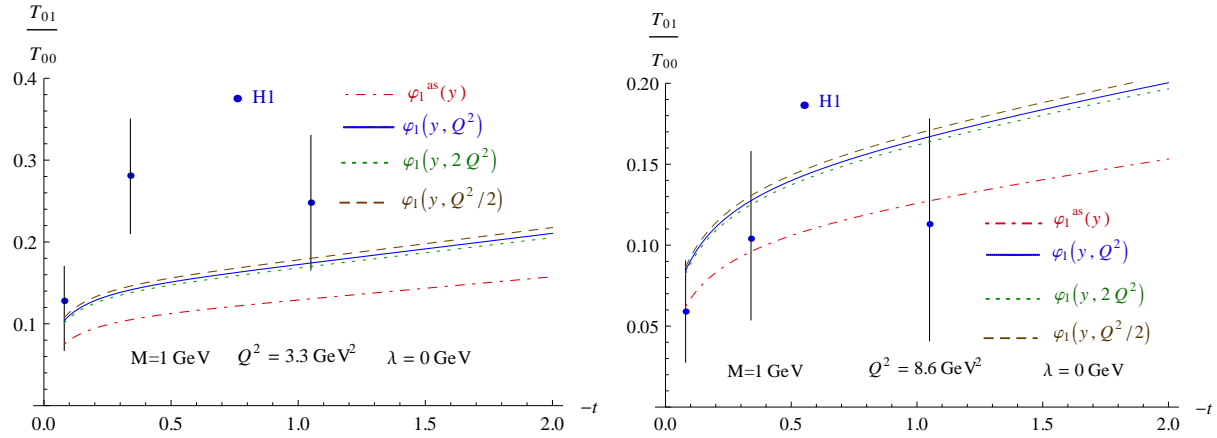


Figure 2.31: Predictions for the ratios T_{01}/T_{00} as a function of $|t|$ for $M = 1$ GeV and $\lambda = 0$ GeV, for different values of the factorization scale μ^2 , compared with H1 data [99]: the blue (solid) line is for $\varphi_1(y, \mu^2 = Q^2)$, the green (dotted) line is for $\varphi_1(y, \mu^2 = 2Q^2)$, the brown (dashed) line is for $\varphi_1(y, \mu^2 = Q^2/2)$, and the red (dashed) line is for $\varphi_1(y, \mu^2 = \infty) = \varphi_1^{as}(y) = 6y(1-y)$. The experimental errors are taken to be the quadratic sum of statistical and systematical errors. Left panel: $Q^2 = 3.3$ GeV². Right panel: $Q^2 = 8.6$ GeV².

Our predictions are based on pQCD and therefore, at small t , can only lead to a powerlike or logarithmic t dependence. We can implement the non-perturbative t -dependence by using the b -slope values extracted from H1 data [99]. Multiplying our predictions for the amplitudes by a factor $e^{-b_i |t-t_{min}|/2}$, where b_i ($i = L, T$) corresponds to ρ electroproduction from γ_L^* or γ_T^* . H1 measured values of b_L and $b_L - b_T$ [99]. The measured values for the latter are $b_L - b_T = -0.03 \pm 0.27^{+0.19}_{-0.17}$ GeV⁻² (for $\langle Q^2 \rangle = 3.3$ GeV²) and $b_L - b_T = -0.65 \pm 0.14^{+0.41}_{-0.51}$ GeV⁻² (for $\langle Q^2 \rangle = 8.6$ GeV²). Here we present our results in fig. 2.32. One can see in the right panel of fig. 2.32 that the precision of the data for the T_{01}/T_{00} ratio does not permit us to discriminate between a zero value for the difference of the transverse and the longitudinal slope parameters, $b_L - b_T$, and a nonzero value of this difference, as measured by H1 at higher values of Q^2 .

Thus our estimate provides the correct sign and order of magnitude for the ratio T_{01}/T_{00}

when compared to H1 data for M of the order of 1 GeV in the whole range of $\langle -t \rangle < 1.08$ GeV².

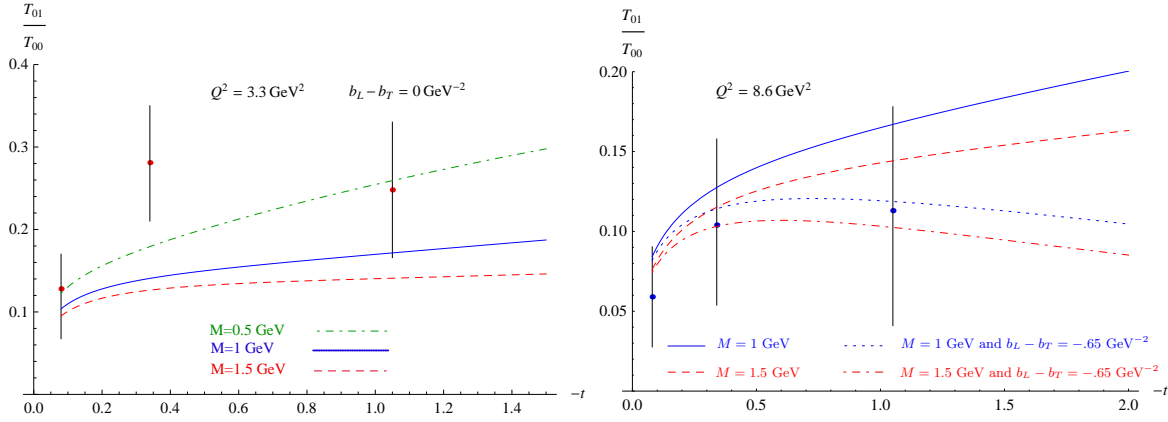


Figure 2.32: Predictions for the ratio T_{01}/T_{00} as a function of $|t|$ for $\lambda = 0$ GeV, for various values of M , compared with H1 data [99]. The experimental errors are taken to be the quadratic sum of statistical and systematical errors. Left panel: $Q^2 = 3.3$ GeV². Right panel: $Q^2 = 8.6$ GeV².

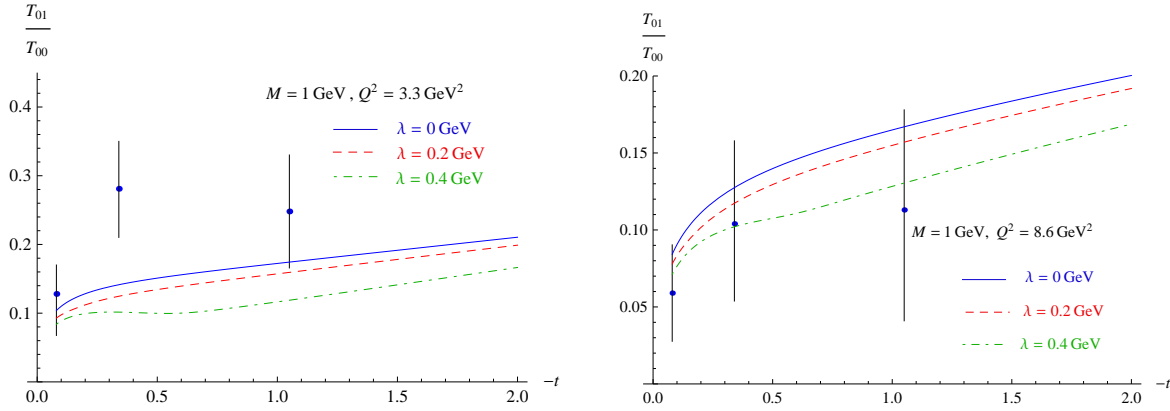


Figure 2.33: Predictions for the ratios T_{01}/T_{00} as a function of $|t|$ for $M = 1$ GeV, for different values of λ , compared with H1 data [99]: the blue (solid) line is for $\lambda = 0$ GeV, the red (dashed) line is for $\lambda = 0.2$ GeV, and the green (dash-dotted) line is for $\lambda = 0.4$ GeV. The experimental errors are taken to be the quadratic sum of statistical and systematical errors. Left panel: $Q^2 = 3.3$ GeV². Right panel: $Q^2 = 8.6$ GeV².

For completeness, as we did for the ratio T_{11}/T_{00} , we also display in fig. 2.33 the effect of varying the cutoff λ on k_T for the ratio T_{01}/T_{00} . Again, the prediction does not change significantly when λ is around Λ_{QCD} . One obtains the same kind of values for M and λ when comparing with the data for the two ratios T_{11}/T_{00} and T_{01}/T_{00} . However, due to a lack of precision of the data for the ratio T_{01}/T_{00} , the parameters M and λ are mainly constrained by the ratio T_{11}/T_{00} .

2.8.5 Discussion of the results

This model provides a fairly good description of the data despite the simplicity of the nucleon impact factor for reasonable values of M . Let us sum up the characteristics of this model,

- the predictions are not very sensitive to the typical transverse scale M of the dipole configuration inside the nucleon,
- the predictions are not very sensitive to the choice of the renormalization scale μ_F that we used,
- the λ -dependence of the predictions shows that the dominant contribution is given by the exchange of hard gluons in t -channel ($\underline{k}^2 \gg \Lambda_{QCD}^2$), but also that the effects of soft gluons are sizable.

This last point justifies the QCD twist expansion based on the dominance of the scattering on the target of small transverse-size quark-antiquark and quark-antiquark-gluon colorless states. It also justifies the fact that a sizable contribution is given by large dipole configurations and should be decreased by saturation effects in the nucleon. So what we can learn from this first approach is that we can describe the HERA data with pQCD but this description have to be improved in order to implement the dynamics of larger dipole sizes.

This approach could be generalized to access other scattering amplitude ratios that have also been measured and should be confronted with a k_T -factorization approach. This requires nontrivial analytical calculations for $t \neq t_{min}$ of the twist-3 amplitudes (which was not needed for the ratio T_{01}/T_{00}) which is a hard task, since it involves, in particular, the computation of the $\gamma_L^* \rightarrow \rho_T$ impact factor. This deserves a separate study.

Data also exist for ϕ leptonproduction. In this case quark-mass effects should be taken into account, in particular, because this allows the transversely polarized ϕ to couple through its chiral-odd twist-2 DA. The fact that the ratio T_{11}/T_{00} is not the same (after trivial mass rescaling) for ρ and ϕ mesons suggests that it is an important effect.

In the next chapter we will make the connection of the twist expansion of the impact factor with the color dipole formalism. The color dipole scattering amplitude in the forward limit being well known from models fitting DIS data, this will allow to get a much more sophisticated model including the saturation dynamics of the nucleon, involving no free parameter and able to predict the normalizations and the energy dependences of the helicity amplitudes in the forward limit.

Chapter 3

LCCF in the impact parameter representation

3.1 Introduction

In the previous section we have built a phenomenological model for the helicity amplitudes of the process $\gamma^*(\lambda_\gamma) p \rightarrow \rho(\lambda_\rho) p$ based on the computations of the impact factors of Refs. [130, 131] in the collinear approximation. This model relies on the models for the DAs given in [142] based on conformal expansion and a model for the proton impact factor [143] with a free parameter M . Despite the fact that this model allows to get a fairly good agreement with the data from HERA, this model does not provide the normalizations of the helicity amplitudes as well as their energy dependences. It seems also that the saturation effects could lead to sizable modifications of the predictions when the t -channel gluon momenta is smaller than the saturation scale.

In this chapter, we will present a way to improve the previous model by connecting the computation performed in the collinear factorization scheme with the color dipole model approach. As a result, we will get a model without free parameter which is able to,

- predict the normalization of the helicity amplitudes,
- predict the energy dependence of the helicity amplitudes,
- include the saturation dynamics of the nucleon target.

The comparison with HERA data of the normalizations, the Q^2 - and the x -dependencies, is a test for both the dipole models and the collinear factorization beyond the leading twist of the ρ -meson.

This chapter is split in two parts. In the first part of the chapter we present the computation in the impact parameter representation of the two- and three-parton impact factor contributions, factorizing in the impact factor when it is possible, the wave function of the virtual photon. These results in the impact parameter representation are strictly equivalent to the results in momentum space presented in the chap. 2. We will see however that this

approach is more natural to generalize the twist expansion of the impact factor as it does not involve hard part derivative terms and it makes clearly appear the moments of the ρ -meson wave functions which are parameterized by the DAs. A non-trivial result of this approach is that the results are consistent with the dipole picture only after using the EOMs of QCD. It is also shown that the interaction of the two t -channel gluons with the quark antiquark gluon intermediate state, involves only color dipole interactions at finite N_c (no quadrupole term).

In the second part of the chapter, we present the predictions for the polarized cross-sections σ_L and σ_T of the processes $\gamma_L^* p \rightarrow \rho_L p$ and $\gamma_T^* p \rightarrow \rho_T p$, obtained from the results of the first part of the chapter, in combination with dipole cross-section models. These predictions are compared with HERA data and we discuss the role of the higher twist corrections and the role of the saturation effects in the predictions of the model. Particularly we compare the distributions of dipole sizes obtained from the twist expansion of the ρ -meson, to distributions obtained with r_\perp -dependent models for the overlap of the wave functions of the virtual photon and the ρ -meson.

3.2 The $q\bar{q}$ intermediate state contributions

3.2.1 Equivalent LCCF procedure in impact parameter representation

In the color dipole picture the dipole scattering amplitude depends on the transverse dipole size \underline{r} , while in the LCCF approach described in the chap. 2, the Taylor expansion around the light-cone direction does not exhibit the transverse parton momentum dependence, being Fourier conjugate to \underline{r} . We can nevertheless get information about the transverse space due to the presence of the transverse momenta k_\perp of the t -channel gluons that gives to the quark antiquark pair a transverse size \underline{r} in the hard part of the process. Note that in principle one could take the Fourier transform with respect to \underline{k} of the impact factor results eqs. (2.276, 2.277) of chap. 2 to combine them with a dipole model, however one would miss the underlying dynamics of the dipoles behind a complicated Fourier transform. In our approach we first express the hard parts in terms of their Fourier transforms in the transverse impact parameter space and then we perform the Taylor expansion of the hard part around the dominant light-cone direction.

We first factorize spinor and color indices using Fierz identity,

$$\mathcal{A}_{q\bar{q}}^{\gamma^* \rightarrow \rho} = \int \frac{d^4 \ell}{(2\pi)^4} H_{q\bar{q}}(\ell) S_{q\bar{q}}(\ell) = -\frac{1}{4} \int \frac{d^4 \ell}{(2\pi)^4} \text{tr}(H_{q\bar{q}}(\ell) \Gamma^\alpha) S_{q\bar{q}}^{\Gamma_\alpha}(\ell). \quad (3.1)$$

Using Sudakov variables for the loop momentum $\ell = \alpha p + \beta n + \ell_\perp$ and for its Fourier

conjugate coordinates $z = \alpha_z p + \beta_z n + z_\perp$, the ℓ integration reads

$$\begin{aligned}
i\mathcal{A}_{q\bar{q}} &= -\frac{1}{4} \int dy \int \frac{d^2 \ell_\perp}{(2\pi)^2} \text{Tr}[H_{q\bar{q}}(y, \ell_\perp) \Gamma^\alpha] \int \frac{d\alpha_\ell}{2\pi} \int \frac{d\beta_\ell}{2\pi} \int \frac{d\lambda}{2\pi} e^{i\lambda(\alpha_\ell - y)} \\
&\times \int d^4 z e^{-i\ell \cdot z} \langle \rho(p) | \bar{\psi}(z) \Gamma_\alpha \psi(0) | 0 \rangle \\
&= -\frac{1}{4} \int dy \int \frac{d^2 \ell_\perp}{(2\pi)^2} \text{Tr}[H_{q\bar{q}}(y, \ell_\perp) \Gamma^\alpha] \int \frac{d\lambda}{2\pi} e^{-i\lambda y} \int d^2 z_\perp e^{-i\ell_\perp \cdot z_\perp} \\
&\times \langle \rho(p) | \bar{\psi}(\lambda n + z_\perp) \Gamma_\alpha \psi(0) | 0 \rangle,
\end{aligned} \tag{3.2}$$

where we kept the information about the transverse momentum in the hard part. Note that this is the main difference at this point with the steps described in Sec. 2.2.4 of the chap. 2. The main point is now to keep a trace of this transverse dynamics by expressing the hard part in terms of its Fourier transform in the impact parameter space. We use the same shorthand notations than in chap. 2,

$$H_{q\bar{q}}^{\Gamma^\alpha}(y, \ell_\perp) \equiv \text{tr}[H_{q\bar{q}}(y, \ell_\perp) \Gamma^\alpha],$$

and we define its Fourier transform in the transverse plane,

$$\tilde{H}_{q\bar{q}}^{\Gamma^\alpha}(y, x_\perp) = \int \frac{d^2 \underline{\ell}}{(2\pi)^2} H_{q\bar{q}}^{\Gamma^\alpha}(y, \underline{\ell}) e^{-i\underline{\ell} \cdot \underline{r}}.$$

The expression we get for the amplitude reads

$$\begin{aligned}
i\mathcal{A}_{q\bar{q}} &= -\frac{1}{4} \int dy \int \frac{d^2 \ell_\perp}{(2\pi)^2} \int d^2 x_\perp \tilde{H}_{q\bar{q}}^{\Gamma^\alpha}(y, x_\perp) e^{-ix_\perp \cdot \ell_\perp} \int \frac{d\lambda}{2\pi} e^{-i\lambda y} \\
&\times \int d^2 z_\perp e^{-i\ell_\perp \cdot z_\perp} \langle \rho(p) | \bar{\psi}(\lambda n + z_\perp) \Gamma_\alpha \psi(0) | 0 \rangle.
\end{aligned} \tag{3.3}$$

For now, the integral over $\underline{\ell}$ links the hard and soft parts and in order to factorize the amplitude we use the Taylor expansion of the hard part around the dominant light-cone direction,

$$\begin{aligned}
H_{q\bar{q}}^{\Gamma^\alpha}(y, \ell_\perp) &= \sum_{k=0}^{\infty} \frac{1}{k!} \left[(\ell - yp) \cdot \frac{\partial}{\partial \ell} \right]^k H_{q\bar{q}}^{\Gamma^\alpha}(y, 0_\perp) \\
&\xrightarrow{\text{twist } 3} \sum_{k=0}^1 \frac{1}{k!} \left[\ell_\perp \cdot \frac{\partial}{\partial \ell_\perp} \right]^k H_{q\bar{q}}^{\Gamma^\alpha}(y, 0_\perp) \\
&= \int d^2 \underline{r} \tilde{H}_{q\bar{q}}^{\Gamma^\alpha}(y, r_\perp) \sum_{k=0}^1 \frac{(i\underline{\ell} \cdot \underline{r})^k}{k!}.
\end{aligned} \tag{3.4}$$

Up to twist 3, the Taylor expansion is truncated at $k = 1$. All the information about the two-parton hard part contribution is encoded in $\tilde{H}_{q\bar{q}}^{\Gamma^\alpha}(y, r_\perp)$ which involves *only* the computation of six Feynman diagrams. In the momentum space approach in Sec. 2.2.4, one would need to compute the derivative of the hard part in the limit $\ell \rightarrow yp$,

$$\frac{\partial^k}{\partial \ell_{\perp\mu}^k} H_{q\bar{q}}^{\Gamma^\alpha}(y, 0_\perp),$$

which using the collinear Ward identity leads to a number of diagrams to compute which increases with the number of derivatives. The price we pay is the integral over \underline{r} the transverse dipole size and to compute the hard part with the parton transverse momenta.

Replacing the hard part (3.4) in (3.3) leads to

$$\begin{aligned} i\mathcal{A}_{q\bar{q}} &= -\frac{1}{4} \int dy \int d^2x_\perp \tilde{H}_{q\bar{q}}^{\Gamma_\alpha}(y, x_\perp) \\ &\times \int^{\ell_\perp^2 < \mu_F^2} \frac{d^2\ell_\perp}{(2\pi)^2} \int d^2z_\perp \sum_{k=0}^1 \frac{1}{k!} (-i\ell_\perp \cdot x_\perp)^k e^{-i\ell_\perp \cdot z_\perp} \\ &\times \int \frac{d\lambda}{2\pi} e^{-i\lambda y} \langle \rho(p) | \bar{\psi}(\lambda n + z_\perp) \Gamma_\alpha \psi(0) | 0 \rangle. \end{aligned}$$

Note that the Taylor expansion terms of $\exp(-i\ell_\perp \cdot x_\perp)$ are giving the moments of the ρ -meson wave function. After integration by parts with respect to the integral over z_\perp the amplitude reads

$$\begin{aligned} i\mathcal{A}_{q\bar{q}} &= -\frac{1}{4} \int dy \int d^2x_\perp \tilde{H}_{q\bar{q}}^{\Gamma_\alpha}(y, x_\perp) \int^{\ell_\perp^2 < \mu_F^2} \frac{d^2\ell_\perp}{(2\pi)^2} \int d^2z_\perp e^{-i\ell_\perp \cdot z_\perp} \\ &\times \sum_{k=0}^1 \frac{(-1)^k}{k!} (x_\perp \cdot \frac{\partial}{\partial z_\perp})^k \int \frac{d\lambda}{2\pi} e^{-i\lambda y} \langle \rho(p) | \bar{\psi}(\lambda n + z_\perp) \Gamma_\alpha \psi(0) | 0 \rangle \\ &= -\frac{1}{4} \int dy \int d^2x_\perp \tilde{H}_{q\bar{q}}^{\Gamma_\alpha}(y, x_\perp) \sum_{k=0}^1 \frac{1}{k!} \\ &\int^{\ell_\perp^2 < \mu_F^2} \frac{d^2\ell_\perp}{(2\pi)^2} \int d^2z_\perp e^{-i\ell_\perp \cdot z_\perp} \int \frac{d\lambda}{2\pi} e^{-i\lambda y} \langle \rho(p) | \bar{\psi}(\lambda n + z_\perp) (x_\perp \cdot \overleftrightarrow{\partial}^\perp)^k \Gamma_\alpha \psi(0) | 0 \rangle. \end{aligned}$$

It can be then parameterized by the DAs as

$$\begin{aligned} i\mathcal{A}_{q\bar{q}} &= -\frac{1}{4} \int dy \int d^2x_\perp \tilde{H}_{q\bar{q}}^{\Gamma_\alpha}(y, x_\perp) \int^{\ell_\perp^2 < \mu_F^2} \frac{d^2\ell_\perp}{(2\pi)^2} \int d^2z_\perp e^{-i\ell_\perp \cdot z_\perp} \int \frac{d\lambda}{2\pi} e^{-i\lambda y} \\ &\times \left(\langle \rho(p) | \bar{\psi}(\lambda n + z_\perp) \Gamma_\alpha \psi(0) | 0 \rangle + x_\perp^\mu \langle \rho(p) | \bar{\psi}(\lambda n + z_\perp) \overleftrightarrow{\partial}_\mu^\perp \Gamma_\alpha \psi(0) | 0 \rangle \right) \\ &= -\frac{m_\rho f_\rho}{4} \int dy \int d^2x_\perp \{ (e^* \cdot n) \varphi_1(y; \mu_F^2) \tilde{H}_{q\bar{q}}^\phi(y, x_\perp) \\ &\quad + \varphi_3(y; \mu_F^2) \tilde{H}_{q\bar{q}}^{\phi*}(y, x_\perp) + i\varphi_A(y; \mu_F^2) \tilde{H}_{q\bar{q}}^{R* \gamma^5}(y, x_\perp) \\ &\quad - i(x_\perp \cdot e_\perp^*) \varphi_1^T(y; \mu_F^2) \tilde{H}_{q\bar{q}}^\phi(y, x_\perp) + (x_\perp \cdot R_\perp^*) \varphi_A^T(y; \mu_F^2) \tilde{H}_{q\bar{q}}^{\phi \gamma^5}(y, x_\perp) \}, \end{aligned} \quad (3.5)$$

with $\tilde{H}_{q\bar{q}}^{\Gamma_\alpha} a_\alpha \equiv \tilde{H}_{q\bar{q}}^{\Gamma_\alpha a_\alpha}$.

In the following part we will compute the hard parts $H_{q\bar{q}}^{\gamma^\mu}(y, \ell_\perp)$ and $H_{q\bar{q}}^{\gamma^5 \gamma^\mu}(y, \ell_\perp)$, and then we will derive the expressions of their Fourier transforms in the transverse coordinate space $\tilde{H}_{q\bar{q}}^{\gamma^\mu}(y, x_\perp)$ and $\tilde{H}_{q\bar{q}}^{\gamma^5 \gamma^\mu}(y, x_\perp)$.

3.2.2 Impact factor calculation for the $q\bar{q}$ contribution

We now compute the hard parts in momentum space $H_{q\bar{q}}^{\gamma^\mu}(y, \ell_\perp)$ and $H_{q\bar{q}}^{\gamma^5 \gamma^\mu}(y, \ell_\perp)$ for the $\gamma_T^*(\lambda_\gamma) \rightarrow \rho_T(\lambda_T)$ impact factor. The partons are kept on the mass-shell and in the collinear

limit ($\ell_\perp \rightarrow 0$), this kinematics is the same than in the chap. 2 which allows to compare the final results after integration over \underline{x} of the Fourier transforms.

We recall the Sudakov decompositions of the momenta

$$\begin{aligned}\ell_1 &= yp_1 + \ell_\perp + \frac{\ell^2}{ys}p_2, \\ \ell_2 &= \bar{y}p_1 - \ell_\perp + \frac{\ell^2}{\bar{y}s}p_2, \\ p_\rho &= p_1 + \frac{\ell^2}{s} \frac{1}{y\bar{y}}p_2.\end{aligned}\tag{3.6}$$

The momentum of the incoming photon is

$$q = p_1 - \frac{Q^2}{s}p_2,\tag{3.7}$$

while the momenta of the gluons in t -channel are

$$\begin{aligned}k_1 &= \frac{\kappa + \underline{k}^2 + Q^2}{s}p_2 + k_\perp, \\ k_2 &= \frac{\kappa + \underline{k}^2 - p_\rho^2}{s}p_2 + k_\perp.\end{aligned}\tag{3.8}$$

The six diagrams of the hard part involving the $q\bar{q}$ intermediate state are similar than the diagrams of fig. 2.7 in the Sec. 2.2.1 and we use the same labeling. After computing all the 6 diagrams (a), (b), (c), (d), (e), (f), we perform the integral over κ by the method of residues to get the contribution to the impact factor, according to the definition of the impact factor (2.237) in sec. 2.7 of chap. 2. Four poles in κ appear,

- Diagram (a) and (e) : $\kappa_1 = \frac{(\underline{\ell} - y\underline{k})^2}{y\bar{y}} - i\eta$
- Diagram (b) and (c) : $\kappa_2 = \frac{(\underline{\ell} + \bar{y}\underline{k})^2}{y\bar{y}} - i\eta$
- Diagram (b) and (e) : $\kappa_3 = \frac{-1}{\bar{y}}((\underline{k} + \underline{\ell})^2 - \underline{\ell}^2 + \bar{y}(\underline{k}^2 + Q^2)) + i\eta$
- Diagram (d) and (f) : $\kappa_4 = \frac{-1}{y}((\underline{k} - \underline{\ell})^2 - \underline{\ell}^2 + y(\underline{k}^2 + Q^2)) + i\eta.$

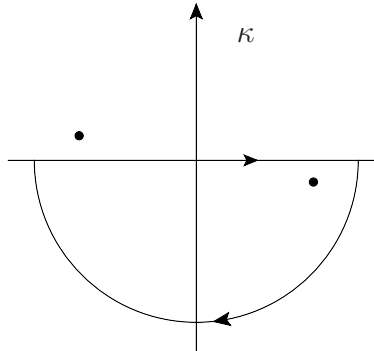


Figure 3.1: Integral contour \mathcal{C}^- along the lower κ - complex plane.

The hard sub-process amplitudes denoted $i\mathcal{M}$, associated to each diagrams (a), (b), (c) and (e) that will give a non-zero contribution when we integrate over κ closing the contour in the lower κ plane \mathcal{C}_- illustrated in fig. 3.1, read for the different structures $\Gamma^\alpha \equiv \{\gamma^\mu, \gamma^\mu \gamma^5\}$

- diagram (a):

$$\begin{aligned} i\mathcal{M}_a^{\Gamma^\alpha} &= \frac{ie}{\sqrt{2}} \frac{g^2 \delta^{ab}}{2N_c} \frac{2}{s} \frac{\text{Tr}[\not{\epsilon}_\gamma(-\bar{y}\not{p}_1 + \frac{\ell^2 + yQ^2}{ys}\not{p}_2 + \not{\ell}_\perp)\not{p}_2(-\bar{y})\not{p}_1\not{p}_2\Gamma^\alpha]}{-\frac{\bar{y}}{y}(\underline{\ell}^2 + \mu^2)(\kappa - \kappa_1)} \\ &= \frac{2ie}{\sqrt{2}} \frac{g^2 \delta^{ab}}{2N_c} y \frac{\text{Tr}[\not{\epsilon}_\gamma(-\bar{y}\not{p}_1 + \not{\ell}_\perp)\not{p}_2\Gamma^\alpha]}{(\underline{\ell}^2 + \mu^2)(\kappa - \kappa_1)}. \end{aligned} \quad (3.9)$$

- diagram (b)

$$\begin{aligned} i\mathcal{M}_b^{\Gamma^\alpha} &= -\frac{ie}{\sqrt{2}} \frac{g^2 \delta^{ab}}{2N_c} \frac{2}{s} \frac{\text{Tr}[\not{p}_2(y\not{p}_1 + \not{k}_\perp + \not{\ell}_\perp)\not{\epsilon}_\gamma(-\bar{y}\not{p}_1 + \not{k}_\perp + \not{\ell}_\perp)\not{p}_2\Gamma^\alpha]}{y\bar{y}(\kappa - \kappa_2)(\kappa - \kappa_3)} \\ &= \frac{2ie}{\sqrt{2}} \frac{g^2 \delta^{ab}}{2N_c} \frac{1}{y\bar{y}(\kappa - \kappa_2)(\kappa - \kappa_3)} \\ &\quad \times \{\bar{y}\text{Tr}[\not{p}_2(\not{k}_\perp + \not{\ell}_\perp)\not{\epsilon}_\gamma\Gamma^\alpha] - y\text{tr}(\not{\epsilon}_\gamma(\not{k}_\perp + \not{\ell}_\perp)\not{p}_2\Gamma^\alpha)\}. \end{aligned} \quad (3.10)$$

- diagram (c)

$$i\mathcal{M}_c^{\Gamma^\alpha} = -\frac{2ie}{\sqrt{2}} \frac{g^2 \delta^{ab}}{2N_c} \bar{y} \frac{\text{Tr}[\not{p}_2(y\not{p}_1 + \not{\ell}_\perp)\not{\epsilon}_\gamma\Gamma^\alpha]}{(\underline{\ell}^2 + \mu^2)(\kappa - \kappa_2)}. \quad (3.11)$$

- diagram (e)

$$\begin{aligned} i\mathcal{M}_e^{\Gamma^\alpha} &= -\frac{2ie}{\sqrt{2}} \frac{g^2 \delta^{ab}}{2N_c} \frac{1}{y\bar{y}(\kappa - \kappa_1)(\kappa - \kappa_4)} \\ &\quad \times \{\bar{y}\text{tr}(\not{p}_2(\not{k}_\perp - \not{\ell}_\perp)\not{\epsilon}_\gamma\Gamma^\alpha) - y\text{Tr}(\not{\epsilon}_\gamma(\not{k}_\perp - \not{\ell}_\perp)\not{p}_2\Gamma^\alpha)\}. \end{aligned} \quad (3.12)$$

Computing the impact factor hard part contribution with residue method along the contour \mathcal{C}_- ,

$$H_{q\bar{q}}^{\Gamma^\alpha} = \frac{1}{2s} \int_{\mathcal{C}_-} \frac{d\kappa}{2\pi} i\mathcal{M}_{q\bar{q}}^{\Gamma^\alpha} = -\frac{i}{2s} \mathcal{R}es_\kappa(i\mathcal{M}_{q\bar{q}}^{\Gamma^\alpha}), \quad (3.13)$$

with

$$\kappa_1 - \kappa_4 = \frac{1}{y\bar{y}}((\underline{\ell} - \underline{k})^2 + \mu^2), \quad (3.14)$$

$$\kappa_2 - \kappa_3 = \frac{1}{y\bar{y}}((\underline{\ell} + \underline{k})^2 + \mu^2), \quad (3.15)$$

leads to

$$\begin{aligned} H_{q\bar{q}}^{\Gamma^\alpha}(y, \underline{\ell}) &= \frac{eg^2 \delta^{ab}}{\sqrt{2}2N_c s} \left\{ \frac{y\text{tr}[\not{\epsilon}_\gamma(\not{\ell}_\perp - \bar{y}\not{p}_1)\not{p}_2\Gamma^\alpha] - \bar{y}\text{tr}[\not{p}_2(y\not{p}_1 + \not{\ell}_\perp)\not{\epsilon}_\gamma\Gamma^\alpha]}{\underline{\ell}^2 + \mu^2} \right. \\ &\quad - \frac{y\text{tr}[\not{\epsilon}_\gamma(\not{\ell}_\perp - \not{k}_\perp)\not{p}_2\Gamma^\alpha] - \bar{y}\text{tr}[\not{p}_2(\not{\ell}_\perp - \not{k}_\perp)\not{\epsilon}_\gamma\Gamma^\alpha]}{(\underline{\ell} - \underline{k})^2 + \mu^2} \\ &\quad \left. - \frac{y\text{tr}[\not{\epsilon}_\gamma(\not{\ell}_\perp + \not{k}_\perp)\not{p}_2\Gamma^\alpha] - \bar{y}\text{tr}[\not{p}_2(\not{\ell}_\perp + \not{k}_\perp)\not{\epsilon}_\gamma\Gamma^\alpha]}{(\underline{\ell} + \underline{k})^2 + \mu^2} \right\}. \end{aligned}$$

The vector and the axial-vector hard parts read respectively

$$H_{q\bar{q}}^{\gamma^\mu}(y, \underline{\ell}) = -4 \frac{eg^2}{\sqrt{2}} \frac{\delta^{ab}}{2N_c} e_\gamma^\mu \frac{y\bar{y}}{\underline{\ell}^2 + \mu^2} - 4 \frac{eg^2}{s\sqrt{2}} \frac{\delta^{ab}}{2N_c} (y - \bar{y}) p_2^\mu \times \left\{ \frac{\underline{e}_\gamma \cdot \underline{\ell}}{\underline{\ell}^2 + \mu^2} - \frac{\underline{e}_\gamma \cdot (\underline{\ell} + \underline{k})}{(\underline{\ell} + \underline{k})^2 + \mu^2} - \frac{\underline{e}_\gamma \cdot (\underline{\ell} - \underline{k})}{(\underline{\ell} - \underline{k})^2 + \mu^2} \right\} \quad (3.16)$$

and

$$H_{q\bar{q}}^{\gamma^\mu \gamma^5}(y, \underline{\ell}) = 4i \frac{eg^2}{s\sqrt{2}} \frac{\delta^{ab}}{2N_c} \times \varepsilon^{\mu\nu\rho\sigma} \left(\frac{e_{\gamma\nu} \ell_{\perp\rho} p_{2\sigma}}{\underline{\ell}^2 + \mu^2} - \frac{e_{\gamma\nu} (\ell_{\perp\rho} + k_{\perp\rho}) p_{2\sigma}}{(\underline{\ell} + \underline{k})^2 + \mu^2} - \frac{e_{\gamma\nu} (\ell_{\perp\rho} - k_{\perp\rho}) p_{2\sigma}}{(\underline{\ell} - \underline{k})^2 + \mu^2} \right). \quad (3.17)$$

The Fourier transforms of propagators in (3.16, 3.17) are related to the modified Bessel functions $K_\nu(x)$

$$\frac{1}{\underline{\ell}^2 + \mu^2} = \int \frac{d^2 \underline{x}}{2\pi} K_0(\mu|\underline{x}|) e^{i\underline{\ell} \cdot \underline{x}}, \quad (3.18)$$

$$\frac{\underline{\ell}}{\underline{\ell}^2 + \mu^2} = -i \int \frac{d^2 \underline{x}}{2\pi} \mu \frac{\underline{x}}{|\underline{x}|} K_1(\mu|\underline{x}|) e^{i\underline{\ell} \cdot \underline{x}}. \quad (3.19)$$

The Fourier transforms of the vector and axial-vector hard parts read thus

$$\tilde{H}_{q\bar{q}}^{\gamma^\mu}(y, \underline{x}) = 4 \frac{eg^2}{(2\pi)\sqrt{2}} \frac{\delta^{ab}}{2N_c} (-y\bar{y} K_0(\mu|\underline{x}|) e_\gamma^\mu + p_2^\mu (y - \bar{y}) i\mu \frac{\underline{e}_\gamma \cdot \underline{x}}{|\underline{x}|} K_1(\mu|\underline{x}|) [(1 - e^{i\underline{k} \cdot \underline{x}})(1 - e^{-i\underline{k} \cdot \underline{x}}) - 1]) \Big), \quad (3.20)$$

$$\tilde{H}_{q\bar{q}}^{\gamma^\mu \gamma^5}(y, \underline{x}) = 4 \frac{eg^2}{s(2\pi)\sqrt{2}} \frac{\delta^{ab}}{2N_c} \mu K_1(\mu|\underline{x}|) \left[\varepsilon^{\mu\nu\rho\sigma} e_{\gamma\nu} \frac{x_{\perp\rho}}{|\underline{x}|} p_{2\sigma} \right] [(1 - e^{i\underline{k} \cdot \underline{x}})(1 - e^{-i\underline{k} \cdot \underline{x}}) - 1]. \quad (3.21)$$

The previous results (3.20, 3.21) for the hard parts integrated over κ can be inserted in eq. (3.5) to obtain the impact factor $q\bar{q}$ contribution as the soft parts are independent of κ . Decomposing the result into the vector contribution $\Phi_{q\bar{q}}^{\gamma_T^* \rightarrow \rho_T, V}$ that will lead to term proportional to φ_3 , φ_1^T and, axial-vector contribution $\Phi_{q\bar{q}}^{\gamma_T^* \rightarrow \rho_T, A}$ that leads to term proportional to φ_A and φ_A^T , we get

$$\Phi_{q\bar{q}}^{\gamma_T^* \rightarrow \rho_T, V} = -\frac{C^{ab}Q^2}{2} \int dy \int \frac{d^2 \underline{x}}{2\pi} \left\{ -2y\bar{y} \varphi_3(y) K_0(\mu|\underline{x}|) \underline{e}_\gamma \cdot \underline{e}_\rho^* + (y - \bar{y}) \varphi_1^T(y) (\underline{e}_\rho^* \cdot \underline{x}) \frac{\underline{x} \cdot \underline{e}_\gamma}{|\underline{x}|} \mu K_1(\mu|\underline{x}|) [(1 - e^{i\underline{k} \cdot \underline{x}})(1 - e^{-i\underline{k} \cdot \underline{x}}) - 1] \right\} \quad (3.22)$$

and

$$\Phi_{q\bar{q}}^{\gamma_T^* \rightarrow \rho_T, A} = \frac{-C^{ab}Q^2}{s} \int dy \int \frac{d^2 x_\perp}{2\pi} \varphi_A^T(y) \frac{2}{s} \varepsilon_{x_\perp e_\rho^* p_1 p_2} \varepsilon_{x_\perp e_\gamma p_1 p_2} \times \mu K_1(\mu|\underline{x}|) ((1 - e^{i\underline{k} \cdot \underline{x}})(1 - e^{-i\underline{k} \cdot \underline{x}}) - 1), \quad (3.23)$$

where we define

$$C^{ab} = -\frac{eg^2}{\sqrt{2}}m_\rho f_\rho \frac{\delta^{ab}}{2N_c} \frac{1}{Q^2}. \quad (3.24)$$

Note that the term with φ_A in eq. (3.5) vanishes due to the structure of the expression (3.21). Using the fact that

$$\varepsilon_{x_\perp e_{\rho\perp}^* p_1 p_2} \varepsilon_{x_\perp e_{\gamma\perp} p_1 p_2} = \frac{s^2}{4} (x_\perp^2 (e_{\gamma\perp} \cdot e_{\rho\perp}^*) - (e_{\gamma\perp} \cdot x_\perp)(x_\perp \cdot e_{\rho\perp}^*)) ,$$

the axial-vector contribution takes the form

$$\begin{aligned} \Phi_{q\bar{q}}^{\gamma_T^* \rightarrow \rho_T, A} &= -\frac{C^{ab}Q^2}{2} \int dy \int \frac{d^2 \underline{x}}{2\pi} \varphi_A^T(y) \left[\underline{e}_\rho^* \cdot \underline{e}_\gamma - \frac{(\underline{e}_\rho^* \cdot \underline{x})(\underline{x} \cdot \underline{e}_\gamma)}{|\underline{x}|^2} \right] \\ &\times \mu|\underline{x}|K_1(\mu|\underline{x}|)((1 - e^{i\mathbf{k} \cdot \underline{x}})(1 - e^{-i\mathbf{k} \cdot \underline{x}}) - 1). \end{aligned} \quad (3.25)$$

The whole 2-parton contribution thus reads

$$\Phi_{q\bar{q}}^{\gamma_T^* \rightarrow \rho_T} = \Phi_{q\bar{q}}^{\gamma_T^* \rightarrow \rho_T, V} + \Phi_{q\bar{q}}^{\gamma_T^* \rightarrow \rho_T, A} \quad (3.26)$$

$$\begin{aligned} &= -\frac{C^{ab}Q^2}{2} \int dy \int \frac{d^2 \underline{x}}{2\pi} \left\{ -2y\bar{y}\varphi_3(y)K_0(\mu|\underline{x}|) \underline{e}_\gamma \cdot \underline{e}_\rho^* \right. \\ &+ \left[((y - \bar{y})\varphi_1^T(y) - \varphi_A^T(y)) \frac{(\underline{e}_\rho^* \cdot \underline{x})(\underline{x} \cdot \underline{e}_\gamma)}{|\underline{x}|^2} + \varphi_A^T(y) \underline{e}_\rho^* \cdot \underline{e}_\gamma \right] \\ &\times \mu|\underline{x}|K_1(\mu|\underline{x}|)((1 - e^{i\mathbf{k} \cdot \underline{x}})(1 - e^{-i\mathbf{k} \cdot \underline{x}}) - 1) \Big\}. \end{aligned} \quad (3.27)$$

This result does not seem to be proportional to the familiar dipole factor

$$\mathcal{N}(\underline{x}, \underline{k}) = (1 - e^{i\mathbf{k} \cdot \underline{x}})(1 - e^{-i\mathbf{k} \cdot \underline{x}}) \quad (3.28)$$

describing the coupling to the two t -channel gluons.

Using the following relations,

$$\int \frac{d^2 \underline{x}}{2\pi} \mu|\underline{x}|K_1(\mu|\underline{x}|) = 2 \int \frac{d^2 \underline{x}}{2\pi} K_0(\mu|\underline{x}|) = \frac{2}{\mu^2} \quad (3.29)$$

$$\int \frac{d^2 \underline{x}}{2\pi} \underline{e}_\rho^* \cdot \underline{x} \frac{\underline{x} \cdot \underline{e}_\gamma}{|\underline{x}|} \mu K_1(\mu|\underline{x}|) = \underline{e}_\gamma \cdot \underline{e}_\rho^* \int \frac{d^2 \underline{x}}{2\pi} K_0(\mu|\underline{x}|), \quad (3.30)$$

we can rewrite $\Phi_{q\bar{q}}^{\gamma_T^* \rightarrow \rho_T}$ in the form,

$$\begin{aligned} \Phi_{q\bar{q}}^{\gamma_T^* \rightarrow \rho_T} &= -\frac{C^{ab}Q^2}{2} \int dy \int \frac{d^2 \underline{x}}{2\pi} \\ &\times \left\{ [-(2y\bar{y}\varphi_3(y) + (y - \bar{y})\varphi_1^T + \varphi_A^T(y))] K_0(\mu|\underline{x}|) \underline{e}_\gamma \cdot \underline{e}_\rho^* \right. \\ &+ \left[((y - \bar{y})\varphi_1^T(y) - \varphi_A^T(y)) \frac{\underline{e}_\rho^* \cdot \underline{x} \underline{x} \cdot \underline{e}_\gamma}{|\underline{x}|^2} + \varphi_A^T(y) \underline{e}_\rho^* \cdot \underline{e}_\gamma \right] \\ &\times \mu|\underline{x}|K_1(\mu|\underline{x}|)\mathcal{N}(\underline{x}, \underline{k}) \Big\}. \end{aligned} \quad (3.31)$$

The term in the r.h.s.

$$[-(2y\bar{y}\varphi_3(y) + (y - \bar{y})\varphi_1^T + \varphi_A^T(y))] K_0(\mu|\underline{x}|) \underline{e}_\gamma \cdot \underline{e}_\rho^*,$$

vanishes in the WW approximation. This is due to the EOMs of QCD eqs. (2.129) and (2.130) relating the WW solutions of the DAs as shown in Sec. 2.4.1. Combining eqs. (2.129) and (2.130), one can get the relation,

$$2y \bar{y} \varphi_3^{WW}(y) + (y - \bar{y}) \varphi_1^{TWW} + \varphi_A^{TWW}(y) = 0. \quad (3.32)$$

This term also vanishes for the genuine twist 3 solutions of the DAs as we will show in Sec. 3.4.1 after computing the $q\bar{q}g$ contributions. At the end the $q\bar{q}$ contribution reads

$$\begin{aligned} \Phi_{q\bar{q}}^{\gamma_T^* \rightarrow \rho_T} &= -\frac{C^{ab}Q^2}{2} \int dy \int \frac{d^2 \underline{x}}{2\pi} \\ &\times \left\{ \left[(y - \bar{y}) \varphi_1^T(y) - \varphi_A^T(y) \right] \frac{\underline{e}_\rho^* \cdot \underline{x} \underline{x} \cdot \underline{e}_\gamma}{|\underline{x}|^2} + \varphi_A^T(y) \underline{e}_\rho^* \cdot \underline{e}_\gamma \right\} \\ &\times \mu |\underline{x}| K_1(\mu |\underline{x}|) \mathcal{N}(\underline{x}, \underline{k}), \end{aligned} \quad (3.33)$$

where the dipole scattering amplitude factorizes out.

3.2.3 Interpretation of the result obtained in the WW approximation

The WW approximation which consists in neglecting all contributions from the $q\bar{q}g$ Fock state, reads

$$\begin{aligned} \Phi_{q\bar{q}}^{\gamma_T^* \rightarrow \rho_T WW} &= -\frac{C^{ab}Q^2}{2} \int dy \int \frac{d^2 \underline{x}}{2\pi} \left\{ [(y - \bar{y}) \varphi_1^{TWW}(y) - \varphi_A^{TWW}(y)] \right. \\ &\times \left. \frac{(\underline{e}_\rho^* \cdot \underline{x})(\underline{x} \cdot \underline{e}_\gamma)}{|\underline{x}|^2} + \varphi_A^{TWW}(y) \underline{e}_\rho^* \cdot \underline{e}_\gamma \right\} \mu |\underline{x}| K_1(\mu |\underline{x}|) \mathcal{N}(\underline{x}, \underline{k}). \end{aligned} \quad (3.34)$$

Similarly to the momentum space analysis, one can split the result (3.34) into the spin non-flip $\Phi_{q\bar{q}, n.f.}^{\gamma_T^* \rightarrow \rho_T}$ and the spin flip $\Phi_{q\bar{q}, f.}^{\gamma_T^* \rightarrow \rho_T}$ contributions

$$\begin{aligned} \Phi_{q\bar{q}, n.f.}^{\gamma_T^* \rightarrow \rho_T WW} &= -\frac{C^{ab}Q^2}{2} \int dy (\varphi_A^{TWW} + (y - \bar{y}) \varphi_1^{TWW}) \\ &\times \int \frac{d^2 \underline{x}}{2\pi} \frac{1}{2} \underline{e}_\rho^* \cdot \underline{e}_\gamma \mu |\underline{x}| K_1(\mu |\underline{x}|) \mathcal{N}(\underline{x}, \underline{k}) \end{aligned} \quad (3.35)$$

and

$$\begin{aligned} \Phi_{q\bar{q}, f.}^{\gamma_T^* \rightarrow \rho_T WW} &= -\frac{C^{ab}Q^2}{2} \int dy (\varphi_A^{TWW} - (y - \bar{y}) \varphi_1^{TWW}) \\ &\times \int \frac{d^2 \underline{x}}{2\pi} \left(\frac{1}{2} \underline{e}_\rho^* \cdot \underline{e}_\gamma - \frac{(\underline{e}_\rho^* \cdot \underline{x})(\underline{e}_\gamma \cdot \underline{x})}{|\underline{x}|^2} \right) \mu |\underline{x}| K_1(\mu |\underline{x}|) \mathcal{N}(\underline{x}, \underline{k}). \end{aligned} \quad (3.36)$$

Both spin flip and spin non-flip impact factors can be put in an elegant form similar to the overlaps of virtual photon wave functions in the case of DIS,

$$\begin{aligned} \Phi_{2\text{-parton}}^{\gamma_T^* \rightarrow \rho_T}(\underline{k}, Q, \mu_F^2) &= \\ &\frac{\delta^{ab}}{2} \int dy \int d\underline{r} \psi_{(q\bar{q})}^{\gamma_T^*(\lambda_\gamma) \rightarrow \rho_T(\lambda_\rho) WW}(y, \underline{r}; Q, \mu_F^2) \mathcal{A}(\underline{r}, \underline{k}), \end{aligned} \quad (3.37)$$

with,

$$\mathcal{A}(\underline{r}, \underline{k}) = \frac{4\pi\alpha_s}{N_c} \mathcal{N}(\underline{x}, \underline{k}), \quad (3.38)$$

the dipole scattering amplitude according to our definition of the impact factors and

$$\psi_{(q\bar{q})}^{\gamma_T^* \rightarrow \rho_T}(y, \underline{r}; Q, \mu_F^2) = \frac{m_\rho f_\rho}{\sqrt{2}} \sum_{(h, \bar{h})} \phi_{(h, \bar{h})}^{\rho_T, (\lambda_\rho)}(y; \mu_F^2) \Psi_{(h, \bar{h})}^{\gamma_T^* (\lambda_\gamma)}(y, \underline{r}; Q^2), \quad (3.39)$$

the overlap of the wave function of the virtual photon $\Psi_{(h, \bar{h})}^{\gamma_T^* (\lambda_\gamma)}(y, \underline{r}; Q^2)$ with the moments of the wave function of the ρ -meson $\phi_{(h, \bar{h})}^{\rho_T, (\lambda_\rho), WW}(y; \mu_F^2)$. We remind that the indices h and \bar{h} denote the quark antiquark helicities, spin $\pm 1/2$ corresponds to $h = \pm$. Note that we put apart the factor $\frac{\delta^{ab}}{2} = \text{Tr}(t^a t^b)$ that will contribute to a global color factor in the helicity amplitude of $\frac{N_c^2 - 1}{4}$. The coefficient $\frac{m_\rho f_\rho}{\sqrt{2}}$, explicitly factorized out, is related to the partonic content of the ρ^0 -meson as a $\frac{u\bar{u} - d\bar{d}}{\sqrt{2}}$ state such that the meson involved below is understood as a one flavor quark-antiquark state. For clarity, we recall the expressions of the virtual photon wave functions following the conventions of Ref. [65] used for the GBW saturation model,

$$\Psi_{(h, \bar{h})}^{\gamma_L^*}(y, \underline{r}; Q^2) = \delta_{\bar{h}, -h} \frac{e}{2\pi} \sqrt{\frac{N_c}{\pi}} \frac{\mu^2}{Q} K_0(\mu |\underline{r}|), \quad (3.40)$$

$$\Psi_{(h, \bar{h})}^{\gamma_T^* (\lambda_\gamma)}(y, \underline{r}; Q^2) = \delta_{\bar{h}, -h} \frac{ie}{2\pi} \sqrt{\frac{N_c}{\pi}} (y \delta_{h, \lambda_\gamma} + \bar{y} \delta_{h, -\lambda_\gamma}) \frac{(\underline{r} \cdot \underline{e}^{(\lambda_\gamma)})}{|\underline{r}|} \mu K_1(\mu |\underline{r}|). \quad (3.41)$$

We can extract from our result the relevant twist 3 moments of the ρ -meson wave function,

$$\begin{aligned} \phi_{(h, \bar{h})}^{\rho_T, (\lambda_\rho), WW}(y, \underline{r}; \mu_F^2) &= -\delta_{\bar{h}, -h} i \sqrt{\frac{\pi}{4N_c}} (\underline{e}^{(\lambda_\rho)*} \cdot \underline{r}) \\ &\times (\varphi_A^{TWW}(y; \mu_F^2) + (\delta_{h, \lambda_\rho} - \delta_{h, -\lambda_\rho}) \varphi_1^{TWW}(y; \mu_F^2)). \end{aligned} \quad (3.42)$$

Note that these combinations of " $\varphi_1^T \pm \varphi_A^T$ " are directly linked to the auxiliary DAs $g_\perp^{\uparrow\downarrow}$ and $g_\perp^{\uparrow\uparrow}$ of [142],

$$\begin{aligned} & -(\varphi_A^{TWW}(y) + (\delta_{h, \lambda_\rho} - \delta_{h, -\lambda_\rho}) \varphi_1^{TWW}(y)) \\ &= \bar{y} (\varphi_3^{WW}(y) + \varphi_A^{WW}(y)) \delta_{h, \lambda_\rho} + y (\varphi_3^{WW}(y) - \varphi_A^{WW}(y)) \delta_{h, -\lambda_\rho} \\ &= \bar{y} g_\perp^{\uparrow\uparrow}(y) \delta_{h, \lambda_\rho} + y g_\perp^{\uparrow\downarrow}(y) \delta_{h, -\lambda_\rho} \\ &= 2y\bar{y} \sum_n [g_n^{\uparrow\downarrow} P_n^{(1,0)}(\xi) \delta_{h, -\lambda_\rho} + g_n^{\uparrow\uparrow} P_n^{(0,1)}(\xi) \delta_{h, \lambda_\rho}], \end{aligned} \quad (3.43)$$

with $\xi = y - \bar{y}$. As we have decomposed the combination of DAs in the sum of the contributions for each quark and antiquark pair of specific helicity states, it is natural that we found a parameterization proportional to the auxiliary DAs $g_\perp^{\uparrow\downarrow}$ and $g_\perp^{\uparrow\uparrow}$ which are the twist 3 DAs of fixed spin projection on the light-cone.

We want to emphasize the fact that the results for $\phi_{(h, \bar{h})}^{\rho_T, (\lambda_\rho), WW}$ are the same for the spin non-flip ($\lambda_\gamma = \lambda_\rho$) and spin flip ($\lambda_\gamma = -\lambda_\rho$) impact factors. This fact is not obvious at all from the results of Sec. 2.7.4 in the chap. 2 for the spin non-flip and spin flip results in

momentum space (see for example below the expressions (3.45, 3.46)). We see again that the results come more naturally in the impact parameter representation. The obtained factorized structures (3.37) are illustrated in fig. 3.2.

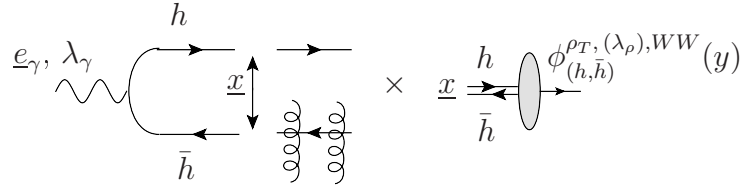


Figure 3.2: The 2-parton contribution to the $\gamma^* \rightarrow \rho_T$ impact factor in the dipole factorized form.

3.2.4 Equivalence of momentum and impact parameter calculations

We want now to derive the results in the momentum space representation of Ref. [131] presented in Sec. 2.7.4 in chap. 2, by integrating over the dipole size \underline{x} . For this aim, we shall use the following formula,

$$\int \frac{d^2 \underline{x}}{2\pi} \mu \frac{\underline{x}_i \underline{x}_j}{|\underline{x}|} K_1(\mu |\underline{x}|) e^{i \underline{\ell} \cdot \underline{x}} = \frac{1}{\underline{\ell}^2 + \mu^2} \left(\delta_{ij} - 2 \frac{\underline{\ell}_i \underline{\ell}_j}{\underline{\ell}^2 + \mu^2} \right), \quad (3.44)$$

which leads us to the same results as in eqs (2.276, 2.277), sec. 2.7.4 in the chap. 2,

$$\begin{aligned} \Phi_{q\bar{q}, n.f.}^{\gamma_T^* \rightarrow \rho_T WW} &= -\frac{C^{ab} Q^2}{2} \int dy (\varphi_A^{T WW} + (y - \bar{y}) \varphi_1^{T WW}) \\ &\quad \times T_{n.f.} \frac{2 \underline{k}^2 (\underline{k}^2 + 2\mu^2)}{\mu^2 (\underline{k}^2 + \mu^2)^2}, \end{aligned} \quad (3.45)$$

$$\begin{aligned} \Phi_{q\bar{q}, f.}^{\gamma_T^* \rightarrow \rho_T WW} &= -\frac{C^{ab} Q^2}{2} \int dy (\varphi_A^{T WW} - (y - \bar{y}) \varphi_1^{T WW}) \\ &\quad \times T_f \frac{-4 \underline{k}^2}{(\underline{k}^2 + \mu^2)^2}. \end{aligned} \quad (3.46)$$

This fact can be seen as a self-consistency check of our calculation.

3.2.5 The impact parameter representation of the $\gamma_L^* \rightarrow \rho_L$ impact factor

Using the eq. (3.5), in the case of longitudinally polarized ρ -meson and virtual photon, leads to

$$\begin{aligned} i\mathcal{A}_{q\bar{q}} &= -\frac{1}{4} \int dy \int d^2 x_\perp \tilde{H}_{q\bar{q}}^{\gamma_\alpha}(y, x_\perp) \int \frac{d\lambda}{2\pi} e^{-i\lambda y} \langle \rho(p) | \bar{\psi}(\lambda n) \gamma_\alpha \psi(0) | 0 \rangle_{\mu_F^2} \\ &= -\frac{m_\rho f_\rho}{4} \int dy \varphi_1(y; \mu_F^2) (e^* \cdot n) \int d^2 x_\perp \tilde{H}_{q\bar{q}}^{\rho_1}(y, x_\perp). \end{aligned} \quad (3.47)$$

The hard part reads

$$p_{1\mu} H_{q\bar{q}}^{\gamma\mu}(y, \underline{\ell}) = -\frac{4Qeg^2\delta^{ab}}{\sqrt{2}2N_c} y \bar{y} \left(\frac{2}{\underline{\ell}^2 + \mu^2} - \frac{1}{(\underline{\ell} + \underline{k})^2 + \mu^2} - \frac{1}{(\underline{\ell} - \underline{k})^2 + \mu^2} \right). \quad (3.48)$$

Its Fourier transform reads

$$\begin{aligned} \tilde{H}_{q\bar{q}}^{\phi_1}(y, \underline{x}) &= -\frac{4Qe}{(2\pi)\sqrt{2}2N_c} y \bar{y} K_0(\mu|\underline{x}|) g^2 \delta^{ab} \mathcal{N}(\underline{x}, \underline{k}) \\ &= -\frac{\delta^{ab}}{2} \mathcal{A}(\underline{x}, \underline{k}) \sqrt{\frac{2\pi}{N_c}} \sum_{h, \bar{h}} \Psi_{h, \bar{h}}^{\gamma_L^*}(y, \underline{x}). \end{aligned} \quad (3.49)$$

The impact factor reads then

$$\Phi^{\gamma_L^* \rightarrow \rho_L}(\underline{k}, Q, \mu_F^2) = \left(\frac{\delta^{ab}}{2} \right) \int dy \int d\underline{r} \psi_{(q\bar{q})}^{\gamma_L^* \rightarrow \rho_L}(y, \underline{r}; Q, \mu_F^2) \mathcal{A}(\underline{r}, \underline{k}), \quad (3.50)$$

where $\psi_{(q\bar{q})}^{\gamma_L^* \rightarrow \rho_L}$ is the overlap,

$$\psi_{(q\bar{q})}^{\gamma_L^* \rightarrow \rho_L}(y, \underline{r}; Q, \mu_F^2) = \frac{m_\rho f_\rho}{\sqrt{2}} \sum_{(h, \bar{h})} \phi_{(h\bar{h})}^{\rho_L}(y; \mu_F^2) \Psi_{(h, \bar{h})}^{\gamma_L^*}(y, \underline{r}; Q^2). \quad (3.51)$$

The extracted relevant moment of ρ -meson longitudinal wave function reads

$$\phi_{(h, \bar{h})}^{\rho_L}(y; \mu_F^2) = \delta_{\bar{h}, -h} \sqrt{\frac{\pi}{4N_c}} (e_L^* \cdot n) \varphi_1(y; \mu_F^2). \quad (3.52)$$

Comparing eqs. (3.52) and (3.42), we can see that the only difference between all these results are the choice of the DAs. This in fact is due to the simple form of eq. (3.5) in the impact parameter space, where the hard parts factorize and are contracted with different Lorentz structures.

Performing the integral over \underline{x} we recover, as expected, the same result as in momentum space

$$\begin{aligned} \Phi^{\gamma_L^* \rightarrow \rho_L} &= \frac{eg^2\delta^{ab}f_\rho Q}{\sqrt{2}2N_c} \int dy y \bar{y} \varphi_1(y) \int \frac{d^2 \underline{x}}{2\pi} K_0(\mu|\underline{x}|) (1 - e^{i\mathbf{k} \cdot \underline{x}}) (1 - e^{-i\mathbf{k} \cdot \underline{x}}) \\ &= \frac{2eg^2\delta^{ab}f_\rho}{\sqrt{2}2N_c Q} \int dy \varphi_1(y) \frac{\underline{k}^2}{\underline{k}^2 + \mu^2}. \end{aligned}$$

3.3 The $q\bar{q}g$ intermediate state contribution to the $\gamma_T^* \rightarrow \rho_T$ impact factor

The $q\bar{q}g$ intermediate state, where the gluon carries a sizable amount of energy of the virtual photon ($y_g \sim y_1 \sim \bar{y}_2$), participates to the full twist 3 result of the impact factor. Its contribution involves several color dipole configurations that can interact with the t -channel gluons.

In sec. 3.3.1, we first present the factorization procedure to get a factorized form involving the transverse Fourier transforms of the three-parton hard parts and the twist 3 moments of the meson wave function. Then, in sec. 3.3.2 we prove by analyzing the color structure of the diagrams that there are only dipole interactions and no other multipole interactions. After that, we classify in sec. 3.3.2 the hard sub-process Feynman diagrams in order to identify the relevant dipole configuration that interacts with the t -channel gluons, we explain in sec. 3.3.3 how the collinear approximation simplifies the computations of the Fourier transforms of the hard parts. Finally, in sec. 3.3.4 the result is split into a spin flip and a spin non-flip contribution as for the two-parton contribution.

3.3.1 LCCF in impact parameter representation for the $q\bar{q}g$ amplitude

The steps here are essentially the same as for the $q\bar{q}$ contribution. Using the Fierz decomposition one gets

$$\begin{aligned} i\mathcal{A}_{q\bar{q}g} &= \int \frac{d^4\ell_1}{(2\pi)^4} \frac{d^4\ell_g}{(2\pi)^4} \text{tr}[H_{q\bar{q}g}^\alpha(\ell_1, \ell_g) S_{q\bar{q}g\alpha}(\ell_1, \ell_g)] \\ &= -\frac{1}{4} \int \frac{d^4\ell_1}{(2\pi)^4} \frac{d^4\ell_g}{(2\pi)^4} \text{tr}[H_{q\bar{q}g}^\alpha(\ell_1, \ell_g) \Gamma^\beta] S_{q\bar{q}g\alpha}^{\Gamma^\beta}(\ell_1, \ell_g). \end{aligned} \quad (3.53)$$

We use the Sudakov decomposition of the momenta of the partons i , $\ell_i = \alpha_i p + \beta_i n + \ell_{i\perp}$ and of the Fourier conjugate coordinates $z_i = \alpha_{z_i} p + \beta_{z_i} n + z_{i\perp}$ in the argument of the non-local correlator defining the soft part $S_{q\bar{q}g}$. We factorize the amplitude in the momentum space, and we reduce it to a convolution in the longitudinal fractions y_i of the ρ meson momentum p carried by the partons. It reads

$$\begin{aligned} i\mathcal{A}_{q\bar{q}g} &= -\frac{1}{4} \int dy_1 dy_g \int \frac{d^2\ell_{1\perp}}{(2\pi)^2} \frac{d^2\ell_{g\perp}}{(2\pi)^2} H_{q\bar{q}g}^{\alpha, \Gamma^\beta}(y_1, y_g, \ell_{1\perp}, \ell_{g\perp}) \\ &\times \int \frac{d\lambda_1}{2\pi} e^{-i\lambda_1 y_1} \int \frac{d\lambda_g}{2\pi} e^{-i\lambda_g y_g} \int d^2 z_{1\perp} e^{-i\ell_{1\perp} \cdot z_{1\perp}} \int d^2 z_{g\perp} e^{-i\ell_{g\perp} \cdot z_{g\perp}} \\ &\times \langle \rho(p) | \bar{\psi}(\lambda_1 n + z_{1\perp}) i\Gamma_\beta g A_\alpha^\perp(\lambda_g n + z_{g\perp}) \psi(0) | 0 \rangle, \end{aligned} \quad (3.54)$$

with $H_{q\bar{q}g}^{\alpha, \Gamma^\mu}(y_i, y_j, \ell_{i\perp}, \ell_{j\perp})$.

Let us introduce its Fourier transform $\tilde{H}_{q\bar{q}g}^{\Gamma^\beta}(y_i, y_j, x_{i\perp}, x_{j\perp})$ defined as

$$\begin{aligned} &H_{q\bar{q}g}^{\alpha, \Gamma^\beta}(y_i, y_j, \ell_{i\perp}, \ell_{j\perp}) \\ &= \int d^2 x_{i\perp} d^2 x_{j\perp} \tilde{H}_{q\bar{q}g}^{\alpha, \Gamma^\beta}(y_i, y_j, x_{i\perp}, x_{j\perp}) e^{-i(\ell_{i\perp} \cdot x_{i\perp} + \ell_{j\perp} \cdot x_{j\perp})}. \end{aligned} \quad (3.55)$$

At twist 3, the Taylor expansion of the $q\bar{q}g$ hard part around the dominant light-cone direction gives the contribution

$$H_{q\bar{q}g}^{\alpha, \Gamma^\beta}(y_i, y_j, 0_\perp, 0_\perp) = \int d^2 x_{1\perp} d^2 x_{g\perp} \tilde{H}_{q\bar{q}g}^{\alpha, \Gamma^\beta}(y_1, y_g, x_{1\perp}, x_{g\perp}) \quad (3.56)$$

and the amplitude simplifies as,

$$i\mathcal{A}_{q\bar{q}g} = -\frac{1}{4} \int dy_1 dy_g \int d^2 x_{1\perp} d^2 x_{g\perp} \tilde{H}_{q\bar{q}g}^{\alpha, \Gamma^\beta}(y_1, y_g, x_{1\perp}, x_{g\perp}) \\ \times \int \frac{d\lambda_1}{2\pi} e^{-i\lambda_1 y_1} \int \frac{d\lambda_g}{2\pi} e^{-i\lambda_g y_g} \langle \rho(p) | \bar{\psi}(\lambda_1 n) i\Gamma_\beta g A_\alpha^\perp(\lambda_g n) \psi(0) | 0 \rangle_{\mu_F^2}. \quad (3.57)$$

We recall the parameterization of the $q\bar{q}g$ correlators appearing in eq. (3.57),

$$\int \frac{d\lambda_1}{2\pi} \frac{d\lambda_g}{2\pi} e^{-i\lambda_1 y_1 - i\lambda_g y_g} \langle \rho(p) | \bar{\psi}(\lambda_1 n) i\gamma_\mu g A_\alpha^\perp(\lambda_g n) \psi(0) | 0 \rangle_{\mu_F^2} \\ = -im_\rho f_\rho \zeta_{3\rho}^V(\mu_F^2) B(y_1, y_2; \mu_F^2) p_\mu e_{\rho\perp\alpha}, \quad (3.58)$$

$$\int \frac{d\lambda_1}{2\pi} \frac{d\lambda_g}{2\pi} e^{-i\lambda_1 y_1 - i\lambda_g y_g} \langle \rho(p) | \bar{\psi}(\lambda_1 n) i\gamma_5 \gamma_\mu g A_\alpha^\perp(\lambda_g n) \psi(0) | 0 \rangle_{\mu_F^2} \\ = -im_\rho f_\rho \zeta_{3\rho}^A(\mu_F^2) i D(y_1, y_2; \mu_F^2) p_\mu \varepsilon_{\alpha e_{\rho\perp} p n}, \quad (3.59)$$

leading to

$$i\mathcal{A}_{q\bar{q}g} = \frac{im_\rho f_\rho}{4} \int dy_1 dy_g \int d^2 x_{1\perp} d^2 x_{g\perp} \\ \times \left[\tilde{H}_{q\bar{q}g}^{e_{\rho\perp}, \not{p}}(y_1, y_g, x_{1\perp}, x_{g\perp}) \zeta_{3\rho}^V B(y_1, y_1 + y_g) \right. \\ \left. + \tilde{H}_{q\bar{q}g}^{R_\perp, \not{p}\gamma_5}(y_1, y_g, x_{1\perp}, x_{g\perp}) i \zeta_{3\rho}^A D(y_1, y_1 + y_g) \right], \quad (3.60)$$

where we use our usual shorthand notation

$$\tilde{H}_{q\bar{q}g}^{a, \Gamma^\mu b_\mu} \equiv \tilde{H}_{q\bar{q}g}^{\alpha, \Gamma^\mu} a_\alpha b_\mu. \quad (3.61)$$

The 3-parton contribution (3.60) in terms of $S(y_1, y_2)$, $M(y_1, y_2)$ reads

$$i\mathcal{A}_{q\bar{q}g} = \frac{im_\rho f_\rho}{4} \int dy_1 dy_g \int d^2 x_{1\perp} d^2 x_{g\perp} \\ \times \left[\frac{S(y_1, y_1 + y_g)}{2} (\tilde{H}_{q\bar{q}g}^{e_{\rho\perp}, \not{p}}(y_1, y_g, x_{1\perp}, x_{g\perp}) + i \tilde{H}_{q\bar{q}g}^{R_\perp, \not{p}\gamma_5}(y_1, y_g, x_{1\perp}, x_{g\perp})) \right. \\ \left. + \frac{M(y_1, y_1 + y_g)}{2} (\tilde{H}_{q\bar{q}g}^{e_{\rho\perp}, \not{p}}(y_1, y_g, x_{1\perp}, x_{g\perp}) - i \tilde{H}_{q\bar{q}g}^{R_\perp, \not{p}\gamma_5}(y_1, y_g, x_{1\perp}, x_{g\perp})) \right]. \quad (3.62)$$

The next section is mainly devoted to the computations of the Fourier transforms

$$\tilde{H}_{q\bar{q}g}^{e_{\rho\perp}, \not{p}}(y_1, y_g, x_{1\perp}, x_{g\perp}) \pm i \tilde{H}_{q\bar{q}g}^{R_\perp, \not{p}\gamma_5}(y_1, y_g, x_{1\perp}, x_{g\perp}).$$

3.3.2 The color dipole configurations of the hard part

Diagrams and kinematics

The kinematics of the $q\bar{q}g$ intermediate state, illustrated in the fig. 3.3, reads

$$\ell_1 = y_1 p_1 + \ell_{1\perp} + \frac{\ell_1^2}{y_1 s} p_2, \quad (3.63)$$

$$\ell_2 = \bar{y}_2 p_1 + \ell_{2\perp} + \frac{\ell_2^2}{\bar{y}_2 s} p_2, \quad (3.64)$$

$$\ell_g = y_g p_1 + \ell_{g\perp} + \frac{\ell_g^2}{y_g s} p_2, \quad (3.65)$$

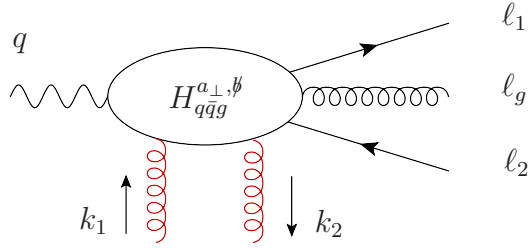


Figure 3.3: The kinematics for 3-parton contributions.

with $y_1 + \bar{y}_2 + y_g = 1$ and $\ell_{1\perp} + \ell_{2\perp} + \ell_{g\perp} = 0$. Each parton is on-shell and this kinematics simplifies to the kinematics of the Sec. 2.7.4 in the collinear limit $\underline{\ell}_i \rightarrow 0$.

The momentum of the ρ meson which is the sum of the momentum of the partons reads

$$p_\rho = p_1 + \frac{1}{s} \left(\frac{\ell_1^2}{y_1} + \frac{\ell_2^2}{\bar{y}_2} + \frac{\ell_g^2}{y_g} \right) p_2 = p_1 + \frac{p_\rho^2}{s} p_2, \quad (3.66)$$

and the invariant mass squared of the partonic system is

$$p_\rho^2 = \frac{\ell_1^2}{y_1} + \frac{\ell_2^2}{\bar{y}_2} + \frac{\ell_g^2}{y_g}. \quad (3.67)$$

Note that the collinear limit, $\underline{\ell}_1 = \underline{\ell}_2 = \underline{\ell}_g = 0$, implies that we neglect higher twist effects from the ρ -meson mass. The momenta of the t -channel gluons and virtual photon are still defined by eqs. (3.7) and (3.8).

The "extended" amplitude defined as function of $\ell_{1\perp}$ and $\ell_{g\perp}$

$$\begin{aligned} i\mathcal{A}_{q\bar{q}g, ext.}(\ell_{1\perp}, \ell_{g\perp}) &= \frac{im_\rho f_\rho}{4} \int dy_1 dy_g \\ &\times \left[\frac{S(y_1, y_1 + y_g)}{2} (H_{q\bar{q}g}^{e_{\rho\perp}^*, \not{p}}(y_1, y_g, \ell_{1\perp}, \ell_{g\perp}) + i H_{q\bar{q}g}^{R_{\perp}^*, \not{p}\gamma_5}(y_1, y_g, \ell_{1\perp}, \ell_{g\perp})) \right. \\ &\left. + \frac{M(y_1, y_1 + y_g)}{2} (H_{q\bar{q}g}^{e_{\rho\perp}^*, \not{p}}(y_1, y_g, \ell_{1\perp}, \ell_{g\perp}) - i H_{q\bar{q}g}^{R_{\perp}^*, \not{p}\gamma_5}(y_1, y_g, \ell_{1\perp}, \ell_{g\perp})) \right], \quad (3.68) \end{aligned}$$

gives back the twist 3 contribution of the amplitude $i\mathcal{A}_{q\bar{q}g}$ in the limit $\{\ell_{1\perp}, \ell_{g\perp}\} \rightarrow 0$. Note that this extended amplitude $i\mathcal{A}_{q\bar{q}g, ext.}$ mixes twist 3 terms (which are the only one remaining in the collinear limit $\ell_{1\perp} = \ell_{g\perp} = 0$), with higher twist terms induced by the non-vanishing transverse momenta $\ell_{1\perp}$ and $\ell_{g\perp}$. The computation of $i\mathcal{A}_{q\bar{q}g, ext.}$ relevant when taking the collinear limit involves all the three-parton diagrams displayed in figs. 2.8, 2.9 and 2.10 in Sec. 2.2.1 of the chap. 2. These diagrams were divided into the following types,

- the 12 "abelian" diagrams (e.g. aG1 shown in fig. 3.4),
- the 12 "non-abelian with a single triple gluon vertex" (e.g. atG1, fig. 3.5),
- the 4 "non-abelian with two triple gluon vertex" (e.g. gttG1, fig. 3.6).

Similarly to the computation in the $q\bar{q}$ intermediate state contribution, we perform the integral over κ of $i\mathcal{A}_{q\bar{q}g}$, using the residue method applied to the contour \mathcal{C}_- to get the impact

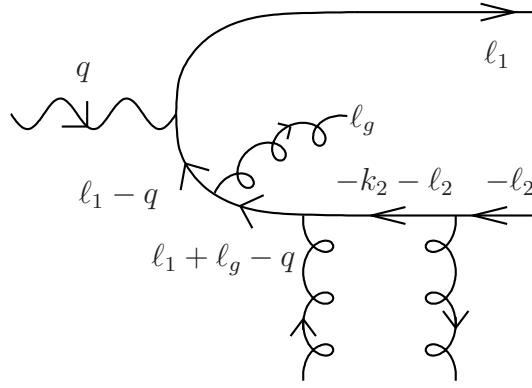


Figure 3.4: The detailed structure of the diagram (aG1).

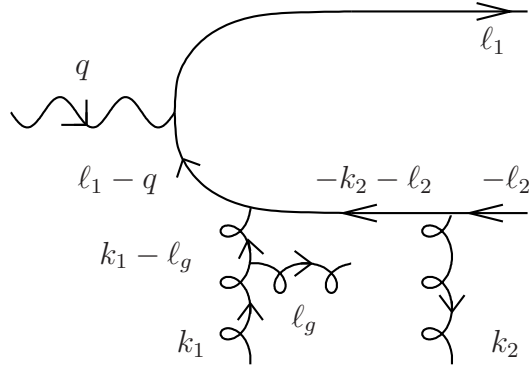


Figure 3.5: The detailed structure of the "non-Abelian" (with one triple gluon vertex) diagram (atG1).

factor contribution of the "extended" impact factor $\Phi_{q\bar{q}g, ext.}^{\gamma_T^* \rightarrow \rho_T}$, which contains the relevant dependence on the transverse momenta.

We show below the explicit results of the aG1 vector and axial contributions to the

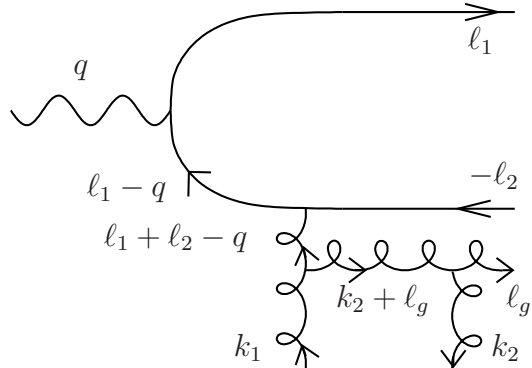


Figure 3.6: The detailed structure of the diagram (gttG1).

extended impact factor $\Phi_{q\bar{q}g, ext.}^{\gamma_T^* \rightarrow \rho_T}$ after integration over κ . The aG1 vector contribution reads

$$\begin{aligned} \Phi_{aG1, ext.}^V &= \frac{e_q g^2}{2} f_\rho m_\rho \frac{\delta^{ab}}{2N_c} \int_0^1 dy_1 dy_2 B(y_1, y_2) \\ &\times \left\{ \underline{e}_\rho^* \cdot \underline{e}_\gamma (\bar{y}_2 \underline{\ell}_1^2 - y_1 \underline{\ell}_2 \cdot \underline{\ell}_1 + y_1 \bar{y}_2 Q^2) + y_1 ((\underline{\ell}_1 \cdot \underline{e}_\gamma)(\underline{\ell}_2 \cdot \underline{e}_\rho^*) + (\underline{\ell}_1 \cdot \underline{e}_\rho^*)(\underline{\ell}_2 \cdot \underline{e}_\gamma)) \right\} \\ &\times \frac{y_1 y_g}{(\underline{\ell}_1^2 + \mu_1^2)(y_g \bar{y}_g \underline{\ell}_1^2 + 2y_1 y_g \underline{\ell}_1 \cdot \underline{\ell}_g + y_1 \bar{y}_1 \underline{\ell}_g^2 + y_1 \bar{y}_2 y_g Q^2)}, \end{aligned} \quad (3.69)$$

and the aG1 axial contribution reads

$$\begin{aligned} \Phi_{aG1, ext.}^A &= \frac{e_q g^2}{2} f_\rho m_\rho \frac{\delta^{ab}}{2N_c} \int_0^1 dy_1 dy_2 D(y_1, y_2) \\ &\times \left\{ \underline{e}_\rho^* \cdot \underline{e}_\gamma (\bar{y}_2 \underline{\ell}_1^2 + y_1 \underline{\ell}_2 \cdot \underline{\ell}_1 + y_1 \bar{y}_2 Q^2) - y_1 [(\underline{\ell}_1 \cdot \underline{e}_\gamma)(\underline{\ell}_2 \cdot \underline{e}_\rho^*) + (\underline{\ell}_1 \cdot \underline{e}_\rho^*)(\underline{\ell}_2 \cdot \underline{e}_\gamma)] \right\} \\ &\times \frac{y_1 y_g}{(\underline{\ell}_1^2 + \mu_1^2)(y_g \bar{y}_g \underline{\ell}_1^2 + 2y_1 y_g \underline{\ell}_1 \cdot \underline{\ell}_g + y_1 \bar{y}_1 \underline{\ell}_g^2 + y_1 \bar{y}_2 y_g Q^2)}. \end{aligned} \quad (3.70)$$

Classification of the diagrams in color dipole configurations

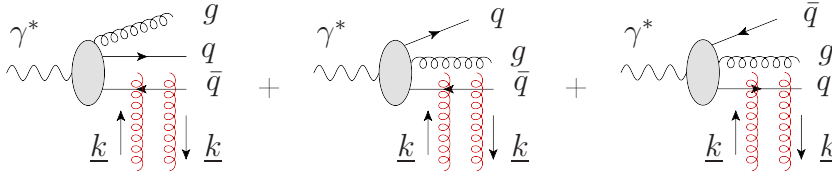


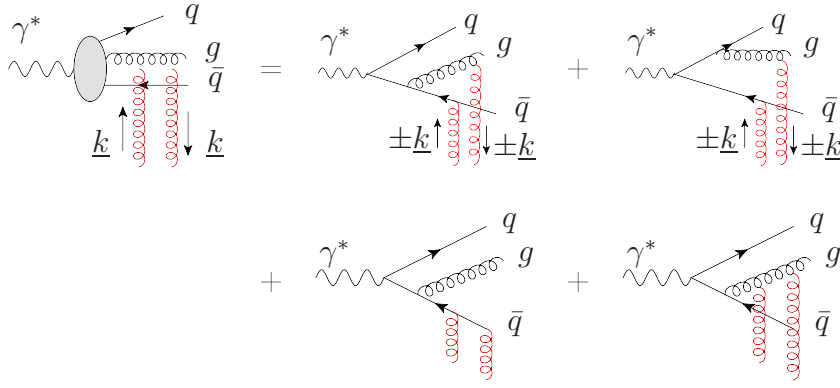
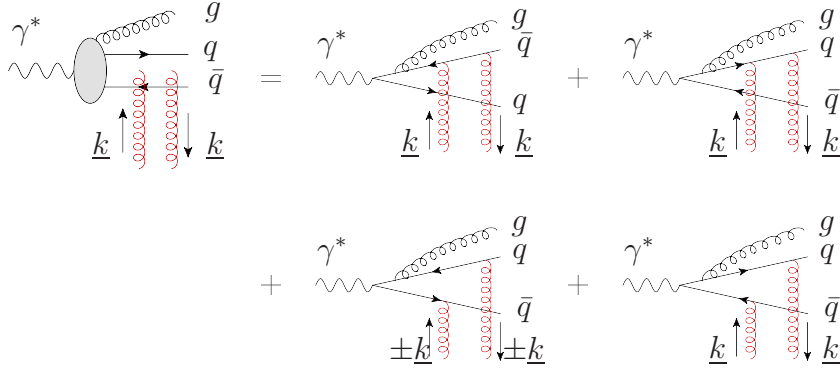
Figure 3.7: The $\{q\bar{q}\}$, $\{\bar{q}g\}$ and $\{qg\}$ dipoles interacting with the t -channel gluons.

We want to extract the relevant color dipoles made of a color-anticolor singlet pair in the fundamental representation, constructed either from a $q\bar{q}$ pair, denoted by $\{q\bar{q}\}$, or from a quark and the "antiquark part" of the gluon (denoted by $\{qg\}$), or from an antiquark and the "quark part" of the gluon (denoted by $\{\bar{q}g\}$), as the gluon belongs to the adjoint representation of $SU(N_c)$.

The diagrams are collected depending on the pair of partons that interacts with the t -channel gluons, see fig. 3.7. Due to the topology of the associated diagrams, the dipole $\{q\bar{q}\}$ is suppressed by $1/N_c^2$, the corresponding diagram being non-planar. The 6 diagrams corresponding to the interaction of the $\{\bar{q}g\}$ system with the t -channel gluons are the contributions in $\frac{\delta^{ab}}{2N_c} \frac{N_c}{C_F}$ of aG1, httG1, atG1, etG1, dtG1, btG2, shown in fig. 3.8. The results of the diagrams associated to the $\{qg\}$ system, cG1, gttG1, ctG1, ftG1, btG1, dtG2 are obtained from the diagrams of the $\{\bar{q}g\}$ system by exchanging the role of the quark and the anti-quark. The diagrams associated to the $\{q\bar{q}\}$ system are the contributions in $\frac{\delta^{ab}}{2N_c} \left(\frac{N_c}{C_F} - 2 \right)$ of aG1, bG2, dG1 and the symmetric diagrams under exchange of the quark and the anti-quark, cG1, dG2, bG1, shown in fig. 3.9.

Dipole interactions

We will show that the color structure of the diagrams associated to the factorized hard part of the $q\bar{q}g$ intermediate state can be simplified into the color structure of a single dipole that

Figure 3.8: The $\{\bar{q}g\}$ dipole content.Figure 3.9: The $\{q\bar{q}\}$ dipole content.

interacts with two t -channel gluons. We need for this to consider the abelian diagrams and the non-abelian diagrams. For the abelian type of diagram, one gets

$$\text{Diagram 1} = -\frac{1}{2} \frac{1}{N_c} \text{Diagram 2} \quad (3.71)$$

while the non-abelian structure reduces to

$$\text{Diagram 3} = N_c \text{Diagram 4} \quad (3.72)$$

This second identity can be easily derived based on the relation

$$\text{Tr}([t^a, t^b] t^c) = \frac{i}{2} f_{abc}, \quad (3.73)$$

which can be represented graphically as

$$\frac{i}{2} f_{abc} = \text{Diagram 5} - \text{Diagram 6}, \quad (3.74)$$

thus allowing to pass from the adjoint representation to the fundamental one. We thus conclude from eqs. (3.71, 3.72) that in color space we only expect color dipole contributions even at finite N_c .

3.3.3 Fourier transforms of the 3-parton diagrams in the collinear limit

In the following parts, we respectively denote \underline{x}_i and $\underline{\ell}_i$ the transverse position and momentum of the parton i . Using the analogy that exists [53] between a Lorentz sub-group in the infinite momentum frame that leaves invariant the hypersurface orthogonal to the dominant light-cone direction with the Galilean transformations in two-dimensional mechanics, the idea to simplify the computation is to make a change of variables dictated by the two-body problem in classical mechanics. The $q\bar{q}g$ system defined by $\{y_1, \underline{\ell}_1\}$, $\{\bar{y}_2, \underline{\ell}_2\}$ and $\{y_g, \underline{\ell}_g\}$ can be simplified by considering the center of mass

$$G_{ij} \equiv \{y_i + y_j, \underline{L}_{ij} = \underline{\ell}_i + \underline{\ell}_j\},$$

and the reduced particle

$$R_{ij} \equiv \{m_{ij} = \frac{y_i y_j Q}{y_i + y_j}, \underline{\ell}_{ij} = \frac{y_i \underline{\ell}_j - y_j \underline{\ell}_i}{(y_i + y_j)}\},$$

variables, where i and j are the partons forming the system that interacts with the t -channel gluons. This simplifies the expressions of the extended impact factor results. It turns out that in the collinear limit the relevant momentum is associated to the reduced particle of the two-parton system that interacts with the t -channel gluons. As an example, the Fourier transform of the hard part associated to the 2-parton system $\{\bar{q}g\}$, reads

$$\begin{aligned} \tilde{H}^{\{\bar{q}g\}}(\underline{x}_1, \underline{x}_2, \underline{x}_g) &= \int \frac{d^2 \underline{L}}{(2\pi)^2} \frac{d^2 \underline{\ell}_2}{(2\pi)^2} \frac{d^2 \underline{\ell}_g}{(2\pi)^2} H^{\{\bar{q}g\}}(\underline{L}, \underline{\ell}_2, \underline{\ell}_g) \delta^2(\underline{L}) \\ &\quad \times \exp(-i((\underline{L} - \underline{\ell}_2 - \underline{\ell}_g) \cdot \underline{x}_1 + \underline{\ell}_2 \cdot \underline{x}_2 + \underline{\ell}_g \cdot \underline{x}_g)) \\ &= \int \frac{d^2 \underline{\ell}_2}{(2\pi)^2} \frac{d^2 \underline{\ell}_g}{(2\pi)^2} H^{\{\bar{q}g\}}(\underline{\ell}_2, \underline{\ell}_g) \\ &\quad \times \exp(-i(\underline{L}_{\bar{q}g} \cdot (\underline{x}_{G_{\bar{q}g}} - \underline{x}_1) + \underline{\ell}_{\bar{q}g} \cdot \underline{x})), \end{aligned} \quad (3.75)$$

with $\underline{L} = \underline{\ell}_1 + \underline{\ell}_2 + \underline{\ell}_g$ and $\underline{x}_G = y_1 \underline{x}_1 + \bar{y}_2 \underline{x}_2 + y_g \underline{x}_g$ the momentum and the position of the center of mass G of the 3-parton system. We now perform the change of variables $(\underline{\ell}_2, \underline{\ell}_g) \rightarrow (\underline{\ell}_{\bar{q}g}, \underline{L}_{\bar{q}g})$, which involves the Jacobian $(\bar{y}_2 + y_g)/\bar{y}_1 = 1$, leading to

$$\tilde{H}^{\{\bar{q}g\}}(\underline{x}_1, \underline{x}_2, \underline{x}_g) = \int \frac{d^2 \underline{\ell}_{\bar{q}g}}{(2\pi)^2} \frac{d^2 \underline{L}_{\bar{q}g}}{(2\pi)^2} H^{\{\bar{q}g\}}(\underline{\ell}_{\bar{q}g}, \underline{L}_{\bar{q}g}) \exp(-i(\underline{L}_{\bar{q}g} \cdot (\underline{x}_{G_{\bar{q}g}} - \underline{x}_1) + \underline{\ell}_{\bar{q}g} \cdot \underline{x})). \quad (3.76)$$

Let us denote $F_{\text{Diagr}, V}^{\{ij\}}(\underline{\ell}_{ij}, \underline{L}_{ij}, y_i, y_j)$ and $F_{\text{Diagr}, A}^{\{ij\}}(\underline{\ell}_{ij}, \underline{L}_{ij}, y_i, y_j)$ respectively the integrands of the vector and axial-vector contributions of the diagram 'Diagr' related to the 2-parton system $\{ij\}$, to the "extended" impact factor.

Taking the diagram atG1 as an example for clarity, its vector contribution $F_{\text{atG1}, V}^{\{\bar{q}g\}}$ and

its axial vector contribution $F_{atG1,A}^{\{\bar{q}g\}}$ read explicitly,

$$\begin{aligned}
F_{atG1,V}^{\{\bar{q}g\}}(\underline{\ell}_{\bar{q}g}, \underline{L}_{\bar{q}g}, \bar{y}_2, y_g) &= \frac{C^{ab}Q^2}{2} \frac{N_c}{C_F} \frac{1}{2} (S(y_1, y_2) + M(y_1, y_2)) \frac{1}{4\bar{y}_1 Q} \\
&\times \left\{ \underline{e}_\rho^* \cdot \underline{e}_\gamma \left(\frac{\underline{L}_{\bar{q}g}^2}{2\mu_1^2/Q} + \frac{Q}{2} + \frac{\underline{L}_{\bar{q}g} \cdot (\underline{\ell}_{\bar{q}g} + \underline{k})}{2\bar{y}_1 \bar{y}_2 Q} \right) \right. \\
&\quad \left. - \frac{(\underline{L}_{\bar{q}g} \cdot \underline{e}_\gamma)(\underline{e}_\rho^* \cdot (\underline{\ell}_{\bar{q}g} + \underline{k}))}{2\bar{y}_2 y_g Q / (\bar{y}_1 + \bar{y}_2)} - \frac{(\underline{L}_{\bar{q}g} \cdot \underline{e}_\rho^*)(\underline{e}_\gamma \cdot (\underline{\ell}_{\bar{q}g} + \underline{k}))}{2\bar{y}_2 Q} \right\} \\
&\times \frac{1}{\left(\frac{\underline{L}_{\bar{q}g}^2}{2\mu_1^2/Q} + \frac{Q}{2} \right) \left(\frac{\underline{L}_{\bar{q}g}^2}{2\mu_1^2/Q} + \frac{Q}{2} + \frac{(\underline{\ell}_{\bar{q}g} + \underline{k})^2}{2\mu_{\bar{q}g}^2/Q} \right)}, \tag{3.77}
\end{aligned}$$

$$\begin{aligned}
F_{atG1,A}^{\{\bar{q}g\}}(\underline{\ell}_{\bar{q}g}, \underline{L}_{\bar{q}g}, \bar{y}_2, y_g) &= \frac{C^{ab}Q^2}{2} \frac{N_c}{C_F} \frac{1}{2} (S(y_1, y_2) - M(y_1, y_2)) \frac{1}{4\bar{y}_1 Q} \\
&\times \left\{ \underline{e}_\rho^* \cdot \underline{e}_\gamma \left(\frac{\underline{L}_{\bar{q}g}^2}{2\mu_1^2/Q} + \frac{Q}{2} - \frac{\underline{L}_{\bar{q}g} \cdot (\underline{\ell}_{\bar{q}g} + \underline{k})}{2\bar{y}_2 y_g Q / (\bar{y}_1 + \bar{y}_2)} \right) \right. \\
&\quad \left. + \frac{(\underline{L}_{\bar{q}g} \cdot \underline{e}_\rho^*)(\underline{e}_\gamma \cdot (\underline{\ell}_{\bar{q}g} + \underline{k}))}{2\bar{y}_2 y_g Q / (\bar{y}_1 + \bar{y}_2)} + \frac{(\underline{L}_{\bar{q}g} \cdot \underline{e}_\gamma)(\underline{e}_\rho^* \cdot (\underline{\ell}_{\bar{q}g} + \underline{k}))}{2\bar{y}_2 Q} \right\} \\
&\times \frac{1}{\left(\frac{\underline{L}_{\bar{q}g}^2}{2\mu_1^2/Q} + \frac{Q}{2} \right) \left(\frac{\underline{L}_{\bar{q}g}^2}{2\mu_1^2/Q} + \frac{Q}{2} + \frac{(\underline{\ell}_{\bar{q}g} + \underline{k})^2}{2\mu_{\bar{q}g}^2/Q} \right)}, \tag{3.78}
\end{aligned}$$

with $\mu_1^2 = y_1 \bar{y}_1 Q^2$, $\mu_{\bar{q}g}^2 = \frac{y_g \bar{y}_2}{y_g + \bar{y}_2} Q^2$. We will denote for an arbitrary pair of partons i, j ,

$$\mu_{ij}^2 = \frac{y_i y_j}{y_i + y_j} Q^2.$$

As our treatment aims to get the proper result only in the collinear approximation, we cannot have access to the full transverse information about the dipoles dynamics but only about dynamics of the dipole which is probed by the t -channel gluons. In other words, the information carried by $\underline{L}_{\bar{q}g}$ is only partial and not relevant in the collinear approximation so we can send the non-interacting dipole momentum $\underline{L}_{\bar{q}g}$ to zero to simplify the result of the extended impact factor. This gives,

$$\begin{aligned}
F_{atG1,V}^{\{\bar{q}g\}}(\underline{\ell}_{\bar{q}g}, \underline{0}, \bar{y}_2, y_g) &= \frac{C^{ab}}{2} \frac{N_c}{C_F} \frac{1}{2} (S(y_1, y_2) + M(y_1, y_2)) \\
&\times \frac{\mu_{\bar{q}g}^2}{\bar{y}_1} \frac{\underline{e}_\rho^* \cdot \underline{e}_\gamma}{2 (\mu_{\bar{q}g}^2 + (\underline{\ell}_{\bar{q}g} + \underline{k})^2)}, \tag{3.79}
\end{aligned}$$

$$\begin{aligned}
F_{atG1,A}^{\{\bar{q}g\}}(\underline{\ell}_{\bar{q}g}, \underline{0}, \bar{y}_2, y_g) &= \frac{C^{ab}}{2} \frac{N_c}{C_F} \frac{1}{2} (S(y_1, y_2) - M(y_1, y_2)) \\
&\times \frac{\mu_{\bar{q}g}^2}{\bar{y}_1} \frac{\underline{e}_\rho^* \cdot \underline{e}_\gamma}{2 (\mu_{\bar{q}g}^2 + (\underline{\ell}_{\bar{q}g} + \underline{k})^2)}. \tag{3.80}
\end{aligned}$$

We can now express eqs. (3.79, 3.80) in terms of their Fourier transforms to get the

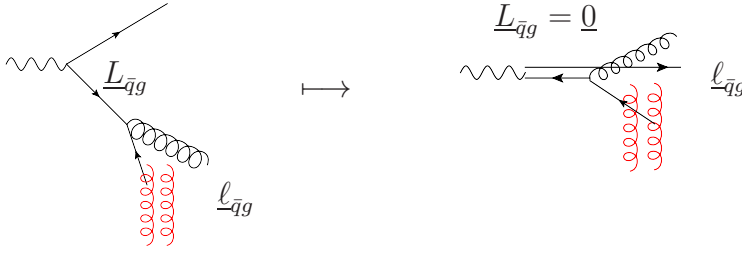


Figure 3.10: The relevant momentum $\underline{\ell}_{\bar{q}g}$ of the interaction with t -channel gluons in the collinear approximation.

information about the interacting dipole dynamics,

$$\begin{aligned}
 F_{atG1,V}^{\{\bar{q}g\}}(\underline{\ell}_{\bar{q}g}, \underline{0}, \bar{y}_2, y_g) &= \frac{C^{ab}}{2} \frac{N_c}{C_F} \frac{1}{2} (S(y_1, y_2) + M(y_1, y_2)) \\
 &\times \frac{\underline{e}_\rho^* \cdot \underline{e}_\gamma}{2} \int \frac{d^2 \underline{x}}{(2\pi)} \frac{\mu_{\bar{q}g}^2}{\bar{y}_1} K_0(\mu_{\bar{q}g} |\underline{x}|) e^{i(\underline{\ell}_{\bar{q}g} + \underline{k}) \cdot \underline{x}}, \\
 F_{atG1,A}^{\{\bar{q}g\}}(\underline{\ell}_{\bar{q}g}, \underline{0}, \bar{y}_2, y_g) &= \frac{C^{ab}}{2} \frac{N_c}{C_F} \frac{1}{2} (S(y_1, y_2) - M(y_1, y_2)) \\
 &\times \frac{\underline{e}_\rho^* \cdot \underline{e}_\gamma}{2} \int \frac{d^2 \underline{x}}{(2\pi)} \frac{\mu_{\bar{q}g}^2}{\bar{y}_1} K_0(\mu_{\bar{q}g} |\underline{x}|) e^{i(\underline{\ell}_{\bar{q}g} + \underline{k}) \cdot \underline{x}}.
 \end{aligned}$$

Finally, what remains in the collinear limit is

$$\begin{aligned}
 F_{atG1,V}^{\{\bar{q}g\}}(\underline{0}, \underline{0}, \bar{y}_2, y_g) &= \frac{C^{ab}}{2} \frac{N_c}{C_F} \frac{1}{2} (S(y_1, y_2) + M(y_1, y_2)) \\
 &\times \frac{\underline{e}_\rho^* \cdot \underline{e}_\gamma}{2} \int \frac{d^2 \underline{x}}{(2\pi)} \frac{\mu_{\bar{q}g}^2}{\bar{y}_1} K_0(\mu_{\bar{q}g} |\underline{x}|) e^{i\bar{k} \cdot \underline{x}}, \\
 F_{atG1,A}^{\{\bar{q}g\}}(\underline{0}, \underline{0}, \bar{y}_2, y_g) &= \frac{C^{ab}}{2} \frac{N_c}{C_F} \frac{1}{2} (S(y_1, y_2) - M(y_1, y_2)) \\
 &\times \frac{\underline{e}_\rho^* \cdot \underline{e}_\gamma}{2} \int \frac{d^2 \underline{x}}{(2\pi)} \frac{\mu_{\bar{q}g}^2}{\bar{y}_1} K_0(\mu_{\bar{q}g} |\underline{x}|) e^{i\bar{k} \cdot \underline{x}}.
 \end{aligned}$$

The total contribution of the diagram atG1 is the sum of the above vector and axial vector contributions

$$F_{atG1}^{\{\bar{q}g\}}(\underline{0}, \underline{0}, \bar{y}_2, y_g) = \frac{C^{ab}}{2} \frac{N_c}{C_F} S(y_1, y_2) \frac{\underline{e}_\rho^* \cdot \underline{e}_\gamma}{2} \int \frac{d^2 \underline{x}}{(2\pi)} \frac{\mu_{\bar{q}g}^2}{\bar{y}_1} K_0(\mu_{\bar{q}g} |\underline{x}|) e^{i\bar{k} \cdot \underline{x}}. \quad (3.81)$$

Let us emphasize that the integral over \bar{y}_2 and y_g of $F_{atG1}^{\{\bar{q}g\}}(\underline{0}, \underline{0}, \bar{y}_2, y_g)$ given in eq. (3.81) is the twist 3 impact factor contribution of the diagram atG1 for the $\{\bar{q}g\}$ dipole, where we have extracted the relevant information about the interacting dipole of size \underline{x} .

The computations of contributions of all the other 3-parton diagrams proceed in the same way. We first compute the diagrams associated to a dipole configuration, in terms of the center of mass and the reduced particle momenta and masses, to obtain $F^{\{ij\}}(\underline{\ell}_{ij}, \underline{L}_{ij}, y_i, y_j)$. We compute then the Fourier transform $\tilde{f}^{\{ij\}}(\underline{x}, y_i, y_j)$ of $F^{\{ij\}}(\underline{\ell}_{ij}, \underline{L}_{ij} = \underline{0}, y_i, y_j)$ as \underline{L}_{ij} is never shifted by the t -channel gluon transverse momenta \underline{k} . Finally, the impact factor is

expressed in terms of $\tilde{f}^{\{ij\}}(\underline{x}, y_i, y_j)$, where $\underline{x} = \underline{x}_i - \underline{x}_j$ is the size of the dipole $\{ij\}$, i.e. the variable conjugated to the momentum $\underline{\ell}_{ij}$. The impact factor has thus the general form

$$\Phi_{q\bar{q}g}^{\gamma_T^* \rightarrow \rho_T} = \sum_{\{ij\}} \Phi_{q\bar{q}g}^{\gamma_T^* \rightarrow \rho_T \{ij\}} \quad (3.82)$$

$$= \sum_{\{ij\}} \int dy_i dy_j \int \frac{d^2 \underline{x}}{(2\pi)^2} \tilde{f}^{\{ij\}}(\underline{x}, y_i, y_j). \quad (3.83)$$

The results of the diagrams in momentum space exhibit two kinds of structure denoted by $S_1(\underline{\ell}, \mu)$ and $S_{2mn}(\underline{\ell}, \mu_A, \mu_B)$

$$S_1(\underline{\ell}, \mu) = \frac{\mu^2}{\underline{\ell}^2 + \mu^2}, \quad (3.84)$$

$$S_{2mn}(\underline{\ell}, \mu_A, \mu_B) = \frac{\underline{\ell}_m \underline{\ell}_n}{(\underline{\ell}^2 + \mu_A^2)(\underline{\ell}^2 + \mu_B^2)}, \quad (3.85)$$

where m and n are 2-dimensional euclidean indices and μ, μ_A, μ_B are the energies scales at stake. The Fourier transforms of formulas (3.84) and (3.85) are

$$S_1(\underline{\ell}, \mu) = \int \frac{d^2 \underline{x}}{(2\pi)} \mu^2 K_0(\mu |\underline{x}|) e^{i\underline{\ell} \cdot \underline{x}}, \quad (3.86)$$

and

$$\begin{aligned} S_{2mn}(\underline{\ell}, \mu_A, \mu_B) &= \int \frac{d^2 \underline{x}}{(2\pi)} \frac{e^{-i\underline{\ell} \cdot \underline{x}}}{\mu_A^2 - \mu_B^2} \frac{\partial}{\partial \underline{x}_m} \frac{\partial}{\partial \underline{x}_n} (K_0(\mu_A |\underline{x}|) - K_0(\mu_B |\underline{x}|)) e^{i\underline{\ell} \cdot \underline{x}} \\ &= \int \frac{d^2 \underline{x}}{(2\pi)} \frac{1}{\mu_A^2 - \mu_B^2} \left\{ \frac{\delta_{mn}}{2} \left[\mu_A^2 \left(\frac{K'_0(\mu_A |\underline{x}|)}{\mu_A |\underline{x}|} + K''_0(\mu_A |\underline{x}|) \right) \right. \right. \\ &\quad \left. \left. - \mu_B^2 \left(\frac{K'_0(\mu_B |\underline{x}|)}{\mu_B |\underline{x}|} + K''_0(\mu_B |\underline{x}|) \right) \right] \right. \\ &\quad \left. + \left(\frac{\delta_{mn}}{2} - \frac{\underline{x}_m \underline{x}_n}{|\underline{x}|^2} \right) \left[\mu_A^2 \left(\frac{K'_0(\mu_A |\underline{x}|)}{\mu_A |\underline{x}|} - K''_0(\mu_A |\underline{x}|) \right) \right. \right. \\ &\quad \left. \left. - \mu_B^2 \left(\frac{K'_0(\mu_B |\underline{x}|)}{\mu_B |\underline{x}|} - K''_0(\mu_B |\underline{x}|) \right) \right] \right\}. \end{aligned} \quad (3.87)$$

This expression can be simplified by noting that the modified Bessel function $K_\nu(\lambda)$ satisfies the equation

$$\lambda^2 K''_\nu(\lambda) + \lambda K'_\nu(\lambda) = (\lambda^2 + \nu^2) K_\nu(\lambda). \quad (3.88)$$

The expression (3.87) thus reads

$$\begin{aligned} S_{2mn}(\underline{\ell}, \mu_A, \mu_B) &= \int \frac{d^2 \underline{x}}{(2\pi)} \frac{e^{i\underline{\ell} \cdot \underline{x}}}{\mu_A^2 - \mu_B^2} \\ &\quad \left\{ \frac{\delta_{mn}}{2} [\mu_A^2 K_0(\mu_A |\underline{x}|) - \mu_B^2 K_0(\mu_B |\underline{x}|)] \right. \\ &\quad \left. - \left(\frac{\delta_{mn}}{2} - \frac{\underline{x}_m \underline{x}_n}{|\underline{x}|^2} \right) [\mu_A^2 K_2(\mu_A |\underline{x}|) - \mu_B^2 K_2(\mu_B |\underline{x}|)] \right\}, \end{aligned} \quad (3.89)$$

where we have used the relation

$$-\frac{1}{\lambda}K'_0(\lambda) + K''_0(\lambda) = K_2(\lambda) \quad (3.90)$$

implied by the standard Bessel recursion formulas [172]. Let us note that the Fourier transforms in eqs. (3.86, 3.89) lead to the appearance of two functions in the 3-parton impact factor, one associated with the spin non-flip transition $\Phi_{q\bar{q}g, \text{nf}}^{\gamma_T^* \rightarrow \rho_T}$ and one associated to the spin flip transition $\Phi_{q\bar{q}g, \text{f}}^{\gamma_T^* \rightarrow \rho_T}$:

$$\Phi_{q\bar{q}g, \text{n.f.}}^{\gamma_T^* \rightarrow \rho_T} \propto \mu^2 K_0(\mu |\underline{x}|), \quad (3.91)$$

$$\Phi_{q\bar{q}g, \text{f.}}^{\gamma_T^* \rightarrow \rho_T} \propto \mu^2 K_2(\mu |\underline{x}|). \quad (3.92)$$

3.3.4 Spin non-flip and spin flip $q\bar{q}g$ impact factor

In this section we show the results we obtain for each color dipole configuration interacting with the gluons in t -channel.

The sum of the contributions in $\frac{\delta^{ab}}{2N_c} \frac{N_c}{C_F}$ of the diagrams (cG1), (ctG1), (ftG1), (httG1), (btG1) and (dtG2), associated with the scattering amplitude of the $\{qg\}$ system on the t -channel gluons, leads to the impact factor

$$\begin{aligned} \Phi_{q\bar{q}g}^{\gamma_T^* \rightarrow \rho_T, \{qg\}} &= \frac{C^{ab}}{2} \frac{N_c}{C_F} \int dy_1 dy_2 \int \frac{d^2 \underline{x}}{(2\pi)} \mathcal{N}(\underline{x}, \underline{k}) \\ &\times \left\{ \frac{\underline{e}_\rho^* \cdot \underline{e}_\gamma}{2} \left[\frac{M(y_1, y_2)}{y_2} \mu_{qg}^2 K_0(\mu_{qg} |\underline{x}|) - \frac{S(y_1, y_2)}{\bar{y}_1} \mu_1^2 K_0(\mu_1 |\underline{x}|) \right] \right. \\ &+ \frac{\bar{y}_1}{y_1 \bar{y}_2} M(y_1, y_2) \left[\mu_1^2 K_0(\mu_1 |\underline{x}|) - \mu_{qg}^2 K_0(\mu_{qg} |\underline{x}|) \right] \\ &+ \left(\frac{\underline{e}_\rho^* \cdot \underline{e}_\gamma}{2} - \frac{\underline{e}_\rho^* \cdot \underline{x} \underline{x} \cdot \underline{e}_\gamma}{|\underline{x}|^2} \right) \left(\frac{S(y_1, y_2)}{y_1} - \frac{M(y_1, y_2)}{\bar{y}_2} \right) \\ &\quad \times \left[\mu_{qg}^2 K_2(\mu_{qg} |\underline{x}|) - \mu_1^2 K_2(\mu_1 |\underline{x}|) \right] \Big\} \\ &+ \frac{C^{ab}}{2} \frac{N_c}{C_F} \int dy_1 dy_2 \int \frac{d^2 \underline{x}}{(2\pi)} T_{\text{n.f.}} \frac{S(y_1, y_2)}{\bar{y}_1} \mu_1^2 K_0(\mu_1 |\underline{x}|), \end{aligned} \quad (3.93)$$

with $\mu_2^2 = y_2 \bar{y}_2 Q^2$. Note that $\frac{\mu_2^2}{Q} = y_2 \bar{y}_2 Q$ is associated to the analogous reduced mass of the 2-body system constituted by the antiquark and the center of mass of the quark and the gluon. We show in the tab. 3.1, the kinematic variables associated to the center of mass G and the reduced particle R of the system $\{qg\}$ that we use to obtain, after simplifications described previously, the result (3.93).

The result for the $\{\bar{q}g\}$ dipole is straightforward by exchanging the role of the quark and the antiquark i.e. exchanging y_1 and \bar{y}_2 in (3.93). Adding the results for the $\{qg\}$ and for the $\{\bar{q}g\}$ dipoles and using the symmetry properties of $S(y_1, y_2)$ and $M(y_1, y_2)$ under the exchange

$\{qg\}$	Center of mass G	Reduced particle R
momenta	$\underline{L}_{qg} = \underline{\ell}_1 + \underline{\ell}_g = -\underline{\ell}_2$	$\underline{\ell}_{qg} = \frac{y_1 \underline{\ell}_g - y_g \underline{\ell}_1}{y_g + y_1} = \frac{y_1 \underline{\ell}_g - y_g \underline{\ell}_1}{y_2}$
positions	$\underline{x}_G = \frac{y_1 \underline{x}_1 + y_g \underline{x}_g}{y_2}$	$\underline{x} = \underline{x}_g - \underline{x}_1$
masses	$m_G = y_2 Q$	$m_R = \frac{\mu_{qg}^2}{Q} = \frac{y_1 y_g Q}{y_2}$

Table 3.1: Kinematic variables of the center of mass G and of the reduced particle R of the system $\{qg\}$

of $y_1 \rightarrow \bar{y}_2$, the spin non-flip part $\Phi_{q\bar{q}g, \text{n.f.}}^{\gamma_T^* \rightarrow \rho_T, \{qg\} + \{\bar{q}g\}}$ and the spin flip part $\Phi_{q\bar{q}g, \text{f.}}^{\gamma_T^* \rightarrow \rho_T, \{qg\} + \{\bar{q}g\}}$ read

$$\begin{aligned}
\Phi_{q\bar{q}g, \text{n.f.}}^{\gamma_T^* \rightarrow \rho_T, \{qg\} + \{\bar{q}g\}} &= \frac{-C^{ab}}{2} \frac{N_c}{C_F} \int dy_1 dy_2 \int \frac{d^2 \underline{x}}{(2\pi)} \mathcal{N}(\underline{x}, \underline{k}) \frac{\underline{e}_\rho^* \cdot \underline{e}_\gamma}{2} \\
&\times \left\{ \frac{S(y_1, y_2)}{\bar{y}_1} [\mu_1^2 K_0(\mu_1 |\underline{x}|) + \mu_{\bar{q}g}^2 K_0(\mu_{\bar{q}g} |\underline{x}|)] \right. \\
&- \frac{M(y_1, y_2)}{y_2} [\mu_2^2 K_0(\mu_2 |\underline{x}|) + \mu_{qg}^2 K_0(\mu_{qg} |\underline{x}|)] \\
&+ \left(\frac{y_2 \bar{y}_1}{y_1 \bar{y}_2} \right) \frac{S(y_1, y_2)}{\bar{y}_1} [\mu_2^2 K_0(\mu_2 |\underline{x}|) - \mu_{\bar{q}g}^2 K_0(\mu_{\bar{q}g} |\underline{x}|)] \\
&- \left. \left(\frac{y_2 \bar{y}_1}{y_1 \bar{y}_2} \right) \frac{M(y_1, y_2)}{y_2} [\mu_1^2 K_0(\mu_1 |\underline{x}|) - \mu_{qg}^2 K_0(\mu_{qg} |\underline{x}|)] \right\} \\
&+ \frac{C^{ab}}{2} \frac{N_c}{C_F} \int dy_1 dy_2 \int \frac{d^2 \underline{x}}{(2\pi)} \frac{\underline{e}_\rho^* \cdot \underline{e}_\gamma}{2} \\
&\times \left[\frac{S(y_1, y_2)}{\bar{y}_1} \mu_1^2 K_0(\mu_1 |\underline{x}|) - \frac{M(y_1, y_2)}{y_2} \mu_2^2 K_0(\mu_2 |\underline{x}|) \right], \tag{3.94}
\end{aligned}$$

and

$$\begin{aligned}
\Phi_{q\bar{q}g, \text{f.}}^{\gamma_T^* \rightarrow \rho_T, \{qg\} + \{\bar{q}g\}} &= \frac{C^{ab}}{2} \frac{N_c}{C_F} \int dy_1 dy_2 \int \frac{d^2 \underline{x}}{(2\pi)} \mathcal{N}(\underline{x}, \underline{k}) \left(\frac{\underline{e}_\rho^* \cdot \underline{e}_\gamma}{2} - \frac{\underline{e}_\rho^* \cdot \underline{x} \underline{x} \cdot \underline{e}_\gamma}{|\underline{x}|^2} \right) \\
&\times \left(\frac{S(y_1, y_2)}{y_1} - \frac{M(y_1, y_2)}{\bar{y}_2} \right) [\mu_{qg}^2 K_2(\mu_{qg} |\underline{x}|) - \mu_1^2 K_2(\mu_1 |\underline{x}|) \\
&+ \mu_{\bar{q}g}^2 K_2(\mu_{\bar{q}g} |\underline{x}|) - \mu_2^2 K_2(\mu_2 |\underline{x}|)] . \tag{3.95}
\end{aligned}$$

The spin non-flip and spin flip impact factors associated to the scattering amplitude of the dipole $\{q\bar{q}\}$ on the t -channel gluons are given by the contributions of type $\frac{\delta^{ab}}{2N_c} (\frac{N_c}{C_F} - 2)$ from

the diagrams (aG1), (cG1), (bG1), (dG2), (bG2), (dG1). The results read

$$\begin{aligned}
\Phi_{q\bar{q}g, \text{n.f.}}^{\gamma_T^* \rightarrow \rho_T, \{q\bar{q}\}} &= \frac{C^{ab}}{2} \left(\frac{N_c}{C_F} - 2 \right) \int dy_1 dy_2 \int \frac{d^2 \underline{x}}{(2\pi)} \mathcal{N}(\underline{x}, \underline{k}) \frac{\underline{e}_\rho^* \cdot \underline{e}_\gamma}{2} \\
&\times \left\{ \frac{S(y_1, y_2)}{\bar{y}_1} \mu_1^2 K_0(\mu_1 |\underline{x}|) - \frac{M(y_1, y_2)}{y_2} \mu_2^2 K_0(\mu_2 |\underline{x}|) \right. \\
&\quad - \frac{S(y_1, y_2)}{y_g} [(\mu_1^2 K_0(\mu_1 |\underline{x}|) - \mu_{q\bar{q}}^2 K_0(\mu_{q\bar{q}} |\underline{x}|)) \\
&\quad \quad \quad \left. + \frac{y_2}{\bar{y}_2} (\mu_2^2 K_0(\mu_2 |\underline{x}|) - \mu_{q\bar{q}}^2 K_0(\mu_{q\bar{q}} |\underline{x}|))] \right] \\
&\quad + \frac{M(y_1, y_2)}{y_g} [(\mu_2^2 K_0(\mu_2 |\underline{x}|) - \mu_{q\bar{q}}^2 K_0(\mu_{q\bar{q}} |\underline{x}|)) \\
&\quad \quad \quad \left. + \frac{\bar{y}_1}{y_1} (\mu_1^2 K_0(\mu_1 |\underline{x}|) - \mu_{q\bar{q}}^2 K_0(\mu_{q\bar{q}} |\underline{x}|))] \right\} \\
&- \frac{C^{ab}}{2} \left(\frac{N_c}{C_F} - 2 \right) \int dy_1 dy_2 \int \frac{d^2 \underline{x}}{(2\pi)} \frac{\underline{e}_\rho^* \cdot \underline{e}_\gamma}{2} \\
&\times \left(\frac{S(y_1, y_2)}{\bar{y}_1} \mu_1^2 K_0(\mu_1 |\underline{x}|) - \frac{M(y_1, y_2)}{y_2} \mu_2^2 K_0(\mu_2 |\underline{x}|) \right), \tag{3.96}
\end{aligned}$$

and

$$\begin{aligned}
\Phi_{q\bar{q}g, \text{f.}}^{\gamma_T^* \rightarrow \rho_T, \{q\bar{q}\}} &= \frac{C^{ab}}{2} \left(\frac{N_c}{C_F} - 2 \right) \int dy_1 dy_2 \int \frac{d^2 \underline{x}}{(2\pi)} \mathcal{N}(\underline{x}, \underline{k}) \left(\frac{\underline{e}_\rho^* \cdot \underline{e}_\gamma}{2} - \frac{\underline{e}_\rho^* \cdot \underline{x} \underline{x} \cdot \underline{e}_\gamma}{|\underline{x}|^2} \right) \\
&\times \left(\frac{S(y_1, y_2)}{y_1} - \frac{M(y_1, y_2)}{\bar{y}_2} \right) \left[\frac{\bar{y}_2}{y_g} (\mu_{q\bar{q}}^2 K_2(\mu_{q\bar{q}} |\underline{x}|) - \mu_1^2 K_2(\mu_1 |\underline{x}|)) \right. \\
&\quad \left. + \frac{y_1}{y_g} (\mu_{q\bar{q}}^2 K_2(\mu_{q\bar{q}} |\underline{x}|) - \mu_2^2 K_2(\mu_2 |\underline{x}|)) \right]. \tag{3.97}
\end{aligned}$$

We show in tab. 3.2 the kinematic variables associated to the system $\{q\bar{q}\}$. The total 3-parton

$\{q\bar{q}\}$	Center of mass G	Reduced particle R
momenta	$\underline{L}_{q\bar{q}} = \underline{\ell}_1 + \underline{\ell}_2 = -\underline{\ell}_g$	$\underline{\ell}_{q\bar{q}} = \frac{\bar{y}_2 \underline{\ell}_1 - y_1 \underline{\ell}_2}{y_1 + \bar{y}_2} = \frac{\bar{y}_2 \underline{\ell}_1 - y_1 \underline{\ell}_2}{\bar{y}_g}$
positions	$\underline{x}_G = \frac{y_1 \underline{x}_1 + \bar{y}_2 \underline{x}_2}{\bar{y}_g}$	$\underline{x} = \underline{x}_1 - \underline{x}_2$
masses	$m_G = \bar{y}_g Q$	$m_R = \frac{\mu_{q\bar{q}}^2}{Q} = \frac{y_1 \bar{y}_2 Q}{\bar{y}_g}$

Table 3.2: Kinematic variables of the center of mass G and of the reduced particle R of the system $\{q\bar{q}\}$

results for the spin non-flip amplitude is thus

$$\begin{aligned}
\Phi_{q\bar{q}g, \text{n.f.}}^{\gamma_T^* \rightarrow \rho_T} = & -\frac{C^{ab}}{2} \int dy_1 dy_2 \int \frac{d^2 \underline{x}}{(2\pi)} \mathcal{N}(\underline{x}, \underline{k}) \frac{\underline{e}_\rho^* \cdot \underline{e}_\gamma}{2} \\
& \times \left\{ 2 \left[\frac{S(y_1, y_2)}{\bar{y}_1} \mu_1^2 K_0(\mu_1 |\underline{x}|) - \frac{M(y_1, y_2)}{y_2} \mu_2^2 K_0(\mu_2 |\underline{x}|) \right] \right. \\
& + \frac{N_c}{C_F} \left[\frac{S(y_1, y_2)}{\bar{y}_1} \mu_{q\bar{g}}^2 K_0(\mu_{q\bar{g}} |\underline{x}|) - \frac{M(y_1, y_2)}{y_2} \mu_{qg}^2 K_0(\mu_{qg} |\underline{x}|) \right. \\
& + \left(\frac{y_2 \bar{y}_1}{\bar{y}_2 y_1} \right) \times \left(\frac{S(y_1, y_2)}{\bar{y}_1} [\mu_2^2 K_0(\mu_2 |\underline{x}|) - \mu_{q\bar{g}}^2 K_0(\mu_{q\bar{g}} |\underline{x}|)] \right. \\
& \quad \left. \left. - \frac{M(y_1, y_2)}{y_2} [\mu_1^2 K_0(\mu_1 |\underline{x}|) - \mu_{qg}^2 K_0(\mu_{qg} |\underline{x}|)] \right) \right] \\
& + \left(\frac{N_c}{C_F} - 2 \right) \left[\frac{S(y_1, y_2)}{y_g} ([\mu_1^2 K_0(\mu_1 |\underline{x}|) - \mu_{q\bar{q}}^2 K_0(\mu_{q\bar{q}} |\underline{x}|)] \right. \\
& \quad \left. + \frac{y_2}{\bar{y}_2} [\mu_2^2 K_0(\mu_2 |\underline{x}|) - \mu_{q\bar{q}}^2 K_0(\mu_{q\bar{q}} |\underline{x}|)] \right) \\
& \quad \left. - \frac{M(y_1, y_2)}{y_g} ([\mu_2^2 K_0(\mu_2 |\underline{x}|) - \mu_{q\bar{q}}^2 K_0(\mu_{q\bar{q}} |\underline{x}|)] \right. \\
& \quad \left. \left. + \frac{\bar{y}_1}{y_1} [\mu_1^2 K_0(\mu_1 |\underline{x}|) - \mu_{q\bar{q}}^2 K_0(\mu_{q\bar{q}} |\underline{x}|)] \right) \right] \Bigg\} \\
& + \frac{C^{ab}}{2} \underline{e}_\rho^* \cdot \underline{e}_\gamma \int dy_1 dy_2 \left(\frac{S(y_1, y_2)}{\bar{y}_1} - \frac{M(y_1, y_2)}{y_2} \right), \tag{3.98}
\end{aligned}$$

while the spin flip 3-parton impact factor is

$$\begin{aligned}
\Phi_{q\bar{q}g, \text{f.}}^{\gamma_T^* \rightarrow \rho_T} = & \frac{C^{ab}}{2} \int dy_1 dy_2 \int \frac{d^2 \underline{x}}{(2\pi)} \mathcal{N}(\underline{x}, \underline{k}) \left(\frac{\underline{e}_\rho^* \cdot \underline{e}_\gamma}{2} - \frac{(\underline{e}_\rho^* \cdot \underline{x})(\underline{x} \cdot \underline{e}_\gamma)}{|\underline{x}|^2} \right) \\
& \times \left(\frac{S(y_1, y_2)}{y_1} - \frac{M(y_1, y_2)}{\bar{y}_2} \right) \left\{ \frac{N_c}{C_F} [\mu_{qg}^2 K_2(\mu_{qg} |\underline{x}|) - \mu_1^2 K_2(\mu_1 |\underline{x}|) \right. \\
& \quad \left. + \mu_{q\bar{g}}^2 K_2(\mu_{q\bar{g}} |\underline{x}|) - \mu_2^2 K_2(\mu_2 |\underline{x}|)] \right. \\
& + \left(\frac{N_c}{C_F} - 2 \right) \left[\frac{\bar{y}_2}{y_g} (\mu_{q\bar{q}}^2 K_2(\mu_{q\bar{q}} |\underline{x}|) - \mu_1^2 K_2(\mu_1 |\underline{x}|)) \right. \\
& \quad \left. + \frac{y_1}{y_g} (\mu_{q\bar{q}}^2 K_2(\mu_{q\bar{q}} |\underline{x}|) - \mu_2^2 K_2(\mu_2 |\underline{x}|)) \right] \Bigg\}. \tag{3.99}
\end{aligned}$$

In the formula (3.98), the last line is not proportional to the dipole factor $\mathcal{N}(\underline{x}, \underline{k})$. In the following part, we will show that putting together the 2-parton result (beyond WW approximation) and the 3-parton result, all parts of the impact factor which do not have the dipole form cancel each others using the QCD EOM. This will extend to the full twist 3 result, the reasoning leading in the WW approximation from eq. (3.31) to eq. (3.34).

3.4 The twist 3 $\gamma_T^* \rightarrow \rho_T$ impact factor in the dipole picture

In the sec. 3.4.1, we show that the EOMs of QCD are essential to get a factorized form of the impact factor at the full twist 3 level. Next, in sec. 3.4.2, we show that the spin non-flip and spin flip results are equivalent to the treatment in momentum space presented in sec. 2.7.4 and finally, in sec. 3.4.3, we combine two- and three-parton impact factor contributions leading to the final full twist 3 result.

3.4.1 The dipole picture arising from the equations of motion of QCD

Let us recall the two relations (2.113, 2.114) between DAs due to the QCD EOMs,

$$\begin{aligned} & \bar{y}\varphi_3(y; \mu_F^2) + \bar{y}\varphi_A(y; \mu_F^2) + \varphi_1^T(y; \mu_F^2) + \varphi_A^T(y; \mu_F^2) \\ &= - \int_y^1 dy_2 S(y, y_2; \mu_F^2), \end{aligned} \quad (3.100)$$

$$\begin{aligned} & y\varphi_3(y; \mu_F^2) - y\varphi_A(y; \mu_F^2) - \varphi_1^T(y; \mu_F^2) + \varphi_A^T(y; \mu_F^2) \\ &= \int_y^1 dy_2 M(y, y_2; \mu_F^2). \end{aligned} \quad (3.101)$$

Adding (3.100) multiplied by y and (3.101) multiplied by \bar{y} , gives the relation

$$\begin{aligned} & y\bar{y}\varphi_3(y) + (y - \bar{y})\varphi_1^T(y) + \varphi_A^T(y) \\ &= -y \int dy_2 S(y, y_2) + \bar{y} \int dy_2 M(y, y_2). \end{aligned} \quad (3.102)$$

Multiplying (3.102) by $1/(y\bar{y})$ and integrating over y gives finally the relation

$$\begin{aligned} & \int \frac{dy}{y\bar{y}} (2y\bar{y}\varphi_3(y) + (y - \bar{y})\varphi_1^T(y) + \varphi_A^T(y)) \\ &+ \int dy_1 \int dy_2 \left(\frac{S(y_1, y_2)}{\bar{y}_1} - \frac{M(y_1, y_2)}{y_2} \right) = 0, \end{aligned} \quad (3.103)$$

with $\varphi(y) = \varphi^{WW}(y) + \varphi^{gen}(y)$ being the complete DAs, i.e. which include both the WW and the genuine twist 3 contributions. The 2-parton impact factor (3.31), before using the relations due to QCD EOMs, reads

$$\begin{aligned} & \Phi_{q\bar{q}}^{\gamma_T^* \rightarrow \rho_T} = \frac{-C^{ab}Q^2}{2} \underline{e}_\rho^* \cdot \underline{e}_\gamma \int dy \int \frac{d^2 \underline{x}}{2\pi} \mu K_1(\mu|\underline{x}|) \mathcal{N}(\underline{x}, \underline{k}) \\ & \times \left([(y - \bar{y})\varphi_1^T(y) - \varphi_A^T(y)] \underline{e}_\rho^* \cdot \underline{x} \frac{\underline{x} \cdot \underline{e}_\gamma}{|\underline{x}|} + \varphi_A^T(y) \frac{\underline{x}^2}{|\underline{x}|} \underline{e}_\rho^* \cdot \underline{e}_\gamma \right) \\ & + \frac{C^{ab}}{2} \underline{e}_\rho^* \cdot \underline{e}_\gamma \int \frac{dy}{y\bar{y}} [(2y\bar{y}\varphi_3(y) + (y - \bar{y})\varphi_1^T + \varphi_A^T(y))]. \end{aligned} \quad (3.104)$$

Collecting all terms arising from eqs. (3.98) and (3.104) which are not proportional to the dipole factor we obtain

$$\begin{aligned} \underline{e}_\rho^* \cdot \underline{e}_\gamma \frac{C^{ab}}{2} \left[\int \frac{dy}{y\bar{y}} (2y\bar{y}\varphi_3(y) + (y - \bar{y})\varphi_1^T(y) + \varphi_A^T(y)) \right. \\ \left. + \int dy_1 \int dy_2 \left(\frac{S(y_1, y_2)}{\bar{y}_1} - \frac{M(y_1, y_2)}{y_2} \right) \right] = 0, \end{aligned} \quad (3.105)$$

i.e. we observe that they cancel due to the relation (3.103). The final 2-parton impact factor is thus

$$\begin{aligned} \Phi_{q\bar{q}}^{\gamma_T^* \rightarrow \rho_T} = -\frac{C^{ab}Q^2}{2} \int dy \int \frac{d^2\underline{x}}{2\pi} \left\{ [(y - \bar{y})\varphi_1^T(y) - \varphi_A^T(y)] \right. \\ \left. \times \frac{(\underline{e}_\rho^* \cdot \underline{x})(\underline{x} \cdot \underline{e}_\gamma)}{|\underline{x}|^2} + \varphi_A^T(y) \underline{e}_\rho^* \cdot \underline{e}_\gamma \right\} \mu|\underline{x}| K_1(\mu|\underline{x}|) \mathcal{N}(\underline{x}, \underline{k}), \end{aligned} \quad (3.106)$$

and it can be decomposed into the spin non-flip and the spin-flip parts

$$\begin{aligned} \Phi_{q\bar{q}, n.f.}^{\gamma_T^* \rightarrow \rho_T} = -\frac{C^{ab}Q^2}{2} \int dy (\varphi_A^T + (y - \bar{y})\varphi_1^T) \\ \times \int \frac{d^2\underline{x}}{2\pi} \frac{1}{2} \underline{e}_\rho^* \cdot \underline{e}_\gamma \mu|\underline{x}| K_1(\mu|\underline{x}|) \mathcal{N}(\underline{x}, \underline{k}), \end{aligned} \quad (3.107)$$

and

$$\begin{aligned} \Phi_{q\bar{q}, f.}^{\gamma_T^* \rightarrow \rho_T} = -\frac{C^{ab}Q^2}{2} \int dy (\varphi_A^T - (y - \bar{y})\varphi_1^T) \\ \times \int \frac{d^2\underline{x}}{2\pi} \left(\frac{1}{2} \underline{e}_\rho^* \cdot \underline{e}_\gamma - \frac{(\underline{e}_\rho^* \cdot \underline{x})(\underline{e}_\gamma \cdot \underline{x})}{|\underline{x}|^2} \right) \mu|\underline{x}| K_1(\mu|\underline{x}|) \mathcal{N}(\underline{x}, \underline{k}). \end{aligned} \quad (3.108)$$

The results (3.106, 3.107, 3.108) are the extension of the formula (3.34, 3.35, 3.36) to the full solution of the QCD EOMs for the DAs, including the genuine twist 3 solutions.

The 3-parton spin non-flip result after using the relation (3.103) is thus

$$\begin{aligned}
\Phi_{q\bar{q}g, \text{ n.f.}}^{\gamma_T^* \rightarrow \rho_T} = & -\frac{C^{ab}}{2} \int dy_1 dy_2 \int \frac{d^2 \underline{x}}{(2\pi)} \mathcal{N}(\underline{x}, \underline{k}) \frac{\underline{e}_\rho^* \cdot \underline{e}_\gamma}{2} \\
& \times \left\{ 2 \left(\frac{S(y_1, y_2)}{\bar{y}_1} \mu_1^2 K_0(\mu_1 |\underline{x}|) - \frac{M(y_1, y_2)}{y_2} \mu_2^2 K_0(\mu_2 |\underline{x}|) \right) \right. \\
& + \frac{N_c}{C_F} \left[\frac{S(y_1, y_2)}{\bar{y}_1} \mu_{\bar{q}g}^2 K_0(\mu_{\bar{q}g} |\underline{x}|) - \frac{M(y_1, y_2)}{y_2} \mu_{qg}^2 K_0(\mu_{qg} |\underline{x}|) \right. \\
& + \left(\frac{y_2 \bar{y}_1}{\bar{y}_2 y_1} \right) \times \left(\frac{S(y_1, y_2)}{\bar{y}_1} [\mu_2^2 K_0(\mu_2 |\underline{x}|) - \mu_{\bar{q}g}^2 K_0(\mu_{\bar{q}g} |\underline{x}|)] \right. \\
& \quad \left. \left. - \frac{M(y_1, y_2)}{y_2} [\mu_1^2 K_0(\mu_1 |\underline{x}|) - \mu_{qg}^2 K_0(\mu_{qg} |\underline{x}|)] \right) \right] \\
& + \left(\frac{N_c}{C_F} - 2 \right) \left[\frac{S(y_1, y_2)}{y_g} ([\mu_1^2 K_0(\mu_1 |\underline{x}|) - \mu_{q\bar{q}}^2 K_0(\mu_{q\bar{q}} |\underline{x}|)] \right. \\
& \quad + \frac{y_2}{\bar{y}_2} [\mu_2^2 K_0(\mu_2 |\underline{x}|) - \mu_{q\bar{q}}^2 K_0(\mu_{q\bar{q}} |\underline{x}|)] \\
& \quad \left. - \frac{M(y_1, y_2)}{y_g} ([\mu_2^2 K_0(\mu_2 |\underline{x}|) - \mu_{q\bar{q}}^2 K_0(\mu_{q\bar{q}} |\underline{x}|)] \right. \\
& \quad \left. \left. + \frac{\bar{y}_1}{y_1} [\mu_1^2 K_0(\mu_1 |\underline{x}|) - \mu_{q\bar{q}}^2 K_0(\mu_{q\bar{q}} |\underline{x}|)] \right) \right] \Big\} , \quad (3.109)
\end{aligned}$$

and it can be rewritten in a more compact way, using the symmetry properties of the DAs under exchange of y_1 and \bar{y}_2 , as

$$\begin{aligned}
\Phi_{q\bar{q}g, \text{ n.f.}}^{\gamma_T^* \rightarrow \rho_T} = & -C^{ab} \int dy_1 dy_2 \int \frac{d^2 \underline{x}}{(2\pi)} \mathcal{N}(\underline{x}, \underline{k}) \frac{\underline{e}_\rho^* \cdot \underline{e}_\gamma}{2} S(y_1, y_2) \\
& \times \left\{ \frac{1}{\bar{y}_1} \left(2 \mu_1^2 K_0(\mu_1 |\underline{x}|) + \frac{N_c}{C_F} [\mu_{\bar{q}g}^2 K_0(\mu_{\bar{q}g} |\underline{x}|) \right. \right. \\
& \quad \left. \left. + \left(\frac{y_2 \bar{y}_1}{\bar{y}_2 y_1} \right) \times [\mu_2^2 K_0(\mu_2 |\underline{x}|) - \mu_{\bar{q}g}^2 K_0(\mu_{\bar{q}g} |\underline{x}|)] \right) \right] \\
& + \frac{1}{y_g} \left(\frac{N_c}{C_F} - 2 \right) [[\mu_1^2 K_0(\mu_1 |\underline{x}|) - \mu_{q\bar{q}}^2 K_0(\mu_{q\bar{q}} |\underline{x}|)] \\
& \quad + \frac{y_2}{\bar{y}_2} [\mu_2^2 K_0(\mu_2 |\underline{x}|) - \mu_{q\bar{q}}^2 K_0(\mu_{q\bar{q}} |\underline{x}|)]] \Big\} . \quad (3.110)
\end{aligned}$$

3.4.2 Equivalence with the results obtained in momentum space in the light-cone collinear factorization scheme

The integration of the spin non-flip result over \underline{x} is straightforward by using the relation

$$\int \frac{d^2 \underline{x}}{(2\pi)} \mathcal{N}(\underline{x}, \underline{k}) \mu^2 K_0(\mu |\underline{x}|) = \frac{2k^2}{\underline{k}^2 + \mu^2} . \quad (3.111)$$

The result after integration over \underline{x} is

$$\begin{aligned} \Phi_{q\bar{q}g, \text{n.f.}}^{\gamma_T^* \rightarrow \rho_T} &= -C^{ab} \int dy_1 dy_2 \underline{e}_\rho^* \cdot \underline{e}_\gamma S(y_1, y_2) \\ &\times \left\{ \left(2 - \frac{N_c}{C_F} \right) \frac{\alpha}{\bar{y}_g \alpha + y_1 \bar{y}_2} \left(\frac{y_1^2}{\alpha + y_1 \bar{y}_1} + \frac{y_2 \bar{y}_2}{\alpha + y_2 \bar{y}_2} \right) \right. \\ &\quad \left. + \frac{N_c}{C_F} \frac{\alpha}{\alpha \bar{y}_1 + \bar{y}_2 y_g} \frac{\alpha}{\alpha + y_2 \bar{y}_2} + \frac{2}{\bar{y}_1} \frac{\alpha}{\alpha + y_1 \bar{y}_1} \right\}, \end{aligned} \quad (3.112)$$

with $\alpha = \underline{k}^2/Q^2$. The result (3.112) is, as expected, identical to the one obtained in Ref. [131] using the light-cone collinear factorization in the momentum space representation.

For the spin flip result, using the symmetry of the amplitude under the exchange of y_1 and \bar{y}_2 , we get

$$\begin{aligned} \Phi_{q\bar{q}g, \text{f.}}^{\gamma_T^* \rightarrow \rho_T} &= C^{ab} \int dy_1 dy_2 \int \frac{d^2 \underline{x}}{(2\pi)} \mathcal{N}(\underline{x}, \underline{k}) \left(\frac{\underline{e}_\rho^* \cdot \underline{e}_\gamma}{2} - \frac{(\underline{e}_\rho^* \cdot \underline{x})(\underline{x} \cdot \underline{e}_\gamma)}{|\underline{x}|^2} \right) \\ &\times \left(\frac{S(y_1, y_2)}{y_1} \right) \left\{ \frac{N_c}{C_F} [\mu_{qg}^2 K_2(\mu_{qg} |\underline{x}|) - \mu_1^2 K_2(\mu_1 |\underline{x}|) \right. \\ &\quad \left. + \mu_{\bar{q}g}^2 K_2(\mu_{\bar{q}g} |\underline{x}|) - \mu_2^2 K_2(\mu_2 |\underline{x}|)] \right. \\ &\quad \left. + \left(\frac{N_c}{C_F} - 2 \right) \left[\frac{\bar{y}_2}{y_g} (\mu_{q\bar{q}}^2 K_2(\mu_{q\bar{q}} |\underline{x}|) - \mu_1^2 K_2(\mu_1 |\underline{x}|)) \right. \right. \\ &\quad \left. \left. + \frac{y_1}{y_g} (\mu_{q\bar{q}}^2 K_2(\mu_{q\bar{q}} |\underline{x}|) - \mu_2^2 K_2(\mu_2 |\underline{x}|)) \right] \right\}. \end{aligned} \quad (3.113)$$

We now integrate over $\underline{x} = (|\underline{x}| \cos(\theta), |\underline{x}| \sin(\theta))$, with $\underline{k} = (|\underline{k}| \cos(\phi), |\underline{k}| \sin(\phi))$. Using the fact that only the spin flip contributions are non zero, and based on the following identities

$$\frac{[(\underline{e}_\rho^-)^* \cdot \underline{x}][\underline{x} \cdot \underline{e}_\gamma^+]}{|\underline{x}|^2} = \left(-i \frac{|\underline{x}| e^{i\theta}}{\sqrt{2}} \right) \left(-i \frac{|\underline{x}| e^{i\theta}}{\sqrt{2}} \right) \frac{1}{|\underline{x}|^2} = -\frac{1}{2} e^{i2\theta}, \quad (3.114)$$

$$\frac{[(\underline{e}_\rho^+)^* \cdot \underline{x}][\underline{x} \cdot \underline{e}_\gamma^-]}{|\underline{x}|^2} = \left(i \frac{|\underline{x}| e^{-i\theta}}{\sqrt{2}} \right) \left(i \frac{|\underline{x}| e^{-i\theta}}{\sqrt{2}} \right) \frac{1}{|\underline{x}|^2} = -\frac{1}{2} e^{-i2\theta}, \quad (3.115)$$

resulting from the explicit definitions of the polarizations in eq. (2.241), we obtain

$$\begin{aligned} &\int \frac{d^2 \underline{x}}{(2\pi)} \mathcal{N}(\underline{x}, \underline{k}) \mu^2 K_2(\mu |\underline{x}|) \left(\frac{((\underline{e}_\rho^\mp)^* \cdot \underline{x})(\underline{x} \cdot \underline{e}_\gamma^\pm)}{|\underline{x}|^2} \right) \\ &= - \int d\lambda \lambda K_2(\lambda) \int \frac{d\theta}{2\pi} 2 \left(1 - \cos \left[\frac{k\lambda}{\mu} \cos(\theta - \phi) \right] \right) \frac{1}{2} e^{\pm i2\theta} \\ &= -\frac{1}{2} e^{\pm i2\phi} \int d\lambda \lambda K_2(\lambda) \int \frac{d\theta}{2\pi} 2 \left(1 - \cos \left[\frac{k\lambda}{\mu} \cos(\theta) \right] \right) e^{\pm i2\theta} \\ &= -\frac{1}{2} e^{\pm i2\phi} 2 \int d\lambda \lambda K_2(\lambda) J_2 \left(\frac{k\lambda}{\mu} \right) \\ &= \frac{((\underline{e}_\rho^\mp)^* \cdot \underline{k})(\underline{k} \cdot \underline{e}_\gamma^\pm)}{|\underline{k}|^2} \frac{2\underline{k}^2}{\underline{k}^2 + \mu^2}, \end{aligned} \quad (3.116)$$

with $\lambda = \mu |\underline{x}|$. Hence the spin flip impact factor integrated over \underline{x} reads

$$\begin{aligned} \Phi_{q\bar{q}g,f}^{\gamma_T^* \rightarrow \rho_T} &= -2C^{ab}T_f \int dy_1 dy_2 S(y_1, y_2) \\ &\times \left\{ \frac{N_c}{C_F} \left[\alpha \bar{y}_2 \left(\frac{y_1}{(\alpha + y_1 \bar{y}_1)(y_2 \alpha + y_1 y_g)} + \frac{\bar{y}_2}{(\alpha + y_2 \bar{y}_2)(\bar{y}_1 \alpha + \bar{y}_2 y_g)} \right) \right] \right. \\ &\quad \left. + \left(\frac{N_c}{C_F} - 2 \right) \left[\frac{\alpha \bar{y}_2}{\bar{y}_g \alpha + y_1 \bar{y}_2} \left(\frac{y_1}{\alpha + y_1 \bar{y}_1} + \frac{\bar{y}_2}{\alpha + y_2 \bar{y}_2} \right) \right] \right\}, \end{aligned} \quad (3.117)$$

which is the same result as the one obtained in Ref. [131].

3.4.3 Complete twist 3 result of the $\gamma_T^* \rightarrow \rho_T$ impact factor

Combining all the 2-parton and 3-parton results for the spin non-flip and spin flip impact factors $\Phi_{n.f.}^{\gamma^* \rightarrow \rho}$, $\Phi_{f.}^{\gamma^* \rightarrow \rho}$ of the $\gamma_T^* \rightarrow \rho_T$ transition, we finally obtain

$$\begin{aligned} \Phi_{n.f.}^{\gamma_T^* \rightarrow \rho_T} &= -C^{ab} \int \frac{d^2 \underline{x}}{(2\pi)} \mathcal{N}(\underline{x}, \underline{k}) \frac{\underline{e}_\rho^* \cdot \underline{e}_\gamma}{2} \\ &\times \left\{ \frac{Q^2}{2} \int dy (\varphi_A^T(y) + (y - \bar{y}) \varphi_1^T(y)) \mu |\underline{x}| K_1(\mu |\underline{x}|) \right. \\ &\quad + \int dy_1 dy_2 S(y_1, y_2) \left(\frac{1}{\bar{y}_1} \left(2 \mu_1^2 K_0(\mu_1 |\underline{x}|) + \frac{N_c}{C_F} [\mu_{\bar{q}g}^2 K_0(\mu_{\bar{q}g} |\underline{x}|) \right. \right. \\ &\quad \left. \left. + \left(\frac{y_2 \bar{y}_1}{\bar{y}_2 y_1} \right) \times [\mu_2^2 K_0(\mu_2 |\underline{x}|) - \mu_{\bar{q}g}^2 K_0(\mu_{\bar{q}g} |\underline{x}|)] \right) \right) \\ &\quad + \frac{1}{y_g} \left(\frac{N_c}{C_F} - 2 \right) [[\mu_1^2 K_0(\mu_1 |\underline{x}|) - \mu_{q\bar{q}}^2 K_0(\mu_{q\bar{q}} |\underline{x}|)] \\ &\quad \left. \left. + \frac{y_2}{\bar{y}_2} [\mu_2^2 K_0(\mu_2 |\underline{x}|) - \mu_{q\bar{q}}^2 K_0(\mu_{q\bar{q}} |\underline{x}|)] \right] \right) \Bigg\}, \end{aligned} \quad (3.118)$$

and

$$\begin{aligned} \Phi_{f.}^{\gamma_T^* \rightarrow \rho_T} &= C^{ab} \int \frac{d^2 \underline{x}}{(2\pi)} \mathcal{N}(\underline{x}, \underline{k}) \left(\frac{\underline{e}_\rho^* \cdot \underline{e}_\gamma}{2} - \frac{(\underline{e}_\rho^* \cdot \underline{x})(\underline{x} \cdot \underline{e}_\gamma)}{|\underline{x}|^2} \right) \\ &\times \left\{ -\frac{Q^2}{2} \int dy (\varphi_A^T(y) - (y - \bar{y}) \varphi_1^T(y)) \mu |\underline{x}| K_1(\mu |\underline{x}|) \right. \\ &\quad + \int dy_1 dy_2 \left(\frac{S(y_1, y_2)}{y_1} \right) \left[\frac{N_c}{C_F} [\mu_{qg}^2 K_2(\mu_{qg} |\underline{x}|) - \mu_1^2 K_2(\mu_1 |\underline{x}|) \right. \\ &\quad \left. + \mu_{\bar{q}g}^2 K_2(\mu_{\bar{q}g} |\underline{x}|) - \mu_2^2 K_2(\mu_2 |\underline{x}|)] \right. \\ &\quad + \left(\frac{N_c}{C_F} - 2 \right) \left[\frac{\bar{y}_2}{y_g} (\mu_{q\bar{q}}^2 K_2(\mu_{q\bar{q}} |\underline{x}|) - \mu_1^2 K_2(\mu_1 |\underline{x}|)) \right. \\ &\quad \left. \left. + \frac{y_1}{y_g} (\mu_{q\bar{q}}^2 K_2(\mu_{q\bar{q}} |\underline{x}|) - \mu_2^2 K_2(\mu_2 |\underline{x}|)) \right] \right] \Bigg\}. \end{aligned} \quad (3.119)$$

The eqs. (3.118) and (3.119) are the full twist 3 results the $\gamma_T^*(\lambda_\gamma) \rightarrow \rho_T(\lambda_\rho)$ impact factors, in the forward limit. These results are consistent with the dipole picture, as the coupling with the t -channel gluons with a dipole of transverse size \underline{x} factorizes out.

Note that the three-parton contribution could, in principle, be rewritten in a factorized form with a photon wave function characterizing the dissociation of the photon into a quark antiquark gluon intermediate state, and the ρ - meson DAs. Unfortunately, to the best of our knowledge, the 3-body wave function of the photon is unknown.

3.5 Helicity amplitudes and polarized cross-sections

The full twist 3 results eqs. (3.118) and (3.119) of the previous section allow us to build a model for the helicity amplitude T_{11} based on one hand on the previous twist expansion calculations and on the other hand on a dipole model for the dipole scattering amplitude which is known from the fit of DIS data.

We are interested in the two dominant helicity amplitudes T_{00} and T_{11} in the forward limit. T_{00} and T_{11} involve respectively the $\Phi^{\gamma_L^* \rightarrow \rho_L}$ given by eq. (3.120) and $\Phi^{\gamma^* \rightarrow \rho, \text{n.f.}}$ given by eq. (3.118). We can put the two results in the compact form,

$$\Phi^{\gamma_L^* \rightarrow \rho_L}(\underline{k}, Q, \mu_F^2) = \left(\frac{\delta^{ab}}{2} \right) \int dy \int d\underline{r} \psi_{(q\bar{q})}^{\gamma_L^* \rightarrow \rho_L}(y, \underline{r}; Q, \mu_F^2) \mathcal{A}(\underline{r}, \underline{k}), \quad (3.120)$$

$$\begin{aligned} \Phi^{\gamma_T^* \rightarrow \rho_T}(\underline{k}, Q, \mu_F^2) &= \left(\frac{\delta^{ab}}{2} \right) \int dy \int d\underline{r} \psi_{(q\bar{q})}^{\gamma_T^* \rightarrow \rho_T}(y, \underline{r}; Q, \mu_F^2) \mathcal{A}(\underline{r}, \underline{k}) \\ &+ \left(\frac{\delta^{ab}}{2} \right) \int dy_2 \int dy_1 \int d\underline{r} \psi_{(q\bar{q}g)}^{\gamma_T^* \rightarrow \rho_T}(y_1, y_2, \underline{r}; Q, \mu_F^2) \mathcal{A}(\underline{r}, \underline{k}). \end{aligned} \quad (3.121)$$

The functions $\psi_{(q\bar{q})}^{\gamma_L^* \rightarrow \rho_L}$, $\psi_{(q\bar{q})}^{\gamma_T^* \rightarrow \rho_T}$, $\psi_{(q\bar{q}g)}^{\gamma_T^* \rightarrow \rho_T}$ are respectively the amplitudes of production of a ρ -meson from a quark-antiquark (quark-antiquark gluon) system produced far upstream the target in the fluctuations of the virtual photon. We recall their expressions,

$$\psi_{(q\bar{q})}^{\gamma_L^* \rightarrow \rho_L}(y, \underline{r}; \mu_F^2) = \frac{m_\rho f_\rho}{\sqrt{2}} \sum_{(h, \bar{h})} \phi_{(h\bar{h})}^{\rho_L}(y; \mu_F^2) \Psi_{(h, \bar{h})}^{\gamma_L^*}(y, \underline{r}; Q^2), \quad (3.122)$$

$$\psi_{(q\bar{q})}^{\gamma_T^* \rightarrow \rho_T}(y, \underline{r}; \mu_F^2) = \frac{m_\rho f_\rho}{\sqrt{2}} \sum_{(h, \bar{h})} \phi_{(h, \bar{h})}^{\rho_T, (\lambda_\rho)}(y; \mu_F^2) \Psi_{(h, \bar{h})}^{\gamma_T^* (\lambda_\gamma)}(y, \underline{r}; Q^2). \quad (3.123)$$

$$\begin{aligned} \psi_{(q\bar{q}g)}^{\gamma_T^* \rightarrow \rho_T}(y, \underline{r}; \mu_F^2) &= \frac{m_\rho f_\rho}{\sqrt{2}} \left[\left(\sqrt{\frac{\pi}{4N_c}} \frac{S(y_1, y_2; \mu_F^2)}{2} \right) \mathcal{F}^{\gamma_T^*}(y_1, y_2, \underline{r}; Q) \right. \\ &\quad \left. - \left(\sqrt{\frac{\pi}{4N_c}} \frac{M(y_1, y_2; \mu_F^2)}{2} \right) \mathcal{F}^{\gamma_T^*}(\bar{y}_2, \bar{y}_1, \underline{r}; Q) \right], \end{aligned} \quad (3.124)$$

where the function $\mathcal{F}^{\gamma_T^*}$ describes the fluctuations of the transversely polarized photon into a quark-antiquark-gluon color singlet. The function $\mathcal{F}^{\gamma_T^*}$ can be expressed in terms of the longitudinally polarized photon wave function

$$\Psi^{\gamma_L^*}(\mu_i, \underline{r}; Q) = \sum_{(h, \bar{h})} \Psi_{(h, \bar{h})}^{\gamma_L^*} \equiv 2 \frac{e}{2\pi} \sqrt{\frac{N_c}{\pi}} \frac{\mu_i^2}{Q} K_0(\mu_i |\underline{r}|), \quad (3.125)$$

as

$$\begin{aligned}
\mathcal{F}^{\gamma_T^*}(y_1, y_2, \underline{r}; Q) = & \frac{1}{2} \left\{ 2 \left[\frac{\Psi^{\gamma_L^*}(\mu_1, \underline{r}; Q)}{\bar{y}_1 Q} \right] \right. \\
& + \frac{N_c}{C_F} \left[\frac{\Psi^{\gamma_L^*}(\mu_{\bar{q}g}, \underline{r}; Q)}{\bar{y}_1 Q} + \left(\frac{y_2 \bar{y}_1}{\bar{y}_2 y_1} \right) \times \left(\frac{\Psi^{\gamma_L^*}(\mu_2, \underline{r}; Q)}{\bar{y}_1 Q} - \frac{\Psi^{\gamma_L^*}(\mu_{\bar{q}g}, \underline{r}; Q)}{\bar{y}_1 Q} \right) \right] \\
& + \left(\frac{N_c}{C_F} - 2 \right) \left[\left(\frac{\Psi^{\gamma_L^*}(\mu_1, \underline{r}; Q)}{y_g Q} - \frac{\Psi^{\gamma_L^*}(\mu_{q\bar{q}}, \underline{r}; Q)}{y_g Q} \right) \right. \\
& \left. \left. + \frac{y_2}{\bar{y}_2} \left(\frac{\Psi^{\gamma_L^*}(\mu_2, \underline{r}; Q)}{y_g Q} - \frac{\Psi^{\gamma_L^*}(\mu_{q\bar{q}}, \underline{r}; Q)}{y_g Q} \right) \right] \right\}. \tag{3.126}
\end{aligned}$$

Note, that in the large N_c limit $\mathcal{F}^{\gamma_T^*}$ simplifies as

$$\begin{aligned}
\mathcal{F}^{\gamma_T^*}(y_1, y_2, \underline{r}; Q) & \xrightarrow{N_c \rightarrow \infty} \frac{1}{\bar{y}_1 y_1 \bar{y}_2 Q} \\
& \times \{ y_1 \bar{y}_2 \Psi^{\gamma_L^*}(\mu_1, \underline{r}; Q) + y_2 \bar{y}_1 \Psi^{\gamma_L^*}(\mu_2, \underline{r}; Q) - y_g \Psi^{\gamma_L^*}(\mu_{\bar{q}g}, \underline{r}; Q) \}. \tag{3.127}
\end{aligned}$$

In our convention, the helicity amplitudes within the impact factor representation read

$$\frac{T_{\lambda_\rho \lambda_\gamma}}{s} = \frac{\delta^{ab}}{2} \int \frac{d^2 \underline{k}}{\underline{k}^4} \Phi_{ab}^{\gamma_{\lambda_\gamma}^* \rightarrow \rho \lambda_\rho}(\underline{k}, Q, \mu_F^2) \mathcal{F}(x, \underline{k}), \tag{3.128}$$

with $\mathcal{F}(x, \underline{k})$ is the unintegrated gluon distribution as defined in Ref. [22]. Note that we have adapted the coefficient of the dipole scattering amplitude in the impact factor such as that the dipole cross-section defined in Ref. [22] is simply

$$\hat{\sigma}(x, \underline{r}) = \frac{N_c^2 - 1}{4} \int \frac{d^2 \underline{k}}{\underline{k}^4} \mathcal{F}(x, \underline{k}) \mathcal{A}(\underline{k}, \underline{r}). \tag{3.129}$$

Inserting the expressions for the impact factor $\Phi^{\gamma_{\lambda_\gamma}^* \rightarrow \rho \lambda_\rho}$ of eqs. (3.120, 3.122), one gets

$$\frac{T_{00}}{s} = \int dy \int d\underline{r} \psi_{(q\bar{q})}^{\gamma_L^* \rightarrow \rho L}(y, \underline{r}; Q, \mu_F^2) \hat{\sigma}(x, \underline{r}), \tag{3.130}$$

$$\begin{aligned}
\frac{T_{11}}{s} &= \int dy \int d\underline{r} \psi_{(q\bar{q})}^{\gamma_T^* \rightarrow \rho T}(y, \underline{r}; Q, \mu_F^2) \hat{\sigma}(x, \underline{r}) \\
&+ \int dy_2 \int dy_1 \int d\underline{r} \psi_{(q\bar{q}g)}^{\gamma_T^* \rightarrow \rho T}(y_1, y_2, \underline{r}; Q, \mu_F^2) \hat{\sigma}(x, \underline{r}). \tag{3.131}
\end{aligned}$$

We can separate T_{11} in the WW contribution and the genuine contribution

$$\frac{T_{11}^{WW}}{s} = \int dy \int d\underline{r} \psi_{(q\bar{q})}^{\gamma_T^* \rightarrow \rho T, WW}(y, \underline{r}; Q, \mu_F^2) \hat{\sigma}(x, \underline{r}), \tag{3.132}$$

$$\begin{aligned}
\frac{T_{11}^{gen}}{s} &= \int dy \int d\underline{r} \psi_{(q\bar{q})}^{\gamma_T^* \rightarrow \rho T, gen}(y, \underline{r}; Q, \mu_F^2) \hat{\sigma}(x, \underline{r}) \\
&+ \int dy_2 \int dy_1 \int d\underline{r} \psi_{(q\bar{q}g)}^{\gamma_T^* \rightarrow \rho T}(y_1, y_2, \underline{r}; Q, \mu_F^2) \hat{\sigma}(x, \underline{r}). \tag{3.133}
\end{aligned}$$

As announced, the formulas (3.130, 3.131) allow us to combine various models of the scattering amplitude of a dipole on a nucleon with the results obtained by the twist expansion of

the $\gamma^* \rightarrow \rho$ impact factor. We will use the GBW-model and the AAMQS-models described in the chap. 1.3.4.

At $t = t_{min}$ the contributions to the longitudinal and transverse differential cross-sections $\frac{d\sigma_L}{dt}$ and $\frac{d\sigma_T}{dt}$ are respectively related to the helicity amplitudes T_{00} and T_{11}

$$\frac{d\sigma_L}{dt}(t=0) = \frac{|T_{00}(s, t=0)|^2}{16\pi s^2}, \quad (3.134)$$

$$\frac{d\sigma_T}{dt}(t=0) = \frac{|T_{11}(s, t=0)|^2}{16\pi s^2}. \quad (3.135)$$

The t -dependency is expected to be governed by non-perturbative effects of the nucleon which can be phenomenologically parameterized by an exponential dependence of the differential cross-sections

$$\frac{d\sigma_{L,T}}{dt}(t) = e^{-b(Q^2)t} \frac{d\sigma_{L,T}}{dt}(t=0). \quad (3.136)$$

Integrating over t leads to the following results in the polarized cross-sections

$$\sigma_L = \frac{1}{b(Q^2)} \frac{|T_{00}(s, t=0)|^2}{16\pi s^2}, \quad (3.137)$$

$$\sigma_T = \frac{1}{b(Q^2)} \frac{|T_{11}(s, t=0)|^2}{16\pi s^2}. \quad (3.138)$$

The $b(Q^2)$ slope has been measured by ZEUS and H1. We will use here quadratic fits of the $b(Q^2)$ slope data of Ref. [99] shown in fig. 3.11 to determine the cross-section. Note that this t -dependence is obtained by fitting the differential cross-section by the factor $\exp(-b|t|)$ for several values of Q^2 giving the dependence $b(Q^2)$. The agreement of the fits with the H1 data is shown in fig. 3.12.

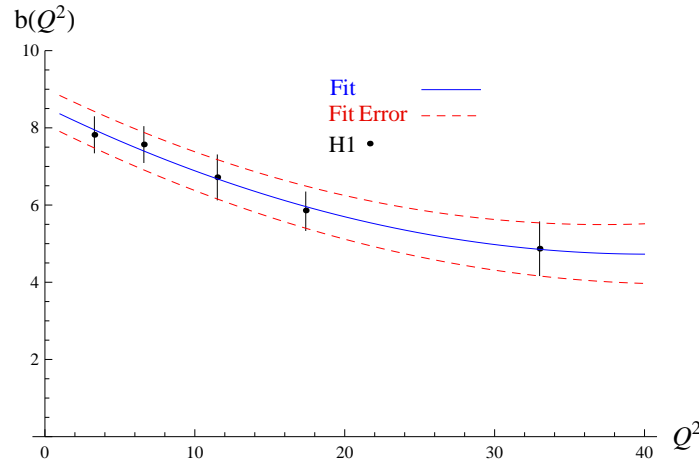


Figure 3.11: Quadratic fits of the b -slope H1 data.

Note that the t -dependence being given by a decreasing exponential function, we can estimate from the b -slope values that the differential cross-section is dominated by the range

$$|t| \lesssim \frac{1}{b(Q^2)} \approx \frac{1}{6} \text{ GeV}^2.$$

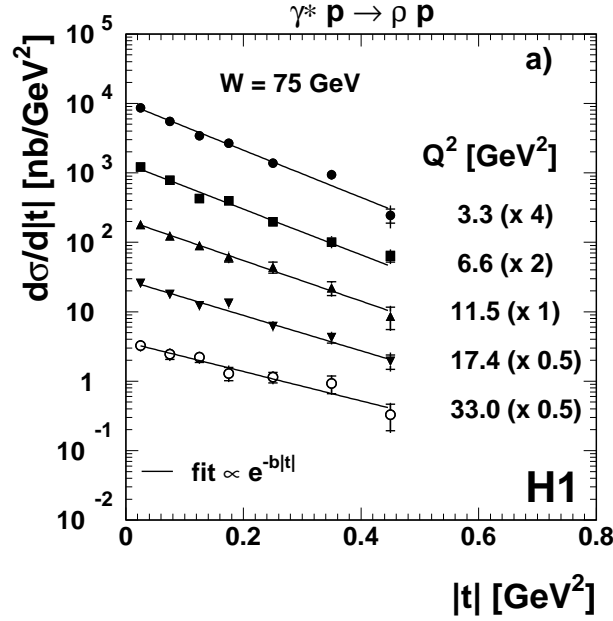


Figure 3.12: t -dependence of the differential cross-section measured by H1 collaboration [99] for several Q^2 values and with a center of mass energy $W = 75$ GeV.

3.6 Comparison with the HERA data

In this section, we compare to H1 [99] and ZEUS [98] data our predictions for,

$$\sigma_T, \sigma_L, R = \frac{\sigma_L}{\sigma_T} \text{ and } r_{00}^{04} = \frac{\varepsilon}{x_{11}^2 + \varepsilon}.$$

We denote σ the total cross-section, $\sigma = \sigma_L + \sigma_T$ according to ZEUS convention in ref. [98] or $\sigma = \varepsilon\sigma_L + \sigma_T$ following H1 notation [99]. We recall that ε is the photon polarization parameter, $\langle\varepsilon\rangle = 0.98$ for H1 and $\langle\varepsilon\rangle = 0.996$ for ZEUS. We remind that the dipole models we will use are the GBW and the AAMQS dipole models.

We prefer to present r_{00}^{04} instead of the ratio T_{11}/T_{00} as the data are available from both H1 and ZEUS collaborations. As the difference between the b -slopes of σ_L (b_L) and σ_T (b_T) is small compared to the value of the b -slope measured by fitting the t -dependence of the total differential cross-section, we will assume that $b = b_L = b_T$. The direct consequence of this is that the ratios of differential cross-sections are constant functions of t . This assumption on the b -slopes allows to relate r_{00}^{04} to the polarized cross-sections,

$$r_{00}^{04} \equiv \frac{\sigma_L}{\sigma}.$$

As it is shown in fig. 3.13, the data of r_{00}^{04} as a function of $|t|$, support this assumption as they are weakly sensitive to the t -value.

The results for σ_T and σ_L are shown in figs. 3.14(a), 3.14(b). As one can see the normalizations of the cross-sections are in very good agreement with the data for large Q^2 ,

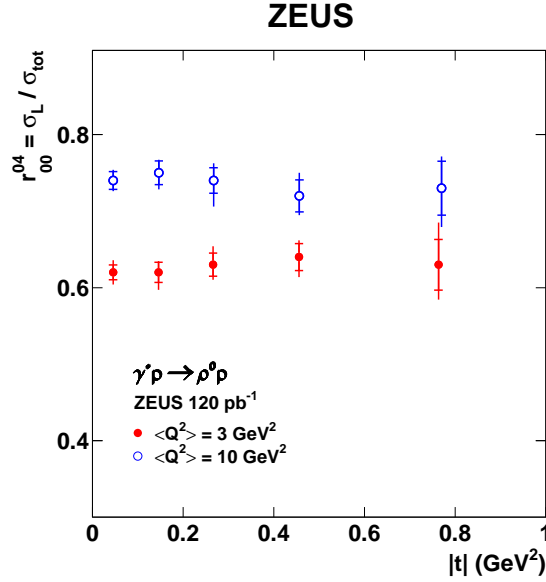


Figure 3.13: Ratio r_{00}^{04} as a function of $|t|$ for different values of Q^2 from ZEUS collaboration Ref. [98].

independently of the dipole model used. This is a non trivial result as the overall normalizations of the predictions are on one hand due to the normalization of the dipole cross-section and on the other hand, based on the coupling constants evaluated from QCD sum rules. The success to reproduce the right normalization at large Q^2 indicates that the factorization procedure we used works properly. The fact that at low Q^2 there is a discrepancy appearing between the data and the predictions, is due to higher twist effects. Indeed, the twist expansion is justified only up to certain value of Q^2 as the neglected terms are expected to be of the order m_ρ/Q . It is also interesting to observe that thanks to HERA data we can evaluate when the higher twist corrections become important. We see that for $Q^2 \sim Q_{\min}^2 \sim 5 \text{ GeV}^2$, the leading twist corrections are not enough to describe the data. Unfortunately the saturation regime which in this kinematics is expected for $Q^2 < Q_s^2 \sim 1 \text{ GeV}^2$ is not accessible with our twist expansion, but as it is shown in fig. 3.15, the dipole models are giving the good x -dependence. We recall that the s dependence of the amplitude is only given by the dipole scattering amplitude as the impact factors are s -independent.

The different contributions, namely the WW (for σ_T only) contribution, the total contributions at,

$$\mu_F^2 = \frac{Q^2 + m_\rho^2}{4},$$

and the asymptotic contributions $\mu_F^2 \rightarrow \infty$ are displayed for σ_T and σ_L in figs. 3.17(a), 3.17(b). As in the GS-model of the chap. 2, the WW contribution dominates the genuine contribution and the AS contribution is close to the other contributions. Comparing the curves of the AS and the total contributions allows to get a good estimation of the dependence of the results in the choice of the factorization scale. Indeed we will see in the next part that

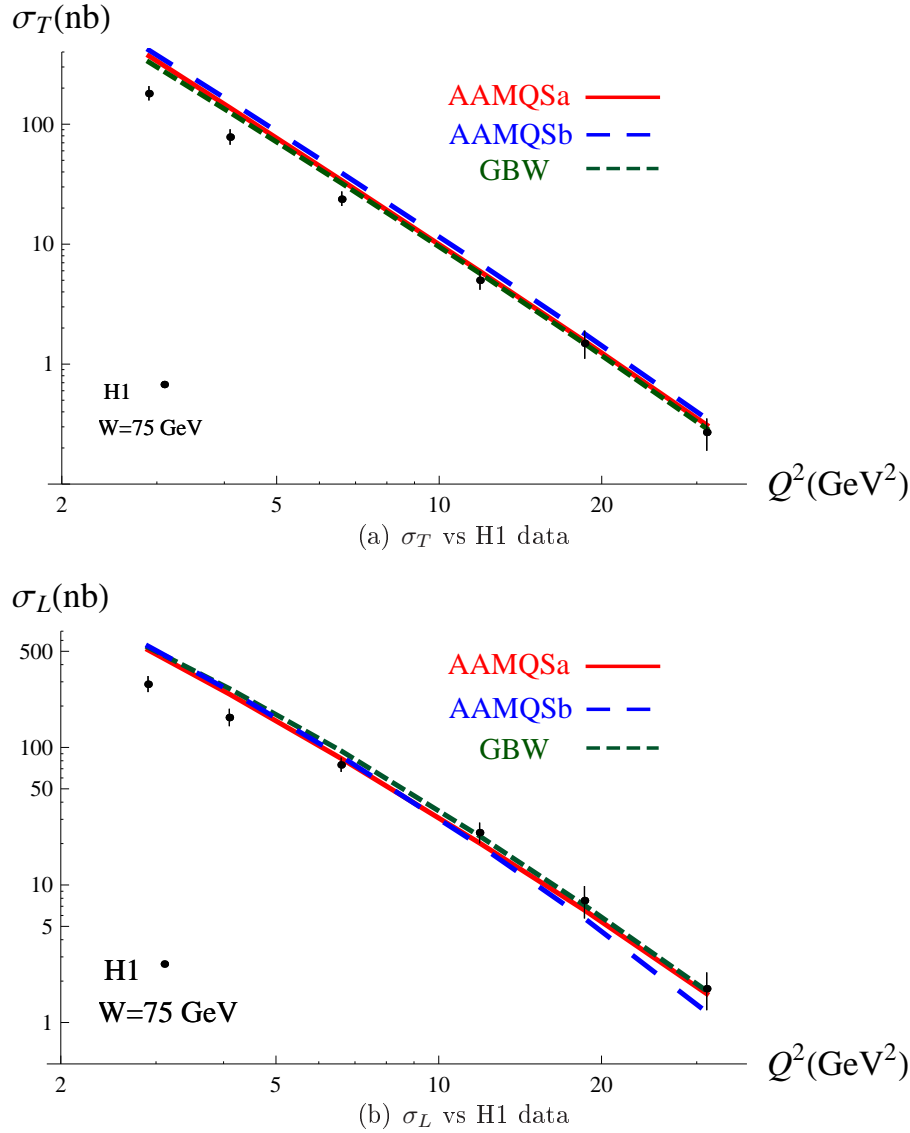


Figure 3.14: Predictions for σ_T and σ_L vs Q^2 , for $W = 75$ GeV, using the AAMQSa (red solid line), AAMQsb (blue large dashed line) and GBW (green dashed line) models compared to the data of H1[99].

this dependence is quite important at the level of the overlap of the γ^* and ρ -meson wave functions but it is hidden by the convolution with the dipole cross-section which filters the range of dipole size where this μ_F -dependence is important.

In figs. 3.18(a), 3.18(b) are shown the total and AS results with the uncertainty due to the error bars on the b -slope values in fig. 3.11.

The results with the AAMQSa dipole model for the ratios R and r_{00}^{04} are shown in figs. 3.19, 3.20. The predictions are compared with both H1 with $W = 75$ GeV and ZEUS with $W = 90$ GeV collaborations. The ratios are independent of the normalization of the dipole cross-section, we can thus only check if we get the good scaling between the transverse, longitudinal and total cross-sections.

The results with the other dipole models are fairly close to the results obtained with the

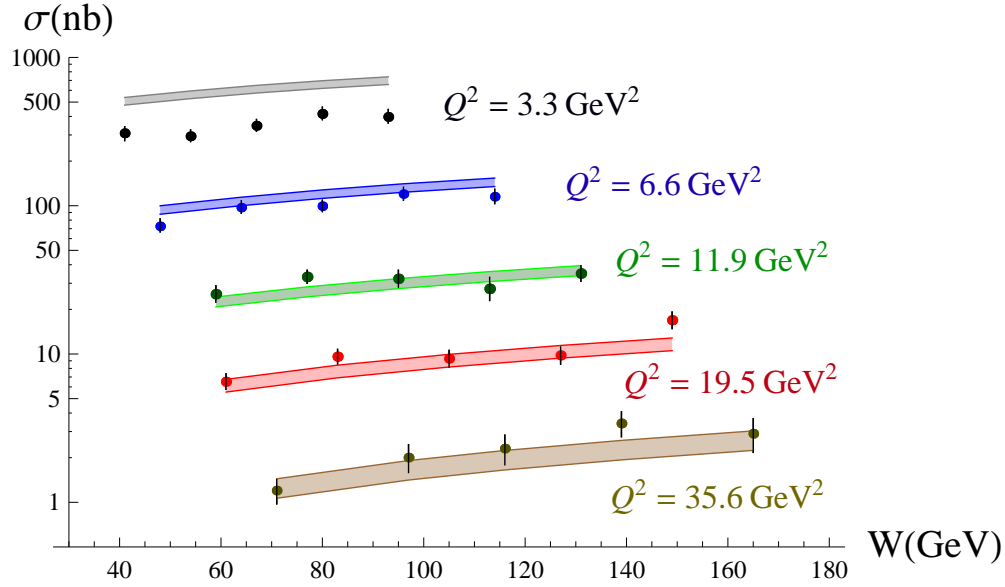


Figure 3.15: Total contribution to the total cross-section σ as the function of W compared to H1 data [99] obtained with the AAMSQa dipole model. The uncertainty due to the b -slope error bars is taken into account.

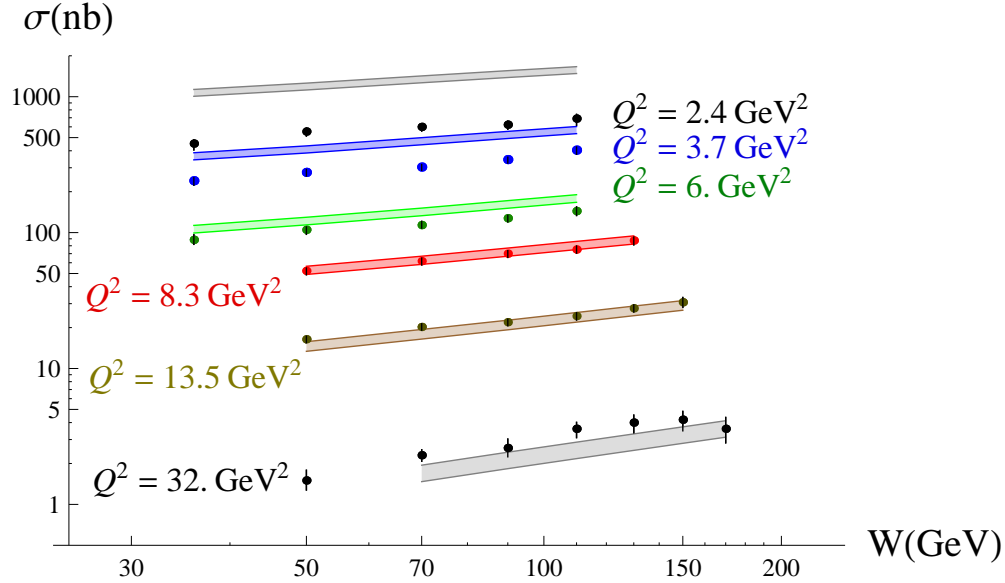
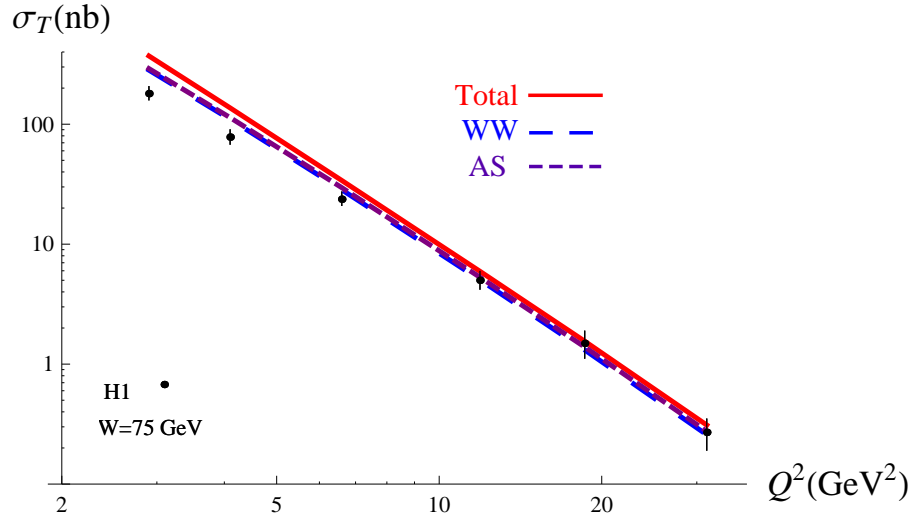


Figure 3.16: Total contribution to the total cross-section σ as the function of W compared to ZEUS data [98] obtained with the AAMSQa dipole model. The uncertainty due to the b -slope error bars is taken into account.

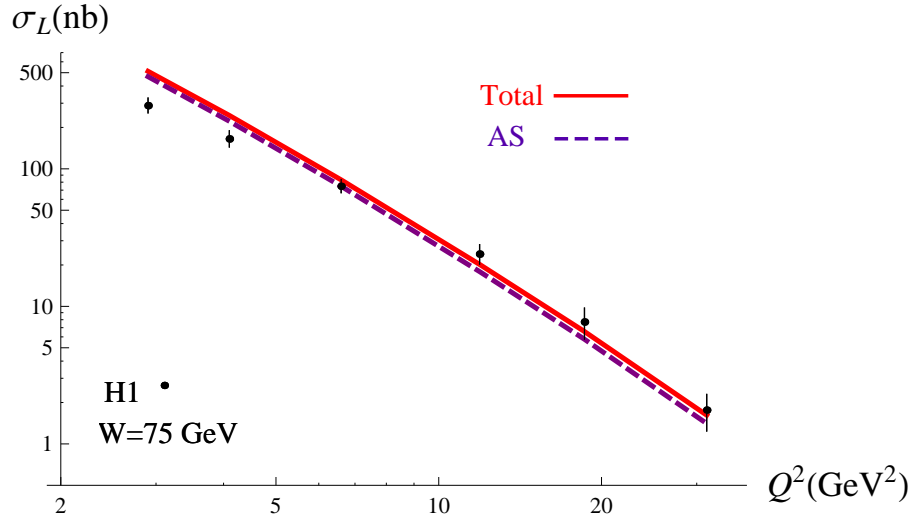
AAMQSa model, they are shown in Ref. [20].

3.7 Interacting dipole distributions

In this section we study the radial distributions of dipoles in the intermediate states that interact with the nucleon via the dipole scattering amplitude.



(a) AS (purple dashed line), WW (blue long dashed line) and Total (red solid line) contributions to σ_T .



(b) AS (purple dashed line) and Total (red solid line) contributions to σ_L .

Figure 3.17: Predictions for σ_T and σ_L vs Q^2 , for $W = 75$ GeV, using the AAMQSa-model, compared to the data of H1[99].

3.7.1 Overlaps and distributions

In Sec. 3.5 we have found the factorized expressions eqs. (3.130, 3.131) for the helicity amplitudes, that we can rewrite as

$$\frac{T_{\lambda_\rho \lambda_\gamma}}{s} = \mathcal{N}_{\lambda_\rho \lambda_\gamma} \int_0^\infty dr \mathcal{P}_{\lambda_\rho \lambda_\gamma}(r, Q^2, \mu_F^2) \hat{\sigma}(x, r), \quad (3.139)$$

with $\mathcal{P}_{\lambda_\rho \lambda_\gamma}(r, Q^2, \mu_F^2)$ being the amplitude of probability to find an intermediate state with a dipole configuration of size $r = |\underline{r}|$ that can interact with the two t -channel gluons and $\mathcal{N}_{\lambda_\rho \lambda_\gamma}$ is a normalization factor. The distribution $\mathcal{P}_{\lambda_\rho \lambda_\gamma}(r, Q^2, \mu_F^2)$ reads

$$\mathcal{P}_{\lambda_\rho \lambda_\gamma}(r, Q^2, \mu_F^2) = \frac{1}{\mathcal{N}_{\lambda_\rho \lambda_\gamma}} r \int dy |\mathcal{W}_{\lambda_\rho \lambda_\gamma}(y, r; \mu_F^2, Q^2)|, \quad (3.140)$$

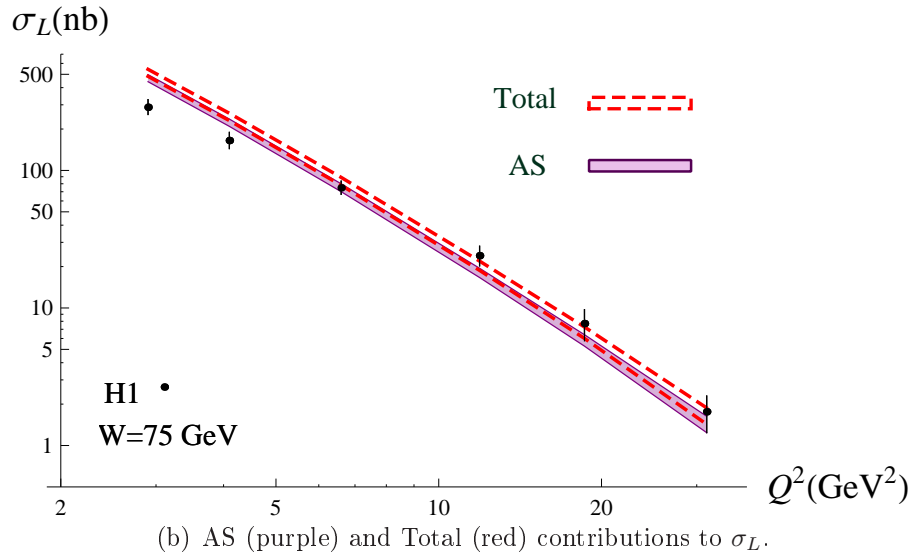
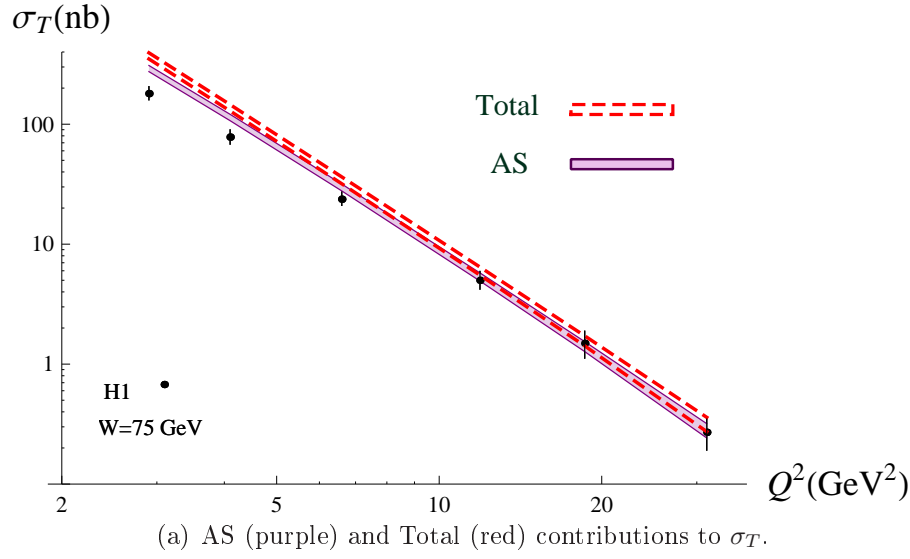


Figure 3.18: Full twist 3 and asymptotic predictions with the b -slope uncertainty, using AAMQSa model.

and

$$\mathcal{N}_{\lambda_\rho \lambda_\gamma} = \int_0^\infty dr r \int dy |\mathcal{W}_{\lambda_\rho \lambda_\gamma}(y_1, y, r; \mu_F^2, Q^2)|, \quad (3.141)$$

where the function $|\mathcal{W}_{\lambda_\rho \lambda_\gamma}(y, r; \mu_F^2, Q^2)|$ is the overlap of the wave functions of the incoming virtual photon state and the final ρ -meson state. The functions \mathcal{W}_{00} and \mathcal{W}_{11} read explicitly,

$$\mathcal{W}_{00}(y, r; \mu_F^2, Q^2) = \psi_{(q\bar{q})}^{\gamma_L^* \rightarrow \rho^L}(y, \underline{r}; Q, \mu_F^2), \quad (3.142)$$

$$\begin{aligned} \mathcal{W}_{11}(y, r; \mu_F^2, Q^2) &= \psi_{(q\bar{q})}^{\gamma_T^* \rightarrow \rho^T}(y, \underline{r}; Q, \mu_F^2) \\ &+ \int_0^y dy_1 \psi_{(q\bar{q}g)}^{\gamma_T^* \rightarrow \rho^T}(y_1, y, \underline{r}; Q, \mu_F^2). \end{aligned} \quad (3.143)$$

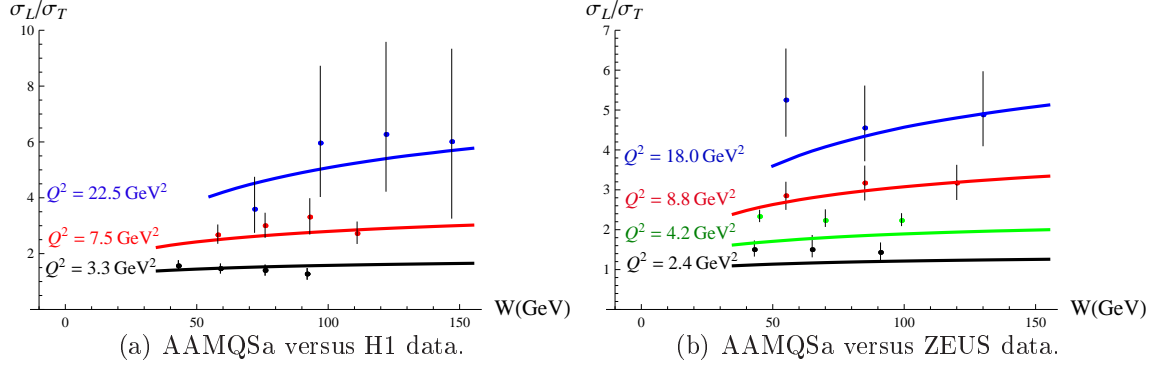


Figure 3.19: The full twist 3 contribution to the ratio of the cross-sections $R = \sigma_L/\sigma_T$ in the limit $t = 0$ versus W and Q^2 compared to the data of H1 [99] in figure (a) and ZEUS [98] in figure (b).

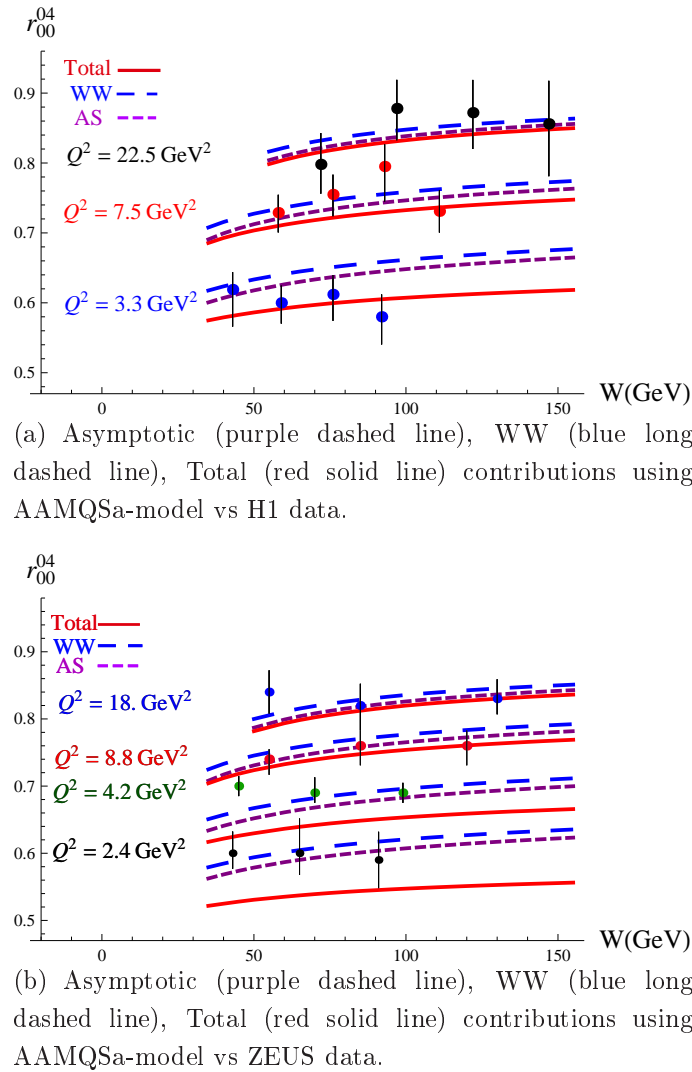


Figure 3.20: Predictions for r_{00}^{04} vs W and Q^2 compared respectively with H1[99] data (figure (a)) and ZEUS[98] data (figure (b)), using the AAMQSa-model.

The overlap \mathcal{W}_{11} can be split in the WW and the genuine contributions

$$\mathcal{W}_{11}^{WW}(y, r; \mu_F^2, Q^2) = \psi_{(q\bar{q})}^{\gamma_T^* \rightarrow \rho_T^{WW}}(y, \underline{r}; Q, \mu_F^2), \quad (3.144)$$

$$\begin{aligned} \mathcal{W}_{11}^{gen}(y, r; \mu_F^2, Q^2) &= \psi_{(q\bar{q})}^{\gamma_T^* \rightarrow \rho_T^{gen}}(y, \underline{r}; Q, \mu_F^2) \\ &+ \int_0^y dy_1 \psi_{(q\bar{q}g)}^{\gamma_T^* \rightarrow \rho_T}(y_1, y, \underline{r}; Q, \mu_F^2). \end{aligned} \quad (3.145)$$

As the r and the Q dependences of the radial distributions enter the amplitudes only through the variable " $\lambda = rQ$ ". We can rescale the distribution by changing the variable r by λ ,

$$P_{\lambda_\rho \lambda_\gamma}(\lambda, \mu_F^2) \equiv \frac{\mathcal{P}_{\lambda_\rho \lambda_\gamma}(\frac{\lambda}{Q}, Q^2; \mu_F^2)}{Q}. \quad (3.146)$$

The distribution $P_{\lambda_\rho \lambda_\gamma}(\lambda, \mu_F^2)$ only depends on Q by the choice of the renormalization scale

$$\mu_F^2(Q^2) = \frac{Q^2 + m_\rho^2}{4}.$$

So in the asymptotic case, $P_{\lambda_\rho \lambda_\gamma}(\lambda, \infty) \equiv P_{\lambda_\rho \lambda_\gamma}^{AS}(\lambda)$ depends only on λ .

Helicity amplitudes read,

$$\frac{T_{\lambda_\rho \lambda_\gamma}}{s} = \mathcal{N}_{\lambda_\rho \lambda_\gamma} \int_0^\infty d\lambda P_{\lambda_\rho \lambda_\gamma}(\lambda, \mu_F^2) \tilde{\sigma}(x, \lambda), \quad (3.147)$$

with

$$\tilde{\sigma}(x, \lambda) = \hat{\sigma}\left(x, \frac{\lambda}{Q}\right) \quad (3.148)$$

the rescaled dipole cross-section.

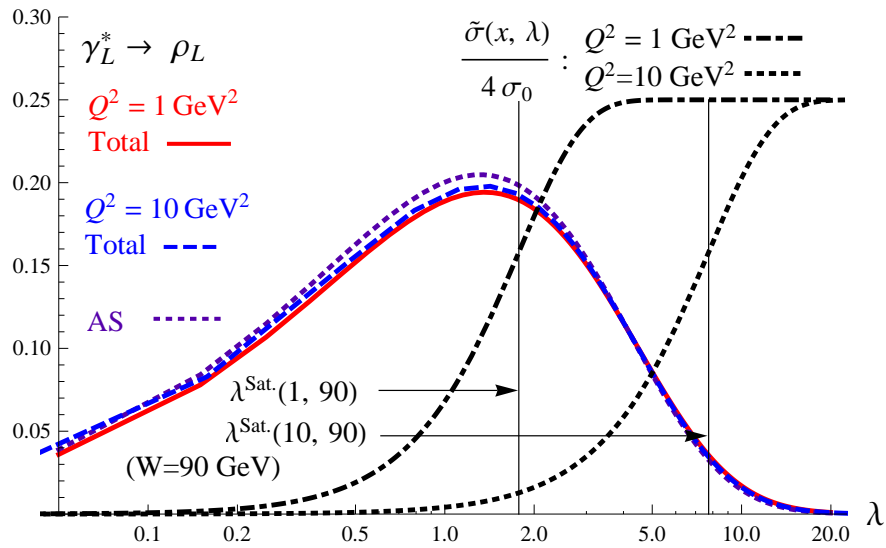


Figure 3.21: Full twist 3 (Total) $P_{00}(\lambda, \mu_F^2(Q^2))$ for $Q^2 = 1 \text{ GeV}^2$ (solid red) and $Q^2 = 10 \text{ GeV}^2$ (dashed blue), AS $P_{00}^{(AS)}(\lambda)$ (dotted purple) and $\tilde{\sigma}(x, \lambda)$ at $W = 90 \text{ GeV}^2$ for $Q^2 = 1 \text{ GeV}^2$ (dotted-dashed black) and $Q^2 = 10 \text{ GeV}^2$ (dashed black).

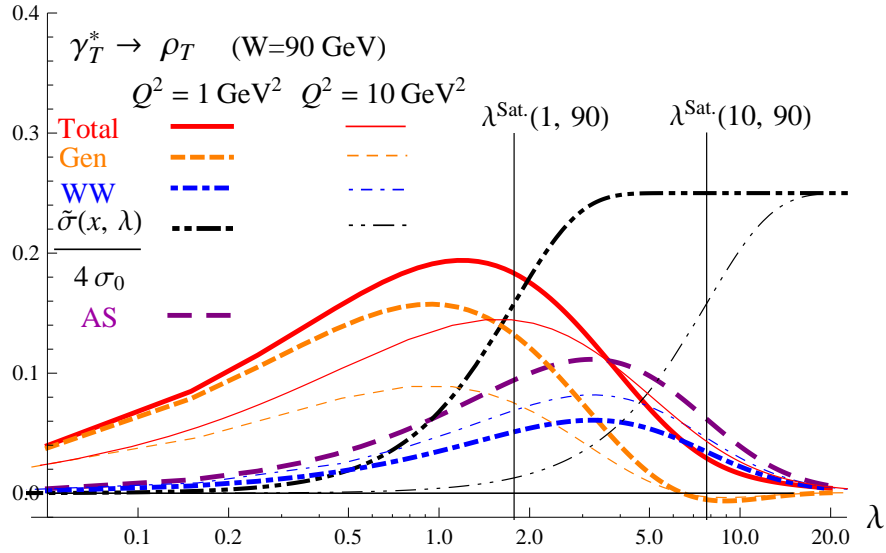


Figure 3.22: The Total $P_{11}(\lambda, \mu_F^2(Q^2))$ (red solid lines) results and their WW (blue dot-dashed lines) and genuine (Gen) (orange dashed lines) contributions, as well as the AS (purple long-dashed line) result $P_{11}^{(AS)}(\lambda)$ and the dipole cross-sections $\tilde{\sigma}(x, \lambda)$ (black dot-dot-dashed lines) at $W = 90 \text{ GeV}^2$, for $Q^2 = 1 \text{ GeV}^2$ (thick lines) and $Q^2 = 10 \text{ GeV}^2$ (thin lines).

In figs. 3.21 and 3.22 are shown the different contributions to the distributions P_{00} and P_{11} for two different values of Q^2 , $Q^2 = Q_a^2 = 10 \text{ GeV}^2$ and $Q^2 = Q_b^2 = 1 \text{ GeV}^2$. As $Q_s(x) = R_0^{-1}(x) \sim 1 \text{ GeV}$, the case $Q^2 = Q_a^2$ corresponds to the diluted regime while the case $Q^2 = Q_b^2$ is at the boundary with the saturation regime.

The dipole cross-section from the GBW-model is also shown in order to see which dipole sizes are filtered by the interaction with the nucleon. We will refer to the "dipole bandwidth" for the range of dipole which have a size above $2R_0(x)$, i.e. $r > 2R_0(x)$, or equivalently by multiplying both sides by Q , $\lambda > \lambda^{\text{Sat.}}(Q^2, W) \equiv 2R_0(x)Q$. Indeed we can see that the dipole cross-section will play the role of a filter for the large dipoles and as one can note looking at the figs. 3.21 and 3.22, $\lambda^{\text{Sat.}}(Q^2, W)$ are good estimates of the inferior bounds of the dipole cross-section bandwidth.

In fig. 3.21, the AS and the total contributions to P_{00} for both virtualities Q_a and Q_b are shown and we can see that the distribution P_{00} is not sensitive to the factorization scale. We can then consider only the AS case as it has a simple analytic form,

$$P_{00}^{(AS)}(\lambda) = \frac{1}{Q} \mathcal{P}_{00}^{(AS)}\left(\frac{\lambda}{Q}, Q^2\right) = 6 \int dy (y\bar{y})^2 \lambda K_0(\sqrt{y\bar{y}}\lambda). \quad (3.149)$$

For the distribution P_{11} we see in fig. 3.22 that the distribution is sensitive to the factorization scale. For the small values, $\mu_F^2 = \mu_F^2(Q_b^2)$, the genuine contribution is as important as the WW-contribution. This fact is not visible on the results for helicity amplitudes because the genuine distribution selects mostly small dipoles that are not in the bandwidth of the dipole cross-section compared to dipoles produced by the WW-contribution. This analysis of the dipole distributions indicates that the genuine contribution, i.e. the quark antiquark gluon intermediate state contribution, should not be omitted in the production

of a transversely polarized ρ -meson at the level of the overlap of the wave functions. This is in contradiction with the usual assumptions of dipole models to assume the transversely polarized ρ -meson state to be saturated by the valence quark antiquark degrees of freedom, leading to the normalization relation (3.150) [55, 145] and the electronic decay width relation eq. (3.151) [115, 145],

$$1 = \sum_{h,\tilde{h}} \int dy \int d^2 \underline{r} \left| \Psi_{h,\tilde{h}}^{\rho T}(y, \underline{r}) \right|^2, \quad (3.150)$$

$$ef_\rho m_\rho (e_\gamma^* \cdot e_\rho) = \sum_{h,\tilde{h}} \int dy \int d^2 \underline{r} \Psi_{h,\tilde{h}}^{\rho T}(y, \underline{r}) \Psi_{h,\tilde{h}}^{\gamma T^*}(y, \underline{r}). \quad (3.151)$$

Indeed, the r.h.s. of eq. (3.151), if one expands at large Q^2 the ρ meson wave function around $\underline{r} = 0$, is our WW result, which therefore misses the genuine contributions arising from three-parton correlators, which can have a significant effect even for large Q^2 values.

We give in tab. 3.3 the average λ defined as,

$$\langle \lambda \rangle_{\lambda_\rho \lambda_\gamma}(\mu_F^2(Q^2)) = \int_0^\infty d\lambda \lambda P_{\lambda_\rho \lambda_\gamma}(\lambda; \mu_F^2). \quad (3.152)$$

Comparing these values with $\lambda^{Sat.}(Q^2, W)$, allows to determine which contribution will

	Total	WW	genuine	AS
$\langle \lambda \rangle_{00}(\mu_F^2)$	~ 3.7	x	x	$\frac{3\pi^2}{8} \approx 3.7$
$\langle \lambda \rangle_{11}(\mu_F^2(1 \text{ GeV}^2))$	6.3	8.7	3.2	$\frac{27\pi^2}{32} \approx 8.3$
$\langle \lambda \rangle_{11}(\mu_F^2(10 \text{ GeV}^2))$	7.3	8.5	3.5	≈ 8.3

Table 3.3: Average values of $\langle \lambda \rangle = \langle r Q \rangle$ for the different contributions to the radial distribution for two values of $\mu_F^2(Q^2)$.

dominate when convoluted with the dipole cross-section. We can also give an estimation, see tab. 3.4, of the percentages $N_{\lambda_\rho \lambda_\gamma}$ of dipoles for a given distribution that are in the bandwidth of the dipole cross-section,

$$N_{\lambda_\rho \lambda_\gamma}(Q^2, W) = \int_{\lambda^{Sat.}(Q^2, W)}^\infty d\lambda P_{\lambda_\rho \lambda_\gamma}(\lambda). \quad (3.153)$$

	AS
$N_{00}(1, 90)$	70%
$N_{00}(10, 90)$	10%
$N_{11}(1, 90)$	90%
$N_{11}(10, 90)$	35%

Table 3.4: Estimation of the percentages of dipoles that have sizes above the saturation scale $2R_0(x)$.

As expected, the more the virtuality Q is high, the weaker is the overlap between the dipole cross-section bandwidth with the distributions leading to a decreasing $N_{\lambda\rho\lambda\gamma}$ with Q^2 . The fact that the $N_{\lambda\rho\lambda\gamma}$'s vary from $\sim 90\%$ to $\sim 10\%$ on the range $Q^2 \in [Q_b^2, Q_a^2]$, indicates that the dipole cross-section is scanning the dipoles distributions with a high sensitivity. This means that the result is very sensitive to the dipole cross-section $\hat{\sigma}(x, r)$ and to the radial distributions $\mathcal{P}_{\lambda\rho, \lambda\gamma}(r, Q^2; \mu_F^2)$ profiles.

It is interesting to get information on the longitudinal fraction of momentum dependences of the overlaps of the wave functions. In other words, do we get more symmetric jet ($y \sim \bar{y} \sim \frac{1}{2}$) or aligned jet ($y \sim 1$ or $\bar{y} \sim 1$) configurations? The overlaps of the wave functions are given in figs. 3.23, 3.24. We restrict ourselves to the study of the AS case. We can

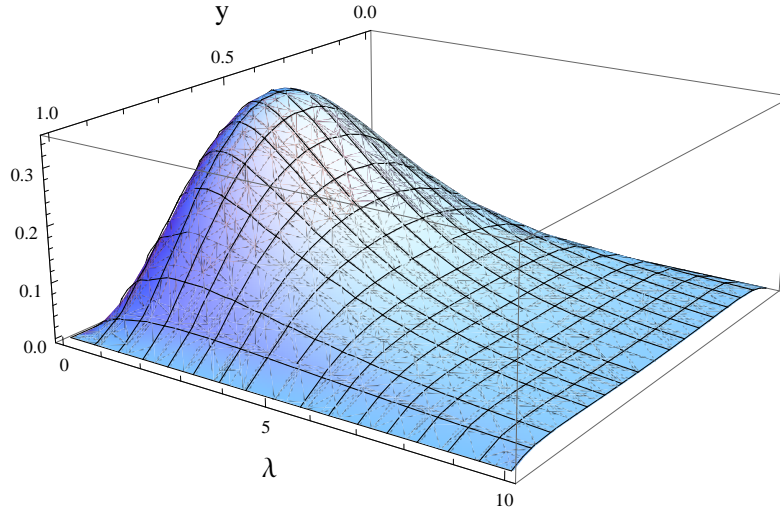


Figure 3.23: Profile of the overlap of the wave functions for the $\gamma_L^* \rightarrow \rho_L$ transition as function of y and λ .

see that we have a symmetric configuration for the $\gamma_L^* \rightarrow \rho_L$ transition while the $\gamma_T^* \rightarrow \rho_T$ transition involves more aligned jet configurations. Note that the aligned jet configurations are important for large values of λ and the oscillations for these large λ -values in the fig. 3.24 are surely due to numerical instabilities. For fixed λ , the y -shape of the overlap is in part due to the shape of the DAs. It is then good to remind that the oscillatory shape of the DAs is due to the fact that the conformal expansion is truncated up to a given conformal spin [142].

In figs. 3.25 and 3.26 are respectively shown the product of the dipole cross-section with the distributions P_{00} and P_{11} . The integrands of T_{00} and T_{11} are globally close to the saturation radius $r \sim 2R_0(x)$ and the peaks are moving on larger dipole sizes when Q^2 decreases. These plots are giving an important information about the k_\perp -behavior of the integrands. Indeed the dipole size r is the Fourier conjugate of the momentum k_\perp meaning that the dominant k_\perp are of the order $1/r$, with r the size corresponding to the maximal value of the integrands shown in figs. 3.25 and 3.26. We can see that the range of k_\perp that gives a significant contribution to the amplitude is of order $1/R_0(x)$ for large Q^2 and of order Q for $Q \sim 1/R_0(x)$. This behavior indicates that within our assumptions, the process is dominated

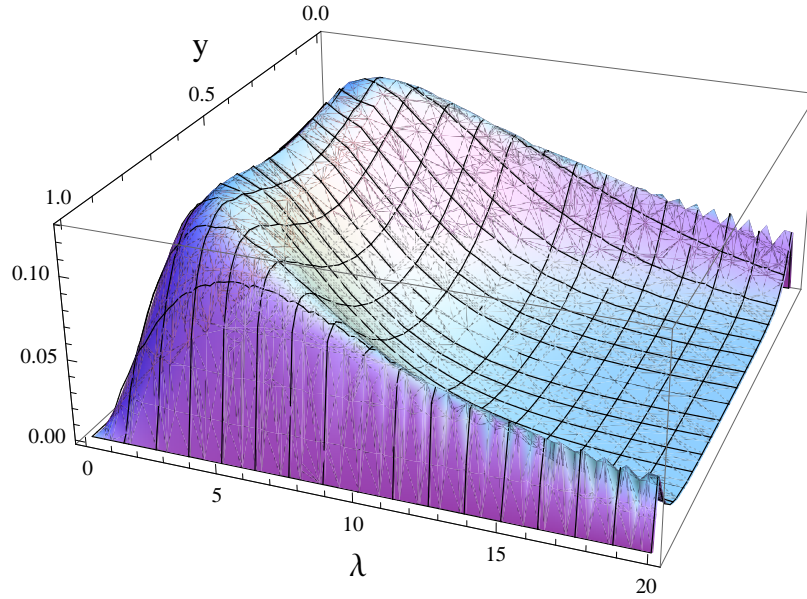


Figure 3.24: Profile of the overlap of the wave functions for the $\gamma_T^* \rightarrow \rho_T$ transition as a function of y and λ .

by some effective scale k_\perp contained in the range $[Q_s, Q]$.

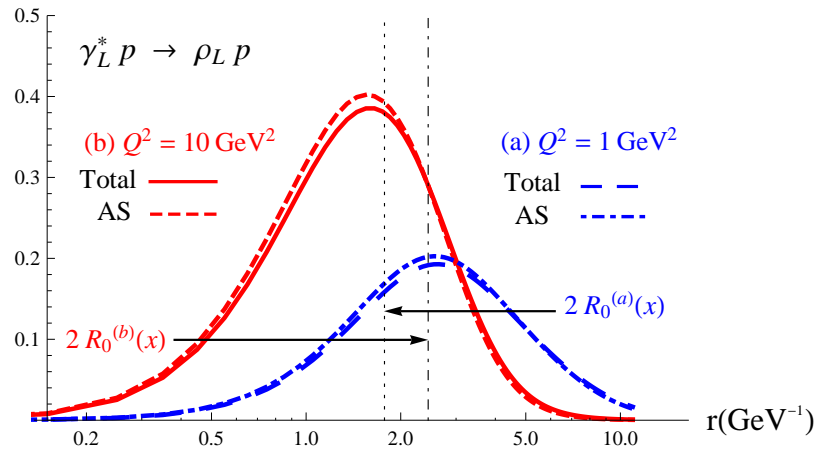


Figure 3.25: The normalized integrand of T_{00} , i.e. $\mathcal{P}_{00}(r, Q^2, \mu_F^2) \hat{\sigma}(x, r)$. The Total integrands at $\mu_F^2(Q^2)$ for $Q^2 = 1 \text{ GeV}^2$ (blue long-dashed line) and $Q^2 = 10 \text{ GeV}^2$ (red solid line), and the AS integrands for $Q^2 = 1 \text{ GeV}^2$ (blue dot-dashed line) and $Q^2 = 10 \text{ GeV}^2$ (red dashed line) integrands of T_{00} for $W = 90 \text{ GeV}$.

3.7.2 Comparison of overlaps

The overlaps we have considered above involve the ρ -meson DAs. Let us compare our model for the wave function overlaps to two other models,

- the "Boosted Gaussian" (BG) model [118],

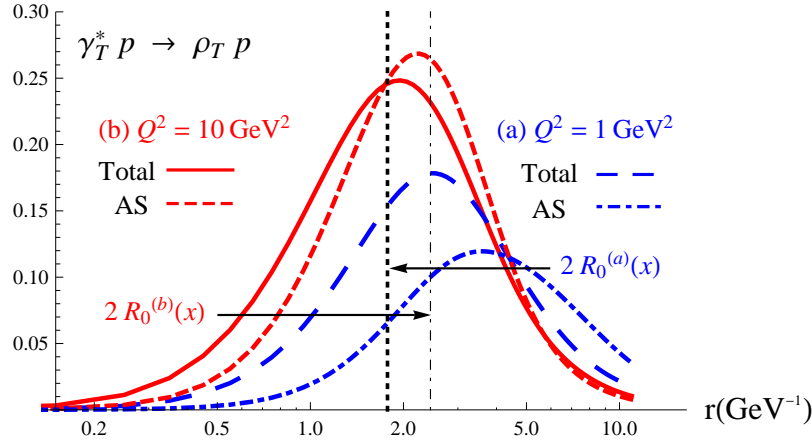


Figure 3.26: The Total contributions at $\mu_F^2(Q^2)$ for $Q^2 = 1 \text{ GeV}^2$ (blue long-dashed line) and $Q^2 = 10 \text{ GeV}^2$ (red solid line), and the AS contributions for $Q^2 = 1 \text{ GeV}^2$ (blue dot-dashed line) and $Q^2 = 10 \text{ GeV}^2$ (red dashed line) to the normalized integrands of T_{11} , i.e. $\mathcal{P}_{11}(r, Q^2, \mu_F^2) \hat{\sigma}(x, r)$, for $W = 90 \text{ GeV}$.

- the "Gaus-LC" model [74].

The ρ -meson wave functions are separated in spinor parts and scalar parts ϕ_T and ϕ_L ,

$$\Psi_{h\bar{h}, \lambda_\rho = \pm 1}^\rho(y, r) = \pm \sqrt{2N_c} \frac{1}{y\bar{y}} \{ i e^{\pm i\theta_r} [y\delta_{h,\pm}\delta_{\bar{h},\mp} - \bar{y}\delta_{h,\mp}\delta_{\bar{h},\pm}] \partial_r + m_f \delta_{h,\pm}\delta_{\bar{h},\pm} \} \phi_T(y, r), \quad (3.154)$$

$$\Psi_{h\bar{h}, \lambda_\rho = 0}^\rho(y, r) = \sqrt{N_c} \delta_{h,-\bar{h}} \left[m_\rho + \delta \frac{m_f^2 - \nabla_r^2}{m_\rho y\bar{y}} \right] \phi_L(y, r). \quad (3.155)$$

The scalar parts read

$$\phi_T^{\text{Gauss-LC}}(y, r) = N_T (y\bar{y})^2 e^{-\frac{r^2}{2R_T^2}}, \quad (3.156)$$

$$\phi_L^{\text{Gauss-LC}}(y, r) = N_L y\bar{y} e^{-\frac{r^2}{2R_L^2}}, \quad (3.157)$$

$$\phi_{L,T}^{\text{BG}}(y, r) = N_{L,T} y\bar{y} \exp \left(-\frac{m_f^2 R_{L,T}^2}{8y\bar{y}} - \frac{2y\bar{y}r^2}{R_{L,T}^2} + \frac{m_f^2 R_{L,T}^2}{2} \right). \quad (3.158)$$

We follow here the conventions and take the values for the parameters of ref. [76]. The values of the parameters are given in tab. 3.5. The overlaps with the virtual photon wave function

Model	N_T	$R_T^2 \text{ GeV}^{-2}$	N_L	$R_L^2 \text{ GeV}^{-2}$	f_ρ^T
Gaus-LC	4.47	21.9	1.79	10.4	f_ρ
Boosted Gaussian	0.911	0.853	12.9	R_L^2	0.182

Table 3.5: Parameters of the "Gaus-LC" and the "Boosted Gaussian" models taken from ref.[76], for $M_\rho = 0.776 \text{ GeV}$, $f_\rho = 0.156 \text{ GeV}$, $m_f = 0.14 \text{ GeV}$ and with $f_\rho^L = f_\rho$.

are

$$\sum_{h,\bar{h}} \Psi_{h,\bar{h}}^{\rho_T^*}(y, \underline{r}) \Psi_{h,\bar{h}}^{\gamma_T^*}(y, \underline{r}) \propto m_f^2 K_0(\mu r) \phi_T(y, r) - (y^2 + \bar{y}^2) \mu K_1(\mu r) \partial_r \phi_T(y, r), \quad (3.159)$$

$$\sum_{h,\bar{h}} \Psi_{h,\bar{h}}^{\rho_L^*}(y, \underline{r}) \Psi_{h,\bar{h}}^{\gamma_L^*}(y, \underline{r}) \propto y \bar{y} K_0(\mu r) \left(m_\rho \phi_L(y, r) + \delta \frac{m_f^2 - \nabla_r^2}{m_\rho y \bar{y}} \phi_L(y, r) \right), \quad (3.160)$$

with $\delta = 0$ for the Gaus-LC model and $\delta = 1$ for the BG model. The longitudinal and transverse radial distributions thus read

$$\mathcal{P}_{L,T}(r) = \frac{1}{\mathcal{N}_{L,T}} r \int dy \sum_{h,\bar{h}} \Psi_{h,\bar{h}}^{\rho_{L,T}^*}(y, \underline{r}) \Psi_{h,\bar{h}}^{\gamma_{L,T}^*}(y, \underline{r}), \quad (3.161)$$

where the factors $\mathcal{N}_{L,T}$ normalize the distributions $\mathcal{P}_{L,T}(r)$. The comparison of our results

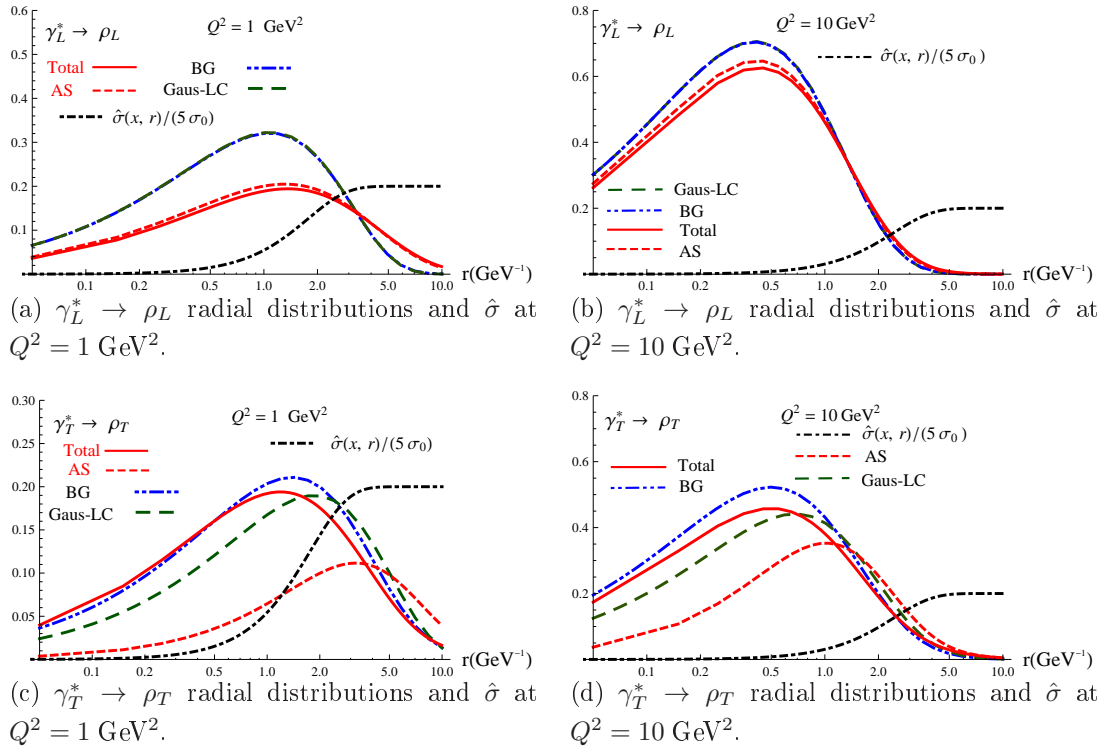


Figure 3.27: The Gauss-LC (green, long dashed), BG (blue, dot-dot-dashed), Total (red, solid) and AS (red, dashed) radial distributions for the $\gamma_L^* \rightarrow \rho_L$ transition (top) and for the $\gamma_T^* \rightarrow \rho_T$ transition (bottom), vs r for $Q^2 = 1 \text{ GeV}^2$ (left) and $Q^2 = 10 \text{ GeV}^2$ (right), as well as the dipole cross-section $\hat{\sigma}(x, r)$ rescaled by the factor $5\sigma_0$ for $W = 90 \text{ GeV}$ (black, dot-dashed).

with the phenomenological models "Gaus-LC" and "BG" allows to understand the role of higher twist corrections on the distributions. We see for example in figs. 3.27(b) that all the results are quite close to each other for $Q^2 = Q_a^2$, leading all to a good description of

the data. For $Q^2 = Q_b^2$, we see in fig. 3.27(a) that the distribution P_{00} spreads more than the distributions from the two other models. The difference is certainly due to higher twist corrections which should be needed for such small virtualities. In fig. 3.27(d) the overlaps are in good agreement for large dipoles in the bandwidth of the cross-section, which means that higher twist corrections are washed out by the dipole cross-section. At small Q^2 , we see in fig. 3.27(c) that the choice $\mu_F^2 \sim Q^2$ allows to get closer from the Gaus-LC and BG models compared to the AS result. Note that the higher twist corrections would play also a role on the normalizations $\mathcal{N}_{\lambda_\rho \lambda_\gamma}$ values.

3.8 Discussion

We have presented a phenomenological model for the helicity amplitudes and the polarized cross-sections of the diffractive ρ -meson electroproduction. The x -dependence of our predictions is encoded in the dipole cross-section model while the Q^2 -dependence comes from the twist 2 and twist 3 calculations of the $\gamma^* \rightarrow \rho$ impact factors. Finally the t -dependence of the differential cross-section is taken from the more recent fits of HERA data. This model does not have free parameter as the dipole cross-section model we use is completely determined by the DIS structure functions. The results have a weak dependence in the factorization scale choice. As expected from many studies (see for example [113] where it is argued that pQCD treatment should be valid for $Q^2 \gtrsim 20 - 30 \text{ GeV}^2$), the model matches the data at large Q^2 and the process can be described in terms of pQCD. Two different effects could generate the discrepancy with the data, the skewness effects which are not included in our study as we took the dipole cross-section from inclusive processes, and the higher twist effects in the ρ -meson factorization. As our predictions are in good agreement with the data at large Q^2 where higher twist corrections can be neglected, we can expect that skewness effects does not change dramatically the predictions. Indeed, the skewness is expected to become large for large Q^2/m_ρ^2 ratio and our predictions agree with data for large Q^2 which indicates that these effects are negligible. Our guess is then that the higher twist corrections should be the dominant corrections to our treatment and thanks to HERA data we can identify the virtuality $Q^2_{\text{min}} \sim 5 \text{ GeV}^2$ where the higher twist corrections become important. The fact that this scale is larger than the saturation scale $Q_s^2(x) \sim 1 \text{ GeV}^2$, indicates that we cannot yet get information on the genuine saturation regime because of higher twist corrections.

The t -dependence of the polarized cross-sections includes the contributions of the other helicity amplitudes that violate the SCHC. The study of the t -dependence of the impact factors would be nice in order to combine the results of dipole models with impact parameter dependence [85, 76] as the DVMP allows to probe the proton shape [145], in particular through local geometric scaling [173, 174].

The next-to-leading order effects - both on the evolution and on the impact factor - should be studied, since it is now known that both may have an important phenomenological effect [175, 176, 177, 178, 179].

On the experimental side, the future Electron-Ion Collider [180] and Large Hadron Electron Collider [181] with a high center-of-mass energy and high luminosities, as well as the International Linear Collider [182, 183, 184] will hopefully open the opportunity to study in more detail the hard diffractive production of mesons [185, 186, 175, 187, 176, 188, 177, 189].

Conclusions

We have presented different techniques used to unravel the hadronic properties uncovered in exclusive processes. The interesting aspect of the approach we pursued here is that it combines two different schemes to model the ρ -meson interactions and the nucleon interactions. The first one involves an extended collinear factorization approach with regularization of the end-point singularities by the transverse momenta k_\perp of the t -channel gluons. It provides an interesting way to study the moments of the ρ -meson wave functions. The second one involves dipole models and confirms the factorization of the interaction of color dipole configurations with the nucleon target. The extension up to twist 3, involving an additional gluon which can take a large amount of energy of the virtual photon, can be interesting in order to study interactions beyond the quark antiquark pair intermediate state approximation.

The new results obtained in this thesis are,

- predictions for the ratios of helicity amplitudes T_{01}/T_{00} and T_{11}/T_{00} [18] combining the twist 2 and twist 3 $\gamma^* \rightarrow \rho$ impact factors with a model of impact factor for the nucleon,
- expressions in impact parameter space representation for the $\gamma_L^* \rightarrow \rho_L$ and $\gamma_T^* \rightarrow \rho_T$ impact factors that are shown to be consistent with the color dipole picture [19],
- predictions for the helicity amplitudes T_{00} and T_{11} as well as for the polarized cross-sections σ_L and σ_T [20], combining the impact parameter representation of the $\gamma^* \rightarrow \rho$ impact factors with dipole cross-section models.

While the first set of predictions using a nucleon impact factor model depends on one free parameter, which is the transverse scale of the nucleon target dynamics M , the second set of predictions has no free parameters and is in good agreement with data for large virtualities. Within this model, we can learn that the $q\bar{q}g$ Fock state plays an important role at the level of the overlap of the virtual photon and the ρ -meson wave functions, while it can be neglected at the level of the helicity amplitude T_{11} due to the convolution with the dipole cross-section.

Many perspectives in order to extend this study are possible. We can make predictions for the future collider projects EIC and LHeC. This study offers also the perspective to combine higher twist calculations of the vector meson productions with impact parameter dependent dipole models, by extending the kinematics to the non-forward limit $t \neq t_{min}$. Indeed the diffractive production of vector meson is a very good process to probe the impact parameter dependence of the dipole-target scattering amplitude and the photon wave function is well-known in the non-forward limit [145]. Another perspective would be also to extend this treatment to the violating s-channel helicity conserving helicity amplitudes that are measured at HERA. A higher twist calculation could be performed to get information on the higher twist corrections in the model presented in chap. 3 for the low values of Q^2 . One could also repeat the calculations including quark mass effects and consequently chiral odd and chiral even DAs to get a similar analysis of other vector mesons such as the ϕ -meson. Another interesting perspective, which we have left for a further study, is to relate the combinations

of DAs that appear in this first principle treatment of the impact factor, to the numerous models that exist for the ρ -meson wave functions. It would provide a test for these models of ρ -meson wave functions.

Appendix

QED and QCD lagrangians, Feynman rules

In our studies we work at energy scales where we can mostly neglect the weak interaction contributions compared to electromagnetic and strong interactions. The weak interaction could contribute for example through the exchange of a Z^0 -boson instead of a virtual photon in $e-p$ collisions but these kinds of contributions can be safely neglected in our present study. We then restrict ourselves to the strong and the electromagnetic interactions involving QCD and QED Lagrangian terms.

Let us recall the Lagrangians and the Feynman rules which are used all along this thesis, we choose to follow the conventions of the Peskin and Schroeder book [190].

QED Feynman rules

Let us consider the QED lagrangian for a theory with only electron, of electric charge $e = -|e|$, and photon fields. The generalization of the following Lagrangian terms and Feynman rules for fermions with electric charge $Q|e|$ is straightforward and consists in replacing $e \rightarrow Q|e|$. The covariant derivative reads

$$D_\mu = \partial_\mu + ieA_\mu \quad (3.162)$$

with A_μ the gauge field of the photon.

The abelian Yang-Mills Lagrangian in the covariant gauge reads

$$\mathcal{L}_{QED} = -\frac{1}{4}(F_{\mu\nu})^2 - \frac{1}{2\xi}(\partial^\mu A_\mu)^2 + \bar{\psi}(i\not{D} - m)\psi \quad (3.163)$$

where $F_{\mu\nu} = \partial_\mu A_\nu - \partial_\nu A_\mu$ is the field strength tensor of the photon, the term $-\frac{1}{2\xi}(\partial^\mu A_\mu)^2$ is the gauge fixing term, where ξ is an arbitrary finite number. The choices to fix $\xi = 0$ and $\xi = 1$ correspond respectively to the Landau and the Feynman gauges. The lagrangian can be decomposed in:

- the photon kinematic term,

$$-\frac{1}{4}(F_{\mu\nu})^2 - \frac{1}{2\xi}(\partial^\mu A_\mu)^2, \quad (3.164)$$

- the electron kinematic term,

$$\bar{\psi}(i\not{\partial} - m)\psi, \quad (3.165)$$

- the interaction term,

$$-\bar{\psi}(eA_\mu)\psi. \quad (3.166)$$

This leads to the following Feynman rules for the propagators of the photon and the electron,

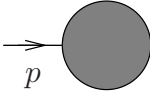
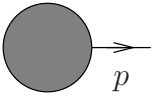
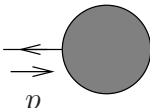
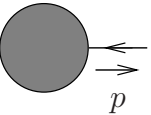
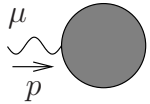
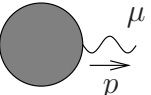
$$\begin{array}{c} \mu \\ \text{~~~~~} \nu \\ \text{~~~~~} \\ \leftarrow p \end{array} \quad \frac{-i}{p^2 + i\varepsilon} \left[g_{\mu\nu} - (1 - \xi) \frac{p_\mu p_\nu}{p^2} \right], \quad (3.167)$$

$$\text{p} \quad \overline{\frac{i}{p - m}}, \quad (3.168)$$

and for the vertex

$$\begin{array}{c} \mu \\ | \\ \text{---} \leftarrow \leftarrow \text{---} \end{array} -ie\gamma^\mu. \quad (3.169)$$

The external lines of the Feynman diagrams for fields of fermions and photons are respectively given by the spinors $u^{(s)}(p)$ for particles and $v^{(s)}(p)$ for antiparticles of spin s and momentum p and polarization vectors $\varepsilon^\lambda(p)$ with λ the polarization,

incoming fermion		$u^{(s)}(p)$
outgoing fermion		$\bar{u}^{(s)}(p)$
incoming antifermion		$\bar{v}^{(s)}(p)$
outgoing antifermion		$v^{(s)}(p)$
incoming photon		$\varepsilon_\mu^{(\lambda)}(p)$
outgoing photon		$\varepsilon_\mu^{*(\lambda)}(p)$

which comes from the projection of the free fields on the incoming and outgoing states.

QCD Lagrangian

The strong interaction is described by QCD which is a local gauge field theory based on the non-abelian SU(3)-color symmetry¹, involving quarks, antiquarks and gluons as elementary constituents of the hadronic matter. The quarks and the antiquarks belong to the fundamental representation of the SU(N)-color group and are carrying a color charge. They couple with the $N^2 - 1$ gauge boson fields (gluons) of SU(N)-color $A^{\mu a} t^a$ that belong to the adjoint representation of SU(N), $\{t^a\}_{a=1..N^2-1}$ being the generators of SU(N). The matrices t^a are traceless hermitian $N \times N$ matrices. Note that the gluons are carrying color charges of the adjoint representation which means that contrary to the abelian case of QED where the photons do not carry an electric charge, the gluons can interact between themselves. This fact will lead to new terms in the Yang-Mills lagrangian of QCD compared to the one of QED. The generators t^a verify the Lie algebra structure relation

$$[t^a, t^b] = i f^{abc} t^c, \quad (3.171)$$

where f^{abc} are the structure constants which are completely antisymmetric under the exchange of the indices a, b, c . The field strength tensor for the gluon fields is given by,

$$F_{\mu\nu}^a = \partial_\mu A_\nu^a - \partial_\nu A_\mu^a + g f_{abc} A_\mu^b A_\nu^c, \quad (3.172)$$

and the covariant derivative reads

$$D_\mu = \partial_\mu - i g t^a A_\mu^a. \quad (3.173)$$

In the covariant gauge the Yang-Mills QCD Lagrangian reads

$$\mathcal{L} = -\frac{1}{4} F_{\mu\nu}^a F^{a\mu\nu} - \frac{1}{2\xi} (\partial_\mu A_\mu^a)^2 + \bar{\psi} (i\gamma^\mu D_\mu - m) \psi + \bar{c} \square c + g \partial^\mu \bar{c}_b f_{bca} A_\mu^a c_c, \quad (3.174)$$

where the fields denoted c are the fields of the Fadeev Popov ghosts that are introduced to represent the functional determinant that appears when inserting in the Lagrangian the gauge-fixing condition. These fields are not associated to physical particles as they are Grassmann fields, i.e. they anticommute as fermionic fields, but in the same time they are scalar fields, i.e. bosons of spin zero. As a consequence they are appearing only when computing loops. The Feynman rules in the covariant gauge are

¹We work from now with N colors instead of 3 in order to keep more general formulas.

$$\begin{array}{c} p \\ \hline i \longrightarrow j \end{array} \quad \frac{i}{\not{p} - m} \delta_{ij}$$

$$\begin{array}{c} p \\ \hline a \text{---} \text{---} \text{---} b \end{array} \quad \frac{-i}{p^2 + i\varepsilon} \left[g_{\mu\nu} - (1 - \xi) \frac{p_\mu p_\nu}{p^2} \right] \delta^{ab}$$

$$\begin{array}{c} p \\ \hline a \cdots \cdots b \\ \hline a, \mu \\ \hline i \longleftarrow j \end{array} \quad \frac{-i\delta^{ab}}{p^2 + i\varepsilon}$$

$$\begin{array}{c} a, \mu \\ \hline i \longleftarrow j \end{array} \quad ig\gamma^\mu t_{ij}^a$$

$$\begin{array}{c} a, \nu_1 \\ \hline k_1 \\ \hline k_2 \text{---} k_3 \\ \hline b, \nu_2 \quad c, \nu_3 \end{array} \quad gf^{abc} [g^{\nu_1\nu_2}(k_1 - k_2)^{\nu_3} + \delta^{\nu_2\nu_3}(k_2 - k_3)^{\nu_1} + \delta^{\nu_1\nu_3}(k_3 - k_1)^{\nu_2}]$$

$$\begin{array}{c} a, \nu_1 \\ \hline d, \nu_4 \text{---} b, \nu_2 \\ \hline c, \nu_3 \end{array} \quad -ig^2 [f^{abe} f^{cde} (g^{\nu_1\nu_3} g^{\nu_2\nu_4} - g^{\nu_1\nu_4} g^{\nu_2\nu_3}) \\ + f^{ace} f^{bde} (g^{\nu_1\nu_2} g^{\nu_3\nu_4} - g^{\nu_1\nu_4} g^{\nu_2\nu_3}) \\ + f^{ade} f^{bce} (g^{\nu_1\nu_2} g^{\nu_3\nu_4} - g^{\nu_1\nu_3} g^{\nu_2\nu_4})]$$

$$\begin{array}{c} a, \mu \\ \hline b \cdots \cdots c \\ \hline p \end{array} \quad -gf^{abc} p^\mu$$

where the dotted lines are the Fadeev-Popov ghosts.

In this thesis we work in most of the cases in the light-cone gauge instead of the covariant gauge. Let us define first the general case of axial gauge where the gauge fixing term is given by

$$\mathcal{L}_{\text{gauge fix.}} = -\frac{1}{2\xi} (n^\mu A_\mu^a)^2, \quad (3.175)$$

with n an arbitrary fixed vector. In this gauge there is no ghost but the price to pay is that the gluonic propagator $D_{\mu\nu}^{ab}(p)$ expression is more complicated

$$D_{\mu\nu}^{ab}(p) = \frac{-i\delta^{ab}}{p^2 + i\varepsilon} \left(g_{\mu\nu} - \frac{n_\mu p_\nu + n_\nu p_\mu}{n \cdot p} + \frac{\xi p^2 + n^2}{(n \cdot p)^2} p_\mu p_\nu \right). \quad (3.176)$$

The light-cone gauge corresponds to the choice $\xi = 0$ and $n^2 = 0$, i.e. n is a light cone vector.

In this case the gluonic propagator simplifies in

$$D_{\mu\nu}^{ab}(p) = \frac{-i\delta^{ab}}{p^2 + i\epsilon} \left(g_{\mu\nu} - \frac{n_\mu p_\nu + n_\nu p_\mu}{n \cdot p} \right), \quad (3.177)$$

which verifies, $n_\mu D^{\mu\nu}(p) = 0$ and the on-shell transversity condition when $p^2 = 0$, $p_\mu D^{\mu\nu}(p) = 0$. Note that the off-shell transversity condition appears clearly when writing $D_{\mu\nu}^{ab}(p)$ as

$$D_{\mu\nu}^{ab} = \frac{-i}{p^2 + i\epsilon} \left(g_{\mu\nu}^\perp - p^2 \frac{n_\mu n_\nu}{(p \cdot n)^2} \right), \quad (3.178)$$

where are appearing the transverse polarizations of the gluons

$$g_{\mu\nu}^\perp = - \sum_{\lambda=1}^2 \varepsilon_\mu^{*(\lambda)} \varepsilon_\nu^{(\lambda)}.$$

References

- [1] R. P. Feynman, *Very high-energy collisions of hadrons*, *Phys.Rev.Lett.* **23** (1969) 1415–1417.
- [2] J. D. Bjorken, *Asymptotic Sum Rules at Infinite Momentum*, *Phys. Rev.* **179** (1969) 1547–1553.
- [3] D. J. Gross and F. Wilczek, *ULTRAVIOLET BEHAVIOR OF NON-ABELIAN GAUGE THEORIES*, *Phys. Rev. Lett.* **30** (1973) 1343–1346.
- [4] D. Gross and F. Wilczek, *Asymptotically Free Gauge Theories. 1*, *Phys.Rev.* **D8** (1973) 3633–3652.
- [5] H. D. Politzer, *RELIABLE PERTURBATIVE RESULTS FOR STRONG INTERACTIONS?*, *Phys. Rev. Lett.* **30** (1973) 1346–1349.
- [6] K. G. Wilson, *Nonlagrangian models of current algebra*, *Phys.Rev.* **179** (1969) 1499–1512.
- [7] N. H. Christ, B. Hasslacher, and A. H. Mueller, *Light cone behavior of perturbation theory*, *Phys. Rev.* **D6** (1972) 3543.
- [8] N. N. Nikolaev and B. G. Zakharov, *Colour transparency and scaling properties of nuclear shadowing in deep inelastic scattering*, *Z. Phys.* **C49** (1991) 607–618.
- [9] N. Nikolaev and B. G. Zakharov, *Pomeron structure function and diffraction dissociation of virtual photons in perturbative QCD*, *Z.Phys.* **C53** (1992) 331–346.
- [10] A. H. Mueller, *Soft gluons in the infinite momentum wave function and the BFKL pomeron*, *Nucl. Phys.* **B415** (1994) 373–385.
- [11] A. H. Mueller and B. Patel, *Single and double BFKL pomeron exchange and a dipole picture of high-energy hard processes*, *Nucl. Phys.* **B425** (1994) 471–488, [[hep-ph/9403256](#)].
- [12] J. Jalilian-Marian, A. Kovner, A. Leonidov, and H. Weigert, *The Wilson renormalization group for low x physics: Towards the high density regime*, *Phys. Rev.* **D59** (1999) 014014, [[hep-ph/9706377](#)].
- [13] J. Jalilian-Marian, A. Kovner, and H. Weigert, *The Wilson renormalization group for low x physics: Gluon evolution at finite parton density*, *Phys. Rev.* **D59** (1999) 014015, [[hep-ph/9709432](#)].
- [14] A. Kovner, J. G. Milhano, and H. Weigert, *Relating different approaches to nonlinear QCD evolution at finite gluon density*, *Phys. Rev.* **D62** (2000) 114005, [[hep-ph/0004014](#)].

- [15] H. Weigert, *Unitarity at small Bjorken x* , *Nucl. Phys.* **A703** (2002) 823–860, [[hep-ph/0004044](#)].
- [16] E. Iancu, A. Leonidov, and L. D. McLerran, *Nonlinear gluon evolution in the color glass condensate. I*, *Nucl. Phys.* **A692** (2001) 583–645, [[hep-ph/0011241](#)].
- [17] E. Ferreiro, E. Iancu, A. Leonidov, and L. McLerran, *Nonlinear gluon evolution in the color glass condensate. II*, *Nucl. Phys.* **A703** (2002) 489–538, [[hep-ph/0109115](#)].
- [18] I. Anikin, A. Besse, A., D. Ivanov, B. Pire, L. Szymanowski, and S. Wallon, *A phenomenological study of helicity amplitudes of high energy exclusive lepton production of the ρ meson*, *Phys. Rev.* **D84** (2011) 054004, [[arXiv:1105.1761](#)].
- [19] A. Besse, L. Szymanowski, and S. Wallon, *The Dipole Representation of Vector Meson Electroproduction Beyond Leading Twist*, *Nucl. Phys.* **B867** (2013) 19–60, [[arXiv:1204.2281](#)].
- [20] A. Besse, L. Szymanowski, and S. Wallon, *Saturation effects in exclusive ρT , ρL meson electroproduction*, [arXiv:1302.1766](#).
- [21] M. Froissart, *Asymptotic behavior and subtractions in the Mandelstam representation*, *Phys. Rev.* **123** (1961) 1053–1057.
- [22] J. R. Forshaw and D. A. Ross, *Quantum chromodynamics and the pomeron*, *Cambridge Lect. Notes Phys.* **9** (1997) 1–248.
- [23] A. Donnachie and P. V. Landshoff, *Total cross-sections*, *Phys. Lett.* **B296** (1992) 227–232, [[hep-ph/9209205](#)].
- [24] R. E. Cutkosky, *Singularities and discontinuities of Feynman amplitudes*, *J. Math. Phys.* **1** (1960) 429–433.
- [25] H. Cheng and T. T. Wu, *Photon-photon scattering close to the forward direction*, *Phys. Rev.* **D1** (1970) 3414–3415.
- [26] G. Frolov and L. Lipatov *Sov. J. Nucl. Phys.* **13** (1971) 333.
- [27] V. Gribov, G. Frolov, and L. Lipatov *Yad. Fiz.* **12** (1970) 994.
- [28] S. Catani, M. Ciafaloni, and F. Hautmann, *Gluon contributions to small x heavy flavor production*, *Phys. Lett.* **B242** (1990) 97.
- [29] S. Catani, M. Ciafaloni, and F. Hautmann, *High-energy factorization and small x heavy flavor production*, *Nucl. Phys.* **B366** (1991) 135–188.
- [30] J. C. Collins and R. K. Ellis, *Heavy quark production in very high-energy hadron collisions*, *Nucl. Phys.* **B360** (1991) 3–30.
- [31] E. M. Levin, M. G. Ryskin, Y. M. Shabelski, and A. G. Shuvaev, *Heavy quark*

- production in semihard nucleon interactions, Sov. J. Nucl. Phys.* **53** (1991) 657.
- [32] J. Bartels, K. J. Golec-Biernat, and K. Peters, *On the dipole picture in the nonforward direction, Acta Phys. Polon.* **B34** (2003) 3051–3068, [[hep-ph/0301192](#)].
 - [33] L. N. Lipatov, *Small- x physics in perturbative QCD, Phys. Rept.* **286** (1997) 131–198, [[hep-ph/9610276](#)].
 - [34] V. S. Fadin, E. A. Kuraev, and L. N. Lipatov, *On the Pommeranchuk Singularity in Asymptotically Free Theories, Phys. Lett.* **B60** (1975) 50–52.
 - [35] E. A. Kuraev, L. N. Lipatov, and V. S. Fadin, *Multi - Reggeon Processes in the Yang-Mills Theory, Sov. Phys. JETP* **44** (1976) 443–450.
 - [36] E. A. Kuraev, L. N. Lipatov, and V. S. Fadin, *The Pommeranchuk Singularity in Nonabelian Gauge Theories, Sov. Phys. JETP* **45** (1977) 199–204.
 - [37] I. I. Balitsky and L. N. Lipatov, *The Pommeranchuk Singularity in Quantum Chromodynamics, Sov. J. Nucl. Phys.* **28** (1978) 822–829.
 - [38] L. N. Lipatov, *Pomeron in Quantum Chromodynamics, Adv. Ser. Direct. High Energy Phys.* **5** (1989) 411–489.
 - [39] F. Gelis, T. Lappi, and R. Venugopalan, *High energy scattering in Quantum Chromodynamics, Int.J.Mod.Phys.* **E16** (2007) 2595–2637, [[arXiv:0708.0047](#)].
 - [40] J. D. Bjorken and E. A. Paschos, *Inelastic Electron Proton and gamma Proton Scattering, and the Structure of the Nucleon, Phys. Rev.* **185** (1969) 1975–1982.
 - [41] J. Callan, Curtis G. and D. J. Gross, *High-energy electroproduction and the constitution of the electric current, Phys.Rev.Lett.* **22** (1969) 156–159.
 - [42] I. Balitsky, *Operator expansion for high-energy scattering, Nucl. Phys.* **B463** (1996) 99–160, [[hep-ph/9509348](#)].
 - [43] Y. V. Kovchegov, *Small- x F_2 structure function of a nucleus including multiple pomeron exchanges, Phys. Rev.* **D60** (1999) 034008, [[hep-ph/9901281](#)].
 - [44] V. N. Gribov and L. N. Lipatov, *Deep inelastic $e p$ scattering in perturbation theory, Sov. J. Nucl. Phys.* **15** (1972) 438–450.
 - [45] L. N. Lipatov, *The parton model and perturbation theory, Sov. J. Nucl. Phys.* **20** (1975) 94–102.
 - [46] G. Altarelli and G. Parisi, *Asymptotic freedom in parton language, Nucl. Phys.* **B126** (1977) 298.
 - [47] Y. L. Dokshitzer, *Calculation of the Structure Functions for Deep Inelastic Scattering and e^+e^- Annihilation by Perturbation Theory in Quantum Chromodynamics, Sov.*

- Phys. JETP* **46** (1977) 641–653.
- [48] V. L. Chernyak and A. R. Zhitnitsky, *Asymptotic Behavior of Hadron Form-Factors in Quark Model. (In Russian)*, *JETP Lett.* **25** (1977) 510.
 - [49] A. Vogt, S. Moch, and J. Vermaseren, *The Three-loop splitting functions in QCD: The Singlet case*, *Nucl.Phys.* **B691** (2004) 129–181, [[hep-ph/0404111](#)].
 - [50] L. Motyka, K. Golec-Biernat, and G. Watt, *Dipole models and parton saturation in ep scattering*, [arXiv:0809.4191](#).
 - [51] J. Bartels and L. Motyka, *Baryon scattering at high energies: Wave function, impact factor, and gluon radiation*, *Eur.Phys.J.* **C55** (2008) 65–83, [[arXiv:0711.2196](#)].
 - [52] Z. Chen and A. H. Mueller, *The Dipole picture of high-energy scattering, the BFKL equation and many gluon compound states*, *Nucl. Phys.* **B451** (1995) 579–604.
 - [53] L. Susskind, *Model of selfinduced strong interactions*, *Phys.Rev.* **165** (1968) 1535–1546.
 - [54] J. D. Bjorken, J. B. Kogut, and D. E. Soper, *Quantum Electrodynamics at Infinite Momentum: Scattering from an External Field*, *Phys. Rev.* **D3** (1971) 1382.
 - [55] G. P. Lepage and S. J. Brodsky, *Exclusive Processes in Perturbative Quantum Chromodynamics*, *Phys. Rev.* **D22** (1980) 2157.
 - [56] D. Y. Ivanov and M. Wusthoff, *Hard diffractive photon proton scattering at large t* , *Eur. Phys. J.* **C8** (1999) 107–114, [[hep-ph/9808455](#)].
 - [57] M. G. R. V. N. Gribov, E. M. Levin, *Singlet structure function at small x : Unitarization of gluon ladders*, *Nucl. Phys. B* **188** (1981) 555–576.
 - [58] **H1 Collaboration** Collaboration, S. Aid *et. al.*, *A Measurement and QCD analysis of the proton structure function $f_2(x, q^{*2})$ at HERA*, *Nucl.Phys.* **B470** (1996) 3–40, [[hep-ex/9603004](#)].
 - [59] **H1 Collaboration** Collaboration, C. Adloff *et. al.*, *A Measurement of the proton structure function $f_2(x, q^{*2})$ at low x and low q^{*2} at HERA*, *Nucl.Phys.* **B497** (1997) 3–30, [[hep-ex/9703012](#)].
 - [60] **ZEUS Collaboration** Collaboration, M. Derrick *et. al.*, *Measurement of the F_2 structure function in deep inelastic $e + p$ scattering using 1994 data from the ZEUS detector at HERA*, *Z.Phys.* **C72** (1996) 399–424, [[hep-ex/9607002](#)].
 - [61] **ZEUS Collaboration** Collaboration, J. Breitweg *et. al.*, *ZEUS results on the measurement and phenomenology of $F(2)$ at low x and low Q^{*2}* , *Eur.Phys.J.* **C7** (1999) 609–630, [[hep-ex/9809005](#)].
 - [62] K. Golec-Biernat, *Saturation and geometric scaling in DIS at small x* , *J.Phys.* **G28** (2002) 1057–1068, [[hep-ph/0109010](#)].

- [63] B. Kopeliovich, L. Lapidus, and A. Zamolodchikov, *DYNAMICS OF COLOR IN HADRON DIFFRACTION ON NUCLEI*, *JETP Lett.* **33** (1981) 595–597.
- [64] G. Bertsch, S. J. Brodsky, A. Goldhaber, and J. Gunion, *Diffractional Excitation in QCD*, *Phys.Rev.Lett.* **47** (1981) 297.
- [65] K. J. Golec-Biernat and M. Wusthoff, *Saturation effects in deep inelastic scattering at low q^2 and its implications on diffraction*, *Phys. Rev.* **D59** (1999) 014017, [[hep-ph/9807513](#)].
- [66] A. M. Stasto, K. J. Golec-Biernat, and J. Kwiecinski, *Geometric scaling for the total $\gamma^* p$ cross-section in the low x region*, *Phys. Rev. Lett.* **86** (2001) 596–599, [[hep-ph/0007192](#)].
- [67] E. Iancu, K. Itakura, and L. McLerran, *Geometric scaling above the saturation scale*, *Nucl.Phys.* **A708** (2002) 327–352, [[hep-ph/0203137](#)].
- [68] **ZEUS** Collaboration, J. Breitweg *et. al.*, *Measurement of the proton structure function F_2 at very low Q^2 at HERA*, *Phys. Lett.* **B487** (2000) 53–73, [[hep-ex/0005018](#)].
- [69] **ZEUS** Collaboration, S. Chekanov *et. al.*, *Measurement of the neutral current cross section and F_2 structure function for deep inelastic $e^+ p$ scattering at HERA*, *Eur. Phys. J.* **C21** (2001) 443–471, [[hep-ex/0105090](#)].
- [70] **H1** Collaboration, C. Adloff *et. al.*, *Deep-inelastic inclusive ep scattering at low x and a determination of α_s* , *Eur. Phys. J.* **C21** (2001) 33–61, [[hep-ex/0012053](#)].
- [71] J. Bartels, K. J. Golec-Biernat, and H. Kowalski, *A modification of the saturation model: DGLAP evolution*, *Phys. Rev.* **D66** (2002) 014001, [[hep-ph/0203258](#)].
- [72] E. Gotsman, E. Levin, M. Lublinsky, and U. Maor, *Towards a new global QCD analysis: Low x DIS data from nonlinear evolution*, *Eur.Phys.J.* **C27** (2003) 411–425, [[hep-ph/0209074](#)].
- [73] E. Iancu, K. Itakura, and S. Munier, *Saturation and BFKL dynamics in the HERA data at small x* , *Phys. Lett.* **B590** (2004) 199–208, [[hep-ph/0310338](#)].
- [74] H. Kowalski and D. Teaney, *An Impact parameter dipole saturation model*, *Phys.Rev.* **D68** (2003) 114005, [[hep-ph/0304189](#)].
- [75] J. L. Albacete, N. Armesto, J. G. Milhano, C. A. Salgado, and U. A. Wiedemann, *Nuclear size and rapidity dependence of the saturation scale from QCD evolution and experimental data*, *Eur.Phys.J.* **C43** (2005) 353–360, [[hep-ph/0502167](#)].
- [76] H. Kowalski, L. Motyka, and G. Watt, *Exclusive diffractive processes at HERA within the dipole picture*, *Phys.Rev.* **D74** (2006) 074016, [[hep-ph/0606272](#)].
- [77] V. Goncalves, M. Kugeratski, M. Machado, and F. Navarra, *Saturation physics at*

- HERA and RHIC: An Unified description*, *Phys.Lett.* **B643** (2006) 273–278, [hep-ph/0608063].
- [78] L. Frankfurt, A. Radyushkin, and M. Strikman, *Interaction of small size wave packet with hadron target*, *Phys.Rev.* **D55** (1997) 98–104, [hep-ph/9610274].
 - [79] J. Jalilian-Marian, A. Kovner, A. Leonidov, and H. Weigert, *The BFKL equation from the Wilson renormalization group*, *Nucl. Phys.* **B504** (1997) 415–431, [hep-ph/9701284].
 - [80] S. Munier and R. B. Peschanski, *Geometric scaling as traveling waves*, *Phys. Rev. Lett.* **91** (2003) 232001, [hep-ph/0309177].
 - [81] S. Munier and R. B. Peschanski, *Traveling wave fronts and the transition to saturation*, *Phys. Rev.* **D69** (2004) 034008, [hep-ph/0310357].
 - [82] S. Munier and R. B. Peschanski, *Universality and tree structure of high energy QCD*, *Phys. Rev.* **D70** (2004) 077503, [hep-ph/0401215].
 - [83] E. Iancu, A. H. Mueller, and S. Munier, *Universal behavior of QCD amplitudes at high energy from general tools of statistical physics*, *Phys. Lett.* **B606** (2005) 342–350, [hep-ph/0410018].
 - [84] Y. V. Kovchegov, *Unitarization of the BFKL pomeron on a nucleus*, *Phys. Rev.* **D61** (2000) 074018, [hep-ph/9905214].
 - [85] C. Marquet, R. B. Peschanski, and G. Soyez, *Exclusive vector meson production at HERA from QCD with saturation*, *Phys. Rev.* **D76** (2007) 034011, [hep-ph/0702171].
 - [86] J. L. Albacete, N. Armesto, J. G. Milhano, and C. A. Salgado, *Non-linear QCD meets data: A Global analysis of lepton-proton scattering with running coupling BK evolution*, *Phys.Rev.* **D80** (2009) 034031, [arXiv:0902.1112].
 - [87] J. L. Albacete, N. Armesto, J. G. Milhano, P. Quiroga-Arias, and C. A. Salgado, *AAMQS: A non-linear QCD analysis of new HERA data at small- x including heavy quarks*, *Eur.Phys.J.* **C71** (2011) 1705, [arXiv:1012.4408].
 - [88] L. D. McLerran and R. Venugopalan, *Boost covariant gluon distributions in large nuclei*, *Phys.Lett.* **B424** (1998) 15–24, [nucl-th/9705055].
 - [89] A. Mueller and D. Triantafyllopoulos, *The Energy dependence of the saturation momentum*, *Nucl.Phys.* **B640** (2002) 331–350, [hep-ph/0205167].
 - [90] J. L. Albacete and Y. V. Kovchegov, *Solving high energy evolution equation including running coupling corrections*, *Phys.Rev.* **D75** (2007) 125021, [arXiv:0704.0612].
 - [91] J. L. Albacete, *Particle multiplicities in Lead-Lead collisions at the LHC from non-linear evolution with running coupling*, *Phys.Rev.Lett.* **99** (2007) 262301,

[arXiv:0707.2545].

- [92] J. R. Forshaw and G. Shaw, *Gluon saturation in the colour dipole model?*, *JHEP* **0412** (2004) 052, [hep-ph/0411337].
- [93] J. R. Forshaw, R. Sandapen, and G. Shaw, *Further success of the colour dipole model*, *JHEP* **0611** (2006) 025, [hep-ph/0608161].
- [94] A. Shuvaev, K. J. Golec-Biernat, A. D. Martin, and M. Ryskin, *Off diagonal distributions fixed by diagonal partons at small x and x_i* , *Phys.Rev.* **D60** (1999) 014015, [hep-ph/9902410].
- [95] J. C. Collins, L. Frankfurt, and M. Strikman, *Factorization for hard exclusive electroproduction of mesons in QCD*, *Phys. Rev.* **D56** (1997) 2982–3006, [hep-ph/9611433].
- [96] **New Muon Collaboration** Collaboration, M. Arneodo *et. al.*, *Exclusive ρ^0 and ϕ muoproduction at large q^{*2}* , *Nucl.Phys.* **B429** (1994) 503–529.
- [97] **E665 Collaboration** Collaboration, M. Adams *et. al.*, *Diffraction production of ρ^0 (770) mesons in muon - proton interactions at 470-GeV*, *Z.Phys.* **C74** (1997) 237–261.
- [98] **ZEUS** Collaboration, S. Chekanov *et. al.*, *Exclusive ρ^0 production in deep inelastic scattering at HERA*, *PMC Phys.* **A1** (2007) 6, [arXiv:0708.1478].
- [99] **H1** Collaboration, F. D. Aaron *et. al.*, *Diffraction Electroproduction of ρ and ϕ Mesons at HERA*, *JHEP* **05** (2010) 032, [arXiv:0910.5831].
- [100] **ZEUS** Collaboration, J. Breitweg *et. al.*, *Exclusive electroproduction of ρ^0 and j/ψ mesons at HERA*, *Eur. Phys. J.* **C6** (1999) 603–627, [hep-ex/9808020].
- [101] **ZEUS** Collaboration, J. Breitweg *et. al.*, *Measurement of the spin-density matrix elements in exclusive electroproduction of ρ^0 mesons at HERA*, *Eur. Phys. J.* **C12** (2000) 393–410, [hep-ex/9908026].
- [102] **H1** Collaboration, C. Adloff *et. al.*, *Elastic electroproduction of ρ mesons at HERA*, *Eur. Phys. J.* **C13** (2000) 371–396, [hep-ex/9902019].
- [103] **HERMES** Collaboration, A. Airapetian *et. al.*, *Spin Density Matrix Elements in Exclusive ρ^0 Electroproduction on 1H and 2H Targets at 27.5 GeV Beam Energy*, *Eur. Phys. J.* **C62** (2009) 659–695, [arXiv:0901.0701].
- [104] **HERMES** Collaboration, A. Borissov, *Spin density matrix elements from ρ^0 and ϕ meson electroproduction at HERMES*, *AIP Conf. Proc.* **1105** (2009) 19–23.
- [105] **The HERMES** Collaboration, A. Airapetian *et. al.*, *Ratios of Helicity Amplitudes for Exclusive ρ^0 Electroproduction*, *Eur. Phys. J.* **C71** (2011) 1609, [arXiv:1012.3676].
- [106] **CLAS** Collaboration, S. A. Morrow *et. al.*, *Exclusive ρ^0 electroproduction on the*

- proton at CLAS*, *Eur. Phys. J. A* **39** (2009) 5–31, [arXiv:0807.3834].
- [107] **COMPASS** Collaboration, V. Y. Alexakhin *et. al.*, *Double spin asymmetry in exclusive ρ^0 muoproduction at COMPASS*, *Eur. Phys. J. C* **52** (2007) 255–265, [arXiv:0704.1863].
 - [108] V. S. Fadin, R. Fiore, and M. I. Kotsky, *Gluon Regge trajectory in the two-loop approximation*, *Phys. Lett. B* **387** (1996) 593–602, [hep-ph/9605357].
 - [109] G. Camici and M. Ciafaloni, *Irreducible part of the next-to-leading BFKL kernel*, *Phys. Lett. B* **412** (1997) 396–406, [hep-ph/9707390].
 - [110] M. Ciafaloni and G. Camici, *Energy scale(s) and next-to-leading BFKL equation*, *Phys. Lett. B* **430** (1998) 349–354, [hep-ph/9803389].
 - [111] V. S. Fadin and L. N. Lipatov, *BFKL pomeron in the next-to-leading approximation*, *Phys. Lett. B* **429** (1998) 127–134, [hep-ph/9802290].
 - [112] A. D. Martin, M. G. Ryskin, and T. Teubner, *The QCD description of diffractive ρ meson electroproduction*, *Phys. Rev. D* **55** (1997) 4329–4337, [hep-ph/9609448].
 - [113] I. Ivanov, N. Nikolaev, and A. Savin, *Diffractive vector meson production at HERA: From soft to hard QCD*, *Phys.Part.Nucl.* **37** (2006) 1–85, [hep-ph/0501034].
 - [114] D. Schildknecht, G. A. Schuler, and B. Surrow, *Vector meson electroproduction from generalized vector dominance*, *Phys.Lett. B* **449** (1999) 328–338, [hep-ph/9810370].
 - [115] H. G. Dosch, T. Gousset, G. Kulzinger, and H. J. Pirner, *Vector meson leptonproduction and nonperturbative gluon fluctuations in QCD*, *Phys. Rev. D* **55** (1997) 2602–2615, [hep-ph/9608203].
 - [116] J. Nemchik, N. N. Nikolaev, and B. G. Zakharov, *Scanning the BFKL pomeron in elastic production of vector mesons at HERA*, *Phys. Lett. B* **341** (1994) 228–237, [hep-ph/9405355].
 - [117] J. Nemchik, N. N. Nikolaev, E. Predazzi, and B. G. Zakharov, *Color dipole phenomenology of diffractive electroproduction of light vector mesons at HERA*, *Z. Phys. C* **75** (1997) 71–87, [hep-ph/9605231].
 - [118] J. R. Forshaw, R. Sandapen, and G. Shaw, *Colour dipoles and ρ , Φ electroproduction*, *Phys. Rev. D* **69** (2004) 094013, [hep-ph/0312172].
 - [119] J. R. Forshaw and R. Sandapen, *Extracting the ρ meson wavefunction from HERA data*, *JHEP* **11** (2010) 037, [arXiv:1007.1990].
 - [120] J. Forshaw and R. Sandapen, *Extracting the Distribution Amplitudes of the ρ meson from the Color Glass Condensate*, *JHEP* **1110** (2011) 093, [arXiv:1104.4753].
 - [121] D. Y. Ivanov and R. Kirschner, *Polarization in diffractive electroproduction of light*

- vector mesons*, *Phys. Rev.* **D58** (1998) 114026, [[hep-ph/9807324](#)].
- [122] S. J. Brodsky, L. Frankfurt, J. F. Gunion, A. H. Mueller, and M. Strikman, *Diffractional lepton production of vector mesons in QCD*, *Phys. Rev.* **D50** (1994) 3134–3144, [[hep-ph/9402283](#)].
 - [123] L. Frankfurt, W. Koepf, and M. Strikman, *Hard diffractive electroproduction of vector mesons in QCD*, *Phys. Rev.* **D54** (1996) 3194–3215, [[hep-ph/9509311](#)].
 - [124] A. V. Radyushkin, *Nonforward parton distributions*, *Phys. Rev.* **D56** (1997) 5524–5557, [[hep-ph/9704207](#)].
 - [125] H. nan Li and G. Sterman, *The Perturbative pion form-factor with Sudakov suppression*, *Nucl. Phys.* **B381** (1992) 129–140.
 - [126] M. Vanderhaeghen, P. A. M. Guichon, and M. Guidal, *Deeply virtual electroproduction of photons and mesons on the nucleon: Leading order amplitudes and power corrections*, *Phys. Rev.* **D60** (1999) 094017, [[hep-ph/9905372](#)].
 - [127] S. V. Goloskokov and P. Kroll, *Vector meson electroproduction at small Bjorken- x and generalized parton distributions*, *Eur. Phys. J.* **C42** (2005) 281–301, [[hep-ph/0501242](#)].
 - [128] S. V. Goloskokov and P. Kroll, *The longitudinal cross section of vector meson electroproduction*, *Eur. Phys. J.* **C50** (2007) 829–842, [[hep-ph/0611290](#)].
 - [129] S. V. Goloskokov and P. Kroll, *The role of the quark and gluon GPDs in hard vector-meson electroproduction*, *Eur. Phys. J.* **C53** (2008) 367–384, [[/08.3569](#)].
 - [130] I. F. Ginzburg, S. L. Panfil, and V. G. Serbo, *Possibility of the experimental investigation of the QCD Pomeron in semihard processes at the gamma gamma collisions*, *Nucl. Phys.* **B284** (1987) 685–705.
 - [131] I. V. Anikin, D. Y. Ivanov, B. Pire, L. Szymanowski, and S. Wallon, *QCD factorization of exclusive processes beyond leading twist: $\gamma_T^* \rightarrow \rho_T$ impact factor with twist three accuracy*, *Nucl. Phys.* **B828** (2010) 1–68, [[arXiv:0909.4090](#)].
 - [132] I. V. Anikin, B. Pire, and O. V. Teryaev, *On the gauge invariance of the DVCS amplitude*, *Phys. Rev.* **D62** (2000) 071501, [[hep-ph/0003203](#)].
 - [133] I. V. Anikin and O. V. Teryaev, *Wandzura-Wilczek approximation from generalized rotational invariance*, *Phys. Lett.* **B509** (2001) 95–105, [[hep-ph/0102209](#)].
 - [134] I. V. Anikin and O. V. Teryaev, *Genuine twist 3 in exclusive electroproduction of transversely polarized vector mesons*, *Phys. Lett.* **B554** (2003) 51–63, [[hep-ph/0211028](#)].
 - [135] A. V. Efremov and O. V. Teryaev, *On spin effects in Quantum Chromodynamics*, *Sov. J. Nucl. Phys.* **36** (1982) 140.

- [136] E. V. Shuryak and A. I. Vainshtein, *Theory of Power Corrections to Deep Inelastic Scattering in Quantum Chromodynamics. 1. Q^2 Effects*, *Nucl. Phys.* **B199** (1982) 451.
- [137] E. V. Shuryak and A. I. Vainshtein, *Theory of Power Corrections to Deep Inelastic Scattering in Quantum Chromodynamics. 2. Q^4 Effects: Polarized Target*, *Nucl. Phys.* **B201** (1982) 141.
- [138] R. K. Ellis, W. Furmanski, and R. Petronzio, *Unraveling Higher Twists*, *Nucl. Phys.* **B212** (1983) 29.
- [139] A. V. Efremov and O. V. Teryaev, *The transversal polarization in Quantum Chromodynamics*, *Sov. J. Nucl. Phys.* **39** (1984) 962.
- [140] A. V. Radyushkin and C. Weiss, *Kinematical twist-3 effects in DVCS as a quark spin rotation*, *Phys. Rev.* **D64** (2001) 097504, [[hep-ph/0106059](#)].
- [141] P. Ball and V. M. Braun, *The ρ Meson Light-Cone Distribution Amplitudes of Leading Twist Revisited*, *Phys. Rev.* **D54** (1996) 2182–2193, [[hep-ph/9602323](#)].
- [142] P. Ball, V. M. Braun, Y. Koike, and K. Tanaka, *Higher twist distribution amplitudes of vector mesons in QCD: Formalism and twist three distributions*, *Nucl. Phys.* **B529** (1998) 323–382, [[hep-ph/9802299](#)].
- [143] J. F. Gunion and D. E. Soper, *Quark Counting and Hadron Size Effects for Total Cross-Sections*, *Phys. Rev.* **D15** (1977) 2617–2621.
- [144] R. K. Ellis, W. Furmanski, and R. Petronzio, *Power Corrections to the Parton Model in QCD*, *Nucl.Phys.* **B207** (1982) 1.
- [145] S. Munier, A. M. Stasto, and A. H. Mueller, *Impact parameter dependent S-matrix for dipole proton scattering from diffractive meson electroproduction*, *Nucl. Phys.* **B603** (2001) 427–445, [[hep-ph/0102291](#)].
- [146] V. M. Braun, G. P. Korchemsky, and D. Mueller, *The uses of conformal symmetry in QCD*, *Prog. Part. Nucl. Phys.* **51** (2003) 311–398, [[hep-ph/0306057](#)].
- [147] S. Wandzura and F. Wilczek, *Sum Rules for Spin Dependent Electroproduction: Test of Relativistic Constituent Quarks*, *Phys.Lett.* **B72** (1977) 195.
- [148] I. I. Balitsky, V. M. Braun, and A. V. Kolesnichenko, *Radiative Decay $\Sigma^+ \rightarrow p \gamma$ in Quantum Chromodynamics*, *Nucl. Phys.* **B312** (1989) 509–550.
- [149] V. M. Braun and I. E. Filyanov, *Conformal invariance and pion wave functions of nonleading twist*, *Z. Phys.* **C48** (1990) 239–248.
- [150] Y. L. Dokshitzer, D. Diakonov, and S. I. Troian, *Hard Processes in Quantum Chromodynamics*, *Phys. Rept.* **58** (1980) 269–395.
- [151] A. Ali, V. M. Braun, and G. Hiller, *Asymptotic solutions of the evolution equation for*

- the polarized nucleon structure function $g_2(x, Q^{*2})$, *Phys.Lett.* **B266** (1991) 117–125.
- [152] A. Ali, V. M. Braun, and H. Simma, *Exclusive radiative B decays in the light cone QCD sum rule approach*, *Z. Phys.* **C63** (1994) 437–454, [[hep-ph/9401277](#)].
 - [153] P. Ball and V. M. Braun, *Higher twist distribution amplitudes of vector mesons in QCD: Twist-4 distributions and meson mass corrections*, *Nucl. Phys.* **B543** (1999) 201–238, [[hep-ph/9810475](#)].
 - [154] P. Ball and G. Jones, *$B \rightarrow \eta^{(\prime)}$ Form Factors in QCD*, *JHEP* **0708** (2007) 025, [[arXiv:0706.3628](#)].
 - [155] P. Ball, V. Braun, and A. Lenz, *Twist-4 distribution amplitudes of the K^* and ϕ mesons in QCD*, *JHEP* **0708** (2007) 090, [[arXiv:0707.1201](#)].
 - [156] G. P. Lepage and S. J. Brodsky, *Exclusive Processes in Quantum Chromodynamics: Evolution Equations for Hadronic Wave Functions and the Form-Factors of Mesons*, *Phys. Lett.* **B87** (1979) 359–365.
 - [157] A. V. Efremov and A. V. Radyushkin, *Factorization and Asymptotical Behavior of Pion Form-Factor in QCD*, *Phys. Lett.* **B94** (1980) 245–250.
 - [158] F. M. Dittes and A. V. Radyushkin, *Two loop contribution to the evolution of the pion wave function*, *Phys. Lett.* **B134** (1984) 359–362.
 - [159] M. H. Sarmadi, *The asymptotic pion form-factor beyond the leading order*, *Phys. Lett.* **B143** (1984) 471.
 - [160] G. R. Katz, *Two loop Feynman gauge calculation of the meson nonsinglet evolution potential*, *Phys. Rev.* **D31** (1985) 652.
 - [161] S. V. Mikhailov and A. V. Radyushkin, *Evolution kernels in QCD: Two loop calculation in Feynman gauge*, *Nucl. Phys.* **B254** (1985) 89.
 - [162] T. Ohrndorf, *Constraints from conformal covariance on the mixing of operators of lowest twist*, *Nucl. Phys.* **B198** (1982) 26.
 - [163] I. I. Balitsky and V. M. Braun, *Evolution Equations for QCD String Operators*, *Nucl. Phys.* **B311** (1989) 541–584.
 - [164] J. Kodaira, Y. Yasui, K. Tanaka, and T. Uematsu, *QCD corrections to the nucleon’s spin structure function $g_2(x, Q^{*2})$* , *Phys.Lett.* **B387** (1996) 855–860, [[hep-ph/9603377](#)].
 - [165] M. A. Shifman, A. I. Vainshtein, and V. I. Zakharov, *QCD and Resonance Physics. Sum Rules*, *Nucl. Phys.* **B147** (1979) 385–447.
 - [166] V. L. Chernyak and A. R. Zhitnitsky, *Exclusive Decays of Heavy Mesons*, *Nucl. Phys.*

B201 (1982) 492.

- [167] V. L. Chernyak and A. R. Zhitnitsky, *Asymptotic Behavior of Exclusive Processes in QCD*, *Phys. Rept.* **112** (1984) 173.
- [168] V. Novikov, L. Okun, M. A. Shifman, A. Vainshtein, M. Voloshin, *et. al.*, *Charmonium and Gluons: Basic Experimental Facts and Theoretical Introduction*, *Phys.Rept.* **41** (1978) 1–133.
- [169] J. Gasser and H. Leutwyler, *Quark Masses*, *Phys.Rept.* **87** (1982) 77–169.
- [170] K. Schilling and G. Wolf, *How to analyze vector meson production in inelastic lepton scattering*, *Nucl.Phys.* **B61** (1973) 381–413.
- [171] H. Navelet, R. B. Peschanski, C. Royon, and S. Wallon, *Proton structure functions in the dipole picture of BFKL dynamics*, *Phys. Lett.* **B385** (1996) 357–364, [[hep-ph/9605389](#)].
- [172] I. Gradshteyn and I. Ryzhik, *Table of Integrals, Series and Products*. 1980.
- [173] E. Ferreiro, E. Iancu, K. Itakura, and L. McLerran, *Froissart bound from gluon saturation*, *Nucl.Phys.* **A710** (2002) 373–414, [[hep-ph/0206241](#)].
- [174] S. Munier and S. Wallon, *Geometric scaling in exclusive processes*, *Eur. Phys. J.* **C30** (2003) 359–365, [[hep-ph/0303211](#)].
- [175] D. Y. Ivanov and A. Papa, *Electroproduction of two light vector mesons in the next-to-leading approximation*, *Nucl. Phys.* **B732** (2006) 183–199, [[hep-ph/0508162](#)].
- [176] D. Y. Ivanov and A. Papa, *Electroproduction of two light vector mesons in next-to-leading BFKL: Study of systematic effects*, *Eur. Phys. J.* **C49** (2007) 947–955, [[hep-ph/0610042](#)].
- [177] F. Caporale, A. Papa, and A. S. Vera, *Collinear improvement of the BFKL kernel in the electroproduction of two light vector mesons*, *Eur. Phys. J.* **C53** (2008) 525–532, [[arXiv:0807.0525](#)].
- [178] D. Colferai, F. Schwennsen, L. Szymanowski, and S. Wallon, *Mueller Navelet jets at LHC - complete NLL BFKL calculation*, *JHEP* **12** (2010) 026, [[arXiv:1002.1365](#)].
- [179] B. Ducloue, L. Szymanowski, and S. Wallon, *Mueller-Navelet jets at LHC: the first complete NLL BFKL study*, *PoS QNP2012* (2012) 165, [[arXiv:1208.6111](#)].
- [180] D. Boer, M. Diehl, R. Milner, R. Venugopalan, W. Vogelsang, *et. al.*, *Gluons and the quark sea at high energies: Distributions, polarization, tomography*, [arXiv:1108.1713](#).
- [181] **LHeC Study Group** Collaboration, J. Abelleira Fernandez *et. al.*, *A Large Hadron Electron Collider at CERN: Report on the Physics and Design Concepts for Machine and Detector*, *J.Phys.* **G39** (2012) 075001, [[arXiv:1206.2913](#)].

- [182] **ILC** Collaboration, J. Brau, (Ed.) *et. al.*, *ILC Reference Design Report Volume 1 - Executive Summary*, [arXiv:0712.1950](#).
- [183] **ILC** Collaboration, G. Aarons *et. al.*, *International Linear Collider Reference Design Report Volume 2: PHYSICS AT THE ILC*, [arXiv:0709.1893](#).
- [184] **ILC** Collaboration, T. Behnke, (Ed.) *et. al.*, *ILC Reference Design Report Volume 4 - Detectors*, [arXiv:0712.2356](#).
- [185] B. Pire, L. Szymanowski, and S. Wallon, *Double diffractive ρ -production in $\gamma^*\gamma^*$ collisions*, *Eur. Phys. J.* **C44** (2005) 545–558, [[hep-ph/0507038](#)].
- [186] R. Enberg, B. Pire, L. Szymanowski, and S. Wallon, *BFKL resummation effects in $\gamma^*\gamma^* \rightarrow \rho\rho$* , *Eur. Phys. J.* **C45** (2006) 759–769, [[hep-ph/0508134](#)].
- [187] B. Pire, M. Segond, L. Szymanowski, and S. Wallon, *QCD factorizations in $\gamma^*\gamma^* \rightarrow \rho_L^0\rho_L^0$* , *Phys. Lett.* **B639** (2006) 642–651, [[hep-ph/0605320](#)].
- [188] M. Segond, L. Szymanowski, and S. Wallon, *Diffractive production of two ρ_L^0 mesons in e^+e^- collisions*, *Eur. Phys. J.* **C52** (2007) 93–112, [[hep-ph/0703166](#)].
- [189] M. Segond, L. Szymanowski, and S. Wallon, *A test of the BFKL resummation at ILC*, *Acta Phys. Polon.* **B39** (2008) 2577–2582, [[arXiv:0802.4128](#)]. proceedings of the School on QCD, low-x physics, saturation and diffraction, Copanello Calabria, Italy, July 1-14 2007.
- [190] M. E. Peskin and D. V. Schroeder, *An Introduction to Quantum Field Theory (Frontiers in Physics)*. Perseus Books, 2008.